STRUCTURAL AND REACTIVITY STUDY OF RHODIUM(I) CARBONYL COMPLEXES AS MODEL NANO ASSEMBLIES

by

CARLA PRETORIUS

Submitted in fulfilment of the requirements in respect of the
Doctoral degree qualification

PHILOSOPHIAE DOCTOR

in the

DEPARTMENT OF CHEMISTRY

in the Faculty of

NATURAL-AND AGRICULTURAL SCIENCES

at the

UNIVERSITY OF THE FREE STATE

Supervisor

Prof. Andreas Roodt

Co-Supervisor

Dr. Alice Brink

JULY 2015

Acknowledgements

Firstly, I would like to thank God for all the blessings that have been bestowed upon me in my life and for giving me so many opportunities to live up to the potential placed in me.

My parents deserve the greatest thank you of all. Pierre and Ronelle Pretorius- I have been very lucky to have such loving and caring parents. You both sacrificed so much in order for me to be where I am today and I will always be thankful to have had you in my life.

Ferdi, you have been such an incredible force that entered my life. Thank you for all the adventures and laughs (and love)- I hope to have many more.

Jacques Pretorius- thank you for being not only a brother but also a best friend. You have been there through so much and always point out the positive things in life.

Prof. A. Roodt- thank you for being both my supervisor in a research capacity but also a mentor in life. I have learnt so much from being under your guidance and I will always respect you. Thank you for all the opportunities to grow and explore my skills as a scientist. I hope to make you proud one day.

Dr. A. Brink, thank you for agreeing to become one of my supervisors. Your time and input in this project is greatly appreciated.

Dr. L. Twigge- Thank you for your assistance in the ^{103}Rh and ^{31}P NMR work that was included in this study. Your help and kindness is appreciated.

Financial assistance from SASOL, University of the Free State and the South African National Research Foundation (NRF) is gratefully acknowledged.

"There are two paths you can go by, but in the long run, there's still time to change the road you're on"

- Led Zeppelin, Stairway to Heaven

Table of Contents

Abbreviations and Symbols

Abbreviation	Meaning
O,O-Bid	Bidentate ligand
acac	Acetylacetonato
tfac	1,1,1-Trifluoro-2,4-pentanedionato
hfac	Hexafluoroacetonato
piv	1,1,1-Trifluoro-5,5-dimethyl-3,5-hexanedionato
dipiv	2,2,6,6-Tetramethyl-3,5-heptanedionato
3Cl-acac	3-Chloro-2,4-pentanedionato
CN-acac	3-Cyano-2,4-pentanedionato
acacac	Triacetylmethanato
pyruv	Methyl-4-oxo-2-oxypent-2-enoato
bzac	3-Benzoylacetonato
F_3-bzac	Benzoyl-1,1,1-trifluoroacetonato
F_3-4Clbzac	Benzoyl-4-chloro-1,1,1-trifluoroacetonato
naphth	4,4,4-Trifluoro-1-(2-naphthyl)-1,3-butanedionato
dbm	1,3-Diphenyl-1,3-propanedionato
$P(otol)_3$	Tri(o-tolyl)phosphine
chloroform-*d*	Deuterated chloroform
benzene-d_6	Deuterated benzene
methylene chloride-d_2	Deuterated methylene chloride
Z	Number of molecules in a unit cell
Å	Angstrom
NMR	Nuclear Magnetic Resonance spectroscopy
IR	Infrared spectroscopy
ν	Stretching frequency on IR
δ	Chemical shift
ppm	Units of chemical shift (parts per million)
π	pi
σ	Sigma
α	Alpha
β	Beta
γ	Gamma
λ	Wavelength
Θ	Theta
°	Degrees
°C	Degrees Celsius
K	Kelvin
ε	Extinction coefficient
g	Gram
M	$mol.dm^{-3}$
k_{obs}	Observed pseudo-first order rate constant
K_{eq}	Equilibrium constant
pK_a	Acid dissociation constant
T	Temperature
UV	Ultraviolet region in light spectrum
Vis	Visible region in light spectrum
TMS	Tetramethylsilane
CO	Carbonyl
DMF	Dimethyl formamide
MeCN	Acetonitrile
PGM	Platinum group metal
μ	Indicates bridging ligand in complexes
CSD	Cambridge Structural Database
s	Singlet in NMR spectroscopy
d	Doublet in NMR spectroscopy

m	Multiplet in NMR spectroscopy
d(⋯)	Distance
Hz	Hertz
J	Coupling constant
PX_3	Tertiary substituted phosphine
t-Bu	Tertiary butyl

ABSTRACT

This study focussed on the investigation of different β-diketonato ligands in coordination to rhodium(I). Square planar [Rh(*O,O'*-Bid)$(CO)_2$] complexes have been shown to effectively facilitate metallophilic interactions between rhodium(I) centres in the construction of infinite one-dimensional metal chains in the solid-state. The classification of these systems as forming nano-wired assemblies has led to similar systems finding wide application in electronic and optical technologies.

The study was focused on investigating the effect of an altered rhodium(I) environment on the metallophilic interactions and subsequent one-dimensional chains formed in the solid-state. These modifications were initiated by using a range of different coordinating β-diketonato ligands to induce either electronic or steric changes to the rhodium(I) centre. To this end, a range of rhodium(I) complexes were synthesized and characterized by IR, UV/Vis and NMR spectroscopy. Single crystal X-ray diffraction was used in the solid-state structure determinations of these complexes showing significant changes in the Rh···Rh distances in each rhodium(I) complex. It also provided valuable information with regards to how the molecules are arranged along these one-dimensional chains. Rh···Rh distances ranging from 3.134(3) Å to 3.617(3) Å were found in the solid-sate for the range of rhodium(I) complexes with the distances correlating to the UV/Vis absorption profile of each complex.

A preliminary substitution reaction and equilibrium study was undertaken to further evaluate how changes at the rhodium(I) centre could affect the reactivity of the rhodium(I) complexes. An important equilibrium was shown to participate in the reaction using ^{31}P NMR and UV/Vis spectroscopy. In this investigation it was seen that using second-order rate constants to describe the reactivity of the complexes correlated to the pK_a values of the uncoordinated β-diketone ligands with an increased rate in substitution associated with a lower pK_a of the free ligand. ^{103}Rh NMR chemical shifts of the rhodium(I) complexes were also found to correlate to the pK_a values of the free ligands as well as highlighting the electronic environment experienced by the metal centre. This provided an effective measure of how electronic changes to the rhodium(I) centre could affect the Rh···Rh interactions of the solid-state structures as well as the physical properties of the compounds.

The study concluded with a comparison of all the parameters by which the rhodium(I) complexes were evaluated to assess how changes induced by using different coordinating β-diketonato ligands influence the one-dimensional chains constructed *via* metallophilic interactions as well as physical properties such as the colour exhibited by the bulk material. These parameters included

pK_a, UV/Vis absorbance properties, IR, ^{103}Rh NMR, reactivity (k_{12} constants), Rh···Rh distances and the torsion angles of the assembled molecules.

Keywords:

Rhodium
Metallophilic interactions
Nano-wires

OPSOMMING

Hierdie studie het gefokus op die ondersoek van β-diketonato ligande wat aan rodium(I) gekoördineer is. Daar is bewys dat vierkantig planêre [Rh(*O,O'*-Bid)$(CO)_2$] komplekse effektief die metalofiliese interaksies tussen rodium(I) kerne in die konstruksie van oneindigende een-dimensionele metaalkettings in die vaste toestand kan fasiliteer. Die klassifikasie van hierdie stelsels om nanodraadsamestellings te vorm het gelei tot soortgelyke stelsels wat wye toepassing in elektroniese en optiese tegnologië gevind het.

Die studie het gefokus op die ondersoek van die effek van `n veranderde rodium(I) omgewing op die metalofiliese interaksies en die opeenvolgende een-dimensionele kettings wat in die vaste toestand gevorm is. Hierdie veranderinge is geïnisieer deur `n reeks verskillend koördinerende β-diketonato ligande te gebruik om óf elektroniese, óf steriese verandering in die rodium(I) kern te bewerkstellig. Met hierdie doel is `n reeks rodium(I) komplekse voorberei en gekarakteriseer deur IR, UV/Sig en KMR spektroskopie. Enkelkristal X-straaldiffraksie is gebruik in die vaste toestand struktuurbepalings van hierdie komplekse wat beduidende veranderinge in die Rh···Rh afstand in elke rodium(I) kompleks getoon het. Dit het ook waardevolle inligting verskaf rakende hoe die molekules in hierdie een-dimensionele kettings gerangskik is. Rh···Rh afstande wat strek vanaf 3.134(3) Å tot 3.617(3) Å is gevind in die vaste toestand vir die reeks rodium(I) komplekse; die afstande stem ooreen met die UV/Sig absorpsieprofiel van elke kompleks.

`n Voorlopige substitusiereaksie- en ewewigstudie is onderneem om die effek van veranderinge by die rodium(I) kern op die reaktiwiteit van die rodium(I) komplekse verder te evalueer. `n Belangrike ewewig neem deel aan die reaksie soos bewys deur die gebruik van ^{31}P KMR en UV/Sig spektroskopie. In hierdie ondersoek is dit waargeneem dat deur tweedeorde tempokonstantes te gebruik om die reaktiwiteit van die komplekse te beskryf, die konstantes ooreengestem het met die pK_a-waardes van die ongekoördineerde β-diketoonligande met `n toename in tempo van substitusie geassosieer met `n laer pK_a van die vry ligand. ^{103}Rh KMR chemiese verskuiwings van die rodium(I) komplekse het ook met die pK_a-waardes van die vry ligande ooreengestem en het die elektroniese omgewing wat die metaalkern ervaar beklemtoon. Hierdie waarneming het `n effektiewe maatstaf verskaf vir hoe elektroniese veranderinge aan die rodium(I) kern die Rh···Rh interaksies van die vaste toestand strukture, asook die fisiese eienskappe van die verbindings, sal beïnvloed.

Die studie is afgesluit deur `n vergelyking van al die parameters waardeur die rodium(I) komplekse geëvalueer was om vas te stel hoe veranderinge wat veroorsaak word deur verskillende koördinerende β-diketonato ligande te gebruik die een-dimensionele kettings wat *via*

metalofiliese interaksies vorm, asook fisiese eienskappe soos die kleur wat deur die massa materiaal vertoon word, beïnvloed. Hierdie parameters het pK_a, UV/Sig absorbansie-eienskappe, IR, ^{103}Rh KMR, reaktiwiteit (k_{12} konstantes), Rh···Rh afstande en die torsiehoeke van die saamgestelde molekule ingesluit.

Sleutelwoorde:

Rodium
Metalofiliese interaksies
Nanodrade

Chapter 1: Introduction

1.1 Introduction

The element rhodium along with iridium, platinum, palladium, ruthenium and osmium form part of the distinguished Platinum Group Metals (PGM's).[1] Discovered in 1803 by W. H. Wollaston the new transition metal was named after the Greek word *rhodon*, meaning rose, in reference to the pink-reddish coloured compounds formed by the metal.[2] However, little interest existed in the applications of this transition metal until its important catalytic properties were discovered.[3]

Rhodium has been found to exhibit remarkable catalytic activity and selectivity in comparison to other metals.[4] Consequently, rhodium-based catalysts have found prominent application in processes such as the hydrogenation of olefins, hydrogenation of arenes, hydroformylation of olefins, olefin-diene co-dimerization and the carbonylation of methanol to acetic acid, to name but a few.[5,6,7,8]

For this reason, research relating to the coordination chemistry of rhodium is seen as a critical step in understanding and developing new rhodium-based catalyst and other technology. In fact, rhodium(I) complexes of the type [Rh(*L,L'*-Bid)$(CO)_2$] (where *L,L'*-Bid refers to a chelating mono-anionic ligand coordinated *via O,O'*, *N,O'* or *S,O'* donor atoms) have been studied at length as catalyst precursors and model compounds for many of the catalytic processes mentioned above.[9,10,11]

Apart from their catalytic application, the typically square planar [Rh(*L,L'*-Bid)$(CO)_2$] complexes are also known to display interesting physical properties such as dichroism. One of the most notable examples being that of [Rh(acac)$(CO)_2$].[12] This rhodium(I) complex

[1] Crundwell, F. K., Moats, M. S., Ramachandran, V., Robinson, T. G., Davenport, W. G., *Extractive Metallurgy of Nickel, Cobalt and Platinum Group Metals*, Elsevier, Oxford, United Kingdom, **2011**, 1.
[2] Cotton, S. A., *Chemistry of Precious Metals*, Blackie Academic & Professional, London, United Kingdom, **1997**, 78.
[3] Kăspar, J., Fornasiero, P., Hickey, N., *Catal. Today*, **2003**, *77*, 419-449.
[4] Yuan, Y., Yan, N., Dyson, P. J., *ACS Catal.*, **2012**, *2*, 1057-1069.
[5] Halpern, J., *Chem. Eng. News*, **2003**, *81*, 114.
[6] Lee, J. D., *Concise Inorganic Chemistry*, London, United Kingdom, **1991**.
[7] Young, J. F., Osborn, J. A., Jardine, F. H., Wilkinson, G., *Chem. Commun.*, **1965**, 131-132.
[8] Thomas, C. M., Süss-Fink, G., *Coord. Chem. Rev.*, **2003**, *243*, 125-142.
[9] Leipoldt, J. G., Bok, L. D. C., Van Vollenhoven, J. S., Pieterse, A. I., *J. Inorg. Nucl. Chem.*, **1978**, *40*, 61-63.
[10] Heaton, B. T., Jacob, C., Markapolous, J., Markapoulou, O., Nähring, J., Skylaris, C. K., Smith, A. K., *J. Chem. Soc. Dalton Trans.*, **1996**, 1701-1706.
[11] Venter, G. J. S., *PhD Thesis*, University of the Free State, Bloemfontein, South Africa, **2013**.
[12] Underhill, A. E., *Philos. Trans. R. Soc. London, Ser. A.*, **1985**, *314*, 125-130.

which was first synthesized in 1967 by Bailley *et al.*[13] is well-known for its prominent red colour with green metallic lustre in the solid-state. Interestingly, this compound has also been found to possess conductive properties which along with the unique colours displayed by the complex are directly attributed to interactions between rhodium(I) centres in the solid-state.[14] Moreover, these so-called metallophilic interactions are found to extend infinitely along neighbouring rhodium(I) molecules to form one-dimensional chains in the solid-state of $[Rh(acac)(CO)_2]$. Figure 1.1 illustrates how these interactions are extended between rhodium(I) centres along one direction within the solid-state of $[Rh(acac)(CO)_2]$.

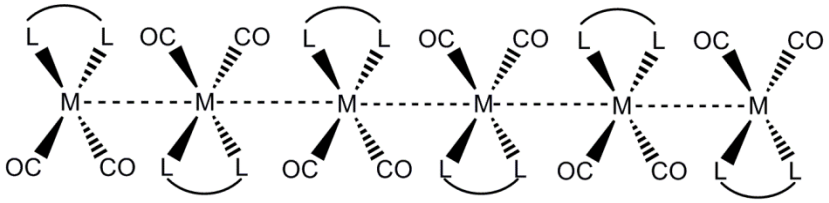

Figure 1.1: Representation of a one-dimensional chain constructed *via* metallophilic interactions between rhodium(I) centres in $[Rh(acac)(CO)_2]$ where L,L' represents the chelation of the O,O' bidentate ligand, acetylacetonato.

The propensity for rhodium(I) nuclei to form metallophilic interactions also lends these complexes to be part of a rather new and emerging research field in material sciences.[15] Materials containing one-dimensional chains are highly sought after due to their electronic, magnetic and photoluminescent properties.[16]

Since metallophilic interactions can be extended into infinite one-dimensional chains they are classified at the nano-scale (1-100 nm) and are often referred to as nano-wires or nano-wired assemblies.[17] As such, metallophilic interactions have been used to construct nano-wires also in other rhodium compounds such as $[Rh(CO)_2Cl(amine)]$[15], [Rh(3,6-dbsq)$(CO)_2$] (3,6-dbsq= 3,6-di-*tert*-butyl-1,2-benzosemiquinon ate)[18] and $[Rh_2(O_2CCF_3)_2(CO)_4]$ (O_2CCF_3= trifluoracetate)[19].

Molecular nano-wires are generally defined as systems that are extended along one direction of the material consisting of repeated molecular units that are either organic or inorganic in nature.[20] It was R. S. Wagner that first pioneered the research into nano-wired

[13] Bailley, N. A., Coates, E., Robertson, G. B., Bonati, F., Ugo, R., *J. Chem. Soc., Chem. Commun.*, **1967**, 1041.
[14] Underhill, A. E., Macchi, P., *Struct. Bonding*, **2012**, *146*, 127-158.
[15] Palmer, L. C., Stupp, S. I., *Acc. Chem. Res.*, **2008**, *41*, 1674-1684.
[16] Yin, X., Warren, S. A., Pn, Y. T., Tsao, K. C., Gray, D. L., Bertke, J., Yang, H*., Angew. Chem. Int. Ed.*, **2014**, *53*, 14087-14091.
[17] Jang, K., Jung, I. G., Nam, H. J., Jung, D. Y., Son, S. U., *J. Am. Chem. Soc.*, **2009**, *131*, 12046-12047.
[18] Mitsumi, M., Goto, H., Umebayashi, S., Ozawa, Y., Kobayashi, M., Yokoyama, T., Tanaka, H., Kuroda, S., Toriumi, K., *Angew. Chem. Int. Ed.*, **2005**, *44*, 4164-4168.
[19] Cotton, F. A., Dikarev, E. V., Petrukhina, M. A., *J. Chem. Soc. Dalton Trans.*, **2000**, 4241-4243.
[20] Dupas, C., Lahmani, M., *Nanoscience: Nanotechnologies and Nanophysics*, Springer-Verlag, Berlin, Germany, **2004**, 325.

structures with his work on silicon micro-wires (whiskers) in the 1960's.[21] Although no viable application could be found for his silicon micro-wires, new research into other fabricated nano-wires was initiated from this work. At present, extensive studies have illustrated the uses of nano-wires in electronic and optical applications and it is expected that they will play a critical role in the functionality of future nano-systems.[22,23]

By implication, an understanding of the fundamental chemistry involved in these structure-directing motifs, such as the [Rh(acac)$(CO)_2$] complex, is crucial in the design of new crystalline and nano-structured functional materials.[24,25] An understanding of the properties of a compound at the molecular level as well as how these molecules are assembled into a larger network can assist in controlled changes in chemical composition, structure, size and morphology to better manipulate the properties associated at the macroscopic scale of the material.[26]

Although it has been shown that materials containing molecules assembled *via* metallophilic interactions show great potential in many applications, as mentioned above, the number of well-defined systems is relatively small.[17,27] It was for this reason that it was decided to investigate some fundamental properties of different rhodium(I) complexes in order to gain better insight into the metallophilic interactions between rhodium(I) centres and build an extended knowledge base in the construction of these nano-wires in the solid-state.

1.2 Aims of Study

As it is known that square planar complexes of the type [Rh(*L,L'*-Bid)$(CO)_2$], such as [Rh(acac)$(CO)_2$], could potentially facilitate metallophilic interactions between rhodium(I) centres in the solid-state, a range of different coordinating β-diketonato ligands similar to acetylacetone were chosen for coordination to rhodium(I) for this study. The various ligands were chosen based on different substituents introduced on the coordinating β-diketonato ligand to bring about specific changes to the rhodium(I) centre in solution and solid state (see Chapter 3).

[21] Xiang, J., *Semiconductor Nanowires*, The Royal Society of Chemistry, London, United Kingdom, **2015**, 3.
[22] Yang, P., Yan, R., Fardy, M., *Nano Lett.*, **2010**, *10*, 1529-1536.
[23] Li, J., Wang, D., LaPierre, R. R., *Advances in III-IV Semiconductor Nanowires and Nanodevices*, Bentham Science Publishers, Sharjah, United Arab Emirates, **2011**, 3.
[24] Enomoto, M., Kishimura, A., Aida, T., *J. Am. Chem. Soc.*, **2001**, *123*, 5608-5609.
[25] Sluch, I. M., Miranda, A. J., Slaughter, L. M., *Cryst. Growth Des.*, **2009**, *9*, 1267-1270.
[26] Kisner, A., *MSc Dissertation*, University of Aachen, Aachen, Germany, **2012**, 1.
[27] Bera, J. K., Dunbar, K. R., *Angew. Chem. Int. Ed.*, **2002**, *41*, 4453-4457.

For example, electron withdrawing/ donating groups were introduced at the methyl (1-) and methine (3-) carbon positions of the different β-diketonato ligands. This was done to evaluate whether a reduction/ increase of electron density at the metal centre could result in changes to the one-dimensional chains and other physical properties associated with the solid-state structures of these complexes. Furthermore, influences of a steric nature were evaluated by introducing bulky substituents such as phenyl rings and *t*-butyl groups on the methyl carbon positions of coordinating β-diketonato ligands and analyzing their effects on the one-dimensional chains of rhodium(I) centres in the solid-state.

The rhodium(I) complexes were subsequently evaluated using different parameters such as the UV/Vis absorption profile, IR stretching frequencies, ^{103}Rh NMR chemical shifts and the substitution rates of the rhodium(I) complexes. These parameters were chosen to assist in evaluating the effect of using different β-diketonato ligands on the rhodium(I) centre and subsequent construction of the one-dimensional metal chains as analyzed systematically by a single crystal X-ray diffraction study.

The overarching investigation was aimed at finding correlations between different properties associated at the molecular level of the different rhodium(I) complexes with the one-dimensional chains constructed *via* metallophilic interactions and subsequent macroscopic properties of the solid-state material, rhodium nano-wired assemblies. Such correlations would contribute to the knowledge base as to how these interactions are formed between singular molecular entities and whether factors such as electronic and steric changes to the rhodium(I) centre influence the construction of the one-dimensional chains. In turn, this can assist in the future design of similar compounds that could potentially be engineered to exhibit specific properties (see Chapter 8).

With the above mentioned in mind, the specific step-wise aims of this study can be summarized as follows:

i) Synthesis and characterization of a range of dicarbonyl-(β-diketonato)-rhodium(I) or [Rh(*O,O'*-Bid)$(CO)_2$] complexes with ligands containing different substituents to induce changes on the rhodium(I) centre.

ii) To characterize the said complexes using IR, UV/Vis, ^{1}H, ^{13}C and ^{103}Rh NMR.

iii) Obtain the solid-state structures of the above mentioned rhodium(I) complexes using single crystal X-ray diffraction.

iv) Undertake a preliminary kinetic and equilibrium investigation into the carbonyl substitution reaction of [Rh(acac)$(CO)_2$] with a bulky phosphine ligand. Such a study would provide a measure of reactivity for the rhodium(I) complexes that

could relate to the changes induced at the rhodium(I) centre using different coordinating β-diketonato ligands.

v) Compare the different parameters by which the rhodium(I) complexes were evaluated to establish trends and relationships between the manipulated rhodium(I) centres and the subsequent one-dimensional chains in the solid-state facilitated *via* metallophilic interactions.

In the following chapter, theory related to this study will be presented followed by the presentation and discussion of experimental results in five chapters. The study will conclude with a comprehensive discussion and comparison of the different parameters by which the rhodium(I) complexes were analyzed to evaluate any trends and relationships that exist for the different complexes in relation to the metallophilic interactions.

Chapter 2: Concise Theoretical Background Related to This Study

2.1 Introduction

The aims of this study as set out in Chapter 1 relates to the coordination of different β-diketone ligands to rhodium(I). The various coordinating ligands were systematically chosen in terms of their different substituents in order to induce either an electronic or steric effect upon the rhodium(I) centre whilst still maintaining the general 6-membered coordination by the *O,O'*-Bid ligands. This was done to better understand the influence of using different substituents in coordinating ligands on the unique metallophilic interactions occurring in such rhodium(I) complexes.

In this chapter, theoretical aspects relating to metallophilic interactions and their uses will be given. Some theory on the methodology of crystal engineering with a focus on metallophilic interactions and its use in the design of nano-material assemblies will be discussed. This will be followed by highlighting applications of materials containing metallophilic interactions. Additionally, motivation for the use of rhodium as prime focus in this study will be given with an emphasis on its unique features and versatility, also for use in catalysis. Since a kinetic and thermodynamic investigation of substitution reactions of rhodium(I) complexes is included in this study with a re-interpretation of the results given in literature, general theory relating to the substitution reactions of square planar complexes will also be given.

2.2 Chemistry and Crystallography-a Perfect Match

In a broad sense, chemistry is involved in the design of functional materials with applications in various fields such as the pharmaceutical and chemical industries. However, in order for chemists to effectively design better drugs or catalysts an understanding of the properties associated with the material and how this relates to the individual molecules and their structure is essential.

The development of X-ray crystallography has given chemists as well as scientists from various other disciplines the unique opportunity of studying the solid-state structures of

compounds at a molecular level. The technique also provides a way to understand how individual molecules are connected into networks at a larger scale.[1] This knowledge can provide scientists with an insight into how characteristics of compounds at the molecular level can be related to the properties of the bulk material.[1]

The relationship between molecules and the structuring of molecules into a network structure was first explored by one of the pioneers of crystallography- W. H. Bragg. By 1921, Bragg became aware of certain structural units such as the benzene ring remaining unchanged in size and form within different crystal structures.[2]

Bragg came across this finding in his study of the crystal structures of naphthalene and anthracene. He discovered that unit cell dimensions could be related to the respective molecular geometry of the different materials (anthracene and naphthalene). Figure 2.1 gives an illustration of the unit cells for these two molecules where two of the axial lengths were found to be nearly identical. The third unit cell dimension was found to be shorter for naphthalene (8.66 Å) and longer in the case of anthracene (11.66 Å). He correctly concluded from these observations that the length of the two molecules had to be along this differing third axis. With this knowledge he calculated the width of a single benzene ring to be 2.5 Å.[2] His findings gave scientists a new understanding into how the physical properties of a molecule could be related to that of its crystal lattice.

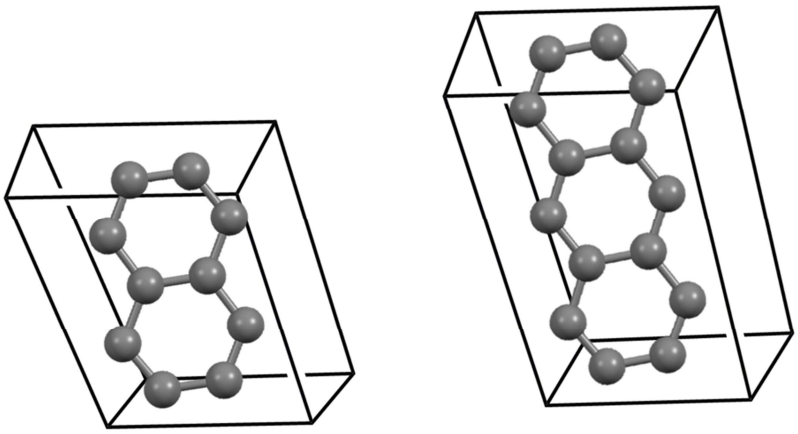

Figure 2.1: Illustration of the unit cells of naphthalene and anthracene respectively as studied by Bragg in 1921.[2]

His research was continued by other crystallographers such as J. D. Bernal in his work to accurately predict formulas of steroids by relating unit cell parameters to different aromatic hydrocarbon structures.[3] It also led to the pioneering work of Dorothy Hodgkin, Max Perutz,

[1] Pignataro, B., *Ideas in Chemistry and Molecular Sciences: Advances in Nanotechnology, Materials and Devices*, Wiley-VCH, Weinheim, Germany, **2010**, 210.
[2] Bragg, W. H., *Proc. Phys. Soc. London.*, **1921**, *34*, 33-50.
[3] Bernal, J. D., Crowfoot, D., *J. Chem. Soc.*, **1935**, 93-100.

James D. Watson and Francis Crick along with many other scientists in the important discoveries of the structures of insulin, haemoglobin and DNA.[4,5,6]

Their work showed that by combining the knowledge of chemistry and crystallography the structure of molecules can be studied to give insight into the relationship of a crystal structure and its properties. These studies can effectively assist scientists with a means by which to design new functional materials.

2.3 The Birth of Crystal Engineering

In 1955, the first use of the term *crystal engineering* appeared.[7] The term was used to describe how new functional materials with desirable properties could be synthesized based on the relationship between the reactivity of compounds and their crystal structures.[8] Today, crystal engineering is recognized as the understanding of intermolecular interactions in the context of crystal packing and how these interactions can be used in the design of new compounds with desired physical and chemical properties.[9]

Intermolecular interactions are often described as the "glue" keeping molecules together in a crystal structure in specific patterns that are often found to repeat within other crystal systems.[7] For instance, the tendency of chlorine atoms to interact with other atoms from group VII, in what are termed halogen interactions, results in molecules containing a chlorine atom to often exhibit halogen interactions in different crystal structures.[10]

Crystal engineering has used this tendency of molecules to form specific interactions to assist in the design of pre-determined patterns in which the assembly of molecules in a crystal lattice may be controlled.[7] Many types of interactions are utilized in this way with hydrogen bonds, C-H$\cdots\pi$ interactions, van der Waals interactions, dipole-dipole interactions and halogen bonding being some of the most prominent known forces.[11]

Of particular focus in this study is the consideration of metallophilic interactions in the design of new molecular systems. These interactions have been found to manifest between metal

[4] Ferry, G., *Dorothy Hodgkin a life*, Bloomsbury Publishing, London, United Kingdom, **1998**.
[5] Ferry, G., *Max Perutz and the Secret of Life*, Random House, London, United Kingdom, **2010**.
[6] Marx, C., *Watson and Crick and DNA*, The Rosen Publishing Group, New York, United States of America, **2005**.
[7] Desiraju, G. R., Vittal, J. J., Ramanan, A., *Crystal Engineering a Textbook*, World Scientific Publishing, London, United Kingdom, **2011**.
[8] Tiekink, E. R. T., Vittal, J. J., *Frontiers in Crystal Engineering*, John Wiley & Sons, West Sussex, United Kingdom, **2006**, 1.
[9] Nastase, S., Tuna, F., Maxim, C., Muryn, C. A., Avarvari, N., Winpenny, R. E. P., Andruh, M., *Cryst. Growth Des.*, **2007**, *7*, 1825-1831.
[10] Desiraju, G. R., *J. Am. Chem. Soc.*, **2013**, *135*, 9952-9967.
[11] Braga, D., Grepioni, F., *Acc. Chem. Res.*, **2000**, *33*, 601-608.

centres of neighbouring molecules rendering an increased dimensionality to the crystal structure.[12] The potential exists to exploit these metallophilic interactions in the design of nano-scaled materials to be used in various new technologies (see Chapter 1) with some of the current applications to be highlighted in the coming sections.

2.4 Metallophilic Interactions

2.4.1 A New Kind of Bonding

The concept of bonding in chemistry is normally associated with the most common examples of covalent, ionic and metallic bonding.[13] The theory of bonding can however be complemented by the important role of intermolecular interactions between molecules such as hydrogen and halogen bonding.[14] Of particular importance in this study is the role of metallophilic interactions in crystal systems. As the name fittingly suggests, this type of interaction refers to an affinity that exists between metal centres.[15]

Metallophilicity is typically regarded as an interaction between closed-shell or pseudo closed-shell metal centres that are spaced together closer than the sum of their van der Waals radii.[16] This definition agrees with the traditional classification of a bond as being closer than the van der Waals radii between two atoms.[17] Metal ions with a d^{10}, d^{8} or s^{2} electron configuration have been found to participate in metallophilic interactions.[18] They are generally understood as a type of weak dispersive interaction between relatively larger reduced metal centres.[19] However, the energy associated with these interactions are not regarded as trivial and are in the same order as hydrogen bonding, with Au(I)···Au(I) interactions typically displaying energies of 7-11 kcal/mol.[20]

The known metals for which metallophilic interactions have been observed are summarized in Figure 2.2[21] with the d^{10} electron configuration for metal centres such as in Au(I)

[12] Abd-El-Aziz, Carraher, C. E., Pittman, C. U., Zeldin, M., *Macromolecules Containing Metal and Metal-Like Elements*, John Wiley & Sons, New Jersey, United States of America, **2005**, 170.
[13] Spencer. J. N., Bodner, G. M., Rickard, L. H., *Chemistry: Structure and Dynamics*, John Wiley & Sons, New Jersey, United States of America, **2012**, 196.
[14] Kaplan, I. G., *Intermolecular Interactions: Physical Picture, Computational Methods and Model Potentials*, John Wiley & Sons, West Sussex, United Kingdom, **2006**, 164.
[15] Kumar, M., Dalela, S., Dinesh, *Int. J. Sci. Res. Publ.*, **2013**, *3*, 1-7.
[16] Pyykkö, P., *Chem. Rev.*, **1997**, *97*, 597-636.
[17] Smart, L., Gagan, M., *The Molecular World, The Third Dimension*, The Open University, Glasgow, United Kingdom, **2002**, 92.
[18] Hunks, W. J., Jennings, M. C., Puddephatt, R. J., *Inorg. Chem.*, **2002**, *41*, 4590-4598.
[19] Pyykkö, P., *Angew. Chem. Int. Ed.*, **2002**, *41*, 3573-3578.
[20] Pathaneni, S. S., Desiraju, G. R., *J. Chem. Soc., Dalton Trans.*, **1993**, 319-322.
[21] Doerrer, L. H., *Dalton Trans.*, **2010**, *39*, 3543-3553.

complexes displaying the most reported cases of metallophilic interactions.[22] In fact, Au(I)···Au(I) interactions are considered the strongest metallophilic interaction due to Au being the most electronegative metal in the periodic table owing to relativistic effects.[23] Relativistic effects are responsible for the expansion of the valence orbitals of the late transition metals. The larger orbitals allow for greater overlap between neighbouring metal centres and in turn result in stronger interactions.[24] Typical lengths for Au···Au interactions have been reported in the range of 2.9 to 3.4 Å which are longer than some hydrogen bonds reported in the 2.2 to 3.2 Å range.[25,26,27]

					B	C	N
					Al	Si	P
Fe	Co	Ni	Cu	Zn	Ga	Ge	As
Ru	Rh	Pd	Ag	Cd	In	Sn	Sb
Os	Ir	Pt	Au	Hg	Tl	Pb	Bi

Figure 2.2: Metals known to display metallophilic interactions (indicated in red) with transition elements highlighted in green and main group elements in blue.[21]

Metallophilic interactions are also mainly associated with metals that exhibit low coordination numbers which are commonly encountered in the heavy transition metals.[28] This preference again arises from relativistic effects which are found to increase past the lanthanide elements.[29] As a result of this, metallophilicity has been closely associated with the heaviest transition metals which are profoundly affected by relativistic effects such as Pt, Au and Hg. They are followed by heavy main group elements such as Tl, Pb, and Bi with fewer examples existing in Ag and Rh complexes.[21]

2.4.2 Definition of a Bond using Van der Waals Radii Criteria

Metallophilic interactions are not only limited to same metal systems (see Section 2.4.1) but have also been recognized in mixed metal systems. By using the same criteria of van der

[22] Scherbaum, F., Grohmann, A., Huber, B., Kruger, C., Schmidbaur, H., *Angew. Chem., Int. Ed. Engl.*, **1988**, *27*, 1544-1546.
[23] Pyykkö, P., *Angew. Chem. Int. Ed.,* **2004**, *43*, 4412-4456.
[24] Schmidbaur, H., Schier, A., *Chem. Soc. Rev.*, **2012**, *41*, 370-412.
[25] Jones, P. G., Ahrens, B., *Z. Naturforsch., B: Chem. Sci.*, **1998**, *53*, 653-662.
[26] Ahrland, S., Noren, B., Oskarsson, A., *Inorg. Chem.,* **1985**, *24*, 1330-1333.
[27] Grabowski, S. J., *Hydrogen Bonding- New Insights*, Springer, Dordrecht, The Netherlands, **2006**, 3.
[28] Biffis, A., Baron, M., Tubaro, C., *Advances in Organometallic Chemistry*, Academic Press, Waltham, United States of America, **2015**, 258.
[29] Misra, P., *Applied Spectroscopy and the Science of Nanomaterials*, Springer Science + Business Media, Singapore, **2015**, 157.

Waals radii applied to mixed metal systems, the minimum distance for mixed-metal interactions can be calculated. Table 2.1 as adapted from Doerrer[21] outlines the sum of the van der Waals radii as available from literature for the pairing of different metals.

Table 2.1: Sums of van der Waals radii[30] of selected metals that display metallophilic interactions.[21]

		Pd 1.63	Pt 1.72	Cu 1.4	Ag 1.72	Au 1.66	Hg 1.55	Tl 1.96	Pb 2.02
Pd	**1.63**	3.26	3.35	3.03	3.35	3.29	3.18	3.59	3.65
Pt	**1.72**		3.44	3.12	3.44	3.38	3.27	3.68	3.74
Cu	**1.4**			2.8	3.12	3.06	2.95	3.36	3.42
Ag	**1.72**				3.44	3.38	3.27	3.68	3.74
Au	**1.66**					3.32	3.21	3.62	3.68
Hg	**1.55**						3.1	3.51	3.57
Tl	**1.96**							3.92	3.98
Pb	**2.02**								4.04

2.4.3 General Quantum Mechanics Related to Metallophilic Interactions

As mentioned in Section 2.4.1, metallophilic interactions are encountered between metal centres with closed-shell or pseudo closed-shell electron configurations most notably the d^{10} and d^8 electronic configurations. Figure 2.3 can be used to illustrate how metallophilic interactions are facilitated without the expected repulsion that generally occurs between positively charged metal centres. In Figure 2.3 orbital diagrams are given for typical d^{10}-d^{10} and d^8-d^8 interactions where the d_{x2-y2} orbital is used as the valence orbital for a d^{10} electron configuration and the dz^2 orbital as valence orbital for a d^8 configuration.[21]

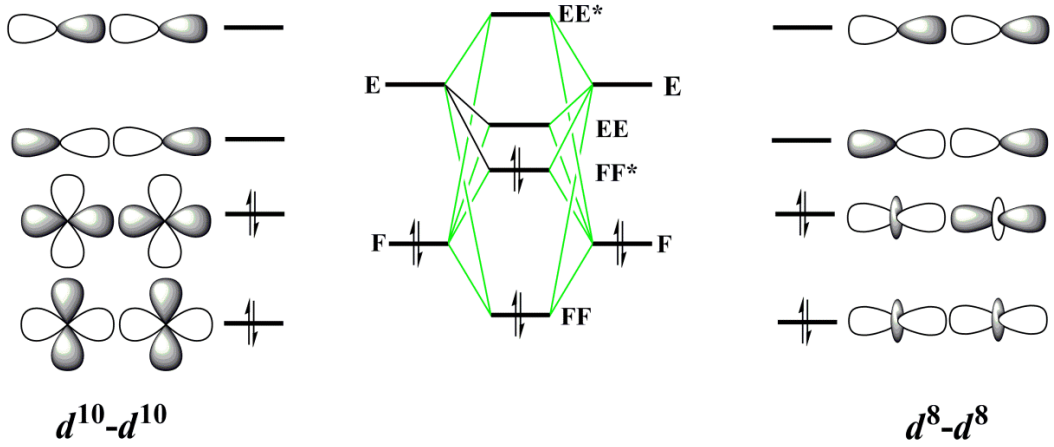

Figure 2.3: Orbital diagrams to illustrate the overlap of orbitals for d^{10}-d^{10} and d^8-d^8 metal ions (F= indicates filled orbitals, E= Empty orbitals, FF= Filled bonding orbitals, EE= Empty bonding orbitals, FF*= Filled antibonding orbitals, EE*= Empty antibonding orbitals).[21]

For the successful overlap of orbitals to take place, a filled orbital (F) must overlap with an identical (F) orbital of a neighbouring molecule. This overlap results in filled bonding orbitals (FF) lower in energy than the (F) orbitals as well as antibonding orbitals (FF*). The empty

[30] Bondi, A., *J. Phys. Chem.*, **1964**, *68*, 441-451.

valence orbitals (E) then become sufficiently low in energy to allow for mixing with the filled orbitals (F) leading to the formation of empty bonding (EE) and antibonding (EE*) orbitals.[21]

The mixing of the filled and unfilled orbitals create the necessary stabilization of the (FF) and (FF*) orbitals which results in a lowering of energy between the metallophilic pair of metal ions in comparison to the separate individual metal ions. This becomes the basis in establishing a metallophilic interaction between a pair of metal centres.[21]

In the case of rhodium the orbitals involved in the establishment of Rh···Rh interactions are the filled $4dz^2$ orbitals that represent the (F) orbitals. The unoccupied $5p_z$ orbitals on adjacent metal centres represent the designated (E) orbitals in the formation of the metallophilic interactions as outlined above.[31]

2.4.4 Other Requirements for Metallophilic Interactions

In addition to the above mentioned electronic requirements in the establishment of metallophilic interactions a steric aspect is also of concern. The geometry of individual molecules must be such that they allow for the effective overlap of the orbitals necessary for the highly spatially orientated metallophilic interactions to exist. Geometries that allow for effective overlap of orbitals between metal centres are presented in Figure 2.4.[21]

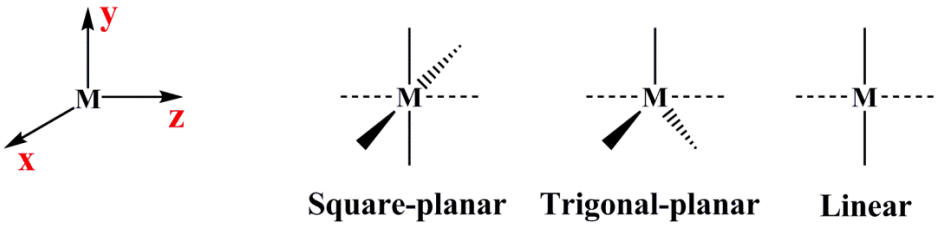

Figure 2.4: Geometries typically associated with metal ions that participate in metallophilic interactions.[21]

Except for the spatial restriction in geometry of the metal complexes, a minimum steric hindrance of the coordinated ligands to the metal ions must also be adhered to for effective stacking of metal centres along the one-directional chain. In this regard, ligands that enforce a highly anisotropic environment are favoured with a presence that is limited to the *xy*-plane.[21]

The importance of steric effects induced by the coordinating ligands is further emphasised by the tendency of molecules to avoid an arrangement of ligands directly atop of one

[31] Gliemann, G., Yersin, H., *Struct. Bonding*, **1985**, *62*, 87-153.

another. An orientation of 180° is sterically favoured between ligands of neighbouring molecules along the metallic chain.[32]

Additionally, the coordinating strength of ligands can have a significant effect on the metal centres' ability to facilitate interactions between the metal ions. Strongly coordinating ligands can destabilize orbital overlap between metal centres thus preventing metallophilic interactions from occurring. The π-donor/ acceptor property of ligands has also been shown to influence metallophilic interactions. The introduction of a π-acceptor coordinating ligand will decrease electron density at the metal centre and result in less repulsion between the metal centres of neighbouring molecules. This in turn, will enable more effective orbital overlap between the metal centres and ultimately result in stronger and shorter interactions.[32,33,34,35]

Metallophilic interactions are not simply limited to two molecules but are potentially extended along an infinite chain of metal centres in which molecules are arranged in a 1-dimensional pattern (see Section 2.3). The most common arrangements of metal centres in these 1-D chains have been found to be linear, zigzag or helical as depicted in Figure 2.5 (a). The arrangement of the individual molecules along the one-dimensional chain also displays specific conformations with regards to the ligand orientation. Staggered (crossed) or eclipsed (parallel) arrangements are the most often encountered arrangements (Figure 2.5 (b)). However, this does not exclude the possibility of other arrangements of molecules brought about due to specific constraints imposed by the coordinating ligands.[36]

Molecules that possess the potential to form metallophilic interactions will remain in monomeric form only when the steric bulk of the coordinating ligands prevent close metal···metal interactions. Additionally, if other interactions of competing strength such as hydrogen bonding are preferred for the stability of the crystal lattice metallophilic interactions might not occur.[37]

For very bulky ligands, the resulting arrangement of monomers or staggered dimers will most probably form *via* metallophilic interactions whilst medium sized ligands will result in the formation of trimers or other oligomers. In all other cases, the metallophilic interactions will result in the construction of a one-dimensional chain connecting an infinite number of molecules.[37]

[32] Connick, W. B., Marsh, R. E., Schaefer, W. P., Gray, H. B., *Inorg. Chem.*, **1997**, *36*, 913-922.
[33] Mégnamisi-Bélombé, M., *J. Solid Chem.*, **1979**, *27*, 389-396.
[34] Ferraris, G., Viterbo, D., *Acta Cryst.*, **1969**, *B25*, 2066-2070.
[35] Krogmann, K., Stephan, D., *Z. Anorg. Allg. Chem.*, **1968**, *362*, 290-300.
[36] Schmidbaur, H., Schier, A., *Chem. Soc. Rev.*, **2008**, *37*, 1931-1951.
[37] Pathaneni, S. S., Desiraju, G. R., *J. Chem. Soc., Dalton Trans.*, **1993**, 319-322.

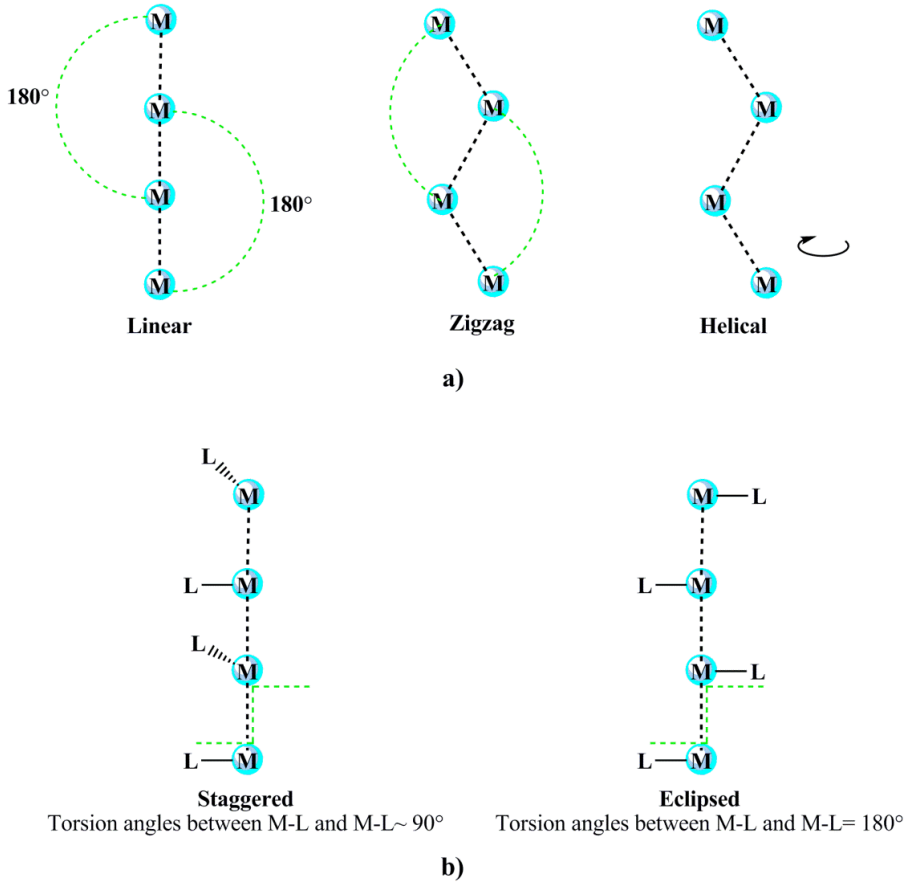

Figure 2.5: a) Different possible spatial arrangements of metal centres along 1-D metal chains; b) Arrangements adopted by molecules with regards to ligand orientation along the infinite 1-D metal chain.

2.4.5 Metallophilic Interactions in PGM's and Influences

As Platinum Group Metals (PGM's) are of significant interest due to their wide application from catalysis[38] to medicine[39] special attention will now be given to some interesting examples involving metallophilic interactions amongst these metals.

One of the most well-known examples of metallophilic interactions involving the metal rhodium is in the $[Rh(acac)(CO)_2]$ complex which was first synthesized by Bailley *et al.*[40] in 1967. This complex has been shown to intrinsically behave as a semiconductor with the conductive properties directly credited to the metallophilic interactions between rhodium(I) centres of the stacked square planar molecules.[41] $[Rh(acac)(CO)_2]$ is also well-known for its red colour with a green metallic lustre which has also been attributed to the metallophilic interactions.[41] In contrast, the iridium counterpart to this complex, $[Ir(acac)(CO)_2]$, displays a

[38] Acres, G. J. K., Swars, K., *Platinum, Supplement A: Technology of the Platinum Group Metals*, Springer-Verlag, Berlin, Germany, **1982**, 99.
[39] Baltzer, N., Copponnex,T., *Precious Metals for Biomedical Applications*, Woodhead Publishing, Cambridge, United Kingdom, **2014**, 6.
[40] Bailley, N. A., Coates, E., Robertson, G. B., Bonati, F., Ugo, R., *J. Chem. Soc., Chem. Commun.*, **1967**, 1041.
[41] Underhill, A. E., Macchi, P., *Struct. Bonding*, **2012**, *146*, 127-158.

deep blue colour with gold metallic lustre due to the presence of Ir···Ir interactions within its structure.[41]

With the discovery that many other square planar rhodium and iridium complexes display these interactions, research was instigated in the design of similar systems. These complexes were considered viable in the formation of functional nano-materials due to their conductive properties. The synthesis of the new systems was mainly focused on finding ligands that could facilitate and assist in the formation of these interactions.[41]

Ligands such as oxalates were investigated by Real *et al.*[42] and showed a similar trend in stacking of the rhodium dicarbonyl molecules as observed for [Rh(acac)$(CO)_2$]. Almost linear chains of 175° were reported along the rhodium metal centres in the 1-D chain with Rh···Rh distances of 3.243 Å. In [Rh(acac)$(CO)_2$], distances between rhodium(I) centres were found in the same range with alternating distances of 3.253 Å and 3.271 Å.[43] The coordinating oxalate ligands were found to be stacked in an eclipsed arrangement (see Figure 2.5 (b)) with angles of 180° between coordinated ligands of adjacent molecules along the one-dimensional metal chain. A similar arrangement was observed for the [Rh(acac)$(CO)_2$] complex. The colour of these crystals were reported as dark-olive green hued in comparison to the red-green crystals of [Rh(acac)$(CO)_2$].[42]

A study by Laurila *et al.*[44] involving a dinuclear rhodium complex with 2,2'-biimidazole carbonyl ligands highlighted that changes along the 1-D metallic chain could result in changes of the physical properties exhibited by the material such as colour. A temperature study was undertaken to assess the effect of temperature on the intra- as well as intermolecular Rh···Rh distances. The bidentate ligands that were utilized for their study are illustrated in Scheme 2.1 with Table 2.2 highlighting the changes that were observed in the intra- as well as intermolecular Rh···Rh distances upon changes in temperature.

[42] Real, J., Bayón, J. C., Lahoz, F. J., López, J. A., *J. Chem. Soc., Chem. Commun.*, **1989**, 1889-1890.
[43] Huq, F., Skapski, A., *J. Cryst. Mol. Struct.*, **1974**, *4*, 411-418.
[44] Laurila, E., Tatikonda, R., Oresmaa, L., Hirva, P., Haukka, M., *Cryst. Eng. Comm.*, **2012**, *14*, 8401-8408.

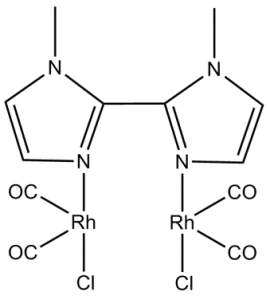

Structure 1

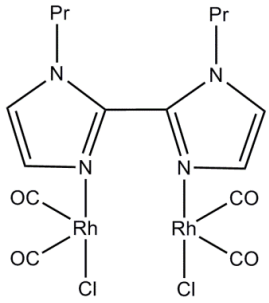

Structure 2

Scheme 2.1: Illustration of the 2,2'-biimidazole ligands coordinated in the dinuclear rhodium complexes in the study of Laurila *et al.*[44]

Table 2.2: Rh···Rh distances and angles between rhodium centres at different temperatures in the study by Laurila *et al.*[44]

Structure	Intermolecular Rh···Rh distance (Å)	Intramolecular Rh···Rh distance (Å)	Angle of Rh···Rh···Rh (°)
1 (100 K)	3.1781(5)	3.4345(6)	174.184(5)
1 (260 K)	3.2095(5)	3.4990(5)	173.909(9)
2 (88 K)	3.1426(5)	3.4255(5)	177.352(17)
2 (100 K)	3.1469(3)	3.4403(3)	179.453(16)
2 (260 K)	3.1737(5)	3.4944(6)	178.888(10)

Relatively small changes were noted for the Rh···Rh distances with a difference of 0.0268 Å reported for the intermolecular Rh···Rh distance of structure **2** upon cooling the crystal from 260 K to 100 K. Changes in the physical properties of the crystals were however very pronounced with the crystals of structure **2** coloured deep purple at 260 K and upon cooling to 100 K the colour became entirely green. This colour change was directly attributed to the changes in the Rh···Rh distances.[44] Their study illustrated how a change in properties of the bulk material can be induced when subtle changes are made to the metal···metal distances.

Metallophilic interactions have also been found between cationic and anionic rhodium complexes with the first rhodium double-salt reported by Laurila *et al.*[45] in 2012. The $[Rh(L)(CO)_2][RhCl_2(CO)_2]$ (L= 2,2'-bipyridine and 1,10-phenanthroline) complexes displayed Rh···Rh interactions with the coordinated 2,2'-bipyridine complex displaying Rh···Rh distances of 3.3174(5) and 3.4116(5) Å along the *c*-axis of the unit cell. The crystals of these compounds were observed to be red in colour with a metallic lustre.[45]

Interestingly, the complex containing the 1,10-phenanthroline ligand was found to consist of two independent metal chains within the crystal lattice. Rh···Rh distances of 3.3155(3) Å and

[45] Laurila, E., Oresmaa, L., Hassinen, J., Hirva, P., Haukka, M., *Dalton Trans.*, **2013**, *42*, 395-398.

3.2734(3) Å for one chain and 3.3211(3) Å and 3.3498(3) Å reported in the second chain. Their study showed that Rh···Rh distances could be altered by changing the coordinating ligand from 2,2'-bipyridine to 1,10-phenanthroline.[45]

The chain containing the 2,2-bipyridine ligand was noted to display a near linear arrangement of metal centres with Rh-Rh-Rh angles of 170.98(1)°. In the double-salt containing 1,10-phenanthroline one chain displayed a linear arrangement of molecules with angles between rhodium centres of 170.28(1)° whilst the second chain displayed a zig-zagged arrangement with angles of 159.57 (1)° (see Figure 2.5(a)).[45]

From charge density studies on these two complexes it was found that the nature of the Rh···Rh interactions can be described as weakly covalent and as such a small amount of electron sharing takes place between the metal centres.[45] The electron sharing capability of these one-dimensional metal chains can be important for future manipulation of these systems into conductive materials to be used as "nano-wires".

One of the oldest examples of a metal complex exhibiting metallophilic interactions is a platinum based compound that was subsequently named after its creator. Magnus' green salt $[Pt(NH_3)_4][PtCl_4]$ is a double-salt system that is highly insoluble and was first described by Magnus[46] in 1828. It was characterized as a polymeric chain in 1957 with the green colour of the salt attributed to the Pt···Pt interactions found within the system.[47] A derivative known as Magnus' pink salt with the same molecular formula was later synthesized to have longer Pt···Pt distances. In contrast to the green colour of the original salt, the new complex exhibited a pink colour due to the longer Pt···Pt interactions.[48] The colour dependency of the compound based on altered Pt···Pt interactions once again highlights the pronounced effect that changes in the one-dimensional chain can have on the physical properties exhibited by the material.[45]

2.5 One-Dimensional Metallic Chains

Metallophilic interactions have been shown in the previous sections to lead towards the self-assembly of nano-structures and supramolecular polymeric materials usually along one direction within the crystal lattice.[49] This has led to research into the applicability of metallophilic interactions in developing conductive materials. The assembly of these so-

[46] Magnus, G., *Pogg. Ann.*, **1828**, *11*, 242.
[47] Atoji, M., Richardson, J. W., Rundle, R. E., *J. Am. Chem. Soc.*, **1957**, *79*, 3017-3020.
[48] Lucier, B. E. G., Johnston,K. E., Xu, W., Hanson, J. C., Senanayake, S. D., Yao, S., Bourassa, M. W., Srebro, M., Autschbach, J., Schurko, R. W., *J. Am. Chem. Soc.*, **2014**, *136*, 1333-1351.
[49] Enomoto, M., Kishimura, A., Aida, T., *J. Am. Chem. Soc.*, **2001**, *123*, 5608-5609.

called one-dimensional metallic chains are highly sought after as they exhibit unique magnetic[50], photophysical[51], conductive[52] and catalytic properties[53]. An electrical nano-wire able to conduct electricity would typically consist of metal atoms that allow for electrical flow along one direction and coordinating ligands around the metal centre that act as an insulating coat.[54]

By definition a one-dimensional (1-D) metallic chain could act as a "nano-wire" since it exhibits metal-like properties (conductive) along one direction of a crystal and non-metallic properties (insulating) orthogonal to this direction.[55] This allows for effective electrical flow only in one direction of the material. Rigid requirements for such a chain exist in terms of electronic and steric properties to allow for effective electrical conduction. The physical and chemical properties of these one-dimensional chains are highly dependent on the chemical nature of the molecules with subtle changes in chemical composition able to alter the physical properties in a noticeable manner.[55]

However, if the necessary requirements are met in the construction of a one-dimensional metallic chain, electron transport along the chain can be facilitated in the preferred orientation of the stacking effect. This can be achieved either by the presence of partially occupied orbitals on the metal centres or a reduction in Coulombic interactions.[55] One problem in the formation of 1-D metallic chains specifically utilizing d^8 metal centres is that an even number of electrons is found within the valence orbitals resulting in no partially occupied orbitals that can be used for electrical flow.[55]

A partially occupied state of orbitals can however be achieved in a d^8 system if one of the following states can be brought into effect[55]:

i) Overlap between the highest occupied (HOMO) and the lowest unoccupied (LUMO) orbitals take place.
ii) Electrons can be removed from the top part of the highest occupied (HOMO) orbital eg. *via* partial oxidation of the metal ion.

One example of where the partial oxidation state was successfully applied to form a conducting 1-D metallic chain was in a range of tetracyanoplatinate(II) complexes. These

[50] Rohmer, M. M., Liu, P. C., Lin, J. C., Chiu, M. J., Lee, C. H., Lee, G. H., Bénard, M., López, X., Peng, S. M., *Angew. Chem. Int. Ed.*, **2007**, *46*, 3533-3536.
[51] Yam, V. W. W., Wong, K. M. C., Zhu, N., *J. Am. Chem. Soc.*, **2002**, *124*, 6506-6507.
[52] Lu, W., Roy, V. A. L., Che, C. M., *Chem. Commun.*, **2006**, 3972-3974.
[53] Kontkanen, M. L., Oresmaa, L., Moreno, M. A., Jänis, J., Laurila, E., Haukka, M., *Appl. Catal., A.*, **2009**, *365*, 130-134.
[54] Bera, J. K., Dunbar, K. R., *Angew. Chem., Int. Ed.*, **2002**, *41*, 4453-4457.
[55] Underhill, A. E., Watkins, D. M., *Chem. Soc. Rev.*, **1980**, *9*, 429-448.

complexes displayed Pt···Pt distances of ~3.09 Å and after oxidation a specific conductivity of ~10^{-4} $\Omega^{-1}cm^{-1}$ was obtained for the material.[56]

To better illustrate how partially oxidized compounds are formed within a one-dimensional chain a comparison can be made to the well-known Jahn-Teller effect. The Jahn-Teller theory[57] states that any non-linear molecular system that exists in a degenerate electronic state will be unstable. A distortion will occur that will allow for a lowering in symmetry that will split the degenerate states resulting in a more stable structure. R. E. Peierls[58] predicted in 1955 that a similar situation will exist for partially occupied orbitals. If an electron is removed from the top part of a chain, the chain will become unstable and will undergo a distortion of the lattice along the metal-chain direction to counter-act this change. The distortion will lead to the existence of occupied and unoccupied orbitals of lower energy and higher energy respectively with a total reduction in the energy of the system. This distortion will render a partially oxidized character to the 1-D metallic chain that allows for effective electrical flow.

Along with systems containing a singular type of metal, mixed metal systems that contain metallophilic interactions have also shown great promise in producing conductive materials as 1-D metallic chains. One such example is of a Pt and Au system in $[Pt(tpy)X][Au(C_6F_5)_2]$ where tpy = 2,2':6',2"-terpyridine and X = halogen. This double salt displays a unique d^{10}-d^8 paring for the Pt(II)···Au(I) interactions that has shown great promise for future electrical applications.[59,60]

2.6 Current Applications of Metallophilic Interactions

As mentioned before metallophilic interactions can be used as driving forces for the self-assembly of nano-structures and supramolecular polymeric materials.[61] Many materials containing metallophilic interactions have been found to display unique spectroscopic[62], photochemical and electrical conductive[63] properties. A few examples of materials displaying some of these unique properties and their applications will now be highlighted.

[56] O'Neill, J. H., Underhill, A. E., Toombs, G. A., *Solid State Commun.*, **1979**, *29*, 557-560.
[57] Burdett, J. K., *Chemical Bonds, A Dialog*, Wiley & Sons, New York, United States of America, **1997**, 129.
[58] Peierls, R. E., *Quantum Theory of Solids*, Oxford University Press, London, United Kingdom, **1955**, 108.
[59] Angle, C. S., Woolard, K. J., Kahn, M. I., Golen, J. A., Rheingold, A. L., Doerrer, L. H., *Acta Cryst*., **2007**, *C63*, m231-m234.
[60] Hayoun, R., Zhong, D. K., Rheingold, A. L., Doerrer, L. H., *Inorg. Chem.*, **2006**, *45*, 6120-6122.
[61] Lu, W., Chan, K. T., Wu, S. X., Chen, Y., Che, C. M., *Chem. Sci.*, **2012**, *3*, 752-755.
[62] Houlding, V. H., Miskowski, V. M., *Coord. Chem. Rev.*, **1991**, *111*, 145-152.
[63] Williams, J. M., *Adv. Inorg. Chem.*, **1983**, *26*, 235-268.

2.6.1 Use of Gold Materials for Photoluminescence

The development of "tunable" optically active materials is a dynamic field of research with such materials finding application in the design of solid-state sensors, electronic switches and laser-based devices.[49]

Materials containing Au(I)···Au(I) interactions are of particular interest in this field as their emission profiles have been found to be highly dependent on different Au···Au distances within the materials.[64] For instance, Au(I) thiolate complexes display photoluminescence at 478 nm which have been attributed to the Au···Au distances of 3.1621(5) Å in the complex. If a different thiolate ligand that induces longer Au···Au distances (3.217(2) Å) is used in the same complex, the emission is moved to a shorter wavelength of 457 nm. These complexes have already been used in the self-assembly of monolayers on silicon at nano-scale to produce thin films in electronic devices.[65]

2.6.2 Silver Luminescence

Very few studies have reported on Ag(I) complexes exhibiting luminescence with the first example only reported by Vogler and Kunkely[66] in 1989. Luminescent complexes of Ag have mainly been restricted to the Ag analogues of the $[CuX_4L_4]$ (X= halogen, L= amine or phosphine) complexes.

However, temperature dependent photoluminescence was observed for a novel $Tl[Ag(CN)_2]$ complex.[67] This complex contains Tl···Ag and Ag···Ag interactions with DFT studies revealing the Ag···Ag interactions to be responsible for the photoluminescent properties of the complex. This is in direct contrast to a similar complex containing Au, $Tl[Au(CN)_2]$, in which Tl···Au and Au···Au interactions were responsible for the reported photoluminescent properties of that complex.[68]

At 10 K it was observed that a broad emission occurred at 420 nm for $Tl[Ag(CN)_2]$ and two excitation maxima were noted at 301 and 314 nm. Excitation at each of these maxima was found to be temperature dependent. The two excitation maxima could directly be correlated to the two different Ag environments observed in the crystal structure of the complex in the Tl···Ag and Ag···Ag interactions.[67]

[64] Katz, M. J., Sakai, K., Leznoff, D. B., *Chem. Soc. Rev.*, **2008**, *37*, 1884-1895.
[65] Wishart, J. F., Rao, B. S. M., *Recent Trends in Radiation Chemistry*, World Scientific Publishing, New Jersey, United States of America, **2010**, 375.
[66] Vogler, A., Kunkely, H., *Chem. Phys. Lett.*, **1989**, *158*, 74-76.
[67] Omary, M. A., Pattersn, H. H., *Inorg. Chem.*, **1998**, *37*, 1060-1066.
[68] Assefa, Z., DeStefano, F., Garepapaghi, M. A., LaCasce, J. H., Ouelette, S., Corson, M. R., Nagle, J. K., Patterson, H. H., *Inorg. Chem.*, **1991**, *30*, 2868-2876.

The emission of the $Tl[Ag(CN)_2]$ complex undergoes a red-shift as the temperature is decreased and the emission peak found to shift from 403 nm at 195 K to 420 nm at 10 K. This implies an average shift of 5 cm^{-1}/K. The temperature dependent luminescent properties of this compound were finally attributed to the formation of a Ag-Ag bonded exciplex as a result of the excitation that takes place along the length of the Ag···Ag interactions. An exciplex is defined as a complex that forms through electronic excitation with a different structure at ground state. This Ag(I) complex was the first example of a solid-state metal-metal bound exciplex reported for any coordination compound.[67]

2.6.3 Formation of Luminescent Dendritic Macromolecules *via* Metallophilic Interactions

Dendrimers have also been shown to display metallophilic interactions upon coordination to metal centres. A group of metallacycles with an achiral Dendron, L2PZ (see scheme 2.2), has resulted in the self-assembly of luminescent superhelical fibers *via* metallophilic interactions.[49] Upon coordination to three metal centres the dendrimers form a stacked structure resembling long tubes called fibrels that connect to form nano-fibers. This was observed for complexes containing Cu(I), Ag(I) and Au(I) metal centres. The fibers fabricated from $[Au(L2PZ)]_3$ display strong birefringence indicating the crystallinity of the nano-structure.[49]

Upon excitation at 280 nm the fibers were found to strongly emit an orange luminescence centred at 605 nm with the excitation attributed to the energy transfer from the dentric ligand to the metal centres. This illustrates the use of metallophilicity to also drive the self-assembly of dentric materials that could result in the design and manipulation of functional mesoscopic materials.[49]

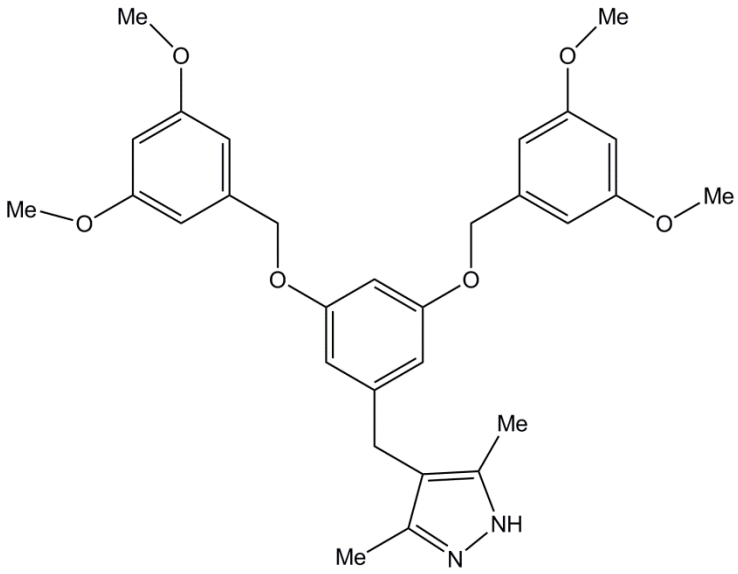

L2PZ

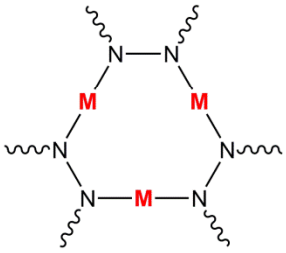

Coordination of Metallacycle

Scheme 2.2: The L2PZ structure and the coordination of metallocycles involving three metal centres.

2.6.4 Reversible Luminescence with Ag-Au Complexes

A gold-silver complex with perhalogenated ligands (see scheme 2.3) has been shown to display reversible mechanochemical switching luminescence.[69] The monomer complex $[Au_2Ag_2(R2)_4(tfa)_2]^{2-}$ (tfa= trifluoroacetate) is strongly green emitting (λ= 540 nm) and by induced polymerization *via* metallophilic interactions a red emitting (λ= 660 nm) material $[Au_2Ag_2(R2)_4(MeCN)_2]_n$ was obtained.[69]

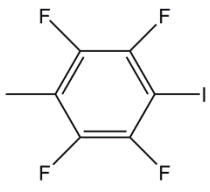

R1

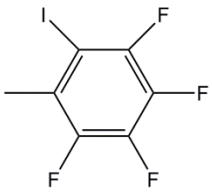

R2

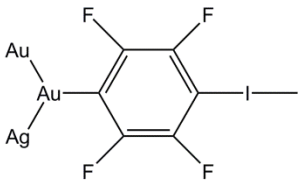

Complex 1

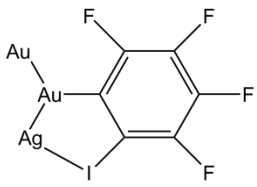

Complex 2

Scheme 2.3: Structures of the perhalogenated ligands employed in coordination to Au for the engineering of luminescent materials.

The addition of solvent (MeCN) to the monomeric species resulted in the luminescence changing first from green to yellow and finally to red. The yellow species that formed was suspected of being a dimeric structure which then upon further self-assembly of molecules led to the formation of the polymeric structure which is red emitting. This process is completely reversible with the red product left at ambient conditions returning to the green emitting structure after several hours.[69]

[69] Lasanta, T., Olmos, M. E., Laguna, A., López-de-Luzuriaga, J. M., Naumov, P., *J. Am. Chem. Soc.*, **2011**, *133*, 16358-16361.

The rate of the reverse reaction was shown to also be dependent on other physical factors with grinding of the sample resulting in the reversal of the luminescence shortened to within minutes. The vastly "tunable" aspects of this complex allows for controlled luminescence that could lead to the development of multicolour sensors in the future.[69]

2.7 Platinum Group Metal Applications: Focus on Rhodium

The fact that PGM's and other late transition metals act as catalysts is related to the electron rich metal centres with lower coordination numbers that allow substrate molecules to interact at the metal centre.[70] This is typically also important for metallophilic interactions. To illustrate the versatility of the PGM's in chemistry, many examples are known however, this study has identified rhodium as a central focus. Thus, a broad discussion of some applications of rhodium in catalysis is included which might relate empirically also to the metallophilic interactions and characteristics thereof.

2.7.1 Discovery and General Uses of Rhodium

Rhodium along with iridium was discovered in 1803 in a similar manner to their preceding neighbours in the periodic table, osmium and ruthenium. Dissolution of a black residue originating from crude platinum in aqua regia led to the isolation of rhodium.[71] W. H. Wollaston named the new transition metal after the Greek word for "rose" due to the rose-coloured solutions of the metal's various salts.[72] Rhodium forms part of the Platinum Group Metals (PGM's) and displays unique characteristics that allow it to actively take part in many important catalytic processes.[73]

2.7.2 Rhodium as Homogeneous Catalyst

Catalysis is typically divided into homogeneous and heterogeneous catalysis. Scheme 2.4 illustrates the basic chemical building blocks obtained from heterogeneous catalysis of crude oil/ syngas and illustrates how some of these building blocks are then utilized in homogeneous catalytic processes to yield higher value products.[74]

[70] Hartley, F. R., *Chemistry of the Platinum Group Metals: Recent Developments*, Elsevier Science Publishers, New York, United States of America, **1991**, 25.
[71] Hunt, L. B., *Platinum Metals Rev.*, **1987**, *31*, 32-41.
[72] Greenwood, N. N., Earnshaw, A., *Chemistry of the Elements*, Butterworth-Heinemann, Oxford, United Kingdom, **1998**, 1113.
[73] Gates, B. C., Knoezinger, H., Jentoft, F. C., *Advances in Catalysis*, Academic Press, Amsterdam, The Netherlands, **2010**, 1.
[74] Bhaduri, S., Mukesh, D., *Homogeneous Catalysis: Mechanisms and Industrial Applications*, John Wiley & Sons, New York, United States of America, **2000**, 2.

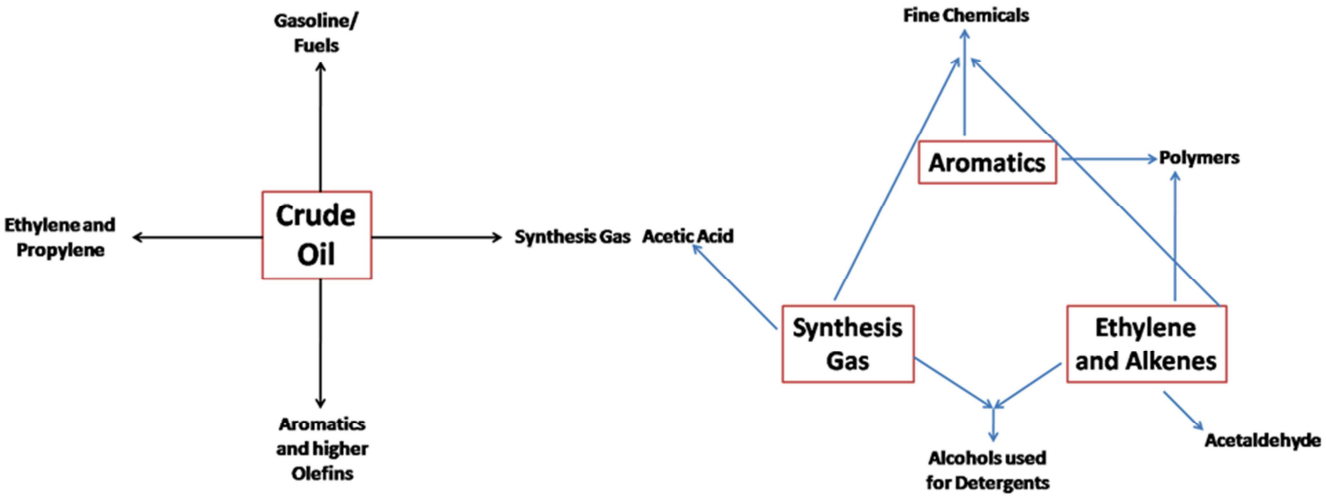

Scheme 2.4: a) Basic chemical building blocks obtained by heterogeneous catalysis treatment of crude oil; b) some of the higher commodity products that can be obtained from homogeneous catalysis using these chemical building blocks.[74]

The manufacture of bulk and fine chemicals has utilized transition metal catalysts to great success. Despite the obvious problems associated with separation of products from homogeneous catalysis the high activity and product selectivity have allowed such processes to be extensively exploited in industry.[75] To this end, some of the most successful innovations in homogeneous catalysis have involved rhodium-based systems. This includes the hydroformylation of alkenes using $[RhH(CO)(PPh_3)_3]$[76]; the carbonylation of methanol[77] utilizing $[Rh(CO)_2I_2]^-$ and the asymmetric hydrogenation of α-amidocinnamic acids[78] that is used in the synthesis of L-DOPA used to control the symptoms of Parkinson's disease. The high selectivity, activity and stability of the catalysts often outweigh the high costs associated with using rhodium.[74]

One of the most important industrial processes to utilize rhodium as catalyst is the Monsanto process which involves the carbonylation of methanol to yield acetic acid.[74] The corresponding technology developed for iridium is known as the Cativa process.[79] The catalytic cycle of the rhodium-catalyzed system is illustrated in Figure 2.6. Standard operating conditions of the Monsanto process are at pressures of 30-60 bar and temperatures of 150-200 ℃ and results in selectivi ty of over 99 % for the production of acetic acid.[80] Several types of reactions that are often encountered in organometallic

[75] Simpson, M. C., Cole-Hamilton, D. J., *Coord. Chem. Rev.*, **1996**, *155*, 163-207.
[76] Jardine, F. H., *Polyhedron*, **1982**, *1*, 569-605.
[77] Howard, M. J., Jones, M. D., Roberts, M. S., Taylor, S. A., *Catal. Today*, **1993**, *18*, 325-354.
[78] Brown, J. M., *Angew. Chem. Int. Ed.*, **1987**, *26*, 190-203.
[79] Wittcoff, H. A., Reuben, B. G., Plotkin, J. S., *Industrial Organic Chemicals*, John Wiley & Sons, New Jersey, United States of America, **2004**, 365.
[80] Thomas, C. M., Süss-Fink, G., *Coord. Chem. Rev.*, **2003**, *243*, 125-142.

chemistry can be associated with the process as illustrated in Figure 2.6.[80] These steps include oxidative addition, migration, insertion and reductive elimination.

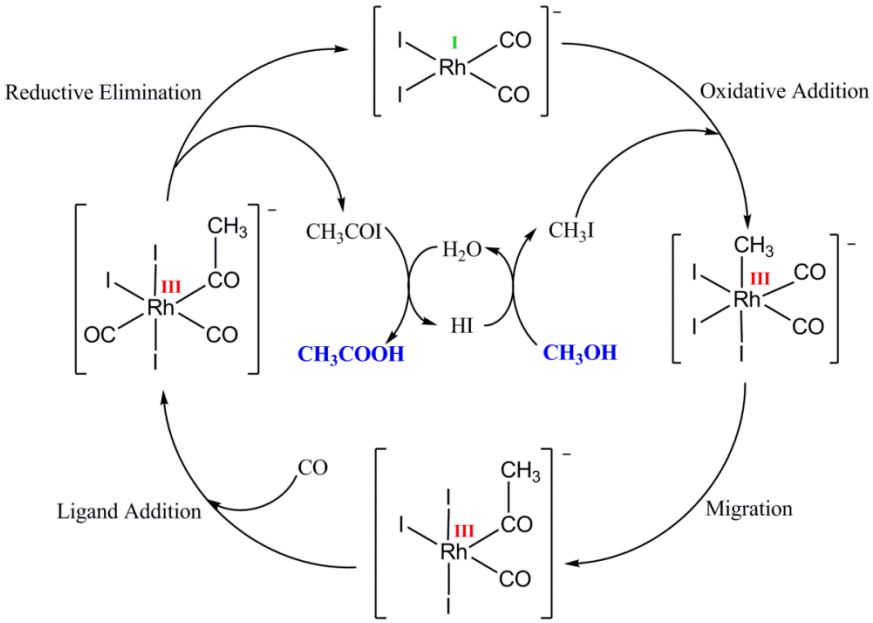

Figure 2.6: The catalytic cycle for the carbonylation of methanol utilizing a rhodium catalyst (Monsanto process).[80]

The first step in the process is the *oxidative addition* of methyl iodide to the rhodium centre with the methyl iodide supplied in the reaction of methanol and HI. The *oxidative addition* step of the Monsanto process is considered the rate-determining step as this is the slowest reaction of the catalytic cycle. First-order dependence exists for the overall rate on the concentrations of rhodium and methyl iodide. An octahedral Rh(III) alkyl species where iodide is coordinated *cis* to the carbonyl groups is formed as an intermediate which then undergoes *migration* of the CO ligand into the methyl bond. This results in a square pyramidal geometry for the Rh(III) acyl product with the new C-C bond formed during this step. Another CO ligand is then coordinated *(ligand addition)* to the rhodium to form an octahedral complex which upon *reductive elimination* of CH_3COI regenerates the original catalyst. Acetic acid as the product is then formed upon hydrolysis of acetyl iodide.[81]

2.8 General Ligand Exchange/ Substitution Reactions

In order to design a catalytic system to give the highest possible yields or selectivity a basic understanding of the catalyst in terms of reactivity is needed. Exchange reactions can reveal

[81] Maitlis, P. M., de Klerk, A. *Greener Fischer-Tropsch Processes for Fuels and Feedstocks*, Wiley-VCH, Weinheim, Germany, **2013**, 140.

a great amount of information regarding the reactivity of a complex and the metal centre.[82] For this reason it was decided to include substitution kinetic investigations in this study and some focus will now be given to ligand exchange reactions for square planar type systems.

Substitution reactions were originally classified according to the system proposed by Ingold and Hughes in their identification of nucleophilic substitution in organic reactions as proceeding *via* a S_N1 or S_N2 pathway.[83] This theory was then expanded upon to include the modern view of dissociative and associative mechanisms (including interchange mechanisms) by Langford and Gray.[84,85] Figure 2.7 provides a representation of the associative and dissociative type mechanisms for ligand substitution reactions.[86]

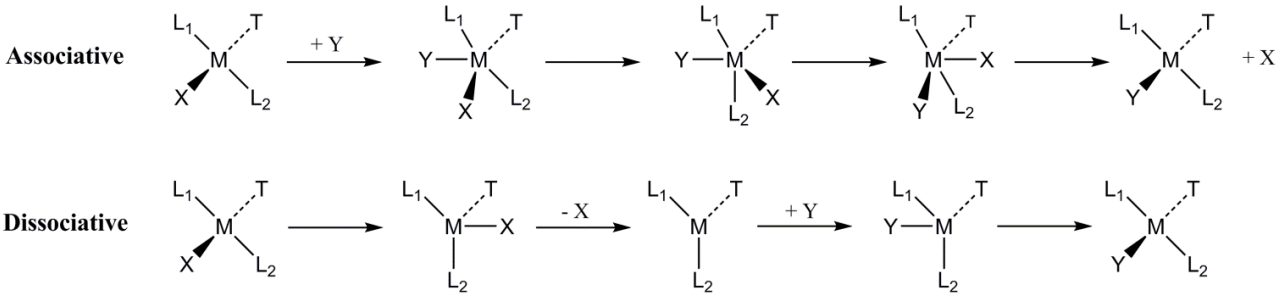

Figure 2.7: The associative and dissociative mechanisms by which substitution reactions occur.[86]

In associative mechanisms, the incoming ligand occupies a vacant site on the metal centre which is followed by a re-orientation of the ligands to create a labile leaving group. This is then followed by the exit of the labile ligand from the coordination sphere. For dissociative mechanisms, the leaving group will first be released by the metal centre with the vacant site either occupied by the incoming ligand or by a solvent molecule.[86]

In the diagrams of Figure 2.7, the ligand **T** indicates the ligand *trans* to the replaceable ligand **X**. The nature of this ligand can have a direct influence on the rate and pathway by which the reaction proceeds. A *trans-directing influence* is brought into effect by the ligand **T** which directs whether **T** or **X** will be substituted in the reaction and is considered to be thermodynamic of nature.[87] Secondly, a *trans labilizing effect* influences the rate at which the substitution will occur and is defined as a kinetic effect.[87] Collectively, these two terms are

[82] Van Eldik, R., Bowman-James, K., *Advances in Inorganic Chemistry*, Academic Press, London, United Kingdom, **2007**, 296.
[83] Gleave, J. L., Hughes, E. D., Ingold, C. K., *J. Chem. Soc.*, **1935**, 236-244.
[84] Langford, C. H., Gray, H. B., *Ligand Substitution Processes*, W. A. Benjamin Inc., New York, United States of America, **1965**, 8.
[85] McAuly, A., *Inorganic Reaction Mechanisms*, Royal Society of Chemistry, London, United Kingdom, **1977**, 163.
[86] Huheey, J. E., Keiter, E. A., Keiter, R. L., *Inorganic Chemistry, Principles of Structure and Reactivity*, Harper Collins College Publishers, New York, United States of America, **1993**, 540.
[87] Lincoln, S. F., Merbach, A. E., *Advances in Inorganic Chemistry*, Academic Press, London, United Kingdom, **1995**, 50.

known as the *trans effect*. A *trans effect* order has been established for different substituents as given in decreasing order[88]:

$$CO, CN^-, C_2H_4 > PR_3, SH_2 > NO_2^- > I^- > Br^- > Cl^- > py \sim NH_3 > OH^- > H_2O$$

Substitution reactions typically involving square planar complexes have been found to preferentially adopt an associative reaction mechanism.[89] The two pathways associated with an associative substitution mechanism for square planar complexes are illustrated in Figure 2.8.[90]

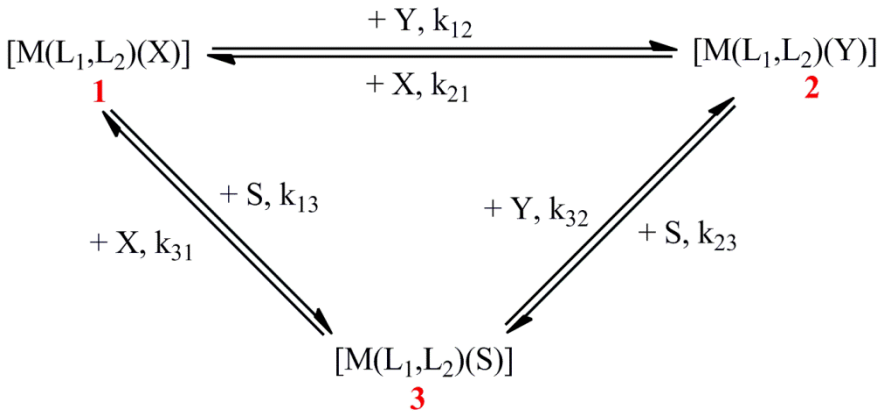

Figure 2.8: Schematic representation of the two reaction pathways in associative susbtitution reactions of square planar complexes.[90] The subscripts of the rate constants represent the numbers of the species involved during the specific reaction, e.g. k_{12} describes the rate constant for the substitution reaction of complex 1 to 2.

The two pathways associated with the mechanism are i) a direct attack of the nucleophile (Y) on the metal centre, [M(L_1,L_2)(X)] (**1**) yielding [M(L_1,L_2)(Y)] (**2**) and ii) a bimolecular attack of the solvent (S) forming a labile solvent species shown as [M (L_1,L_2)(S)] (**3**), followed by a fast attack of the entering ligand (Y) to yield the final substituted complex, [M(L_1,L_2)(Y)] (**2**).

From the reaction mechanism illustrated in Figure 2.8 the expression for the pseudo-first order rate constant (k_{obs}) can be derived as follows with the solvent concentration already incorporated into the k_{13} and k_{32} rate constants[90,91,92]:

$$k_{obs} = k_{12}([Y] + \frac{[X]}{K_{eq}}) + \frac{\frac{k_{13}k_{32}}{K_{eq}k_{31}}[X] + k_{13}\frac{k_{32}}{k_{31}}[Y]}{[X] + \frac{k_{32}}{k_{31}}[Y]} \qquad \text{(Eq. 2.1)}$$

[88] Miessler, G. L., Tarr, D. A., *Inorganic Chemistry*, Pearson Education, New Jersey, United States of America, **2004**, 439.
[89] Porterfield, W. W., *Inorganic Chemistry: A Unified Approach*, Academic Press Inc., San Diego, United States of America, **1993**, 716.
[90] Otto, S., *PhD Thesis*, University of the Free State, **1999**, 13.
[91] Kirsten, L., *MSc Dissertation*, University of Johannesburg, Johannesburg, South Africa, **2005**.
[92] Romeo, R., Arena, G., Scolara, L. M., Plutino, M. R., *Inorg. Chim. Acta*, **1995**, *240*, 81-92.

In equation 2.1, K_{eq} is used to denote the equilibrium constant. In cases where the reactions are not reversible (large K_{eq} constants) the rate law can be simplified to the two-term rate law often employed in square planar substitution reactions[93,94,95,96]:

$$k_{obs} = k_{12}[Y] + k_{13} \quad \text{(Eq. 2.2)}$$

Under non-equilibrium conditions, linear plots of the pseudo-first order rate constants against concentration of incoming ligand will be expressed with a slope equal to the rate constant k_{12} term and the intercept as the k_{13} constant (solvent assisted pathway).[97] However, under equilibrium conditions (small K_{eq} values) the concentration of the leaving group must be considered and the overall rate (Eq. 2.1) describing the observable rate must be used.

Moreover, several factors have been found to influence the rate of substitution reactions with the most notable examples being:

i) The incoming ligand[98]
ii) The labile ligand[98]
iii) The nature of other ligands in the complex[99]
iv) The metal centre[100]

Substitution reaction studies that were conducted by P. Ebenebe[101] in 1998 were found to be of particular interest to this study. Ebenebe[101] investigated the substitution of a carbonyl ligand in square planar rhodium(I) complexes of the type [Rh(*O,O'*-Bid)$(CO)_2$] with a bulky phosphine ligand. The data reported by Ebenebe[101] for the pseudo first-order rate constants in the substitution reaction of [Rh(acac)$(CO)_2$] and tri(o-tolyl)phosphine, ($P(otol)_3$), is summarized in Table 2.3. Data relating to substitution reactions involving several other [Rh(*O,O'*-Bid)$(CO)_2$] complexes are given in Table 2.4.

[93] De Waal, D. J. A., Robb, W., *Inorg. Chim. Acta*, **1978**, *26*, 91-96.
[94] Gray, H. B., Olcott, R. J., *Inorg. Chem.*, **1962**, *1*, 481-485.
[95] Pearson, R. G., Gray, H. B., Basolo, F., *J. Am. Chem. Soc.*, **1960**, *82*, 787-792.
[96] Otto, S., Roodt, A., *J. Organomet. Chem.*, **2006**, *691*, 4626-4632.
[97] Basolo, F., *From Coello to Inorganic Chemistry: A Lifetime of Reactions*, Springer Science + Business Media, New York, United States of America, **2002**, 97.
[98] Cotton, F. A., Wilkinson, G., Gaus, P. L., *Basic Inorganic Chemistry*, John Wiley & Sons, New York, United States of America, **1995**, 201.
[99] Atkins, P. W., Overton, T. L., Rourke, J. P., Weller, M. T., Armstrong, F. A., *Shriver & Atkins Inorganic Chemistry*, Oxford University Press, Oxford, United Kingdom, **2010**, 515.
[100] Wulfsberg, G., *Inorganic Chemistry*, University Science Books, Sausalito, United States of America, **2000**, 853.
[101] Ebenebe, P., *MSc Dissertation*, University of the Free State, Bloemfontein, South Africa, **1998**.

Table 2.3: Observed pseudo first-order rate constants at different concentrations of entering ligand, $P(otol)_3$ in the carbonyl substitution of $[Rh(acac)(CO)_2]$ in acetone at 25 ℃ reported by Ebenebe[101].

$[P(otol)_3]$ (M)	k_{obs} (s^{-1})
3.0×10^{-3}	0.89(1)
7.5×10^{-3}	2.04(1)
1.7×10^{-2}	4.34(5)
3.1×10^{-2}	8.3(1)
4.5×10^{-2}	16(1)
5.9×10^{-2}	23(1)
8.0×10^{-2}	38(1)
1.0×10^{-1}	48(3)

Table 2.4: Pseudo first-order rate constants for the carbonyl substitution of $[Rh(O,O'\text{-Bid})(CO)_2]$ by tri(o-tolyl)phosphine at 25 ℃ reported by Ebe nebe[101].

Complex*	$[P(otol)_3]$ (M)	k_{obs} (s^{-1})
$[Rh(dipiv)(CO)_2]$	0.003	0.61(4)
$[Rh(acac)(CO)_2]$	0.003	0.89(1)
$[Rh(dbm)(CO)_2]$	0.003	2.49(4)
$[Rh(tfac)(CO)_2]$	0.003	49.2(9)
$[Rh(F_3\text{-bzac})(CO)_2]$	0.003	123.6(1)
$[Rh(hfac)(CO)_2]$	0.0006	238.3(4)

* Abbreviations: dipiv= 2,2,6,6-tetramethyl-3,5-heptanedionato; acac= acetylacetonato, dbm= 1,3-diphenyl-1,3-propanedionato, tfac= 1,1,1-trifluoro-2,4-pentanedionato, F_3-bzac= benzoyl-1,1,1-trifluoracetonato, hfac= hexafluoracetonato.

Interestingly, from the work conducted by Ebenebe[101] it was noticed that the data reported for the k_{obs} *vs.* concentration of entering phosphine ligand yielded non-linear relationships. Ebenebe[101] however, assigned two different linear plots to the data concluding that the reaction was occurring along two different mechanistic pathways. Figure 2.9 illustrates these linear plots for the carbonyl substitution of $[Rh(acac)(CO)_2]$ by $P(otol)_3$ assigned by Ebenebe[101]. At lower phosphine concentrations the reaction was thought to occur along the solvolysis pathway (proceeding from species **1** to **3** and proceeding to the final substituted product **2** (see Figure 2.8). At higher concentration of phosphine ligand the reaction was considered to proceed from species **1** to **2** along the direct substitution pathway (Figure 2.8).

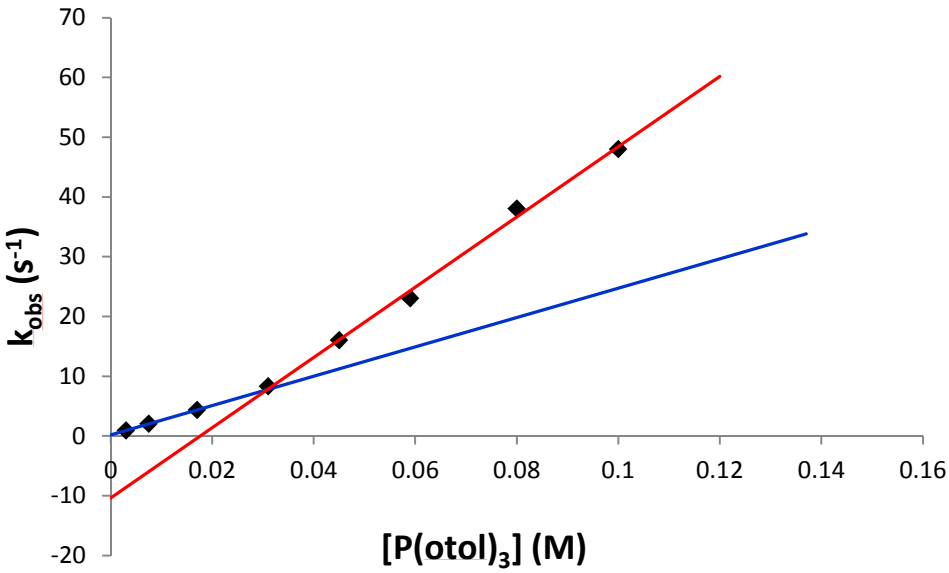

Figure 2.9: The rate constant dependence on [P(otol)$_3$] for the carbonyl substitution in [Rh(acac)(CO)$_2$ reported by Ebenebe[101]. The assignment of two slopes was used to indicate the different pathways by which the reaction was concluded to proceed with varying phosphine concentrations.

This interpretation seemed unlikely with the non-linear tendency of the data suggesting that the K_{eq} term (small values indicating the presence of an equilibrium) significantly affects the substitution reaction and that the full rate law given in Eq. 2.1 holds for the reaction. The kinetic investigations in this study will explore a re-interpretation of data reported by Ebenebe[101] as well as the analysis of a possible equilibrium involved in these substitution reactions (see Chapter 7).

2.9 Conclusion

Several topics of relevance to the current study were discussed in this chapter. Theory relating to metallophilic interactions as well as the wide applications of materials containing such interactions was discussed in this chapter. Focus was also given to rhodium and its wide applications in catalysis as the transition metal forms a central focus in this study. Additionally, concepts concerning square planar substitution reactions were also discussed which directly relates to the preliminary kinetic investigations undertaken in this study (see Chapter 7).

As laid out in the aims of Chapter 1, one of the central objectives of this project is to synthesize novel rhodium(I) complexes that contain different β-diketone ligands. The following chapter will focus on the synthesis and characterization of these rhodium(I) complexes using different β-diketone ligands. It will include a discussion on the general

synthetic procedures as well as correlations that exist between the pK_a values of the uncoordinated ligands and C=O stretching frequencies and/ or ^{103}Rh NMR chemical shifts of the resulting rhodium(I) complexes.

Chapter 3: Synthesis of [Rh(*O,O'*-Bid)$(CO)_2$] and [Rh(*O,O'*-Bid)$(CO)(P(otol)_3)$] Complexes

3.1 Introduction

The synthesis of rhodium(I) complexes with different coordinating β-diketone ligands forms a fundamental part of this study. One of the primary aims of the current study was the solid-state characterization of these compounds utilizing X-ray diffraction which, without successful synthesis of said complexes would be unattainable. The various ligands chosen for chelation to rhodium(I) offer unique electronic and steric changes to the final coordinated complex. These changes could potentially alter the electronic/ steric environment at the rhodium(I) centre which in turn could alter the assembly of the rhodium(I) complexes in the one-dimensional chains constructed *via* metallophilic interactions in the solid-state. Systematic changes in the individual ligands were brought about by varying the substituent positions on the β-diketone backbone (1, 3 and 5 positions, see scheme 3.1) as well as introducing different electron donating/ withdrawing moieties. The 14 ligand systems that were investigated for potential coordination to rhodium(I) are illustrated in scheme 3.2 with the detailed synthesis of each rhodium(I) complex given in Section 3.3.

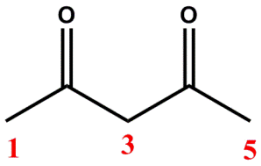

Scheme 3.1: Schematic representation of the carbon positions at which substituent groups were altered in different β-diketone ligands in coordination to rhodium(I).

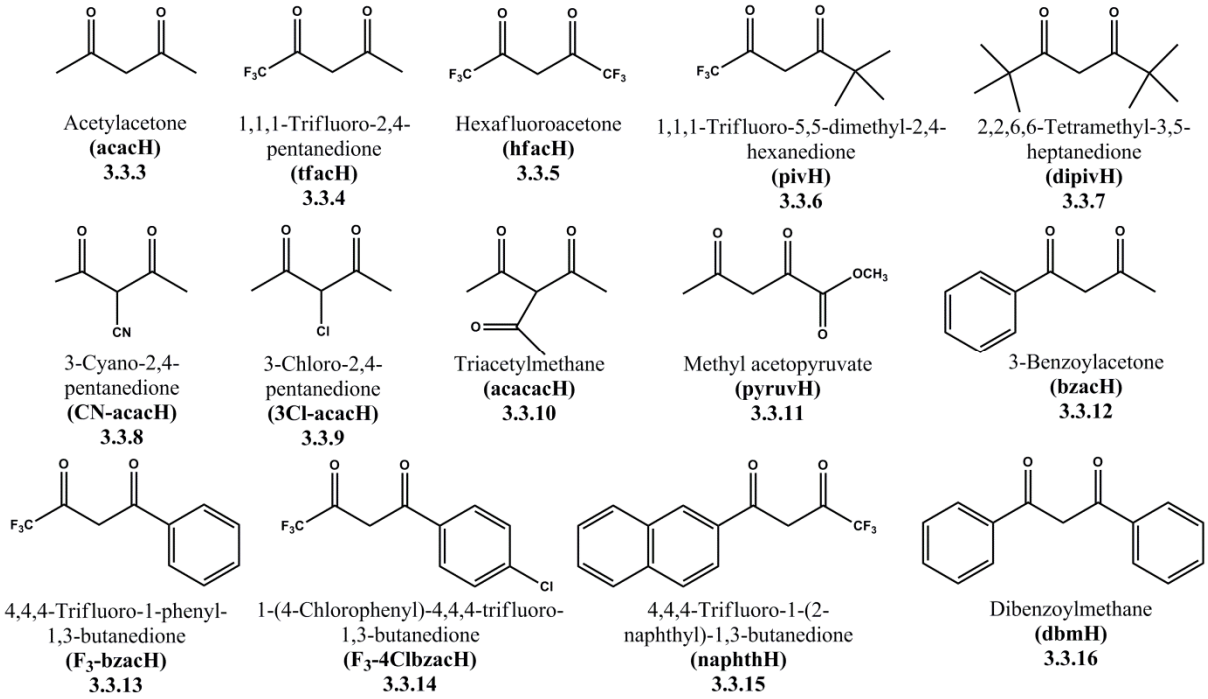

Scheme 3.2: Schematic representation of the β-diketone ligands employed in the synthesis of rhodium(I) complexes (labelling indicates paragraph where the synthesis is described).

3.2 Chemical and Apparatus Detail

3.2.1 Reagents and Solvents

All reagents used for the synthesis and characterization were of analytical grade and obtained from Sigma-Aldrich, South Africa. Solvents were of analytical grade and along with the reagents were used without further purification.

3.2.2 Infrared Spectroscopy

All infrared spectra of synthesized complexes were recorded as neat samples on a Bruker Digilab FTS 2000 Fourier transform spectrometer (ATR) using a He-Ne laser at 632.6 nm, in the range of 3000 to 600 cm^{-1}.

3.2.3 Nuclear Magnetic Resonance Spectroscopy

NMR spectroscopic data were obtained on a Bruker Avance II 600 MHz spectrometer (operating at 600.28 for ^{1}H, 150.96 for ^{13}C, 242.99 for ^{31}P and 18 MHz for ^{103}Rh respectively). Chemical shifts are reported in ppm and given relative to TMS for ^{1}H NMR spectra. In each case the respective deuterated solvent used for analysis will be stated.

3.2.4 UV/Vis Spectroscopy

All UV/Vis spectra for the compounds synthesized were recorded using a Varian Cary 50 Conc UV-Visible spectrophotometer equipped with a Julabo F12-mV temperature cell regulator (accurate within 0.1 ℃) in a 1.000 ± 0.0 01 cm quartz tandem cuvette.

3.3 Synthesis of Starting Reagents, [Rh(*O,O'*-Bid)$(CO)_2$] and [Rh(acac)(CO)$(P(otol)_3)$] Complexes

3.3.1 Rhodium reactant

In all of the synthesis to follow the rhodium reactant to be used in the coordination of β-diketone ligands (Scheme 3.1) to rhodium(I) is the dinuclear complex, [Rh(μ-Cl)$(CO)_2]_2$ (scheme 3.3). This complex may be obtained from two synthetic methods as found in literature.[1,2] The first route involves the *in situ* preparation of the [Rh(μ-Cl)$(CO)_2]_2$ complex by refluxing $RhCl_3.xH_2O$ in DMF until a colour change from red to yellow is observed. This colour change is associated with the formation of the desired complex. The complex is not isolated but the solution is directly used further. The second method involves the pulverising of $RhCl_3.xH_2O$ followed by sublimation at 98 ℃ with CO gas flus hed through the system continuously. Red crystals of the desired product are obtained using this synthetic process.

In all of the reactions to follow, the *in situ* method was utilized in preparing the starting rhodium complex of [Rh(μ-Cl)$(CO)_2]_2$.

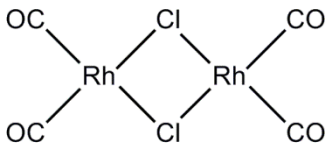

Scheme 3.3: Schematic representation of the [Rh(μ-Cl)$(CO)_2]_2$ complex prepared *in situ* for the synthesis of rhodium(I) complexes with different coordinating β-diketone ligands.

3.3.2 Synthesis of 3-cyano-2,4-pentanedione (CN-acacH)

The title compound was prepared according to the procedure outlined by Silvernail *et al.*[3] Acetylacetone (10.0 g, 100 mmol) was stirred in dichloromethane (27 cm^3) under a nitrogen atmosphere. To this solution chlorosulfonylisocyanate (4.75 cm^3, 55.0 mmol) was added dropwise over several minutes. The reaction mixture was allowed to stir for an additional 30

[1] McCleverty, J. A., Wilkinson, G., *Inorganic Synth.*, **1990**, *28*, 84.
[2] Szafran, Z., Pike, R. M., Singh, M. M., *Microscale Inorganic Laboratory*, **1990**, Wiley, New York.
[3] Silvernail, C. M., Yap, G., Sommer, R. D., Rheingold, A. L., Day, V. W., Belot, J. A., *Polyhedron*, **2001**, *20*, 3113-3117.

minutes before adding dimethylformamide (8.5 cm^3). Water was then added to the mixture to allow for separation of the organic products but before separation could be performed it was noted that the product crystallized as fine orange needle-like crystals within the organic layer and was collected. (Yield: 4.00 g, 58 %)

^{1}H NMR (600 MHz, chloroform-*d*; *ppm*): δ = 2.39 (s, 6H, CH_3). ^{13}C NMR (151 MHz, chloroform-*d*; *ppm*): δ = 197.14 (CO), 116.60 (CN), 24.65 (CH_3).

3.3.3 Synthesis of (acetylacetonato-κ^2*O,O*)dicarbonylrhodium(I), [Rh(acac)$(CO)_2$]

$RhCl_3.3H_2O$ (0.0109 g, 0.0413 mmol) was refluxed in 2 ml of DMF until the red colour was observed to turn yellow (approx. 30 min). The solution was then cooled in an ice-bath before adding acetylacetone (0.0051 cm^3, 0.0497 mmol) to the reaction mixture. The dark red-green product was precipitated by the addition of ice-water and then collected by centrifugation. It was recrystallized from dichloromethane and methanol yielding red needle-like crystals with a green metallic lustre after approximately three days. These crystals were found suitable for single crystal X-ray diffraction studies. (**Yield**: 0.0072 g, 68 %) The structure of [Rh(acac)$(CO)_2$] has been previously synthesized and the crystal structure published by Huq and Skapski in 1974.[4]

IR (ATR): $\nu_{CO(asym)}$ 1995 cm^{-1}; $\nu_{CO(sym)}$ 2062 cm^{-1}. UV/Vis: λ_{max}= 382 nm, ε= 516 $M^{-1}.cm^{-1}$.^{1}H NMR (600 MHz, benzene-d_6; *ppm*): δ = 5.14 (s, 1H, CH), 1.68 (s, 6H, 2 x CH_3). ^{13}C NMR (151 MHz, benzene-d_6; *ppm*): δ = 187.87 (CO), 185.32 (CO), 102.12 (CH), 27.20 (CH_3). ^{103}Rh NMR (18 MHz, methylene chloride-d_2; *ppm*): δ = 284.2.

3.3.4 Synthesis of dicarbonyl(1,1,1-trifluoro-2,4-pentanedionato-κ^2*O,O'*) rhodium(I), [Rh(tfac)$(CO)_2$]

$RhCl_3.3H_2O$ (0.0115 g, 0.0437 mmol) was refluxed in 2 ml of DMF until the red colour turned yellow (approx. 30 min). The solution was then cooled in an ice-bath before adding 1,1,1-trifluoro-2,4-pentanedione (0.0064 cm^3, 0.0524 mmol) to the reaction mixture. The orange product was precipitated by the addition of ice-water and collected by centrifugation. Recrystallization from dichloromethane and methanol yielded orange needle-like crystals suitable for single crystal X-ray diffraction studies after approximately three days. (**Yield**: 0.0086 g, 54 %)

IR (ATR): $\nu_{CO(asym)}$ 2015 cm^{-1}; $\nu_{CO(sym)}$ 2082 cm^{-1}. UV/Vis: λ_{max}= 305 nm, ε= 620 $M^{-1}.cm^{-1}$.^{1}H NMR (600 MHz, methylene chloride-d_2; *ppm*): δ = 6.08 (s, 1H, CH), 2.26 (s, 3H, CH_3). ^{13}C

[4] Huq, F., Skapski, A. C., *J. Cryst. Mol. Struct.*, **1974**, *4*, 411-418.

NMR (151 MHz, methylene chloride-d_2; *ppm*): δ = 196.91 (CO), 183.53 (CO), 97.88 (CH), 28.98 (CH_3). ^{103}Rh NMR (18 MHz, methylene chloride-d_2; *ppm*): δ = 319.2.

3.3.5 Synthesis of dicarbonyl(hexafluoroacetonato-κ^2*O,O*)rhodium(I), [Rh(hfac)$(CO)_2$]

$RhCl_3.3H_2O$ (0.0130 g, 0.0491 mmol) was refluxed in 2 ml of DMF until the red colour was observed to turn yellow (approx. 30 min). The solution was cooled in an ice-bath before adding hexafluoroacetylacetone (0.0083 cm^3, 0.0589 mmol) to the reaction mixture. The orange product was precipitated by the addition of ice-water and collected by centrifugation. An oil was obtained by evaporation of acetone. All attempts at recrystallization of the product using various solvents were unsuccessful in yielding a crystalline product. (**Yield**: 0.0104 g, 76 %)

IR (ATR): $\nu_{CO(asym)}$ 2034 cm^{-1}; $\nu_{CO(sym)}$ 2094 cm^{-1}. UV/Vis: λ_{max}= 315 nm, ε= 630 $M^{-1}.cm^{-1}$.^{1}H NMR (600 MHz, methylene chloride-d_2; *ppm*): δ = 6.49 (s, 1H, CH). ^{13}C NMR (151 MHz, methylene chloride-d_2; *ppm*): δ = 178.34 (CO), 177.77 (CO), 130.08 (CF_3). ^{103}Rh NMR (18 MHz, methylene chloride-d_2; *ppm*): δ = 357.5.

3.3.6 Synthesis of dicarbonyl(1,1,1-trifluoro-5,5-dimethyl-3,5-hexanedionato-κ^2*O,O'*) rhodium(I), [Rh(piv)$(CO)_2$]

$RhCl_3.3H_2O$ (0.0125 g, 0.0472 mmol) was refluxed in 2 ml of DMF until the red colour was observed to turn yellow (approx. 30 min). The solution was cooled in an ice-bath before adding 1,1,1-trifluoro-5,5-dimethyl-2,4-hexanedione (0.0097 cm^3, 0.0566 mmol) to the reaction mixture. The red product was precipitated by the addition of ice-water after which the product was collected by centrifugation. The product was dissolved in dichloromethane and placed in an NMR tube to which methanol was added. After being kept for approximately three days at 4 ℃, purple-green need le-like crystals were observed of suitable quality for XRD analysis. (**Yield**: 0.0079 g, 47 %)

IR (ATR): $\nu_{CO(asym)}$ 2024 cm^{-1}; $\nu_{CO(sym)}$ 2083 cm^{-1}. UV/Vis: λ_{max}= 353 nm, ε= 708 $M^{-1}.cm^{-1}$.^{1}H NMR (600 MHz, methylene chloride-d_2; *ppm*): δ = 5.32 (s, 1H, CH), 2.12 (s, 9H, *t*-Bu). ^{13}C NMR (151 MHz, methylene chloride-d_2; *ppm*): δ = 206.94 (CO), 205.44 (CO), 93.32 (CH), 31.01 (*t*-Bu). ^{103}Rh NMR (18 MHz, methylene chloride-d_2; *ppm*): δ = 306.8.

3.3.7 Synthesis of dicarbonyl(2,2,6,6-tetramethyl-3,5-heptanedionato-κ^2*O,O*) rhodium(I), [Rh(dipiv)(CO)$_2$]

$RhCl_3.3H_2O$ (0.0106 g, 0.04 mmol) was refluxed in 2 ml of DMF until the red colour was observed to turn yellow (approx. 30 min). The solution was cooled in an ice-bath before adding 2,2,6,6-tetramethyl-3,5-heptanedione (0.0099 cm^3, 0.048 mmol) to the reaction mixture. The red product was precipitated by the addition of ice-water and isolated by centrifugation. The product was dissolved in diethyl ether and kept at 4 ℃. After approximately one week purple-green needle-like crystals were collected of suitable quality for single crystal X-ray diffraction. (**Yield**: 0.0089 g, 65 %)

IR (ATR): $\nu_{CO(asym)}$ 1996 cm^{-1}; $\nu_{CO(sym)}$ 2066 cm^{-1}. UV/Vis: λ_{max}= 331 nm, ε= 684 $M^{-1}.cm^{-1}$.^{1}H NMR (600 MHz, methylene chloride-d_2; *ppm*): δ = 5.32 (s, 1H, CH), 2.12 (s, 18H, *t*-Bu). ^{13}C NMR (151 MHz, methylene chloride-d_2; *ppm*): δ = 206.87 (CO), 197.39 (CO), 92.50 (CH), 30.79 (*t*-Bu). ^{103}Rh NMR (18 MHz, methylene chloride-d_2; *ppm*): δ = 270.2.

3.3.8 Synthesis of dicarbonyl(3-cyano-2,4-pentanedionato-κ^2*O,O*)rhodium(I), [Rh(CN-acac)(CO)$_2$]

$RhCl_3.3H_2O$ (0.01003 g, 0.0378 mmol) was refluxed in 2 ml of DMF until the red colour was observed to turn yellow (approx. 30 min). The solution was cooled in an ice-bath before adding 3-cyano-2,4-pentanedione (0.0057 g, 0.0454 mmol) (Section 3.3.2) to the reaction mixture. The purple-green product was precipitated by the addition of ice-water and isolated by centrifugation. The product was recrystallized from a mixture of dichloromethane and methanol. After approximately one week, purple needle-like crystals with a green metallic lustre were obtained and were found suitable for analysis by single crystal X-ray diffraction. (**Yield**: 0.0108 g, 59 %)

IR (ATR): $\nu_{CO(asym)}$ 2011 cm^{-1}; $\nu_{CO(sym)}$ 2074 cm^{-1}. UV/Vis: λ_{max}= 353 nm, ε= 965 $M^{-1}.cm^{-1}$.^{1}H NMR (600 MHz, methylene chloride-d_2; *ppm*): δ = 2.37 (s, 6H, 2 x CH_3). ^{13}C NMR (151 MHz, methylene chloride-d_2; *ppm*): δ = 193.07 (CO), 182.61 (CO), 119.51 (CN), 27.85 (CH_3). ^{103}Rh NMR (18 MHz, methylene chloride-d_2; *ppm*): δ = 294.2.

3.3.9 Synthesis of dicarbonyl(3-chloro-2,4-pentanedionato-κ^2*O,O*)rhodium(I), [Rh(3Cl-acac)(CO)$_2$]

$RhCl_3.3H_2O$ (0.0120 g, 0.0453 mmol) was refluxed in 2 ml of DMF until the red colour was observed to turn yellow (approx. 30 min). The solution was cooled in an ice-bath before adding 3-chloro-2,4-pentanedione (0.0065 cm^3, 0.0543 mmol) to the reaction mixture. The dark orange product was precipitated by the addition of ice-water and collected by

centrifugation. The product was recrystallized from dichloromethane and yielded red needle-like crystals after approximately three days. The crystals were of suitable quality for single crystal X-ray diffraction. (**Yield**: 0.0088 g, 67 %)

IR (ATR): $\nu_{CO(asym)}$ 2020 cm^{-1}; $\nu_{CO(sym)}$ 2078 cm^{-1}. UV/Vis: λ_{max}= 366 nm, ε= 584 $M^{-1}.cm^{-1}$.^{1}H NMR (600 MHz, methylene chloride-d_2; *ppm*): δ = 2.33 (s, 6H, 2 x CH_3). ^{13}C NMR (151 MHz, methylene chloride-d_2; *ppm*): δ = 186.52 (CO), 184.74 (CO), 28.05 (CH_3). ^{103}Rh NMR (18 MHz, methylene chloride-d_2; *ppm*): δ = 297.7.

3.3.10 Synthesis of dicarbonyl(triacetylmethanato-κ^2*O,O*)rhodium(I), [Rh(acacac)(CO)$_2$]

$RhCl_3.3H_2O$ (0.0156 g, 0.0589 mmol) was refluxed in 2 ml of DMF until the red colour was observed to turn yellow (approx. 30 min). The solution was cooled in an ice-bath before adding triacetylmethane (0.0094 cm^3, 0.0706 mmol) to the reaction mixture. The orange-green product was precipitated by the addition of ice-water and isolated by centrifugation. All attempts at recrystallization from different solvents were unsuccessful in yielding crystals suitable for single crystal X-ray diffraction. (**Yield**: 0.0111 g, 63 %)

IR (ATR): $\nu_{CO(asym)}$ 1994 cm^{-1}; $\nu_{CO(sym)}$ 2066 cm^{-1}. UV/Vis: λ_{max}= 330 nm, ε= 602 $M^{-1}.cm^{-1}$.^{1}H NMR (600 MHz, methylene chloride-d_2; *ppm*): δ = 2.41 (s, 3H, CH_3), 2.09 (s, 6H, CH_3). ^{13}C NMR (151 MHz, methylene chloride-d_2; *ppm*): δ = 204.25 (CO), 185.73 (CO), 183.61 (CO), 33.60 (CH_3), 26.34 (CH_3).

3.3.11 Synthesis of dicarbonyl(methyl-4-oxo-2-oxypent-2-enoato-κ^2*O,O'*) rhodium(I), [Rh(pyruv)(CO)$_2$]

$RhCl_3.3H_2O$ (0.0113 g, 0.0426 mmol) was refluxed in 2 ml of DMF until the red colour was observed to turn yellow (approx. 30 min). The solution was cooled in an ice-bath before adding methyl acetopyruvate (0.0074 g, 0.0512 mmol) to the reaction mixture. The yellow product was precipitated by the addition of ice-water and collected by centrifugation. The product was recrystallized from acetone as red needle-like crystals after approximately two days. The crystals were found suitable for single crystal X-ray diffraction. (**Yield**: 0.0077 g, 60 %)

IR (ATR): $\nu_{CO(asym)}$ 2013 cm^{-1}; $\nu_{CO(sym)}$ 2064 cm^{-1}. UV/Vis: λ_{max}= 370 nm, ε= 604 $M^{-1}.cm^{-1}$.^{1}H NMR (600 MHz, methylene chloride-d_2; *ppm*): δ = 3.85 (s, 1H, CH), 2.91 (s, 3H, OCH_3), 1.92 (s, 3H, CH_3). ^{13}C NMR (151 MHz, methylene chloride-d_2; *ppm*): δ = 195.29 (CO), 168.09 (CO), 162.92 (CO), 101.71 (CH), 36.73 (OCH_3), 31.49 (CH_3). ^{103}Rh NMR (18 MHz, methylene chloride-d_2; *ppm*): δ = 311.1.

3.3.12 Synthesis of (3-benzoylacetonato-κ^2*O,O'*)dicarbonylrhodium(I), [Rh(bzac)$(CO)_2$]

$RhCl_3.3H_2O$ (0.1014 g, 0.385 mmol) was refluxed in 2 ml of DMF until the red colour was observed to turn yellow (approx. 30 min). The solution was then cooled in an ice-bath before adding 1-phenyl-1,3-butanedione (0.0906 g, 0.905 mmol) to the reaction mixture. The orange product was precipitated by the addition of ice-water and was then collected by centrifugation. Recrystallization from diethyl ether yielded needle-like crystals with an orange colour and green metallic lustre after approximately two days. These crystals were found suitable for single crystal X-ray diffraction. (**Yield**: 0.0809 g, 66 %)

IR (ATR): $\nu_{CO(asym)}$ 1999 cm^{-1}; $\nu_{CO(sym)}$ 2066 cm^{-1}. UV/Vis: λ_{max}= 379 nm, ε= 640 $M^{-1}.cm^{-1}$.^{1}H NMR (600 MHz, methylene chloride-d_2; *ppm*): δ = 7.74, 7.41, 7.33 (m, 5H, Ar), 6.08 (s, 1H, CH), 3.97 (s, 3H, CH_3). ^{13}C NMR (151 MHz, methylene chloride-d_2; *ppm*): δ = 194.37 (CO), 183.95 (CO), 132.96, 129.54, 127.12 (Ar), 96.91 (CH), 26.01 (CH_3). ^{103}Rh NMR (18 MHz, methylene chloride-d_2; *ppm*): δ = 284.0.

3.3.13 Synthesis of (benzoyl-1,1,1-trifluoroacetonato-κ^2*O,O'*)dicarbonyl rhodium(I), [Rh(F_3-bzac)$(CO)_2$]

$RhCl_3.3H_2O$ (0.0100 g, 0.0377 mmol) was refluxed in 2 ml of DMF until the red colour was observed to turn yellow (approx. 30 min). The solution was cooled in an ice-bath before adding 4,4,4-trifluoro-1-phenyl-1,3-butanedione (0.0098 g, 0.0453 mmol) to the reaction mixture. The dark orange product was precipitated by the addition of ice-water after which the product was collected by centrifugation. Recrystallization from acetone yielded orange needle-like crystals suitable for X-ray diffraction after three days. (**Yield**: 0.0089 g, 63 %) The structure of [Rh(F_3-bzac)$(CO)_2$] has been previously synthesized and the crystal structure published by Leipoldt *et al.* [5]

IR (ATR): $\nu_{CO(asym)}$ 2024 cm^{-1}; $\nu_{CO(sym)}$ 2084 cm^{-1}. UV/Vis: λ_{max}= 371 nm, ε= 1496 $M^{-1}.cm^{-1}$.^{1}H NMR (600 MHz, methylene chloride-d_2; *ppm*): δ = 7.95, 7.61, 7.49 (m, 5H, Ar), 6.75 (s, 1H, CH). ^{13}C NMR (151 MHz, methylene chloride-d_2; *ppm*): δ = 187.13 (CO), 182.87 (CO), 157.35, 136.30, 133.77 (Ar), 129.14 (CF_3), 95.76 (CH). ^{103}Rh NMR (18 MHz, methylene chloride-d_2; *ppm*): δ = 320.4.

[5] Leipoldt, J. G., Bok, L. D. C., Basson, S. S., van Vollenhoven, J. S., Gerber, T. I. A., *Inorganica Chimica Acta*, **1977**, *25*, L63-L64.

3.3.14 Synthesis of (benzoyl-4-chloro-1,1,1-trifluoroacetonato-κ^2*O,O'*) dicarbonylrhodium(I), [Rh(F_3-4Clbzac)($CO)_2$]

$RhCl_3.3H_2O$ (0.0114 g, 0.0430 mmol) was refluxed in 2 ml of DMF until the red colour was observed to turn yellow (approx. 30 min). The solution was cooled in an ice-bath before the addition of 1-(4-chlorophenyl)-4,4,4-tifluoro-1,3-butanedione (0.0129 g, 0.0516 mmol). The orange product was precipitated by the addition of ice-water and collected by centrifugation. A small amount of product was dissolved in dichloromethane and placed in an NMR tube to which methanol was added. This solution was kept at 4 ℃ for approximately two weeks before orange needle-like crystals with a green metallic lustre were observed. These crystals were of suitable quality for single crystal X-ray diffraction. (**Yield**: 0.0094 g, 53 %)

A second portion of product was dissolved in dichloromethane and kept in an NMR tube at room temperature (28 ℃) which yielded a small amou nt of orange needle-like crystals that were analysed by single crystal X-ray diffraction. This second portion of crystals proved to be a polymorph of the structure collected from the above mentioned crystals (see Chapter 4).

IR (ATR): $\nu_{CO(asym)}$ 2028 cm^{-1}; $\nu_{CO(sym)}$ 2077 cm^{-1}. UV/Vis: λ_{max}= 384 nm, ε= 817 $M^{-1}.cm^{-1}$.^{1}H NMR (600 MHz, methylene chloride-d_2; *ppm*): δ = 7.90, 7.45 (m, 4H, Ar), 6.68 (s, 1H, CH). ^{13}C NMR (151 MHz, methylene chloride-d_2; *ppm*): δ = 185.95 (CO), 170.20 (CO), 140.47, 135.43 (Ar), 129.63 (CF_3), 94.09 (CH). ^{103}Rh NMR (18 MHz, methylene chloride-d_2; *ppm*): δ = 325.1.

3.3.15 Synthesis of dicarbonyl(4,4,4-trifluoro-1-(2-naphthyl)-1,3-butane dionato-κ^2*O,O'*) rhodium(I), [Rh(naphth)($CO)_2$]

$RhCl_3.3H_2O$ (0.0149 g, 0.0562 mmol) was refluxed in 2 ml of DMF until the red colour was observed to turn yellow (approx. 30 min). The solution was cooled in an ice-bath before adding 4,4,4-trifluoro-1-(2-naphtyl)-1,3-butanedione (0.0179 g, 0.0675 mmol) to the reaction mixture. The yellow product was precipitated by the addition of ice-water and collected by centrifugation. Orange feather-like crystals were obtained from a dichloromethane solution after approximately four days. Attempts at recrystallization using various solvents did not yield crystals suitable for X-ray diffraction. (**Yield**: 0.0137 g, 57 %)

IR (ATR): $\nu_{CO(asym)}$ 2011 cm^{-1}; $\nu_{CO(sym)}$ 2078 cm^{-1}. UV/Vis: λ_{max}= 350 nm, ε= 850 $M^{-1}.cm^{-1}$.^{1}H NMR (600 MHz, methylene chloride-d_2; *ppm*): δ = 7.93 (m, 4H, Ar), 7.6 (m, 3H, Ar), 6.89 (s, 1H, CH). ^{13}C NMR (151 MHz, methylene chloride-d_2; *ppm*): δ = 186.97 (CO), 163.00 (CO), 136.45-127.49 (Ar), 124.10 (CF_3), 94.59 (CH).

3.3.16 Synthesis of dicarbonyl(1,3-diphenyl-1,3-propanedionato-κ^2O,O) rhodium(I), [Rh(dbm)(CO)$_2$]

$RhCl_3.3H_2O$ (0.0124 g, 0.0468 mmol) was refluxed in 2 ml of DMF until the red colour was observed to turn yellow (approx. 30 min). The solution was cooled in an ice-bath before adding dibenzoylmethane (0.0123 g, 0.0562 mmol) to the reaction mixture. The yellow product was precipitated by the addition of ice-water and collected by centrifugation. The product was then dissolved in dichloromethane with a layer of methanol and left to crystallize at -12 ℃. After three days yellow-orange needle-like crystals were observed of suitable quality for X-ray diffraction analysis. (**Yield**: 0.0098 g, 54 %)

IR (ATR): $\nu_{CO(asym)}$ 1986 cm^{-1}; $\nu_{CO(sym)}$ 2076 cm^{-1}. UV/Vis: λ_{max}= 394 nm, ε= 764 M^{-1}.cm^{-1}.^{1}H NMR (600 MHz, methylene chloride-d_2; *ppm*): δ = 7.96, 7.55, 6.97 (m, 10H, Ar), 3.42 (s, 1H, CH). ^{13}C NMR (151 MHz, methylene chloride-d_2; *ppm*): δ = 184.46 (CO), 182.00 (CO), 132.13, 128.89, 127.95 (Ar), 95.76 (CH). ^{103}Rh NMR (18 MHz, methylene chloride-d_2; *ppm*): δ = 292.2.

3.3.17 Synthesis of (acetylacetonato-κ^2O,O)carbonyl-tri(o-tolyl)phosphine- rhodium(I), [Rh(acac)(CO)(P(otol)$_3$)]

[Rh(acac)(CO)$_2$] (0.020 g, 0.077 mmol) was dissolved in diethyl ether to which tri(o-tolyl)phosphine (0.028 g, 0.093 mmol) was added, resulting in the immediate evolution of gas. The solution was left to crystallize and yielded yellow needle-like crystals after one day. (**Yield**: 0.039 g, 97 %)

IR (ATR): ν_{CO} 1973 cm^{-1}. ^{1}H NMR (600 MHz, methylene chloride-d_2; *ppm*): δ = 7.40, 7.39, 7.38, 7.24, 7.23, 7.22 (m, 12H, Ar), 5.40 (s, 1H, CH), 2.29 (s, 9H, 3 x CH_3), 2.03 (s, 3H, CH_3), 1.47 (s, 3H, CH_3). ^{13}C NMR (151 MHz, methylene chloride-d_2; *ppm*): δ = 187.40 (CO), 131.99, 130.47, 125.80 (Ar), 100.20 (CH), 27.21 (CH_3), 26.51 (CH_3), 23.23 (CH_3). ^{31}P NMR (242.99 MHz, methylene chloride-d_2; *ppm*): δ = 45.40 (d, J_{Rh-P} 173.6 Hz).

3.4 Discussion

This study set out to synthesize and characterize a range of novel rhodium(I) complexes with different coordinating β-diketone ligands. In general the synthetic procedures adopted to produce these rhodium(I) complexes were uncomplicated and led to the successful synthesis of the planned compounds. Scheme 3.4 illustrates the general synthetic procedure followed in obtaining the different rhodium(I) complexes.

One challenge that was encountered during the synthesis was the difficulty in obtaining crystals of sufficient quality for study by single crystal X-ray diffraction. Various crystallization methods had to be attempted in order to obtain suitable crystals. However, once the crystals of the different rhodium(I) complexes were harvested out of solution they remained stable in air for several months.

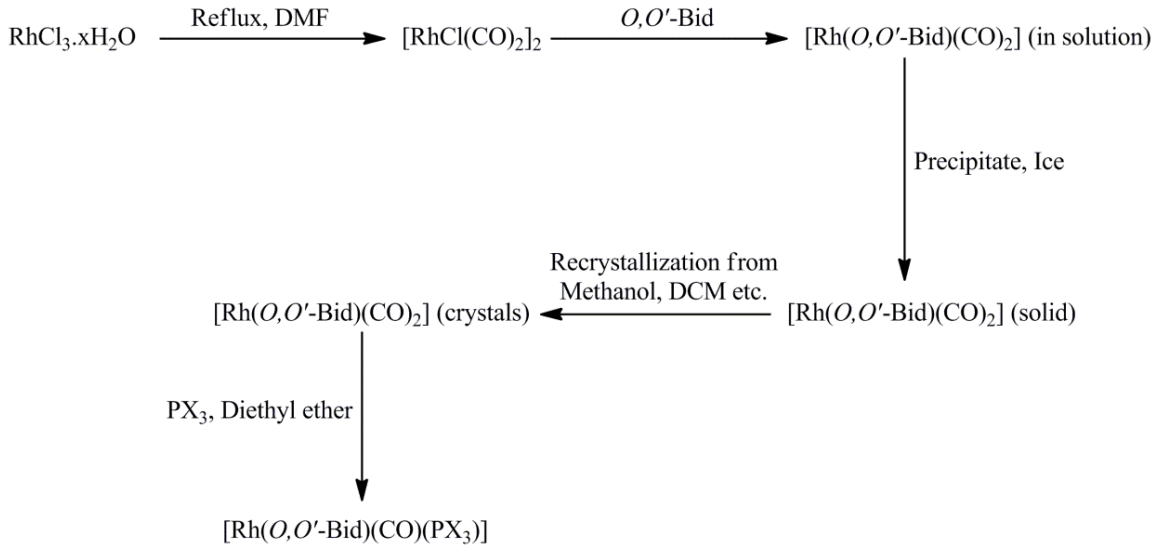

Scheme 3.4: Schematic representation of the general synthetic procedure followed to obtain [Rh(*O,O'*-Bid)(CO)$_2$] and [Rh(*O,O'*-Bid)(CO)(PX$_3$)] complexes with different coordinating β-diketonato ligands, PX$_3$ refers to phosphine ligands.

As mentioned in Section 3.1, the range of ligands chosen to coordinate to rhodium(I) were selected based on their varying electronic and steric properties. These ligands were chosen to evaluate whether the different substituents of the coordinating β-diketone ligand could extend their influence (electronic or steric) onto the metal centre. For example, trilfuoro moieties are well known for their electron withdrawing ability where as other ligands, such as those containing *t*-butyl groups increase the steric bulk of the coordinated rhodium(I) complex as well as being slightly electron donating.[6] Although more detail on the effect of these substituents within the resulting rhodium(I) complexes will be given in Chapters 4, 5 and 6, some trends were observed in respect to the characterization of the range of rhodium(I) complexes.

To illustrate some of these observed trends, a summary of the spectroscopic data for the different complexes synthesized is presented in Table 3.1. It was observed that as the pK_a value of the free ligands decreased, the ν_{CO} stretching frequencies of the coordinated rhodium(I) complexes generally increased. For example, the pK_a of the free ligand 2,2,6,6-tetramethyl-3,5-heptanedione (dipivH, pK_a= 11.77) is much larger than the pK_a of 1,1,1-trifluoro-5,5-dimethyl-2,4-hexanedione (pivH, pK_a= 6.99). In contrast the carbonyl stretching

[6] Peters, G. J., *Deoxynucleoside Analogs in Cancer Therapy*, Humana Press, New Jersey, **2006**, 364.

frequencies for [Rh(dipiv)$(CO)_2$] ($\nu_{CO(asym)}$ 1996 cm^{-1}; $\nu_{CO(sym)}$ 2066 cm^{-1}) was found to be much lower than those found for [Rh(piv)$(CO)_2$] ($\nu_{CO(asym)}$ 2024 cm^{-1}; $\nu_{CO(sym)}$ 2082 cm^{-1}).

Table 3.1: Summary of the spectroscopic data for the synthesized rhodium(I) complexes, [Rh(*O,O'*-Bid)$(CO)_2$]

Complex	pK_a of free ligand	$\nu CO_{(asym),\ (sym)}$ (cm^{-1})	^{103}Rh NMR chemical shift (ppm)	λ_{max} (nm)
[Rh(dipiv)$(CO)_2$]	11.77[7]	1996, 2066	270.2	331
[Rh(dbm)$(CO)_2$]	9.35[7]	1986, 2076	292.2	394
[Rh(acac)$(CO)_2$]	8.95[7]	1995, 2062	284.2	382
[Rh(bzac)$(CO)_2$]	8.7[8]	1999, 2066	284.0	379
[Rh(pyruv)$(CO)_2$]	8.35[9]	2013, 2064	311.1	370
[Rh(F_3-4Clbzac)$(CO)_2$]	7.55[10]	2028, 2077	325.1	384
[Rh(piv)$(CO)_2$]	6.99[11]	2024, 2083	306.8	353
[Rh(3Cl-acac)$(CO)_2$]	6.77[12]	2020, 2078	297.7	366
[Rh(F_3-bzac)$(CO)_2$]	6.3[7]	2024, 2084	320.4	371
[Rh(tfac)$(CO)_2$]	6.3[7]	2015, 2082	319.2	305
[Rh(acacac)$(CO)_2$]*	-	1994, 2066	-	330
[Rh(hfac)$(CO)_2$]	4.6[7]	2034, 2094	357.5	315
[Rh(CN-acac)$(CO)_2$]*	-	2011, 2074	294.2	353
[Rh(naphth)$(CO)_2$]*	-	2011, 2078	-	394

* No data available on pK_a values for the free ligands.

Higher wavenumbers in the infrared stretching frequencies of carbonyl bonds typically suggest weaker bonds caused by a decrease in the π-back donation from the CO bond to the metal centre. This would suggest that as the pK_a value of the free ligands is decreased, less electron density is available at the metal centre for bonding with the carbonyl groups. It must also be noted that the lower pK_a values given in Table 3.1 are associated with ligands containing electron withdrawing groups such as those found in [Rh(tfac)$(CO)_2$] and [Rh(3Cl-acac)$(CO)_2$].

Another observation that was made for the range of rhodium(I) complexes were that the absorbance maxima in DMF solutions revealed maxima within a similar wavelength range (305-394 nm) and all appeared yellow in solution. This was interesting as the solid state

[7] Ebenebe, P., *MSc Dissertation*, University of the Free State, Bloemfontein, South Africa, **1998**, 121.
[8] Watarai, H., Takahashi, I., *Anal. Commun.*, **1998**, *38*, 289-292.
[9] Methyl-2,4-dioxopentanoate (CAS: 20577-61-1), http://en.chembase.cn/molecule-54218.html, accessed: 26-05-15 (Calculated pK_a value).
[10] 1-(4-Chlorophenyl)-4,4,4-trifluorobutane-1,3-dione (CAS: 18931-60-7), http://en.chembase.cn/molecule-34967.html, accessed: 26-05-15 (Calculated pK_a value).
[11] Canada-Vilalta, C., Huffman, J. C., Christou, G., *Polyhedron*, **2001**, *20*, 1785-1793.
[12] 3-Chloro-2,4-pentanedione (CAS: 1694-29-7), http://www.scbt.com/datasheet-251987-3-chloro-2-4-pentanedione.html, accessed: 26-05-15 (Calculated pK_a value).

colouration of many of these compounds were found to differ significantly. For [Rh(acac)$(CO)_2$] crystals (**3.3.3**) a green-red dichroic colour was noted and for [Rh(piv)$(CO)_2$] (**3.3.4**) a green-purple product was observed. [Rh(dbm)$(CO)_2$] (**3.3.16**) crystals were found to be yellow-orange and the [Rh(bzac)$(CO)_2$] (**3.3.12**) crystals to be orange-green. As was discussed in Chapter 2, dichroic effects are often attributed to metallophilic interactions within rhodium(I) structures (Section 2.4.5). From these colour observations it was suspected that some of the synthesized complexes could exhibit metallophilic interactions (see Chapters 4, 5 and 6).

Upon closer examination of the colours exhibited by the different rhodium(I) complexes it was noted that complexes containing aliphatic substituents on the coordinating β-diketone ligands exhibited a red to purple hue in the solid state. In contrast, those complexes containing aromatic substituents on the coordinated β-diketonato ligands were orange or yellow coloured.

The different colouration properties of the solution *vs.* solid-state of these rhodium(I) complexes could suggest that an arrangement adopted by the molecules within the solid-state results in the different colours exhibited by these compounds. Upon dissolving the rhodium(I) complexes the arrangement of molecules may be disrupted and result in all of the rhodium(I) complexes to exhibit a yellow colour. The connection between the colour of the different complexes and their solid-state structures will be discussed further in Chapter 8.

A correlation was also noted between the pK_a values of the free ligands and the ^{103}Rh NMR chemical shifts of the different coordinated rhodium(I) complexes (Table 3.1). Figure 3.1 provides an illustration of this relationship where an increase in pK_a of the free ligand can be seen to lead to a general decrease of the ^{103}Rh NMR chemical shifts for the different complexes. A lower chemical shift value in NMR (up field) is associated with an increase of shielding experienced by the nucleus. This means that if electron density is increased around the rhodium(I) centre an increase in shielding is expected that leads to a lower chemical shift (up field).

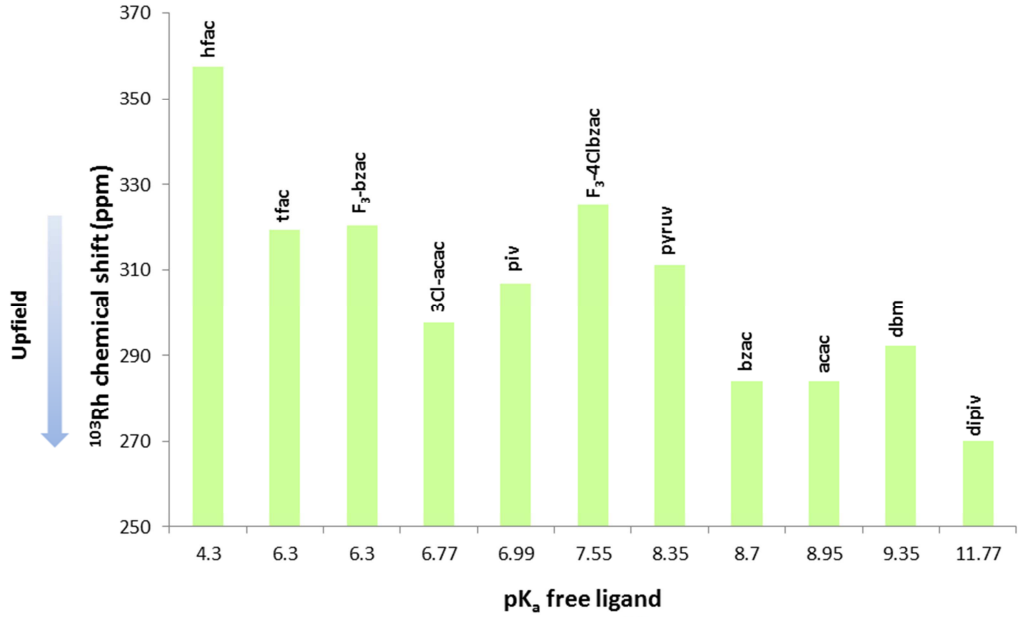

Figure 3.1: Illustration of the relationship between the ^{103}Rh chemical shifts of the rhodium(I) complexes and the pK$_a$ values of the uncoordinated β-diketone ligands.

A relationship was also noted between the ^{103}Rh chemical shifts and the CO stretching frequencies of the different rhodium(I) complexes. This relationship is illustrated for the asymmetric CO stretching frequency in Figure 3.2 and for the symmetric CO stretching frequency (Figure 3.3). As can be seen from Figure 3.2 and 3.3 an increase in stretching frequency is generally associated with an increase in ^{103}Rh chemical shift value. As this was not considered a strong correlation with a lot of fluctuations between the different complexes, no further comparisons were pursued with other parameters evaluated in this study (see Chapter 8).

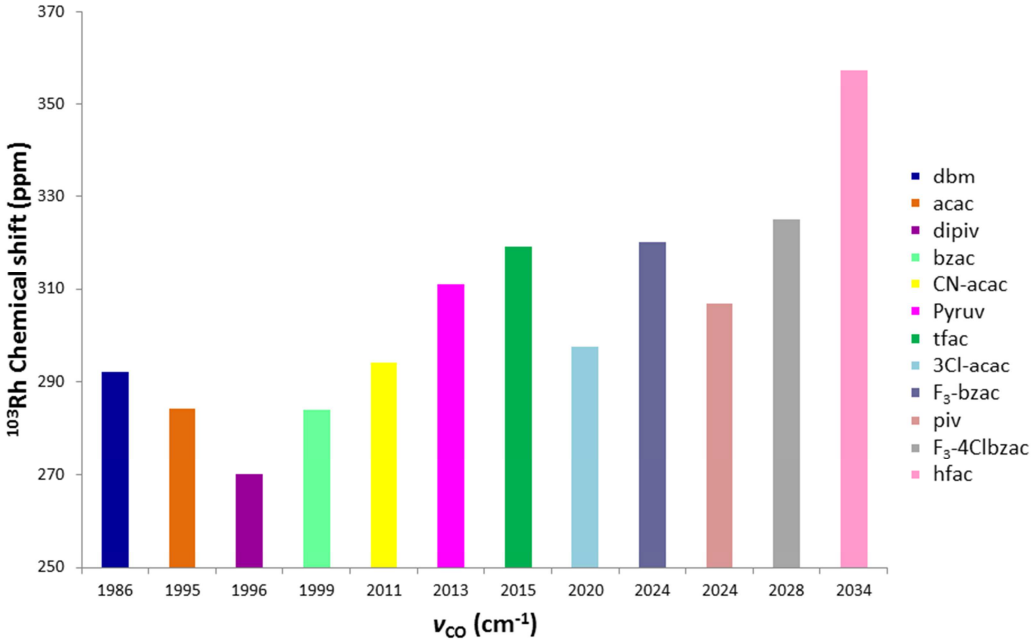

Figure 3.2: Illustration of the relationship between the ^{103}Rh chemical shifts and the asymmetric CO stretching frequencies ($\nu_{CO(asym)}$) of the rhodium(I) complexes.

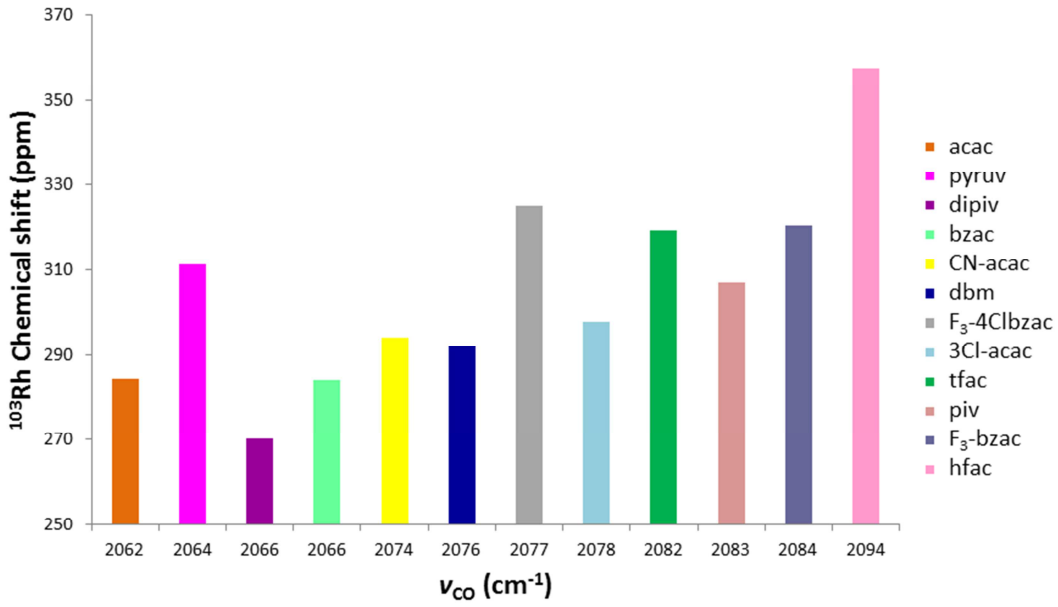

Figure 3.3: Illustration of the relationship between the ^{103}Rh chemical shifts and the symmetric CO stretching frequencies ($\nu_{CO(sym)}$) of the rhodium(I) complexes.

Interesting to note, is also the absence of any stretching frequencies between 2000-2011 cm^{-1} (Figure 3.2) and 2066-2074 cm^{-1} (Figure 3.3). The group of rhodium(I) complexes found above the 2011 cm^{-1} range (Figure 3.2) contain highly electron withdrawing groups such as trifluoro or methoxy moieties on the β-diketonato backbone. The same was observed for the complexes with symmetric CO stretching frequencies above 2074 cm^{-1}. These rhodium(I) complexes all contained a trifluoro moiety with the exception of the [Rh(dbm)(CO)$_2$] complex. This would suggest that the presence of electron withdrawing groups on the coordinated β-diketonato ligand could exert an influence on the strength of the carbonyl bonds within the rhodium(I) complexes.

3.5 Conclusion

The successful synthesis and characterization of a range of rhodium(I) complexes was discussed in this chapter. Some general comments were presented on the synthetic procedures as well as the stability of the complexes. Observations were made upon investigating some of the data obtained from spectroscopic characterization with regards to the ^{103}Rh chemical shifts as well as the carbonyl stretching frequencies of the rhodium(I) complexes.

As mentioned in Section 3.4, several of the syntheses were successful in yielding a number of crystals that were suitable for single crystal X-ray diffraction. The solid state structures obtained from the X-ray diffraction studies of these crystals will be presented in Chapters 4, 5 and 6.

Chapter 4: Crystallographic Study of [Rh(bzac)(CO)$_2$], [Rh(F$_3$-bzac)(CO)$_2$], [Rh(F$_3$-4Clbzac)(CO)$_2$] and [Rh(dbm)(CO)$_2$]

4.1 Introduction

As discussed in Chapter 2 some transition metals are known to display unique metallophilic interactions with the potential to be manipulated in the design of functional nano-materials. This chapter will focus on the crystal structures of four novel rhodium(I) complexes obtained in the study that displayed these metallophilic interactions. The coordinating *O,O'* β-diketone ligands used to coordinate to rhodium were specifically selected for their subtle electronic and steric differences. The different coordinating β-diketonato ligands were chosen to evaluate the influence of an alternating environment on the Rh(I) centre and ultimately, if any, on the metallophilic interactions. The four coordinating ligands that were utilized in coordination to rhodium(I) of which the solid-state structures will be discussed in this Chapter are illustrated in Scheme 4.1.

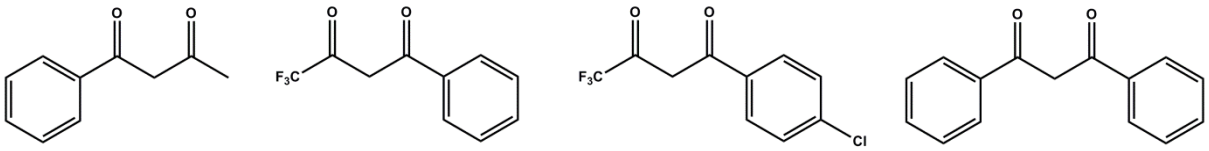

3-Benzoylacetone **(bzacH)**

4,4,4-Trifluoro-1-phenyl-1,3-butanedione **(F_3-bzacH)**

1-(4-Chlorophenyl)-4,4,4-Trifluoro-1,3-butanedione **(F_3-4ClbzacH)**

Dibenzoylmethane **(dbmH)**

Scheme 4.1: Different β-diketone ligands chosen to coordinate to rhodium(I) to facilitate metallophilic interactions between the metal centres.

This chapter will focus on the structural data of the above mentioned complexes with a focus on general molecular geometry and intermolecular interactions that contribute to the stability of the crystal packing. Geometric parameters such as the different bond distances and angles in the molecules will also be highlighted. The dihedral angle which will be referred to in this Chapter is defined as the angle between the phenyl ring and the O-C-C-C-O backbone of the β-diketonato ligand as illustrated in Scheme 4.2.

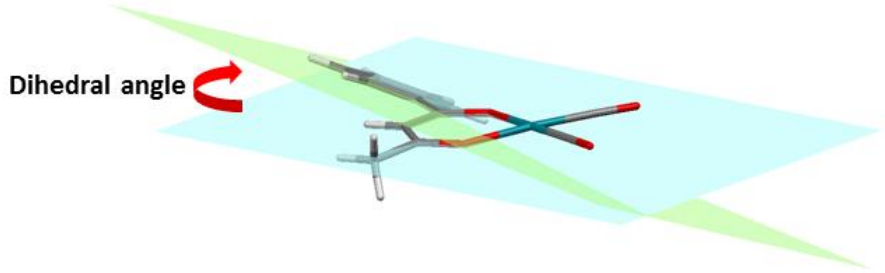

Scheme 4.2: Representation of how the dihedral angle was defined for the [Rh(bzac)(CO)$_2$], [Rh(F$_3$-bzac)(CO)$_2$], [Rh(4Cl-F$_3$bzac)(CO)$_2$] and [Rh(dbm)(CO)$_2$] solid state structures.

4.2 Experimental

The reflection data of [Rh(bzac)(CO)$_2$], [Rh(F$_3$-bzac)(CO)$_2$], [Rh(F$_3$-4Clbzac)(CO)$_2$] and [Rh(dbm)(CO)$_2$] were collected on a Bruker X8 Apex II 4K Kappa CCD diffractometer using graphite monochromated Mo Kα radiation (λ= 0.70926 Å) with ω- and φ-scans at 100(2) K. The Apex II software package[1] was utilized along with the optimum measurement method in collecting more than a hemisphere of reciprocal space as predicted by COSMO.[2] Frame integration and data reduction was performed using the SAINT-Plus and XPREP software packages and SADABS[3] was made use of for multi-scan absorption correction.[4] The structures were solved using SIR92[5], SIR97[6], SIR2002[7], DIRDIF[8] or Superflip[9] with refinement performed using the WinGX software package[10] that incorporates SHELXL[11]. All atoms were refined anisotropically with the exception of hydrogen atoms. The hydrogen atoms were positioned geometrically and refined utilizing a riding model with fixed C-H distances of 0.95 Å (CH) [U_{iso}(H)= 1.2 Ueq] for aromatic hydrogens and methyl H-atoms fixed at 0.98 Å (CH) [U_{iso}(H)= 1.2 Ueq]. Molecular diagrams were generated with the Mercury software package[12] with a 50 % thermal ellipsoid probability for all non-hydrogen atoms. General crystal data and refinement parameters are represented in Table 4.1 with the

[1] **Apex2**, Version 2012.10-0, Bruker AXS Inc.,Madison, Wisconsin, USA, **2012**.
[2] **COSMO**, Version 1.48, Bruker AXS Inc., Madison, Wisconsin, USA, **2003**.
[3] **SADABS**, Version 2012/1, BrukerAXS Inc, Madison, Wisconsin, USA, **2012**.
[4] **SAINT-Plus**, Version 8.27B including XPREP, Bruker AXS Inc., Madison, Wisconsin, USA, **2012**.
[5] Altomare, A., Cascarano, G., Giacovazzo, C., Guagliardi, A., Burla, M. C., Polidori, G., Camalli, M., *J. Appl. Cryst.*, **1994**, *27*, 435-436.
[6] Altomare, A., Burla, M. C., Camalli, M., Cascarano, G. L., Giacovazzo, C., Guagliardi, A., Moliterni, A. G. G., Polidori, G., Spagna, R., *J. Appl. Cryst.*, **1999**, *32*, 115-119.
[7] Burla, M. C., Camalli, M., Carrozzini, B., Cascarano, G. L., Giacovazzo, C., Polidori, G., Spagna, R., *J. Appl. Cryst.*, **2003**, *36*, 1103.
[8] Beurskens, P. T., Admiraal, G., Beurskens, G., Bosman, W. P., Garcia-Granda, S., Gould, R. O., Smits, J. M. M., Smykalla, C., Crystallography Laboratory, University of Nijmegen, Toernooiveld, The Netherlands.
[9] Palatinus, L., Chapuis, G., *J. Appl. Cryst.*, **2007**, *40*, 786-790.
[10] **WinGX**. Farrugia, L. J., *J. Appl. Cryst.*, **2012**, *45*, 849–854.
[11] Sheldrick, G. M., *Acta Cryst.*, **2008**, *A64*, 112-122.
[12] **Mercury**, Macrae, C. F., Bruno, I. J., Chisholm, J. A., Edgington, P. R., McCabe, P., Pidcock, E., Rodriquez-Monge, L., Taylor, R., van de Streek, J., Wood, P. A., *J. Appl. Cryst.*, **2008**, 41, 466-470.

complete list of atomic coordinates, equivalent isotropic parameters and hydrogen coordinates of each data set given in Appendix A.

Table 4.1: General crystal data for [Rh(bzac)(CO)$_2$], [Rh(F$_3$-bzac)(CO)$_2$], [Rh(F$_3$-4Clbzac)(CO)$_2$] and [Rh(dbm)(CO)$_2$].

Crystallographic Data	[Rh(bzac)(CO)$_2$]	[Rh(F$_3$-bzac)(CO)$_2$]	[Rh(F$_3$-4Clbzac)(CO)$_2$] i	[Rh(F$_3$-4Clbzac)(CO)$_2$] ii	[Rh(dbm)(CO)$_2$]
Empirical Formula	$C_{12}H_9O_4Rh$	$C_{12}H_6F_3O_4Rh$	$C_{12}H_5ClF_3O_4Rh$	$C_{12}H_5ClF_3O_4Rh$	$C_{17}H_{11}O_4Rh$
Molecular weight (g/mol)	320.10	374.08	408.52	408.52	382.17
Crystal system, space group	Monoclinic, $P2_1/c$	Orthorhombic, *Pbca*	Orthorhombic, $P2_12_12_1$	Triclinic, $P\bar{1}$	Orthorhombic, $P22_12_1$
a (Å)	7.5887(2)	7.016(4)	6.936(1)	7.080(3)	7.0256(2)
b (Å)	6.7522(1)	11.733(8)	17.116(3)	12.567(6)	19.281(5)
c (Å)	22.5299(5)	30.095(3)	46.121(7)	17.308(8)	21.656(5)
α (°)	90.0	90.0	90.0	72.24(2)	90
β (°)	98.850(1)	90.0	90.0	88.67(1)	90
γ (°)	90.0	90.0	90.0	76.03(1)	90
Volume (Å^3)	1140.70(4)	2477(2)	5475(3)	1421.1(1)	2933.4(2)
Z	4	8	16	4	8
Density calculated (g/ cm^3)	1.864	2.006	1.983	1.909	1.731
Absorption coefficient (mm^{-1})	1.495	1.426	1.489	1.434	1.179
***F* (000)**	632	1456	3168	2760	1520
Crystal size (mm^3)	0.19 x 0.09 x 0.05	0.119 x 0.128 x 0.509	0.498 x 0.246 x 0.209	0.119 x 0.310 x 0.903	0.221 x 0.321 x 0.628
Morphology, colour	Needle, orange	Needle, orange	Needle, orange	Cuboid, orange	Needle, yellow
Θ range for data collection	2.7 to 28.3	3.45 to 28.0	2.65 to 28.0	2.48 to 27.99	3.01 to 28.29
Completeness for collection (%)	99.9	99.9	99.7	99.7	99.8
Index ranges	-10≤ *h* ≥10 -9≤ *k* ≥8 -29≤ *l* ≥30	-9≤ *h* ≥9 -15≤ *k* ≥15 -39≤ *l* ≥39	-9≤ *h* ≥8 -22≤ *k* ≥22 -60≤ *l* ≥60	-9≤ *h* ≥9 -16≤ *k* ≥16 -22≤ *l* ≥22	-9≤ *h* ≥9 -25≤ *k* ≥25 -28≤ *l* ≥28
Reflections collected	15332	38994	79926	38429	96056
Independent reflections	2827	2990	12980	6346	7095
Observed reflections	2497 (R_{int}= 0.020)	2071 (R_{int}= 0.1234)	11157 (R_{int}= 0.0725)	4076 (R_{int}=0.1350)	6690 (R_{int}= 0.0643)
Max. and min. transmission	0.851 and 0.982	0.839 and 0.981	0.524 and 0.746	0.105 and 0.622	0.812 and 0.953
Data/ restraints/ parameters	2827/ 0/ 154	2990/ 0/ 182	12980/ 0/ 765	6346/ 0/ 333	7095/ 0/ 392
Goodness-of-fit on F^2	1.08	1.036	1.071	1.323	1.069
Final R indices	R1= 0.0184 wR2= 0.0485	R1= 0.0414 wR2= 0.0812	R1= 0.0440 wR2= 0.0783	R1= 0.1453 wR2= 0.3535	R1= 0.0225 wR2= 0.0509
R indices	R1= 0.0219 wR2= 0.0515	R1= 0.0706 wR2= 0.0909	R1= 0.0567 wR2= 0.0834	R1= 0.1799 wR2= 0.3878	R1= 0.0250 wR2= 0.0524
Largest diff. Peak and hole (e.Å^{-3})	0.04 and -0.17	0.68 and -0.99	1.07 and -0.97	1.83 and -1.18	0.97 and -0.60

4.3 Crystal Structure of [Rh(bzac)(CO)$_2$]

The complex, (3-benzoylacetonato-κ^2O,O')dicarbonylrhodium(I), crystallized in the monoclinic space group $P2_1/c$ having only one independent molecule in the asymmetric unit. The molecular structure as well as the numbering scheme is represented in Figure 4.1. General crystallographic information pertaining to the crystal structure is referred to in Table 4.1 and selected bond lengths and angles are given in Table 4.2. For comprehensive information regarding bond distances and angles related to the structure refer to Appendix A.

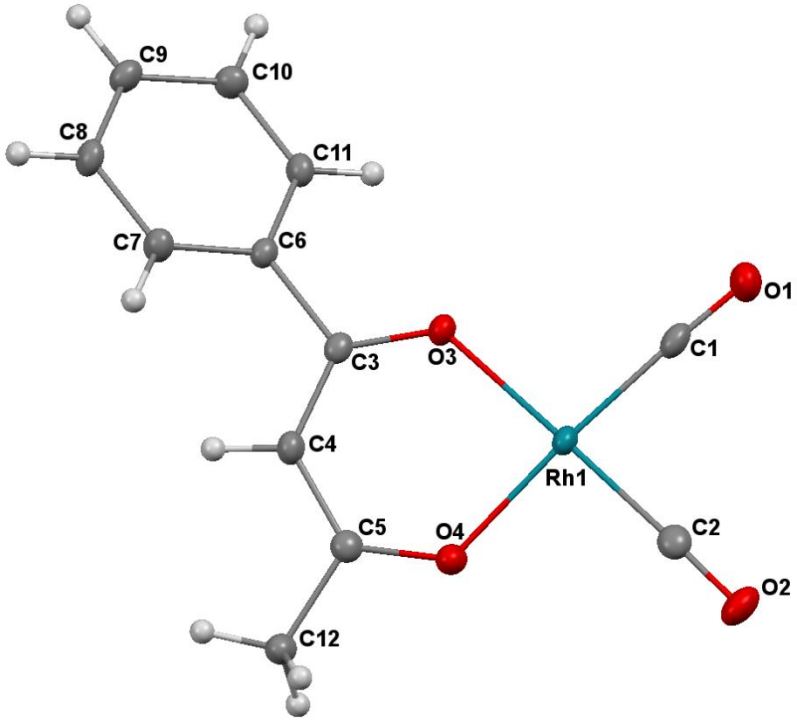

Figure 4.1: Molecular structure of [Rh(bzac)(CO)$_2$] with atom numbering scheme (thermal ellipsoid probability= 50 %). Hydrogen atom labels have been omitted for clarity.

Table 4.2: Selected bond distances and angles of [Rh(bzac)(CO)$_2$].

Atoms	Distance (Å)
Rh1-C1	1.854(2)
Rh1-C2	1.848(2)
Rh1-O3	2.050(1)
Rh1-O4	2.035(1)
C1-O1	1.139(2)
C2-O2	1.138(2)
C3-O3	1.284(2)
C5-O4	1.278(2)
O3···O4[a]	2.904(3)

[a] Bite distance

Atoms	Angle (°)
C1-Rh1-C2	87.98(7)
O3-Rh1-O4	90.62(5)
C1-Rh1-O4	175.86(6)
C2-Rh1-O3	179.13(6)
C3-C4-C5	126.5(1)
C1-Rh1-O3	92.87(6)
C2-Rh1-O4	88.53(6)
C3-O4···C5-O4[b]	177.23(2)
C4-Rh1(1)···C4-Rh1(2)[c]	180.0(2)
Dihedral Angle[d]	24.90(3)

[b] Torsion angle between C3-O4 and C5-O4; [c] Torsion angle between C4-Rh1 and C4-Rh1 of neighbouring molecules; [d] defined as the torsion angle between the O4-C3-C4-C5-O4 plane and the phenyl ring (see scheme 4.2)

The square planar geometry exhibited by the complex consists of the rhodium centre coordinated to two carbon atoms from *cis* orientated carbonyl groups and two oxygen atoms from a coordinated β-diketonato ligand. This geometry is favoured by Rh(I) complexes as well as other complexes containing transition metals with a d^8 electron configuration.[13] The angles between the rhodium centre and coordinated atoms however showed distortion from the ideal geometry of the predicted 90° angles. This distortion is illustrated with measured angles in Figure 4.2.

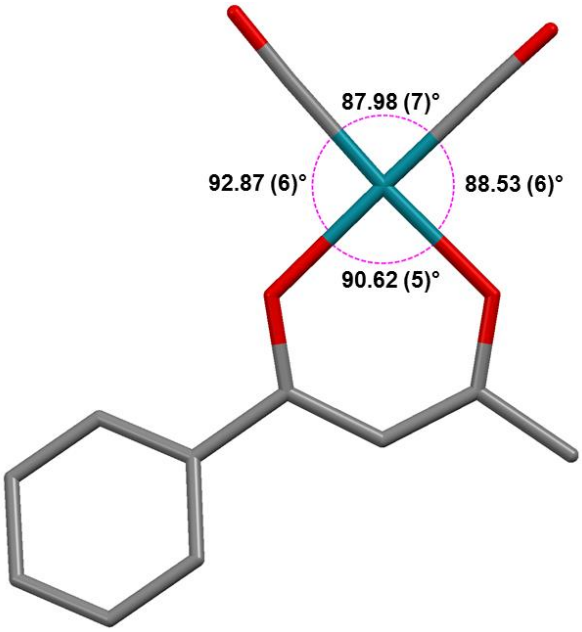

Figure 4.2: Represenation of the distortion of angles as observed in the square planar geometry of [Rh(bzac)(CO)$_2$].

All of the atoms except for the phenyl substituent group of the benzoylacetonato ligand were found to be intersected by an equatorial plane constructed through atoms C1, C2, O3 and

[13] Janes, R., Moore, E., *Metal-Ligand Bonding*, The Open University, Bath Press, Bath, United Kingdom, **2004**, 31.

O4. A dihedral angle of 24.90(3)° between the phenyl ring and plane constructed of O3-C3-C4-C5-O4 atoms was noted.

A geometry search by the crystallographic database MOGUL[14] on the Rh1-C1 and Rh1-C2 bond lengths of 1.854(2) Å and 1.848(2) Å revealed that the bonds were well in the range for carbonyl bond lengths as reported in the CSD[15] with an average reported Rh-C bond length of 1.848 Å. The C1-O1 and C2-O2 bond lengths were determined as 1.138(2) Å and 1.139(2) Å and were also in good agreement with the average bond distance of 1.137 Å reported for this bond type in the CSD[15].

Metallophilic interactions between neighbouring Rh(I) centres are encountered in [Rh(bzac)$(CO)_2$]. The metal centres in the chain displayed alternating rhodium-rhodium distances. As illustrated in Figure 4.4 the alternating Rh···Rh distances of 3.308(3) Å and 3.461(3) Å are repeated indefinitely throughout the crystal lattice. These interactions induce a pseudo-octahedral geometry of sort around each rhodium centre as shown in Figure 4.5 and render an increased dimensionality to the molecule by effectively creating a 1-D chain of metal centres. Additionally, it was noted that the Rh···Rh interaction occurred along the *b*-axis which is the shortest reported cell axis (6.7522(1) Å) in the unit cell. This is consistent with literature reports that metallophilic interactions occur along the shortest cell axis.[16]

Metallophilic interactions are typically classified as being shorter than the sum of the Van der Waals radii between the two metal centres.[17] Unfortunately, for rhodium no Van der Waals radius has been determined and as such no comparison can be made to literature values as opposed to other PGM metals such as Pt or Au.[18] The question thus arises of whether the contacts evaluated can be classified as a formal interaction or whether a dimeric structure is formed with weak Rh-Rh bonds. A MOGUL[14] geometry check on the Rh···Rh interaction revealed that the accepted distance for formal Rh-Rh bonds are approximately in the ~3.1 Å range which implies that the longer Rh···Rh distances measured in the structure cannot be classified as a formal bond but rather as interactions.

[14] **MOGUL**: Retrieval of Crystallographically-Derived Molecular Geometry Information, Bruno, I. J., Cole, J. C., Kessler, M., Luo, J., Motherwell, W. D. S., Purkis, L. H., Smith, B. R., Taylor, R., Cooper, R. I., Harris, S. E., Orpen, A. G., *J. Chem. Inf. Comput. Sci.*, **2004**, *44*, 2133-2144.
[15] **Cambridge Structural Database** (CSD), Version 5.35, November 2013 update. Allen, F. H., *Acta Cryst.*, **2002**, *B58*, 380-388.
[16] Pretorius, C, Roodt, A., *Acta Cryst.*, **2012**, *E68*, m1451-m1452.
[17] Pyykkö, P., *Chem. Rev.*, **1997**, *97*, 597-636.
[18] Doerrer, L. H., *Dalton Trans.*, **2010**, *39*, 3543-3553.

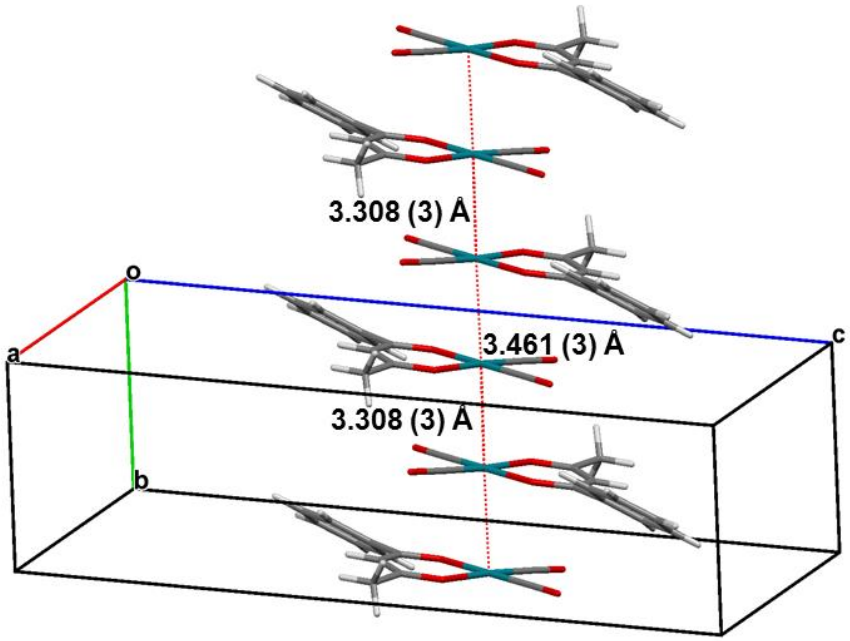

Figure 4.4: Rh···Rh interactions (indicated in red) are observed between neighbouring molecules of [Rh(bzac)(CO)$_2$] to form a one-dimensional metallic chain along the *b*-axis.

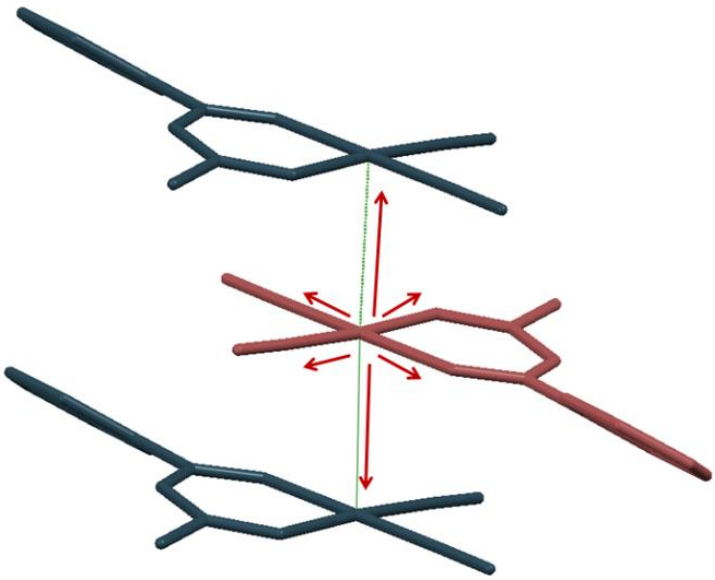

Figure 4.5: The Rh···Rh interactions observed in [Rh(bzac)(CO)$_2$] create a pseudo-octahedral geometry in the complex.

The Rh-Rh distances of 3.308(3) Å and 3.461(3) Å were slightly longer than those reported in literature for [Rh(acac)(CO)$_2$] (3.253 Å and 3.271 Å) (see also Chapter 5).[19] A possible explanation for the increased distance of the short contact could be due to the electron withdrawing effect of the phenyl substituent on the coordinating β-diketonato ligand. As was discussed in Chapter 3 (Section 3.4) this would result in less electron density at the rhodium(I) centre and in turn less effective dz^2 overlap between neighbouring rhodium(I) centres. Th result being longer Rh···Rh interactions.

[19] Huq, F., Skapski, A., *J. Cryst. Mol. Struct.*, **1974**, *4*, 411-418.

Angles of 172.06(3)° between neighbouring rhodium centres (Rh-Rh-Rh) indicate a slight deviation from a perfectly linear arrangement of molecules along the 1-D chain as can be seen in Figure 4.6. Torsion angles between the β-diketonato groups coordinated to the rhodium centres measured 180.0(2)° in an eclipsed arrangement of R-groups in the 1-D chain (see Section 2.4.4, Chapter 2).

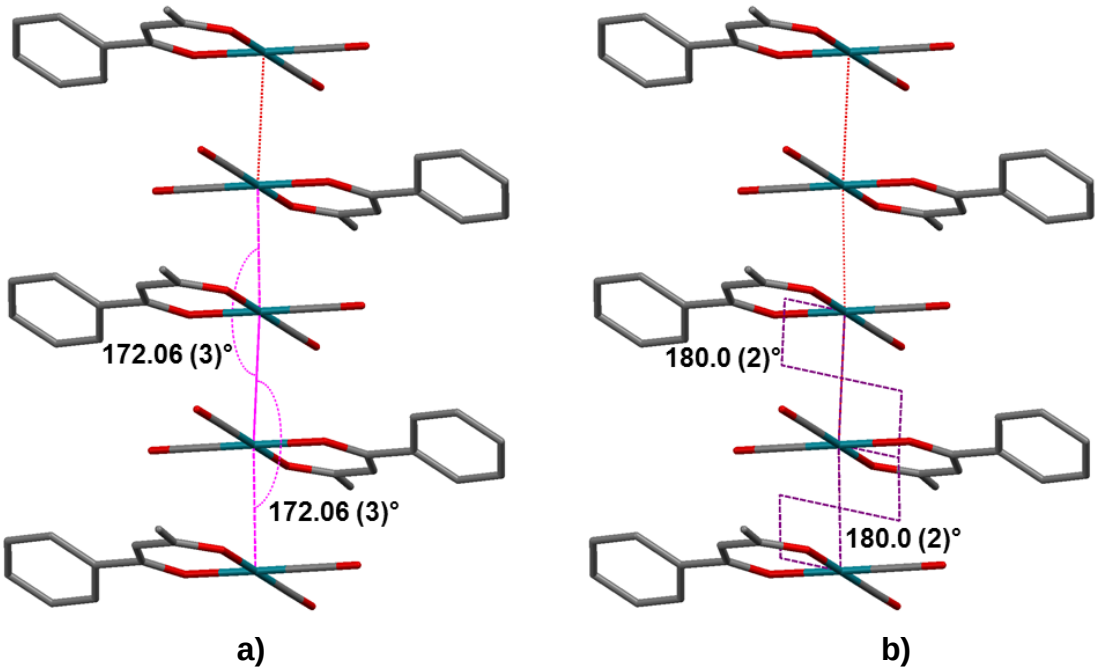

Figure 4.6: a) The angle between neighbouring Rh centres (172.06 (3)°) is repeated throughout the crystal structure in the infinite 1-D chains; b) Torsion angles of 180.0 (2)° between coordinating β-diketonato ligands revealed an eclipsed arrangement of R-groups in [Rh(bzac)(CO)$_2$].

Several other short contacts were observed in the [Rh(bzac)(CO)$_2$] structure with C-H interactions being the most prominent. One intermolecular hydrogen bond was observed between O4 and C12 of neighbouring molecules. The hydrogen bond as well as another soft contact involving the carbonyl group and a methyl hydrogen with C1-H12B determined as 2.718(3) Å is represented in Figure 4.7. Details of the hydrogen bond is summarized in Table 4.3. The illustrated hydrogen bond allows for the formation of a polymeric chain along the *a*-axis in a tail-to-tail motif as shown in Figure 4.8, contributing to the stability of the crystal lattice.

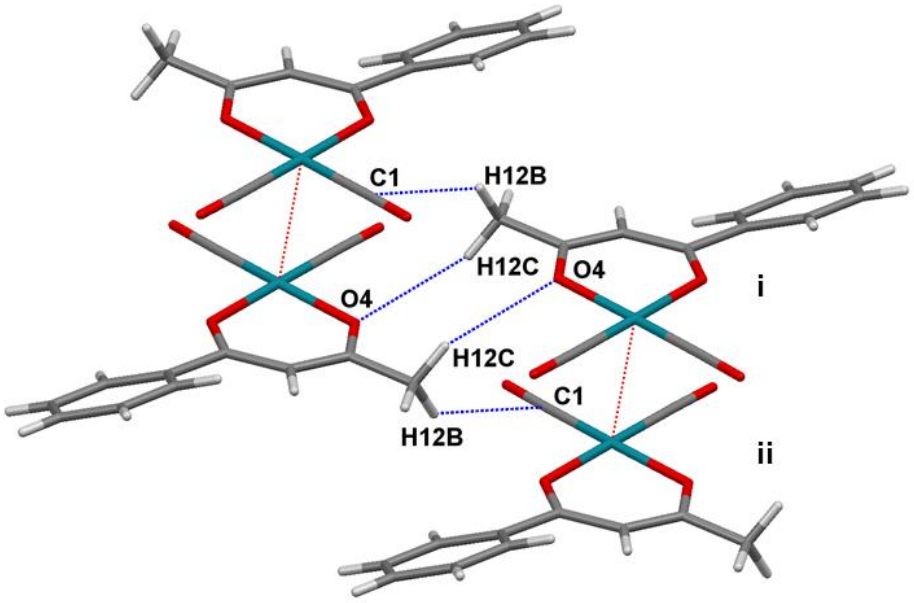

Figure 4.7: Graphical representation of the intermolecular hydrogen bond C12-H12C···O4^{i} (indicated in blue) as well as the soft contact H12B-C1^{ii} in [Rh(bzac)(CO)$_2$] (symmetry code: i) 1-x, -y, 1-z; ii) 1+x, y, z).

Table 4.3: Hydrogen-bond geometry for [Rh(bzac)(CO)$_2$].

D-H···A	dD-H (Å)	dH···A (Å)	dD···A (Å)	Angle D-H···A (°)
C12-H12C···O4^{i}	0.98	2.67	3.65(2)	155.78

Symmetry codes: i) 1-x, -y, 1-z.

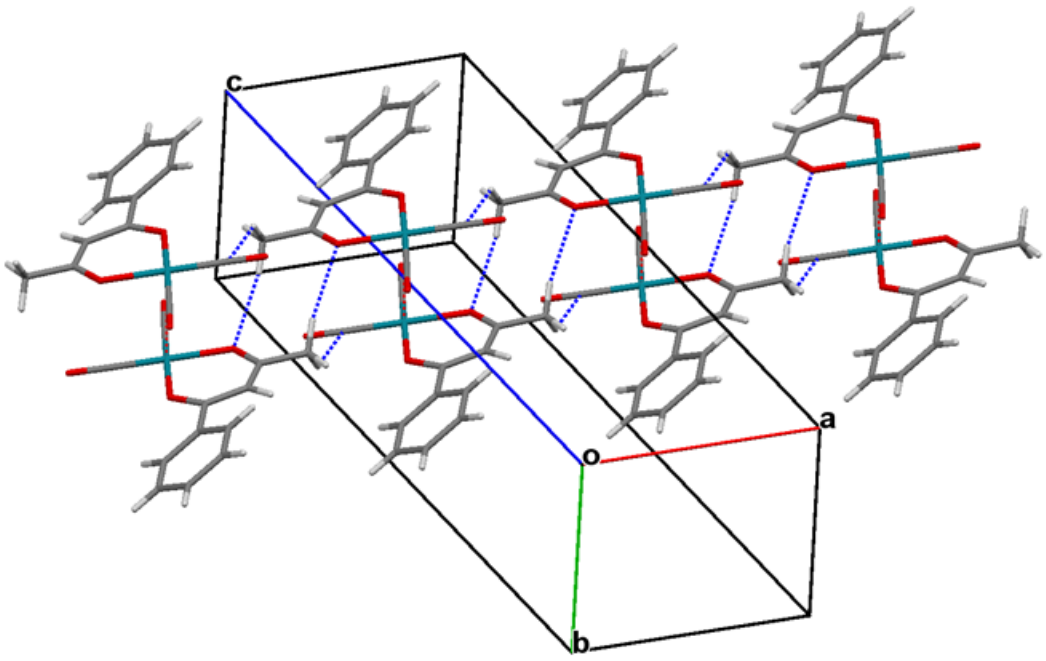

Figure 4.8: Hydrogen bonds in [Rh(bzac)(CO)$_2$] connect in a tail-to-tail motif between coordinated β-diketonato ligands to form a polymeric chain-like structure between neighbouring molecules along the *a*-axis.

The twisted phenyl group in [Rh(bzac)(CO)$_2$] (dihedral angle of 24.90(3)°, see Table 4.2) could possibly be attributed to some soft contacts (Van der Waals interactions) involving the

phenyl group. These interactions are found between different phenyl groups as well as the methine carbon and proton of neighbouring molecules. The H8-C4^{i} contact was determined as 2.794(2) Å and C9-H10^{ii} as 2.859(3) Å (symmetry codes: i) -x, ½+y, ½-z; ii) -1-x, -½+y, ½-z). These interactions are illustrated in Figure 4.9.

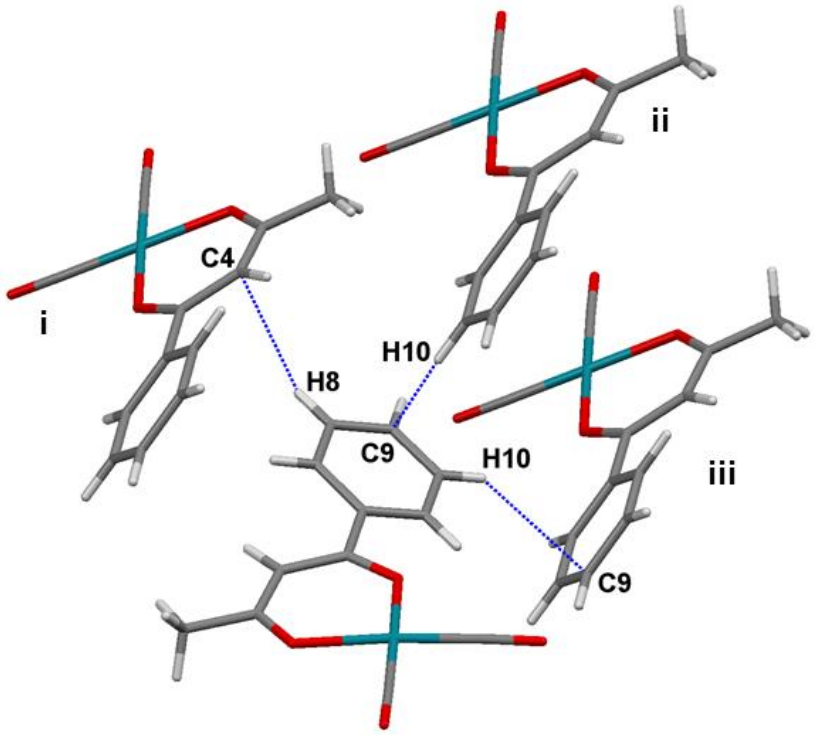

Figure 4.9: Graphical representation of soft contacts (indicated in blue) involving the phenyl ring substituent of the β-diketonato ligand possibly leading to distortion of the ring out of the horizontal plane in the square planar coordinating moiety. (Symmetry code: i) -x, ½+y, ½-z; ii) -1-x, -½+y, ½-z; iii) -1-x, ½+y, ½-z).

The packing for [Rh(bzac)(CO)$_2$] is dominated by the effect of the metallophilic interactions with packing in a head-to-head fashion between neighbouring molecules illustrated in Figure 4.10.

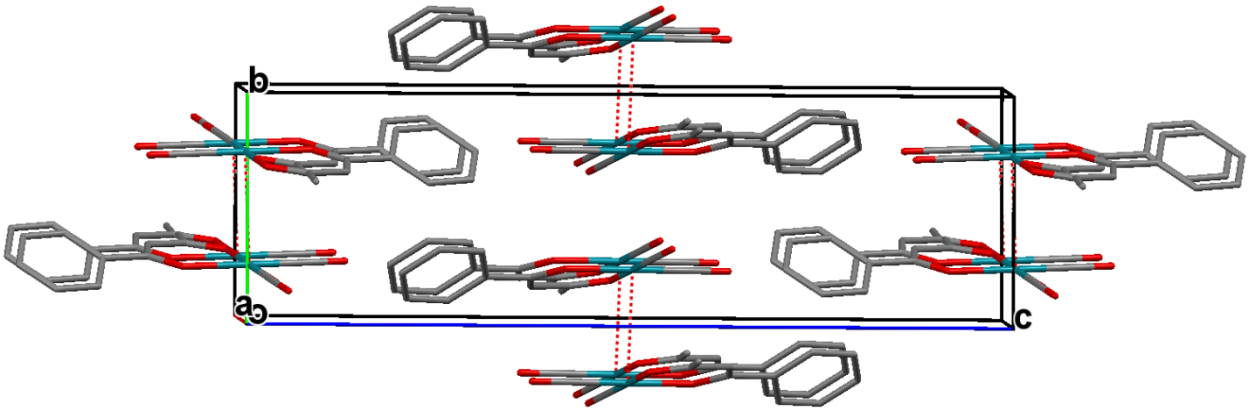

Figure 4.10: Packing of [Rh(bzac)(CO)$_2$] along an off-centered *a*-axis illustrating the dominating influence metallophilic interactions have on the packing of molecules within the crystal lattice.

4.4 Crystal Structure of [Rh(F_3-bzac)($CO)_2$]

This structure is a re-determination of the same complex that was published by Leipoldt *et al.*[20] in 1977. The published structure was a data collection at room temperature and the short communication paper offered very little information with regards to the reliability of the data as key factors such as completeness of the data collection and Goodness-of-Fit etc. could not be established. As such a re-determination of the structure was undertaken.

As was mentioned in Chapter 3 (Section 3.4) obtaining crystals of these rhodium(I) complexes proved rather difficult and as a result only a few crystals of relatively poor quality could be obtained from the synthesis of [Rh(F_3-bzac)($CO)_2$] (see Section 3.3.13, Chapter 3). The poor quality of crystals is reflected in the high R value of 12 % (see Table 4.1) for the data collection. The other data parameters such as the completeness of 99.9 % and a Goodness-of-Fit value of 1.036 indicated that a useful structure determination was still possible.

The unit cell dimensions of the published structure by Leipoldt *et al.*[20] are given in Table 4.4 for comparison to the dimensions of the structure determined in this study. As can be seen from the data no errors have been supplied on the unit cell dimensions of the published structure. The slight deviations observed for the unit cell dimensions as seen in Table 4.4 could possibly be attributed to the temperature at which the data collection was performed with room temperature collections typically resulting in an increase of lattice parameters with the lattice expanding anisotropically with an increase in temperature.[21]

Table 4.4: Comparison of the unit cell dimensions for the structure determined in this study as well as the published structure[20] of [Rh(F_3bzac)($CO)_2$].

Cell dimension	This Study	Published[20]
a	7.016(4)	7.047
b	11.733(8)	12.086
c	30.095(3)	30.486
α	90	90
β	90	90
γ	90	90
Space group	Orthorhombic, *Pbca*	Orthorhombic, *Pbca*
Z	8	8
Z'	1	1
Temperature (K)	100	298

The complex, (benzoyl-1,1,1-trifluoroacetonato-κ^2O,O')dicarbonylrhodium(I), crystallized in the orthorhombic space group *Pbca* with only one independent molecule in the asymmetric

[20] Leipoldt, J. G., Bok, L. D. C., Basson, S. S., van Vollenhoven, J. S., Gerber, T. I. A., *Inorganica Chimica Acta*, **1977**, *25*, L63-L64.
[21] Ohashi, Y., Burnham, C. W., *American Mineralogist*, **1973**, *58*, 843-849.

unit and 8 formula units in the unit cell. The molecular structure is represented in Figure 4.11 along with the atom numbering scheme with selected bond lengths and angles given in Table 4.5. Selected bond lengths and angles found for the published structure are included for comparison.

As can be seen from Table 4.5, the re-determined structure offers much more accurate information with regards to the bond distances and angles as is evident by the large esd values present on the data for the published structure of [Rh(F_3-bzac)($CO)_2$]. Large error values are not uncommon with data originating from several decades ago with the improvement of techniques and software in crystallography that has led to a reduction in the errors observed for data. Additionally, temperature effects could also account for some of the differences observed in the bond lengths and angles between the two structures. Elevated temperatures generally result in larger thermal parameters for atoms as the movement of atoms are less resitricted leading to an increase in reported bond lenghts and angles.[22]

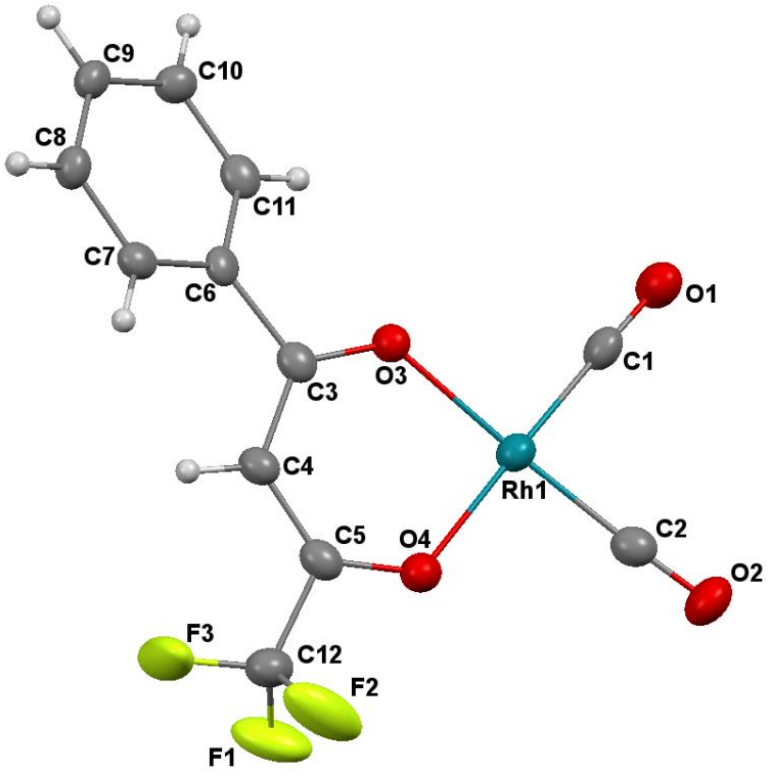

Figure 4.11: Molecular diagram of [Rh(F_3-bzac)($CO)_2$] with atom numbering scheme. Hydrogen atom numbering omitted for clarity. Thermal ellipsoids have been drawn at 50 % probability level.

[22] Müller, P., *Crystallography Reviews*, **2009**, *15*, 57-83.

Table 4.5: Selected bond distances and angles of [Rh(F_3-bzac)$(CO)_2$].

Atoms	This Study	Published[20]
	Distance (Å)	
Rh1-C1	1.832(5)	1.82(3)
Rh1-C2	1.854(4)	1.79(3)
Rh1-O3	2.043(3)	2.02(2)
Rh1-O4	2.030(4)	2.02(2)
C1-O1	1.143(6)	1.16(4)
C2-O2	1.133(5)	1.18(3)
C3-O3	1.270(5)	1.27(3)
C5-O4	1.281(5)	1.28(4)
C12-F3	1.320(6)	1.28(5)
O3···O4[a]	2.872(4)	2.85(3)

[a] Bite distance

Atoms	This Study	Published[20]
	Angle (°)	
C1-Rh1-C2	86.2(2)	87.0(1)
O3-Rh1-O4	89.7(1)	89.8(7)
C1-Rh1-O4	177.1(2)	178.4(2)
C2-Rh1-O3	177.0(1)	178.3(2)
C3-C4-C5	124.3(4)	119.2(2)
C1-Rh1-O3	92.1(1)	91.3(3)
C2-Rh1-O4	92.1(2)	91.9(2)
C3-O4···C5-O4[b]	177.17(3)	178.3(2)
C4-Rh1(1)···C4-Rh1(2)[c]	115.23(1)	114.3(3)
Dihedral angle[d]	23.18(4)	22.4(2)

[b] Torsion angle between C3-O4 and C5-O4; [c] Torsion angle between C4-Rh1 and C4-Rh1 of neighbouring molecules; [d] defined as the torsion angle between the O4-C3-C4-C5-O4 plane and the phenyl ring (see scheme 4.2).

As with the previous structure, the rhodium(I) complex once again displayed a square planar geometry with even greater distortion than that exhibited by the [Rh(bzac)$(CO)_2$] complex as is evident from the angles listed in Table 4.4. C1-Rh1-C2 was determined as 86.2(2)° in comparison to the same angle for [Rh(bzac)$(CO)_2$] given as 87.98(7)° (see Section 4.3). The C2-Rh1-O4 angle for the reported complex was determined as 92.1(2)° in comparison to 88.53(6)° for [Rh(bzac)$(CO)_2$]. Also of note is the difference in bond lengths for the carbonyl bonds with C1-O1 determined as 1.143(6) Å and C2-O2 as 1.133(5) Å. C1-O1 (1.143(6) Å) is slightly longer in comparison to the carbonyl bonds reported for [Rh(bzac)$(CO)_2$] (1.139(2) Å and 1.138(2) Å) with the electronic withdrawing influence of the *trans* located trifluoro substituent on the β-diketonato ligand contributing to the weakened bond.

A plane constructed through the coordinating moiety of C1, C2, O2 and O3 around the coordinative Rh(I) centre, in Figure 4.13, clearly showed that the atoms C1, C2, C3, C4, C5, C6 and C7 were all in the horizontal plane. The phenyl ring is however orientated out of the plane with a dihedral angle of 23.18(4)° (see Table 4.5). The dihedral angle is smaller than that found in the [Rh(bzac)$(CO)_2$] complex (24.90(3)°) (see Table 4.2).

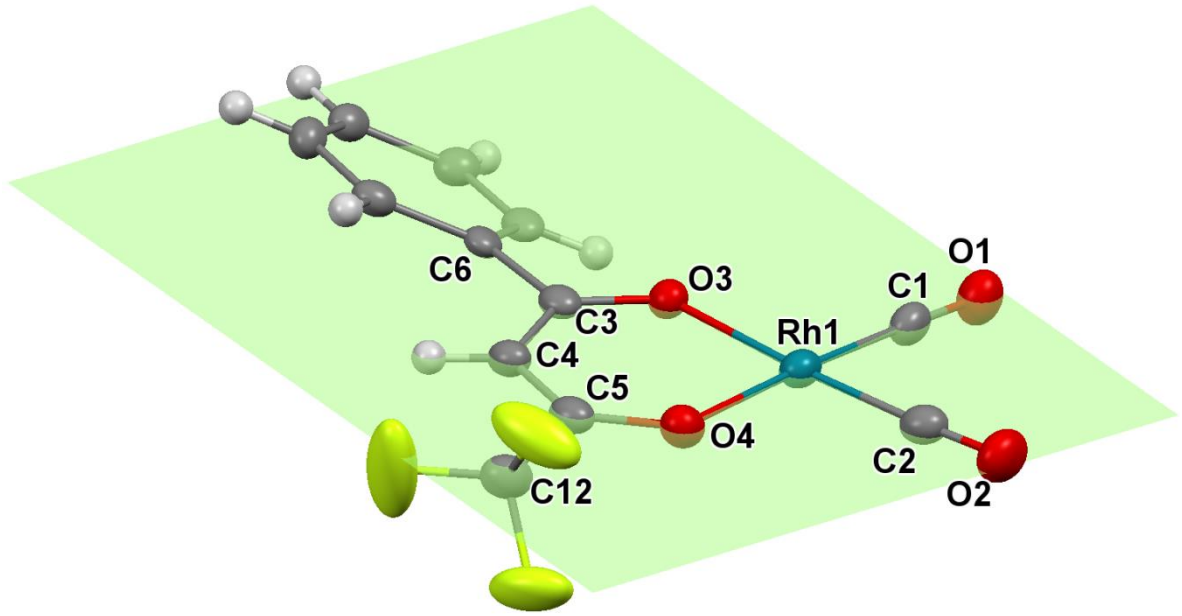

Figure 4.13: The phenyl group of the coordinating trifluorobenzoylacetonato ligand is twisted out of the horizontal plane intersecting all other non-H atoms in [Rh(bzac)(CO)$_2$] (with exception of the fluorine atoms).

It was suspected that the structures of [Rh(F$_3$-bzac)(CO)$_2$] and [Rh(bzac)(CO)$_2$] could be very similar and to that end an overlay of the two molecules is illustrated in Figure 4.12. It is clear from the overlay that the two structures exhibit significant differences in the orientation of the phenyl ring substituents as well as deviation of the carbonyl groups.

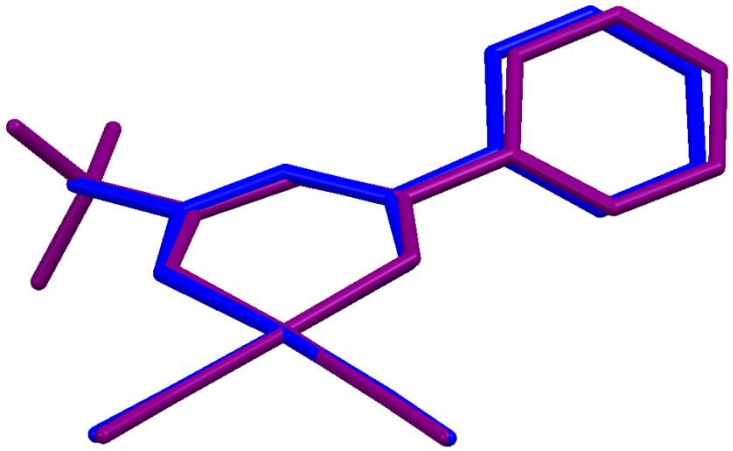

Figure 4.12: Overlay of [Rh(F$_3$-bzac)(CO)$_2$] (purple) and [Rh(bzac)(CO)$_2$] (blue) shows greater distortion of the phenyl ring (in relation to the coordination plane) for the [Rh(bzac)(CO)$_2$] structure. Hydrogen atoms were omitted for clarity.

As with the structure of [Rh(bzac)(CO)$_2$] (Section 4.3), metallophilic interactions were observed in the [Rh(F$_3$-bzac)(CO)$_2$] structure between neighbouring rhodium centres, illustrated in Figure 4.14. The interactions are once again encountered along the shortest cell axis (*a*-axis = 7.016(4) Å) of the unit cell but in contrast to [Rh(bzac)(CO)$_2$], the Rh···Rh interactions exhibited constant distances of 3.529(3) Å between neighbouring Rh centres.

The published structure of [Rh(F_3-bzac)($CO)_2$] was also noted for its metallophilic interactions with Rh···Rh distances determined as 3.537(3) Å.

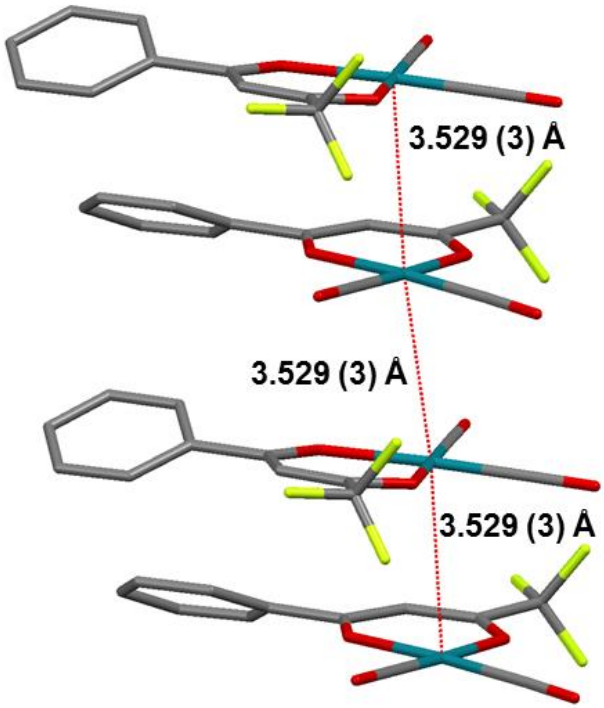

Figure 4.14: Illustration of the Rh···Rh interactions (indicated in red) between neighbouring molecules in [Rh(F_3-bzac)($CO)_2$] along the *a*-axis of the unit cell.

As with the previous structure, the Rh···Rh interactions lead to the construction of a 1-D metal chain with an angle of 167.50(2)° between rhodium centres (Rh-Rh-Rh) as seen in Figure 4.15. This was smaller than the reported angle of 172.06(3)° for [Rh(bzac)($CO)_2$]. Torsion angles of 115.23(1)° for C4-Rh···C4-Rh (see Table 4.5) were found between β-diketonato groups (R-groups) along the one-dimensional metal chain. These angles were also smaller than those found in [Rh(bzac)($CO)_2$] (180.0(2)°). The arrangement of molecules in [Rh(F_3-bzac)($CO)_2$] could be described as a staggered arrangement in contrast to the eclipsed formation adopted by molecules of [Rh(bzac)($CO)_2$] (see Figure 4.6(b); also Section 2.4.4, Chapter 2).

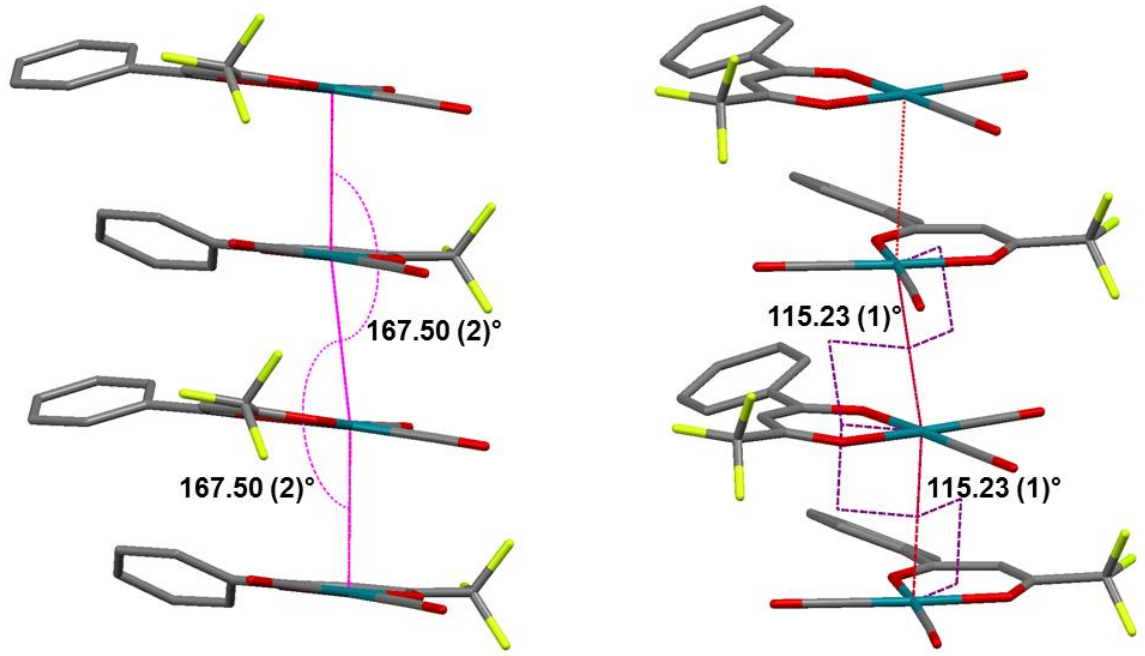

Figure 4.15: a) Angles of 167.50(2)° between neighbouring Rh centres are repeated throughout the crystal structure in the infinite 1-D metal chains; b) Torsion angles of 115.23(1)° between coordinating β-diketonato ligands (C4-Rh···C4-Rh) of neighbouring molecules reveal a staggered arrangement along the 1-D chain.

Halogen bonding involving the fluorine atoms of [Rh(F_3-bzac)($CO)_2$] are encountered in the crystal lattice. IUPAC has recently defined halogen bonding as *occuring between an electrophilic region on a halogen atom belonging to a molecule or molecular fragment with a nucleophilic region of a molecule or molecular fragment*.[23]

Traditionally, fluorine atoms were excluded as potential halogen bond donors. However, heavier halogen atoms such as iodine, bromine and chlorine were unequivocally accepted as participating in halogen bonds. This notion was based on the theory that halogen bonds originate through the interactions of a positively charged σ-hole present on a halogen atom with negative sites of nucleophiles.[24] For the heavier halogens, the existence of these σ-holes were undisputed but only recently has consensus been reached that fluorine may also possess σ-holes that result in halogen bonding.[25]

Halogen bonds are typically encountered along the bond at angles of approximately 180° between donor and acceptor sites. This holds true except in cases where secondary interactions are found to disrupt this arrangement.[25]

[23] Desiraju, G. R., Ho, P. S., Kloo, L., Legon, A. C., Marquardt, R., Metrangolo, P., Politzer, P., Resnatti, G., Rissanen, K., *Pure Appl. Chem.*, **2013**, *85*, 1711-1713.
[24] Lommerse, J. P. M., Stone, A. J., Taylor, R., Allen, F. H., *J. Am. Chem. Soc.*, **1996**, *118*, 3108-3116.
[25] Metrangola, P., Murray, J. S., Pilati, T., Politzer, P., Resnatti, G., Terraneo, G., *Cryst. Growth Des.*, **2011**, *11*, 4238-4246.

The halogen bonds between molecules of [Rh(F_3-bzac)($CO)_2$] are illustrated in Figure 4.16 and data related to the interactions given in Table 4.6. The interactions result in polymeric chains within the crystal lattice along the *b*-axis, resulting in a 3-dimensional connected structure as illustrated in Figure 4.17.

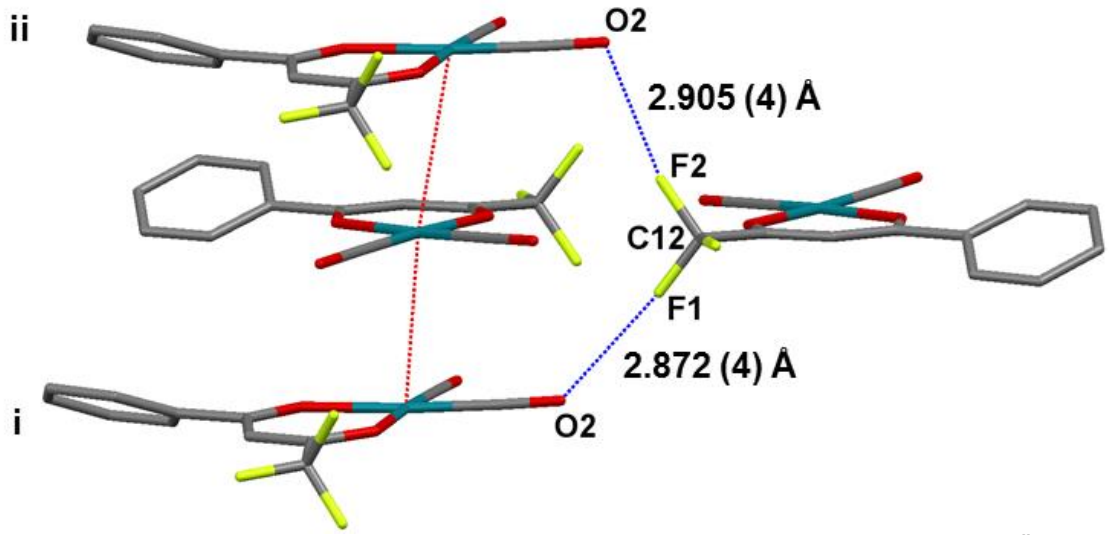

Figure 4.16: Weak C-F···O interactions (indicated in blue) observed for C12-F2···O2^{ii} and C12-F1···O2^{i} in [Rh(F_3-bzac)($CO)_2$].

Table 4.6: Halogen bond geometry for [Rh(F_3-bzac)($CO)_2$] as depicted in Figure 4.16 and 4.17.

D-X···A	dD-X (Å)	dX···A (Å)	dD···A (Å)	Angle D-X···A (°)
C12-F1···O2^{i}	1.315(5)	2.872(4)	4.183(6)	174.6(3)
C12-F2···O2^{ii}	1.318(5)	2.905(4)	4.142(6)	155.8(3)

Symmetry codes: i) 5/2-x, -1/2+y, -z; ii) 3/2-x, -1/2+y, -z.

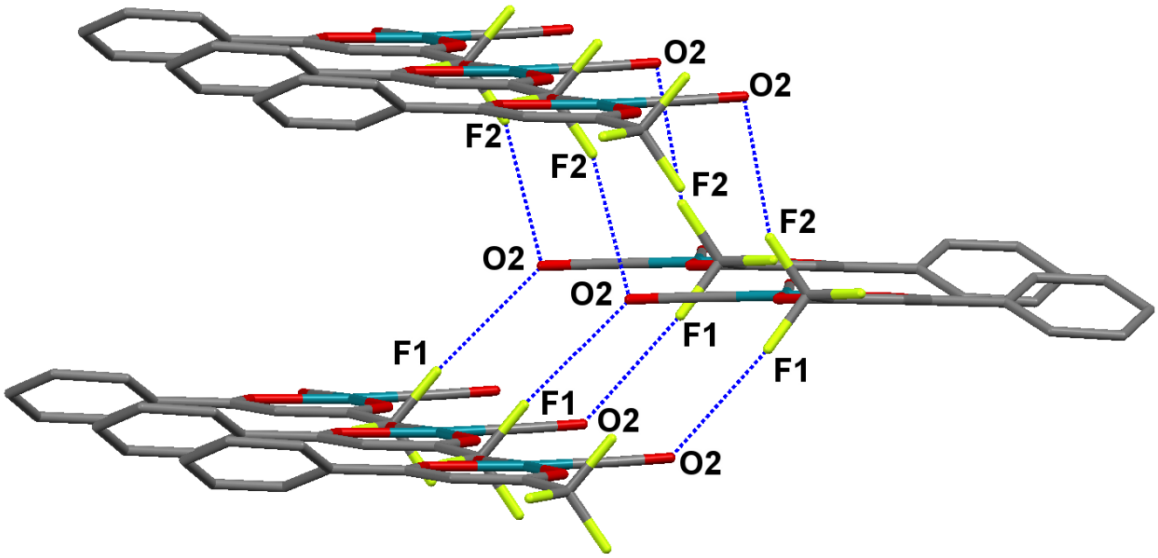

Figure 4.17: Halogen bonds (indicated in blue) connect neighbouring molecules *via* the carbonyl moeity of [Rh(F_3-bzac)($CO)_2$] in a head-to-tail motif forming a polymeric chain along the *b*-axis.

A hydrogen bond was observed between O1 and H9 atoms with a distance of 2.556 Å. This interaction is illustrated in Figure 4.18 and data related to the hydrogen bond given in Table 4.7.

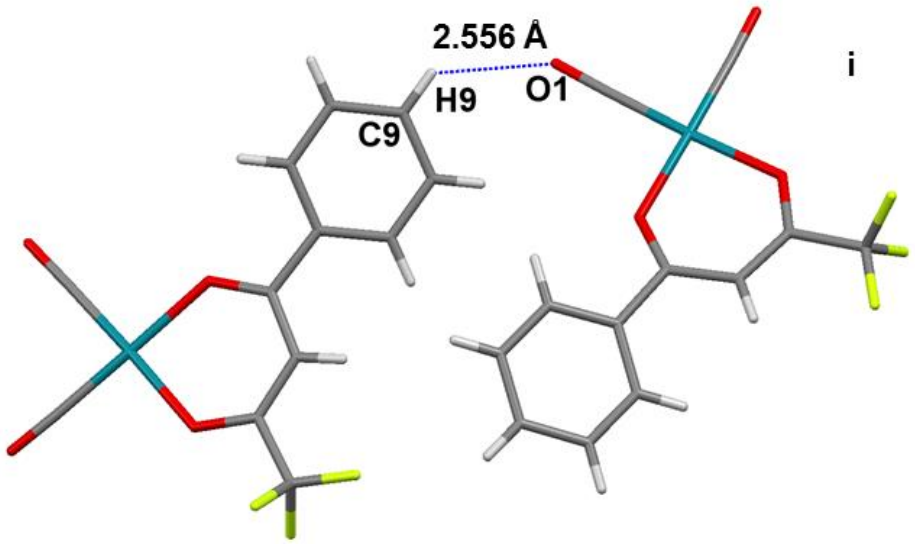

Figure 4.18: Hydrogen bond C9-H9···O1^{i} (indicated in blue) observed in [Rh(F_3-bzac)$(CO)_2$].

Table 4.7: Hydrogen-bond geometry for [Rh(F_3-bzac)$(CO)_2$].

D-H···A	dD-H (Å)	dH···A (Å)	dD···A (Å)	Angle D-H···A (°)
C9-H9···O1^{i}	0.931	2.556	3.220(5)	128.6

Symmetry codes: i) x, -½+y, ½-z.

As with the previous structure the metallophilic interactions contribute significantly to the packing motif in [Rh(F_3-bzac)$(CO)_2$] as can be seen in Figure 4.19.

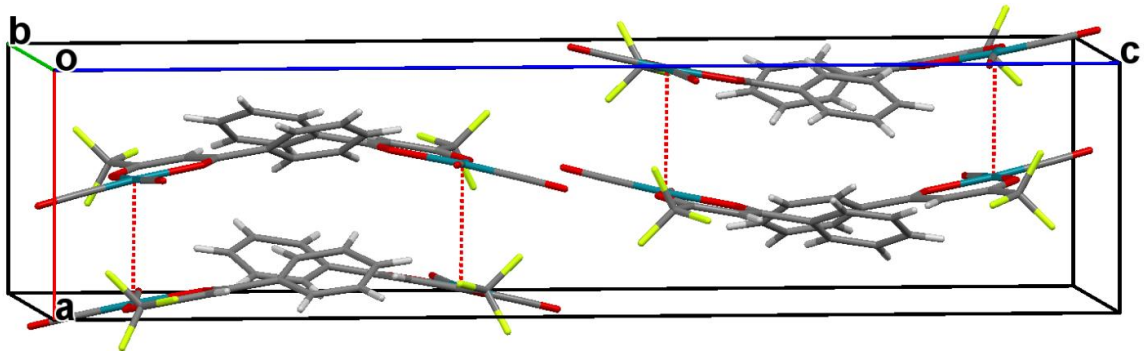

Figure 4.19: Packing of [Rh(F_3-bzac)$(CO)_2$] along an off-centered *b*-axis showing the dominating influence metallophilic interactions (indicated in red) have on the stability of the crystal structure.

4.5 Crystal Structure of [Rh(F_3-4Clbzac)($CO)_2$] (i)

The complex, (benzoyl-4-chloro-1,1,1-trifluoroacetonato-κ^2O,O')dicarbonylrhodium(I), crystallized in the orthorhombic space group $P2_12_12_1$ with four independent molecules in the asymmetric unit and thus 16 formula units in the unit cell. The four independent molecules are represented in Figure 4.20 and selected bond lengths and angles are given in Table 4.8.

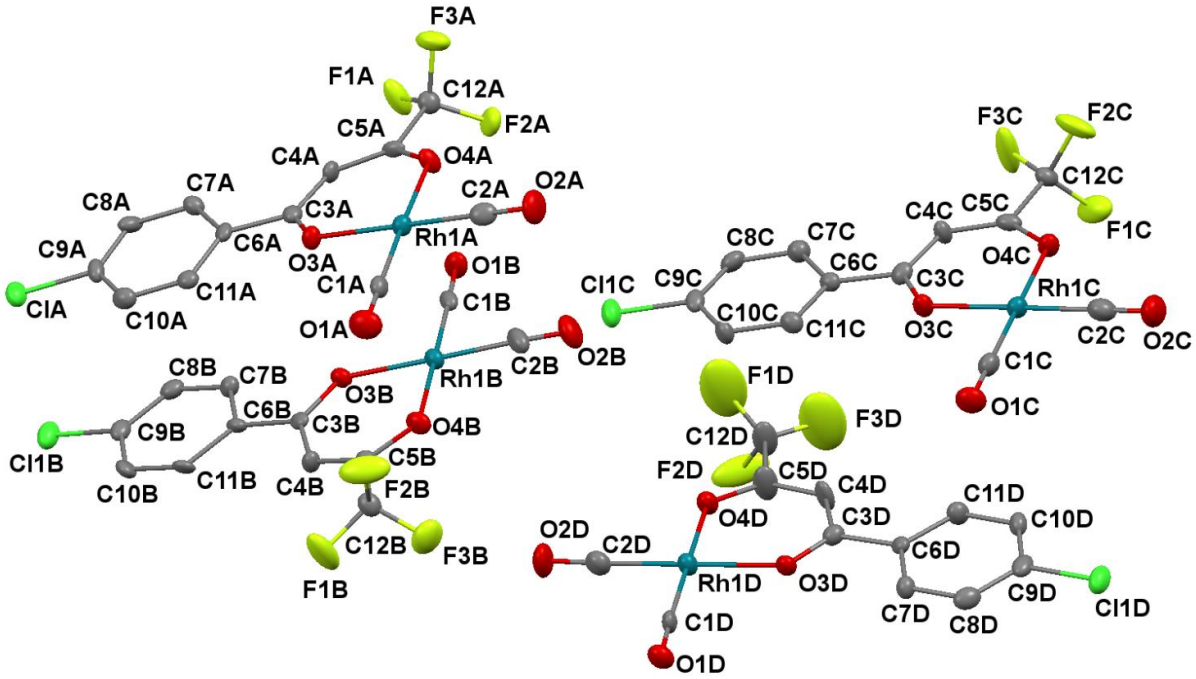

Figure 4.20: Molecular diagram of [Rh(F_3-4Clbzac)($CO)_2$] with atom numbering scheme. Hydrogen atoms have been omitted for the sake of clarity. Thermal ellipsoids have been drawn at 50 % probability level.

Table 4.8: Selected bond distances and angles of [Rh(F_3-4Clbzac)($CO)_2$].

Atoms	Distance (Å)			
	Molecule			
	A	B	C	D
Rh1-C1	1.860(7)	1.842(7)	1.838(7)	1.854(7)
Rh1-C2	1.850(9)	1.841(9)	1.841(8)	1.846(8)
Rh1-O3	2.037(5)	2.037(5)	2.038(4)	2.030(4)
Rh1-O4	2.032(4)	2.037(5)	2.034(5)	2.031(5)
C1-O1	1.113(9)	1.139(9)	1.142(9)	1.120(9)
C2-O2	1.14(1)	1.14(1)	1.14(1)	1.134(9)
C3-O3	1.276(9)	1.276(9)	1.271(8)	1.262(8)
C5-O4	1.278(8)	1.277(8)	1.280(9)	1.266(9)
C12-F3	1.332(9)	1.327(9)	1.318(8)	1.31(1)
C9-Cl1	1.736(7)	1.744(8)	1.733(7)	1.740(7)
O3···O4[a]	2.888(8)	2.893(8)	2.879(7)	2.873(7)

[a] Bite distance

Atoms	Angle (°)			
	Molecule			
	A	B	C	D
C1-Rh1-C2	88.7(4)	90.1(4)	89.5(4)	89.2(4)
O3-Rh1-O4	90.2(2)	90.4(2)	90.1(2)	90.1(2)
C1-Rh1-O4	177.8(3)	179.7(3)	179.3(3)	178.9(3)
C2-Rh1-O3	178.8(3)	179.3(3)	179.3(3)	179.2(3)
C3-C4-C5	124.8(8)	125.7(8)	124.4(8)	125.0(9)
C1-Rh1-O3	90.5(3)	89.7(3)	89.7(3)	90.1(3)
C2-Rh1-O4	90.6(3)	89.8(3)	90.7(3)	90.6(3)
F1-C12-F2	107.6(7)	108.6(7)	106.4(7)	101.5(9)
F2-C12-F3	106.5(7)	106.0(7)	106.3(7)	100.9(9)
F1-C12-F3	106.8(7)	105.4(7)	108.4(7)	113(1)
C3-O4···C5-O4[b]	179.6(7)	179.5(7)	179.6(7)	178.4(8)
C4-Rh1(1)···C4-Rh1(2)[c]	97.55(2)	97.55(2)	96.92(3)	96.92(3)
Dihedral angle[d]	6.55(3)	4.80(3)	1.72(3)	2.64(4)

[b] Torsion angle between C3-O4 and C5-O4; [c] Torsion angle between C4-Rh1 and C4-Rh1 of neighbouring molecules; [d] defined as the torsion angle between the O4-C3-C4-C5-O4 plane and the phenyl ring (see scheme 4.2).

The carbonyl bond distances between the rhodium(I) centre and carbon atoms found in the four molecules are in good agreement with the reported bond distances of [Rh(bzac)$(CO)_2$] (1.854(2) Å and 1.848(2) Å) and [Rh(F_3-bzac)$(CO)_2$] (1.832(5) Å and 1.854(4) Å). In molecule A these bonds were found as Rh1a-C1a (1.860(7) Å) and Rh1a-C2a (1.850(9) Å) and in molecule B as Rh1b-C1b (1.842(7) Å) and Rh1b-C2b (1.841(9) Å). Rh1c-C1c (1.838(7) Å) and Rh1c-C2c (1.841(8) Å) bond distances were encountered for molecule C and Rh1d-C1d (1.854(7) Å) and Rh1d-C2d (1.846(8) Å) were found for molecule D.

The only discernible difference between the four molecules was the dihedral angle between the phenyl ring and the O4-C3-C4-C5-O4 atoms as indicated in scheme 4.2 (Section 4.1). For molecule A this angle was considerably larger with the phenyl ring orientated at an angle of 6.55(3)° in relation to the O4-C3-C4-C5-O4 plane. Molecule C had the smallest dihedral angle (1.72(3)°) with the phenyl ring almost planar to the O4-C3-C4-C5-O4 plane.

All of the molecules displayed a slightly distorted square planar geometry as with the other reported structures of [Rh(bzac)$(CO)_2$] (see Section 4.3) and [Rh(F_3-bzac)$(CO)_2$] (see Section 4.4). As opposed to the previously reported structures the molecules were less distorted from the ideal 90° angles as expected for a square planar geometry as can be seen in Figure 4.22.

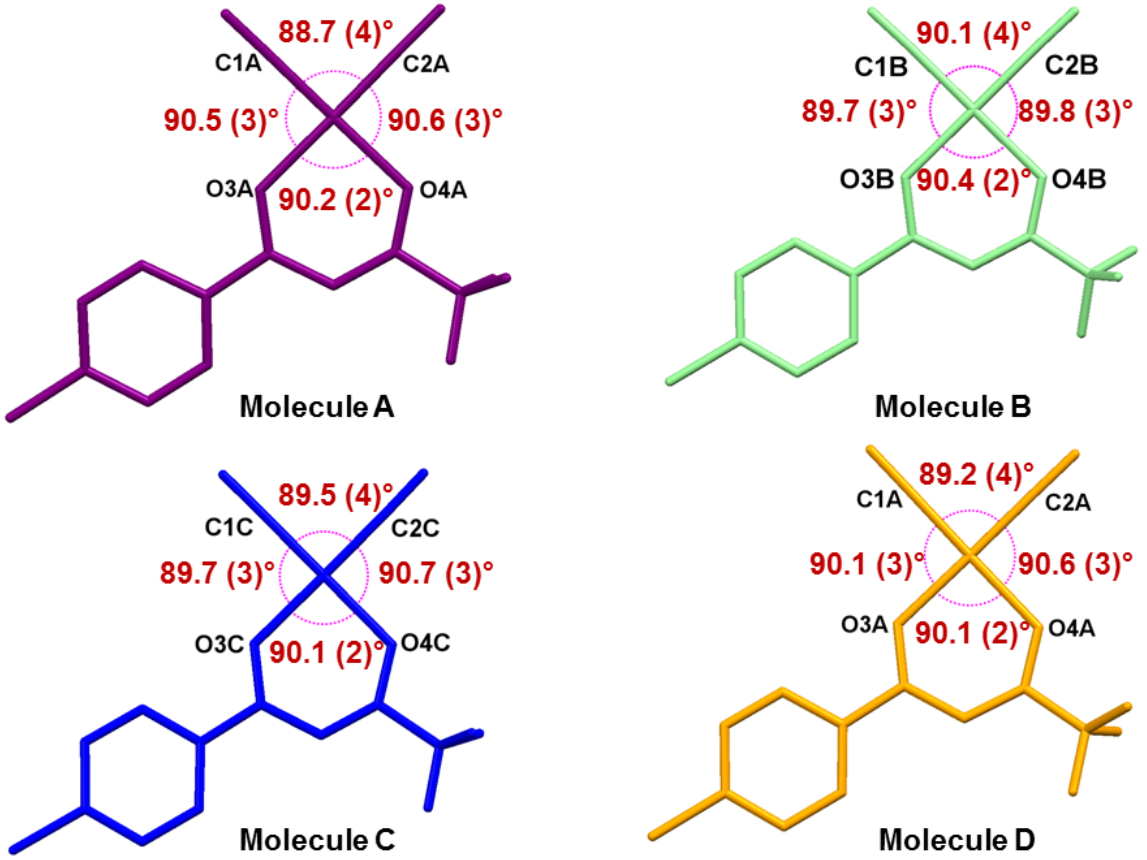

Figure 4.22: Angles indicated illustrate the slight distortion of the square planar geometry of the complex for the four different independent molecules in the asymmetric unit for [Rh(F_3-4Clbzac)$(CO)_2$].

Overlays between the different molecules of the asymmetric unit in [Rh(F_3-4Clbzac)$(CO)_2$] reveal significant differences between the molecules (see Figure 4.23). Between molecules **A** and **B** for example deviations in the orientation of the phenyl group as well as the fluorine atoms of the coordinating β-diketonato ligand can clearly be seen. Between molecules **C** and **D** the position of the carbonyl moieties differ as well as the fluorine atom orientation. These overlays reveal that the four molecules found in the solid state structure of [Rh(F_3-4Clbzac)$(CO)_2$] are indeed different and are not generated by symmetry in any way.

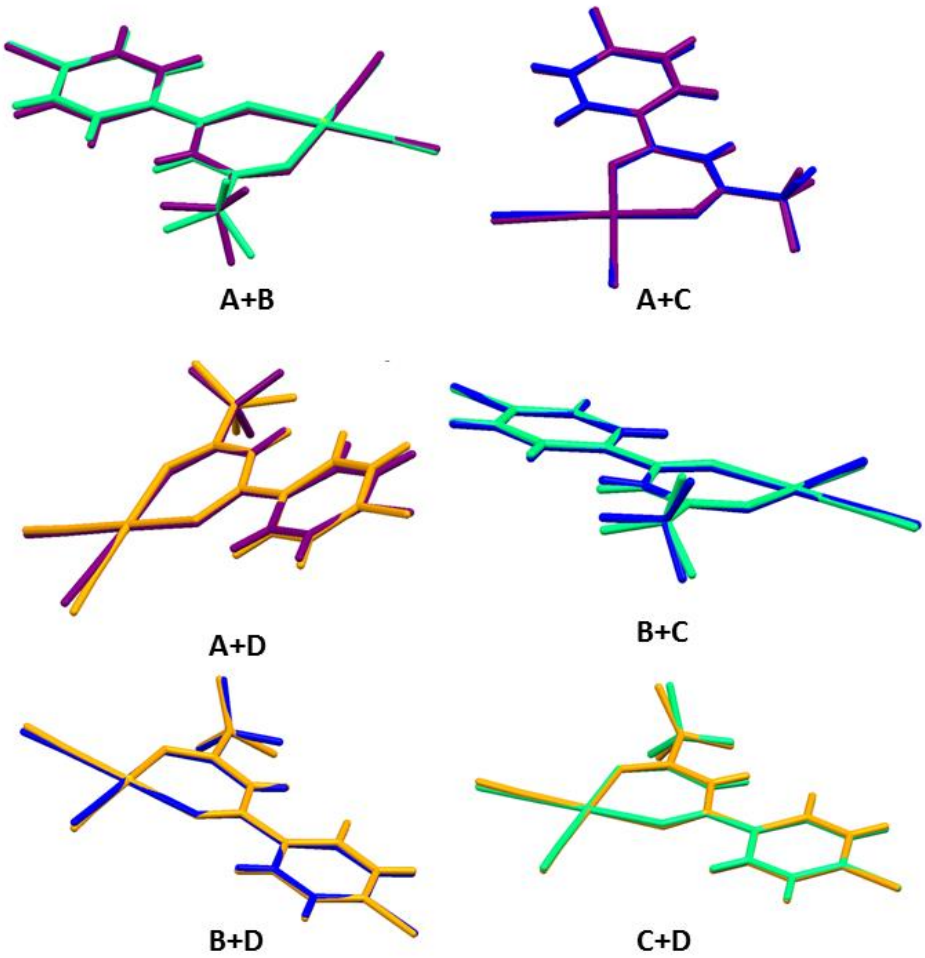

Figure 4.24: Overlay of the four molecules in the asymmetric unit. Primary differences in the molecules are the orientation of the fluorine atoms, different orientations of the phenyl ring and the position of the carbonyl moeities. Representation of molecules: A= purple, B= green, C= blue, D= orange.

As with [Rh(bzac)$(CO)_2$] (Section 4.3) and [Rh(F_3-bzac)$(CO)_2$] (Section 4.4), the structure of [Rh(F_3-4Clbzac)$(CO)_2$] displayed metallophilic interactions between neighbouring rhodium centres as illustrated in Figure 4.25. Rh···Rh interactions were observed between Rh1a and Rh1b (in molecules **A** and **B**) with alternating Rh···Rh distances of 3.469(3) Å and 3.470(3) Å. The other Rh···Rh interaction was observed between Rh1c and Rh1d (molecules **C** and **D**) with alternating Rh···Rh distances of 3.491(3) Å and 3.617(3) Å.

The interactions were noted to occur along the *a*-axis (6.936(1) Å) of the unit cell which is once again the shortest reported cell axis. The Rh1c···Rh1d distance of 3.617(3) Å is also considerably longer than the Rh···Rh distances for [Rh(bzac)$(CO)_2$] (3.308(3) Å and 3.461(3) Å) and [Rh(F_3-bzac)$(CO)_2$] (3.529(3) Å).

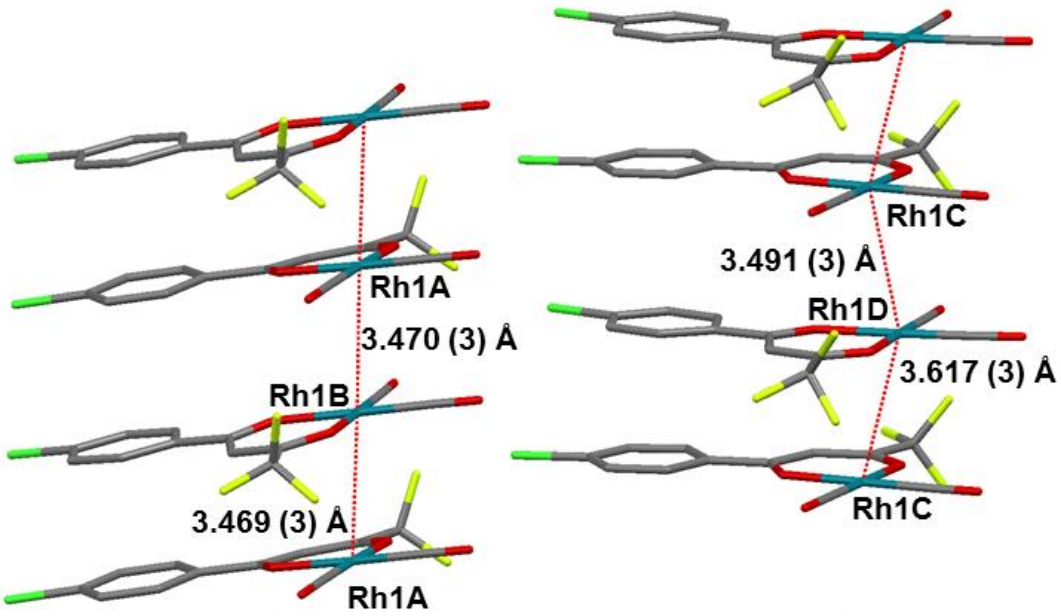

Figure 4.25: Rh···Rh interactions in [Rh(F_3-4Clbzac)($CO)_2$] were found alternating between two pairs of molecules. a) Rh1a···Rh1b displayed interactions of 3.469(3) Å and 3.470(3) Å and b) Rh1c···Rh1d had distances of 3.491(3) Å and 3.617(3) Å.

The 1-D metallic chain constructed out of alternating molecules **A** and **B** displayed an almost completely linear arrangement with angles between Rh centres of 176.34(3)° (Rh1a-Rh1b-Rh1a) as depicted in Figure 4.26(a). In contrast, the chain consisting of alternating molecules **C** and **D** represented in Figure 2.26(b) revealed a zig-zagged geometry with angles of 154.80(3)° between Rh centres (Rh1c-Rh1d-Rh1c) (see Section 2.4.4, Chapter 2).

The torsion angle between coordinating β-diketonato moieties (C4a-Rh1a···Rh1b-C4b) were determined as 97.42(2)° and 97.61(3)° revealing a staggered geometry (Figure 4.27(a)) for the 1-D chain consisting of molecules **A** and **B** in [Rh(F_3-4Clbzac)($CO)_2$]. Similarly, in Figure 4.27(b), the torsion angles of 97.98(4)° and 97.79(3)° between coordinating β-diketonato ligands (C4c-Rh1c···Rh1d-C4d) in molecules **C** and **D** reveal a staggered arrangement along the one dimensional chain.

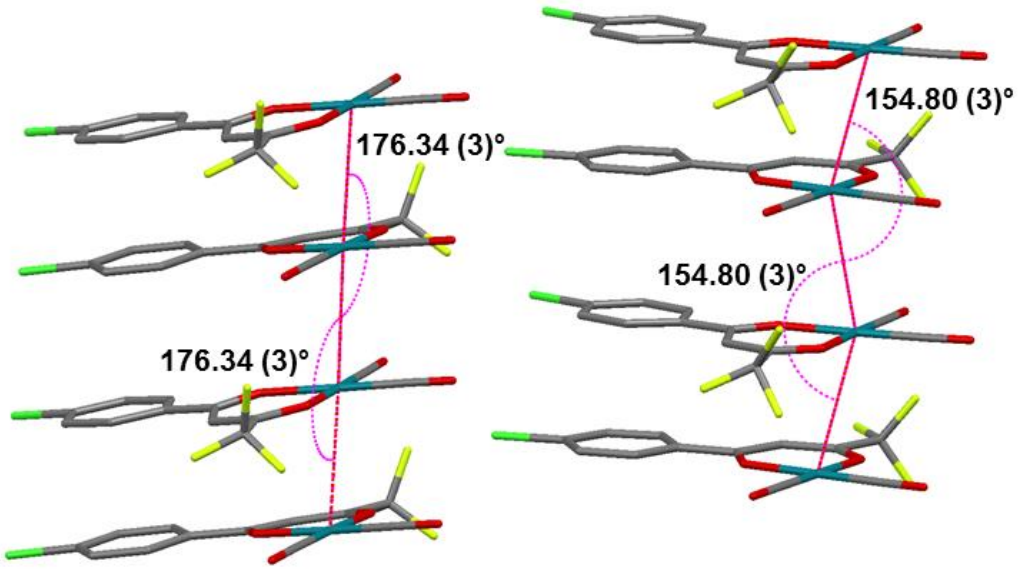

Figure 4.26: a) Rh···Rh interactions observed for molecules A and B in a linear geometry with the angle between neighbouring Rh centres determined as 176.34(3)°; b) Rh···Rh interactions observed for molecules C and D are arranged in a zig-zagged motif along the *a*-axis with the angle between neighbouring Rh centres determined as 154.80(3)°.

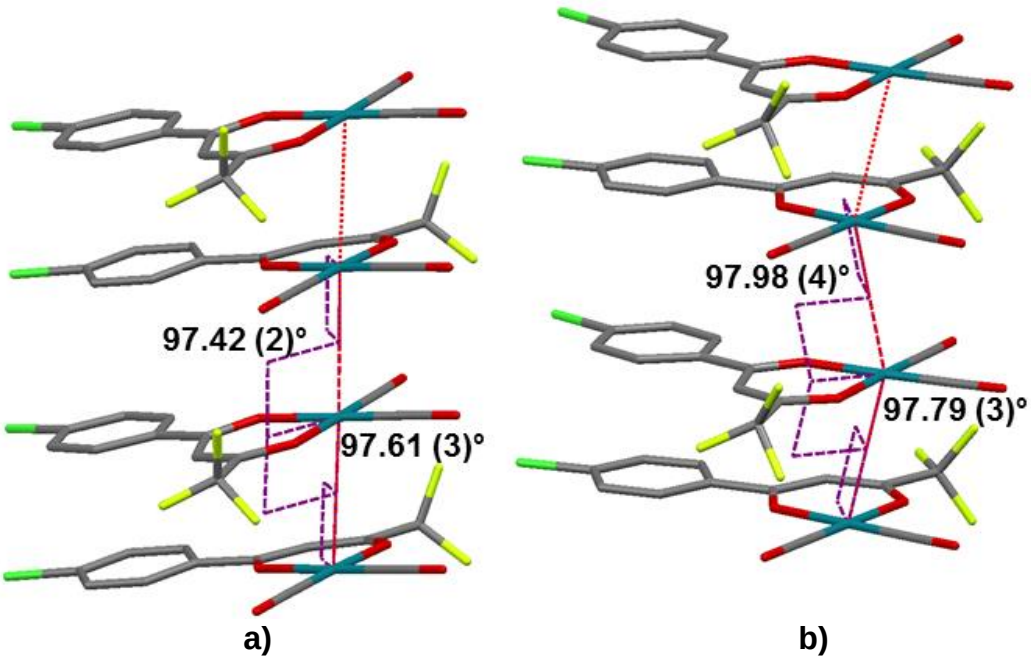

Figure 4.27: a) Torsion angles (97.42(2)° and 97.61(3)°) between coordinating β-diketonato moeities of molecules A and B reveal a staggered geometry in the 1-D chain; b) Torsion angles (97.98(4)° and 97.79(3)°) between coordinating β-diketonato moieties of molecules C and D displayed a staggered geometry.

Cl···Cl soft contacts were observed in the structure and are represented in Figure 4.28. Cl1c was observed to be involve in a bifurcated interaction with O1b and C1b as illustrated in Figure 4.28. Details of the interactions are given in Table 4.9.

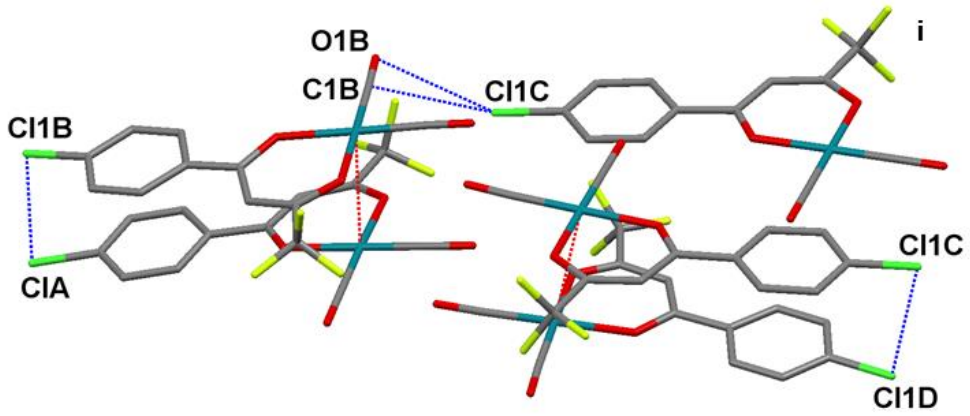

Figure 4.28: Cl···Cl interactions connecting molecules of [Rh(F_3-4Clbzac)$(CO)_2$] to form dimers in the crystal lattice. A Cl···C interaction was also observed between Cl1c and C1b.

Table 4.9: Selected data of the observed Cl···Cl interactions in [Rh(F_3-4Clbzac)$(CO)_2$].

Atoms	Distance (Å)	θ_1	θ_2
Cl1a···Cl1b	3.431(3)	102.85	102.30
Cl1c···Cl1d	3.497(3)	79.43	79.55
C1b···Cl1c^i	3.446(7)	-	-
O1b··· Cl1c^i	3.226(6)	-	-

Symmetry codes: i) -1/2+x,3/2-y,2-z.

Halogen···halogen interactions are typically classified as weak interactions but contribute distinctly to packing in the crystal lattice.[26] Cl···Cl interactions are considered the weakest halogen···halogen type interaction with an energy estimation of only 3 % of a typical Cl-Cl covalent bond.[27] Typical distances are shorter than 3.50 Å for Cl···Cl interactions as this the sum of their van der Waals radii.[28] Three parameters are assigned when evaluating halogen···halogen interactions namely: i) the distance between $X_1 \cdots X_2$, ii) θ_1 = C-$X_1 \cdots X_2$ and iii) θ_2 = $X_1 \cdots X_2$-C. Contacts with $\theta_1 \approx \theta_2$ are referred to as Type-I interactions and those where $\theta_1 \approx 180°$ and $\theta_2 \approx 90°$ are classified as Type-II.[29] Figure 4.29 illustrate the requirements for the two different types of halogen···halogen interactions. From the data summarized in Table 4.9 it is clear that the Cl···Cl interactions found in the crystal lattice are Type-I interactions.

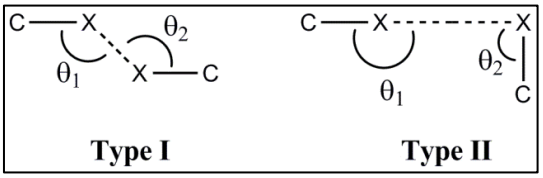

Figure 4.29: Halogen···Halogen interactions occur as two different types with Type-I interactions displaying $\theta_1 \approx \theta_2$ and Type-II interactions with $\theta_1 \approx 180°$ and $\theta_2 \approx 90°$.[29]

Type-I interactions are generally symmetrical and are almost always encountered around a crystallographic inversion centre.[30] The shortest distance reported for Type-I interactions for

[26] Desiraju, G. R., *Crystal Engineering: The Design of Organic Solids*, Elsevier, Amsterdam, The Netherlands, **1989**.
[27] Williams, D. E., Hsu, L. Y., *Acta Cryst. Sect. A.*, **1985**, *41*, 296-301.
[28] Bondi, A., *J. Phys. Chem.*, **1964**, *68*, 441-451.
[29] Hathar, V. R., Guru Row, T. N., *J. Phys. Chem. A.*, **2010**, *114*, 13434-13441.

Cl···Cl has been 3.30 Å. If the contact becomes shorter than this distance a repulsion will occur between the Cl atoms. In contrast, Type-II interactions are commonly associated with screw axes and glide planes and have been described as an attractive interaction.[30] This is according to the Williams model that assigns positive polarization regions to the polar region of the Cl atom and a negative polarization to the equatorial region.[30] The likelyhood of Type-II interactions have been found to increase when proceeding from Cl to Br to I in the halogen group. This is in line with the increase in polarization of halogens going down the periodic group.[31]

In [Rh(F_3-4Clbzac)($CO)_2$], no inversion centres exist as the space group is $P2_12_12_1$. Figure 4.30 illustrates the three 2_1 screw axes that are however present. The reported Type-I Cl···Cl interactions are thus associated with the 2_1 screw axis rather than the expected inversion centre as described above.

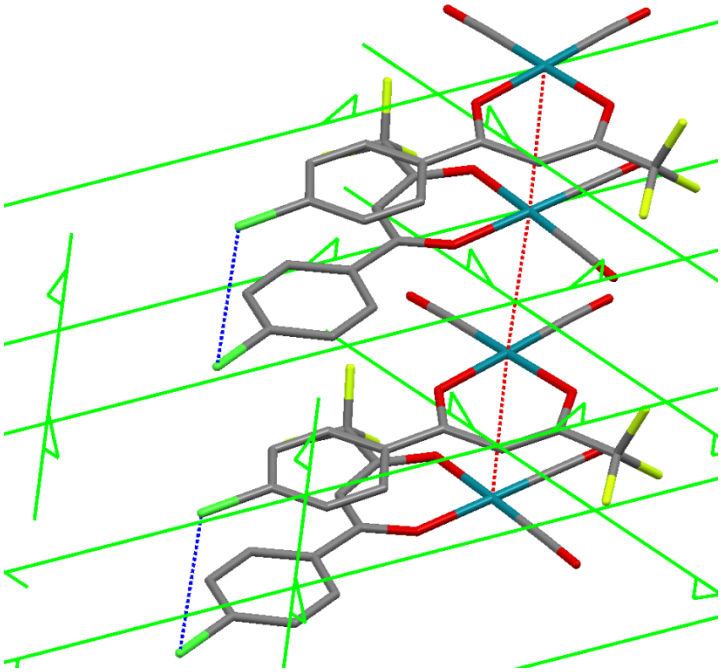

Figure 4.30: Type-I Cl···Cl interactions in [Rh(F_3-4Clbzac)($CO)_2$] occur along the 2_1 screw axis as indicated by green arrows.

Halogen bonds were observed in the crystal lattice of [Rh(F_3-4Clbzac)($CO)_2$] involving the trifluoro moiety of the coordinating β-diketonato ligand. These interactions are illustrated in Figure 4.31 and information related to the interactions summarized in Table 4.10. Soft contacts were also observed between F2a···Cl1d (3.039(5) Å) (symmetry operation: -1/2+x,3/2-y,2-z) and F3d···H11c (2.526 Å).

[30] Bui, T. T. T., Dahaoui, S., Lecomte, C., Desiraju, G. R., Espinosa, E., *Angew. Chem., Int. Ed.*, **2009**, *48*, 3838-3841.
[31] Pedireddi, V. R., Reddy, D. S., Goud, B. S., Craig, D. C., Rae, A. D., Desiraju, G. R., *J. Chem. Soc. Perkin Trans.*, **1993**, *2*, 2353-2360.

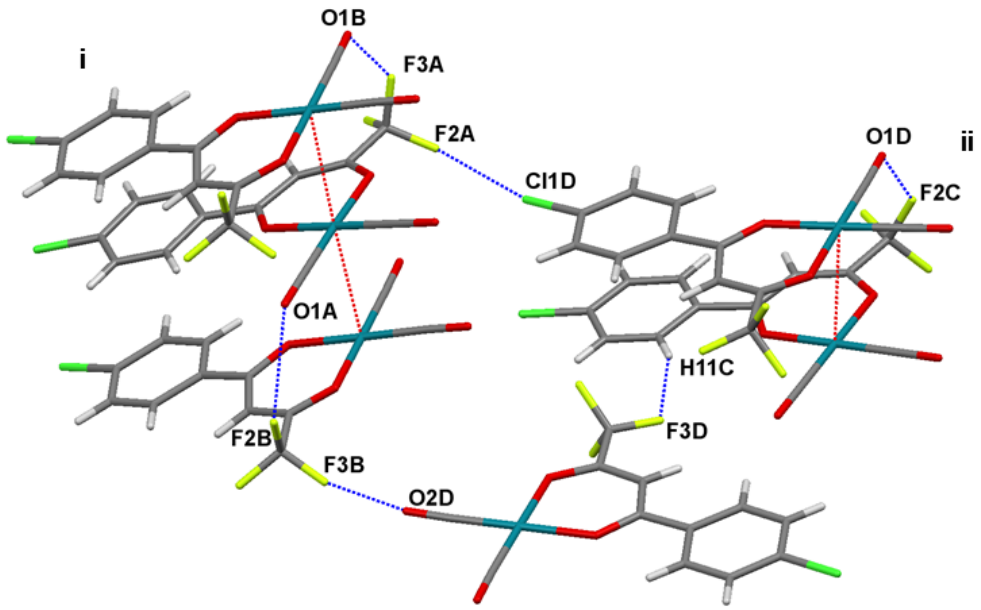

Figure 4.31: a) Soft contacts involving fluorine atoms in [Rh(F_3-4Clbzac)($CO)_2$].

Table 4.10: Halogen bond geometry in [Rh(F_3-4Clbzac)($CO)_2$].

D-X···A	dD-X (Å)	dX···A (Å)	dD···A (Å)	Angle D-X···A (°)
C12a-F3a···O1b^{i}	1.33(2)	2.928(8)	3.91(2)	129.4(5)
C12b-F2b···O1a	1.32(2)	2.924(9)	3.85(2)	126.2(5)
C12b-F3b···O2d	1.33(2)	2.989(8)	4.11(3)	141.9(3)
C12c-F2c···O1d^{ii}	1.33(3)	2.83(1)	3.82(3)	130.2(3)

Symmetry codes: i) -1+x,y,z; ii) -1/2+x,3/2-y,2-z.

The packing motif in [Rh(F_3-4Clbzac)($CO)_2$] is illustrated in Figure 4.32 with a distinct pattern influenced by the two metallophilic chains constructed through the Rh(I) centres of neighbouring molecules.

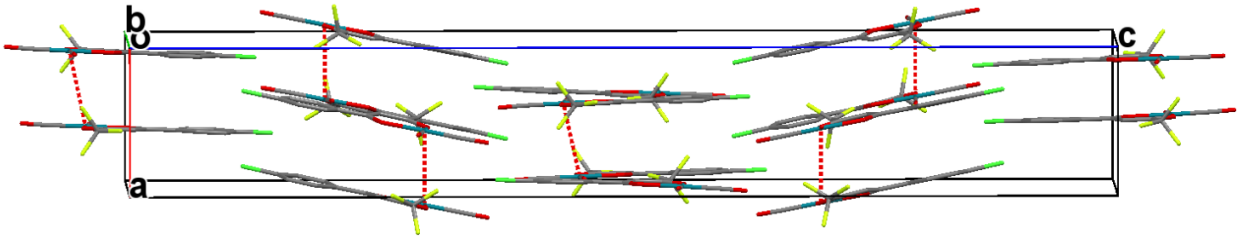

Figure 4.32: Packing of [Rh(F_3-4Clbzac)($CO)_2$] along an off-centered *b*-axis showing a distinct pattern in the crystal lattice influenced by the metallophilic interactions (indicated in red).

4.6 Crystal Structure of an Isolated Polymorph of [Rh(F_3-4Clbzac)($CO)_2$] (ii)

A polymorph of the complex, (benzoyl-4-chloro-1,1,1-trifluoroacetonato-κ^2O,O')dicarbonyl rhodium(I), was isolated as orange cuboid-like crystals. Unfortunately, these crystals were of

relatively poor quality which is reflected in the high R value of 13 % and Goodness-of-fit of 1.309 for the data collection (see Table 4.1). The structure of this complex could however be determined fairly accurately and will be discussed in this section. The crystals of (benzoyl-4-chloro-1,1,1-trifluoroacetonato-κ^2O,O')dicarbonyl rhodium(I) crystallized in the triclinic space group $P\bar{1}$ with two independent molecules in the asymmetric unit as illustrated in Figure 4.33. Selected bond lengths and angles are given in Table 4.11.

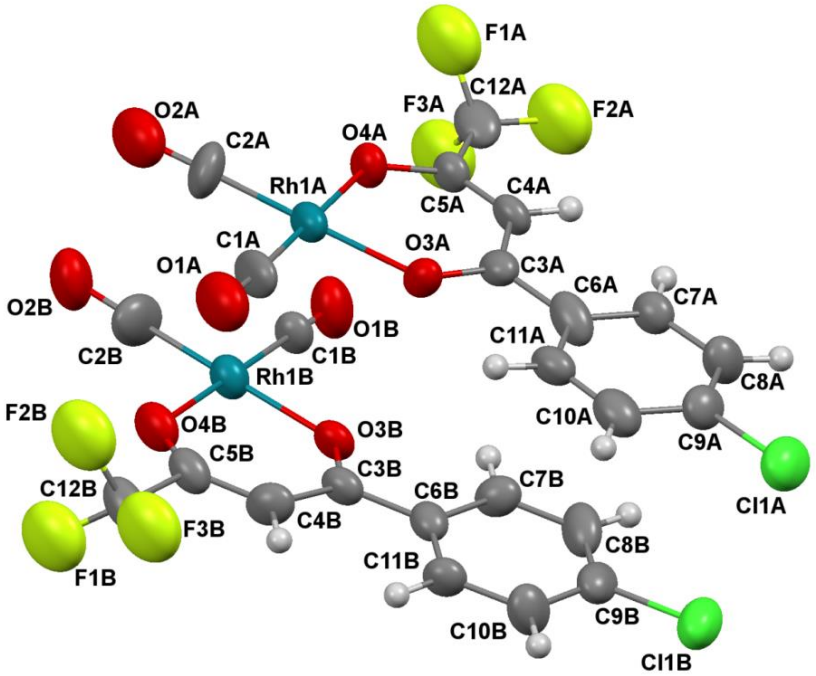

Figure 4.33: Molecular diagram of [Rh(F_3-4Clbzac)$(CO)_2$]. Hydrogen atom numbering has been omitted for clarity and thermal ellipsoids have been drawn at 50 % probability level.

Table 4.11: Selected bond distances and angles of the isolated polymorph of [Rh(F_3-4Clbzac)$(CO)_2$].

Atoms	Distance (Å)	
	Molecule	
	A	B
Rh1-C1	1.85(2)	1.86(2)
Rh1-C2	1.86(2)	1.85(2)
Rh1-O3	2.04(1)	2.00(1)
Rh1-O4	2.04(1)	2.03(1)
C1-O1	1.12(3)	1.12(3)
C2-O2	1.15(3)	1.13(3)
C3-O3	1.29(2)	1.32(3)
C5-O4	1.27(2)	1.22(3)
C12-F1	1.36(2)	1.32(2)
C9-Cl1	1.73(2)	1.73(2)
O3···O4[a]	2.87(1)	2.87(1)

[a] Bite distance

Atoms	Angle (°)	
	Molecule	
	A	B
C1-Rh1-C2	90(1)	89(1)
O3-Rh1-O4	90.3(5)	90.3(5)
C1-Rh1-O4	179.8(8)	179.3(8)
C2-Rh1-O3	177.6(8)	179.0(8)
C3-C4-C5	125(2)	122(2)
C1-Rh1-O3	89.6(8)	90.3(8)
C2-Rh1-O4	90.4(8)	90.4(8)
F1-C12-F2	105(1)	94(1)
F2-C12-F3	102(1)	89(1)
F1-C12-F3	101(1)	121(2)
C3-O4···C5-O4[b]	179.7(2)	179.6(3)
C4-Rh1(1)···C4-Rh1(2)[c]	97.3(4)	97.3(4)
Dihedral angle[d]	1.63(3)	4.65(3)

[b] Torsion angle between C3-O4 and C5-O4; [c] Torsion angle between C4-Rh1 and C4-Rh1 of neighbouring molecules; [d] defined as the torsion angle between the O4-C3-C4-C5-O4 plane and the phenyl ring (see scheme 4.2).

As mentioned above the structure is a polymorph of [Rh(F_3-4Clbzac)$(CO)_2$] which was described in Section 4.5. Table 4.12 gives a comparison of the unit cells of the two different structures of [Rh(F_3-4Clbzac)$(CO)_2$]. The *c*-axis provides the greatest difference between the two unit cells with a lower *Z* number for the structure reported in the triclinic space group $P\bar{1}$.

Table 4.12: Comparison of cell dimensions for the two polymorph structures of [Rh(F_3-4Clbzac)$(CO)_2$].

Cell dimension	[Rh(F_3-4Clbzac)$(CO)_2$] (Section 4.5)	[Rh(F_3-4Clbzac)$(CO)_2$] (polymorph)
a	6.936(1)	7.080(3)
b	17.116(3)	12.567(6)
c	46.121(7)	17.308(8)
α	90	72.23(2)
β	90	88.67(1)
γ	90	76.03(1)
Volume (Å^3)	5475(3)	1421.1(1)
Space group	Orthorhombic, $P2_12_12_1$	Triclinic, $P\bar{1}$
Z	16	4
Z'	4	2

For the two structures of [Rh(F_3-4Clbzac)$(CO)_2$] the *Z'* number differs between four molecules and two molecules in the asymmetric unit. Crystallograhically, high *Z'* structures are typically found to include more intermolecular interactions within their solid state structures where as low *Z'* structures are thought to be more kinetically stable. This implies that thermodynamically or kinetically stable crystal forms can be found between polymoprhs.[32]

[32] Sathishkumar, R., Mahapatra, S., Thakurm T. S., Desiraju, G. R., *Current Research*, **2010**, *99*, 1807-1811.

One of the theories as to which crystal form (kinetic *vs.* theromodynamic) will be favoured during crystallization relates to the proposed mechanism of crystallization. This theory suggests that molecules exist as structured aggregates in pre-crystallization stages within solution. If these aggregates remain unchanged during crystallization a high *Z'* unit will be rendered and if the aggregates break down to more elementary parts a lower *Z'* form will result. High *Z'* crystal forms are viewed as a "snap shot" of a molecule during crystallization with the lowest energy form not yet reached.[32]

In the following paragraphs continuous comparisons and evaluation of the two polymorphs will be given to highlight the differences between the two structures as well the important role that interactions play in the two crystal structures.

As with all of the previously discussed Rh(I) complexes the polymorph structure of [Rh(F_3-4Clbzac)($CO)_2$] displayed a square planar geometry with only very slight distorion from the ideal angles of 90° between atoms in the coordinating geometry (Figure 4.34).

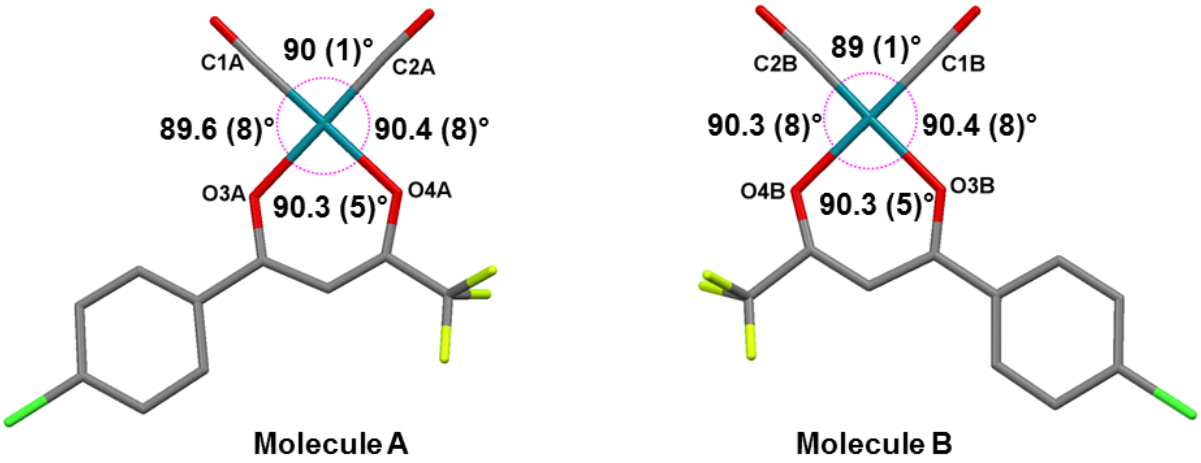

Figure 4.34: Represenation of the square planar geometry displayed with angles of close to 90° in the two molecules of the polymorph of [Rh(F_3-4Clbzac)($CO)_2$].

Between the two molecules found in the asymmetric unit very few differences were noted in terms of bond lengths and angles as given in Table 4.11. An overlay of the two molecules, in Figure 4.35, however shows differences in the orientation of the fluorine atoms as well as the position of the carbonyl moieties. As can be seen from the dihedral angles given in Table 4.11 the phenyl ring of molecule B (4.65(3)°) is also slightly more deviated from the O4-C3-C4-C5-O4 plane than molecule A (1.63(3)°).

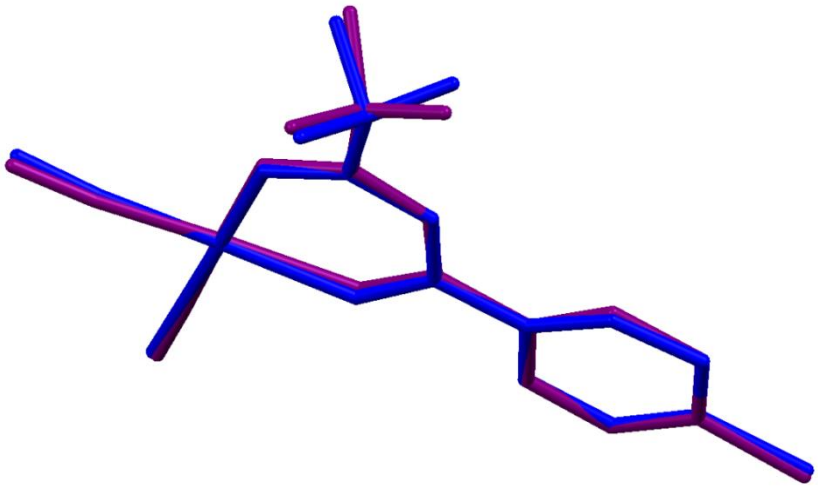

Figure 4.35: Overlay of the two molecules in the asymmetric unit of [Rh(F_3-4Clbzac)$(CO)_2$] (molecule A= purple; molecule B= blue).

The polymorph of [Rh(F_3-4Clbzac)$(CO)_2$] displayed metallophilic interactions between neighbouring rhodium centres as illustrated in Figure 4.37. Rh···Rh interactions were observed between Rh1a and Rh1b (in molecules A and B) with alternating Rh···Rh distances of 3.523(2) Å and 3.593(3) Å. These Rh···Rh distances are much longer than the Rh1a···Rh1b distances reported for the related structure in Section 4.5 (3.469(3) Å and 3.470(3) Å). The distances are closer to the Rh···Rh distances that were observed between Rh1c and Rh1d atoms in the second chain encountered in [Rh(F_3-4Clbzac)$(CO)_2$] which was discussed in Section 4.5 (3.491(3) Å and 3.617(3) Å).

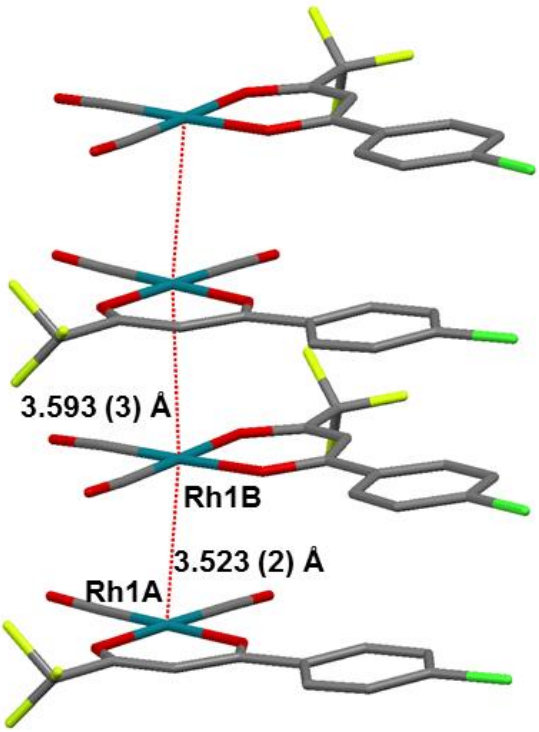

Figure 4.37: Illustration of the Rh···Rh interactions (indicated in red) between neighbouring molecules in [Rh(4Cl-F_3bzac)$(CO)_2$] along the *a*-axis of the unit cell with alternating distances of 3.523(2) Å and 3.593(3) Å.

The interactions were noted to occur along the *a*-axis (7.080(3) Å), as was the interactions described in Section 4.5, which also happens to be the shortest cell axis of the unit cell. The 1-D metal chain constructed out of alternating molecules A and B displayed an almost linear arrangement with angles measured between Rh(I) centres of 168.36(6)° (Rh1a-Rh1b-Rh1a) as can be seen in Figure 4.38(a). These angles are smaller than those for the structure in Section 4.5 which displayed an almost completely linear chain with Rh1a-Rh1b-Rh1a angles of 176.34(3)°. In contrast, the chain of Rh1c-Rh1d-Rh1c (154.80(3)°) centres in Section 4.5 displayed a zig-zagged arrangement.

The torsion angle between neighbouring coordinating β-diketonato moieties (C4a-Rh1a-C4b-Rh1b) were determined as 95.83(2)° and 97.28(3)° along the 1-D chain indicating a staggered geometry for the molecules (Figure 4.38(b)). These torsion angles were in good agreement with the torsions angles determined in the two metallophilic chains of Section 4.5 (97.42(2)°, 97.61(3)° for the chain of Rh1a-Rh1b and 97.98(4)°, 97.79(3)° for the chain of Rh1c-Rh1d).

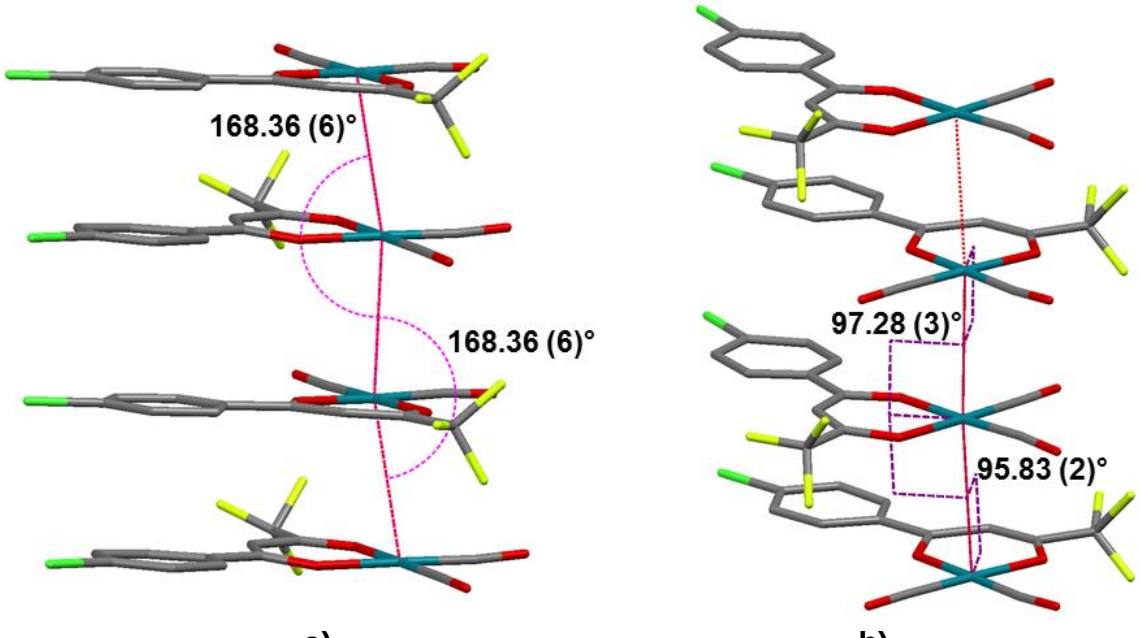

Figure 4.38: a) Rh···Rh interactions observed between neighbouring Rh(I) centres in a linear geometry with angles of 168.36(6)° (Rh1a-Rh1b-Rh1a); b) Torsion angles (95.83(2)° and 97.28(3)°) between coordinating β-diketonato moeities (C4a-Rh1a···C4b-Rh1b) reveal a staggered geometry for molecules along the constructed 1-D chain.

Several soft contacts involving the fluorine atoms situated on the coordinating β-diketonato backbone were observed in the crystal lattice. These interactions are illustrated in Figure 4.39 with information related to the interactions summarized in Table 4.13.

Interesting to note, is the presence of the halogen bond O1b···F3a-C12a which is similar to the observed halogen bond of O1a···F2b-C12b between molecules **A** and **B** in the structure

described in Section 4.5. Similarly, the Cl1b···F1a^{ii} interaction (2.67(2) Å, symmetry code: 1+x,-1+y,z) found in this structure was also observed in Section 4.5 (Cl1d···F2a).

It would seem as if the soft contacts observed in the polymoprh structure in this section are also present in the four molecules observed in the structure described in Section 4.5 for [Rh(F_3-4Clbzac)($CO)_2$]. What is clearly absent however from the polymorph structure is the Cl···Cl interactions that were observed between stacking of molecules **A** and **B** along the 1-D chain in Section 4.5 (Figure 4.28).

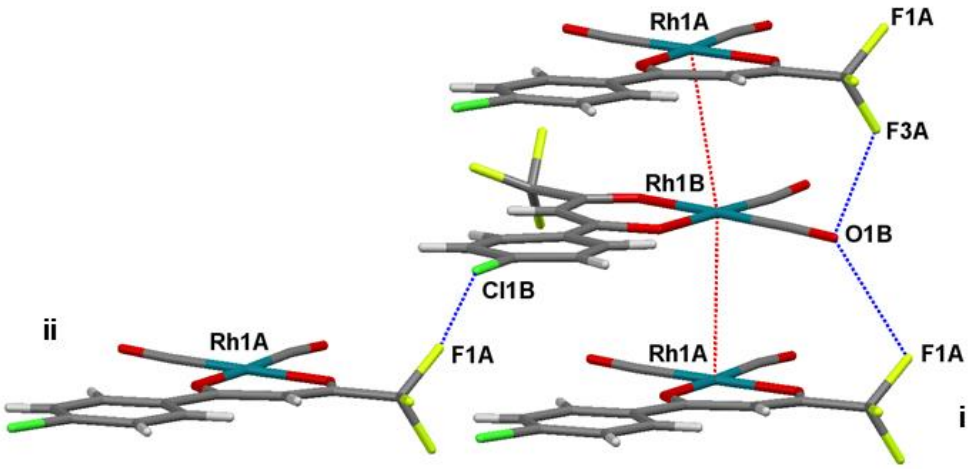

Figure 4.39: Soft contacts involving fluorine atoms in the polymorph of [Rh(F_3-4Clbzac)($CO)_2$].

Table 4.13: Halogen bond geometry in the polymorph of [Rh(F_3-4Clbzac)($CO)_2$].

D-X···A	dD-X (Å)	dX···A (Å)	dD···A (Å)	Angle D-X···A (°)
C12a-F3a···O1b	1.34(2)	2.94(2)	3.98(2)	132.2(3)
C12a-F1a···O1b^{i}	1.36(2)	2.99(2)	3.58(2)	108.2(2)

Symmetry codes: i) 1+x, y, z; ii) 1+x,-1+y,z.

The packing diagram of the polymorph of [Rh(F_3-4Clbzac)($CO)_2$] is given in Figure 4.40 with the distinct influence of metallophilic interactions again evident in the packing of molecules in the crystal lattice.

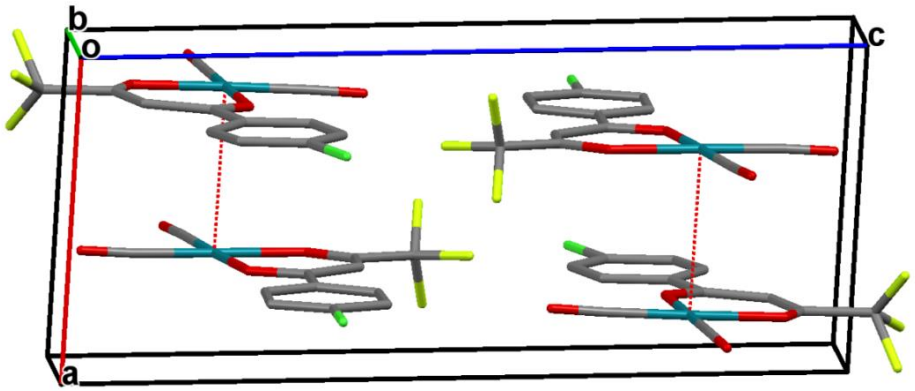

Figure 4.40: Packing of the polymorph of [Rh(F_3-4Clbzac)($CO)_2$] along an off-centered *b*-axis clearly illustrating the effect of metallophilic interactions on the packing of molecules within the crystal lattice.

4.7 Crystal Structure of [Rh(dbm)(CO)$_2$]

The complex, dicarbonyl(1,3-diphenyl-1,3-propanedionato-κ^2O,O) rhodium(I), crystallized in the orthorhombic space group $P22_12_1$ with two independent molecules in the asymmetric unit. The molecular structure is represented in Figure 4.41 with the atom numbering scheme. Selected bond lengths are reported in Table 4.14.

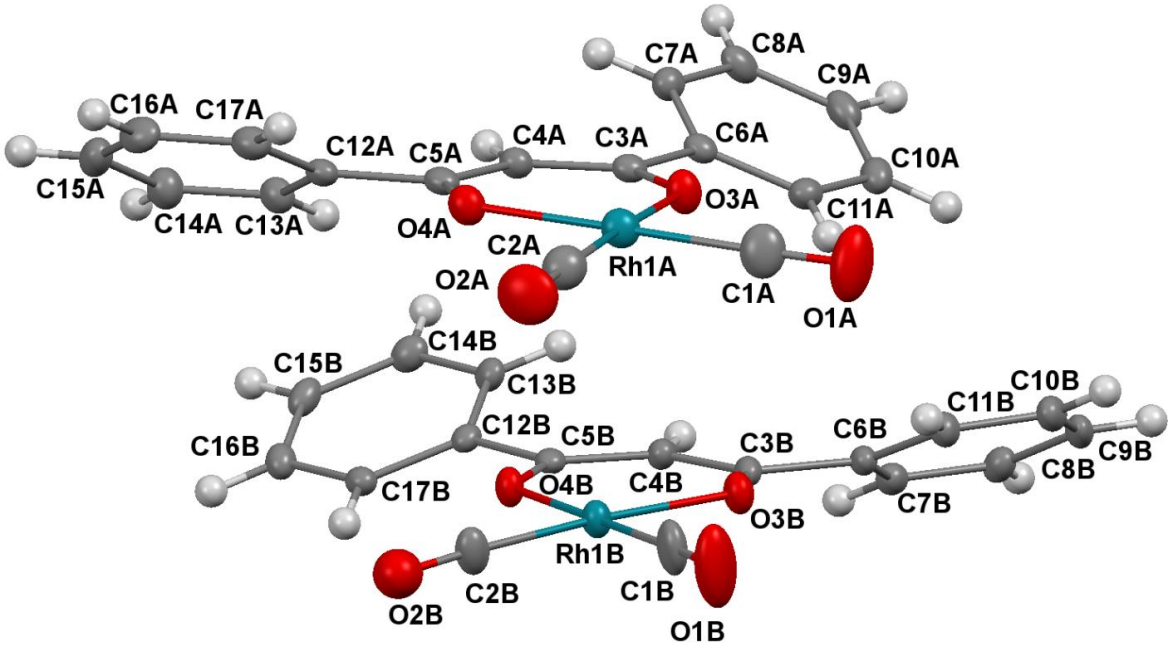

Figure 4.41: Molecular diagram of [Rh(dbm)(CO)$_2$] with atom numbering scheme. Hydrogen atom numbering has been omitted for the sake of clarity and thermal ellipsoids have been drawn at 50 % probability level.

Table 4.14: Selected bond distances of [Rh(dbm)(CO)$_2$].

Atoms	Distance (Å)	
	Molecule	
	A	B
Rh1-C1	1.854(6)	1.846(6)
Rh1-C2	1.845(6)	1.829(4)
Rh1-O3	2.015(3)	2.024(3)
Rh1-O4	2.025(3)	2.028(3)
C1-O1	1.130(7)	1.129(7)
C2-O2	1.141(7)	1.145(6)
C3-O3	1.290(5)	1.275(5)
C5-O4	1.292(5)	1.288(5)
O3···O4[a]	2.868(3)	2.878(3)

[a] Bite distance

Atoms	Angle (°) Molecule	
	A	B
C1-Rh1-C2	91.5(2)	86.4(2)
O3-Rh1-O4	90.49(9)	90.51(9)
C1-Rh1-O4	177.8(1)	178.5(1)
C2-Rh1-O3	177.6(1)	176.2(1)
C3-C4-C5	126.2(3)	125.8(3)
C1-Rh1-O3	87.6(1)	90.4(1)
C2-Rh1-O4	91.0(1)	92.2(1)
C3-O4···C5-O4[b]	179.2(3)	176.6(3)
C4-Rh1(1)···C4-Rh1(2)[c]	143.3(3)	143.3(3)
Dihedral angle(1)[d]	24.68(3)	27.29(3)
Dihedral angle(2)[d]	24.68(5)	23.20(7)

[b] Torsion angle between C3-O4 and C5-O4; [c] Torsion angle between C4-Rh1 and C4-Rh1 of neighbouring molecules; [d] defined as the torsion angle between the O4-C3-C4-C5-O4 plane and the phenyl ring (see scheme 4.2).

The molecules in the asymmetric unit displayed the expected square planar geometry for the Rh(I) complex. The distortion from the ideal geometry is represented in Figure 4.42. Of note is the extent to which the distortion exists between the two molecules. Molecule **A** displayed severe distortion in the C1-Rh1-O3 angle of 87.7(3)° whilst molecule **B** showed the greatest distortion with an angle of 86.32(2)° for C18-Rh2-C19.

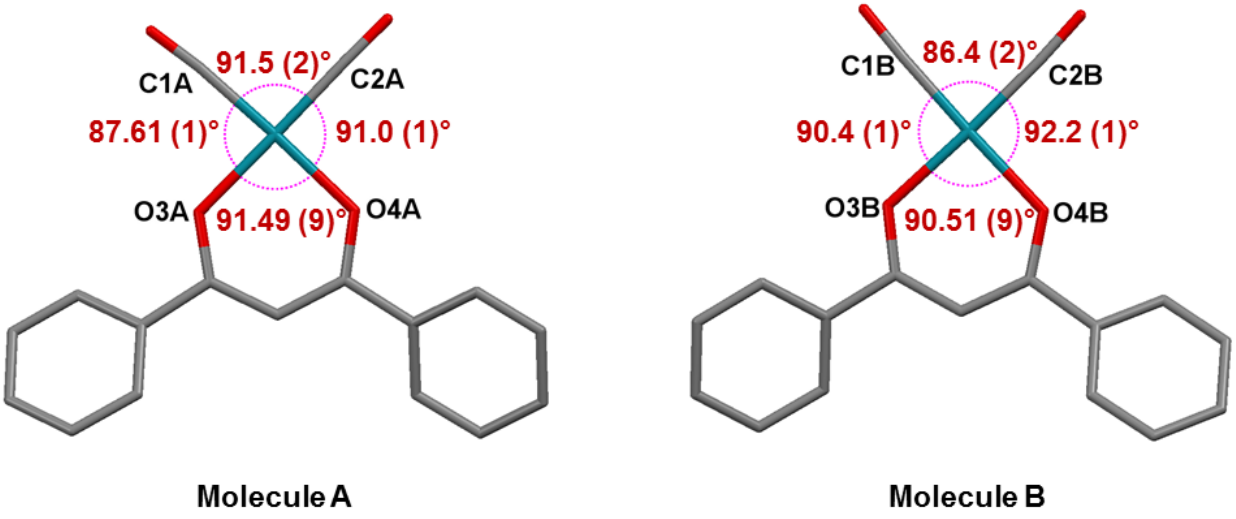

Figure 4.42: Represenation of the distortion of angles as observed in the square planar geometry of the two independent molecules of [Rh(dbm)(CO)$_2$].

All of the bond lengths were in good agreement with those reported in the previous structures. Of note is the shortened Rh-O bond (Rh1a-O3a = 2.015(3) Å) in the coordinating β-diketonato moiety in the complex. In the previous structures these bonds were reported in the 2.03-2.05 Å range (Sections 4.3, 4.4, 4.5 and 4.6).

Significant differences were noted for the dihedral angles of the phenyl rings of the two molecules. These differences are highlighted by an overlay of the two molecules given in Figure 4.43.

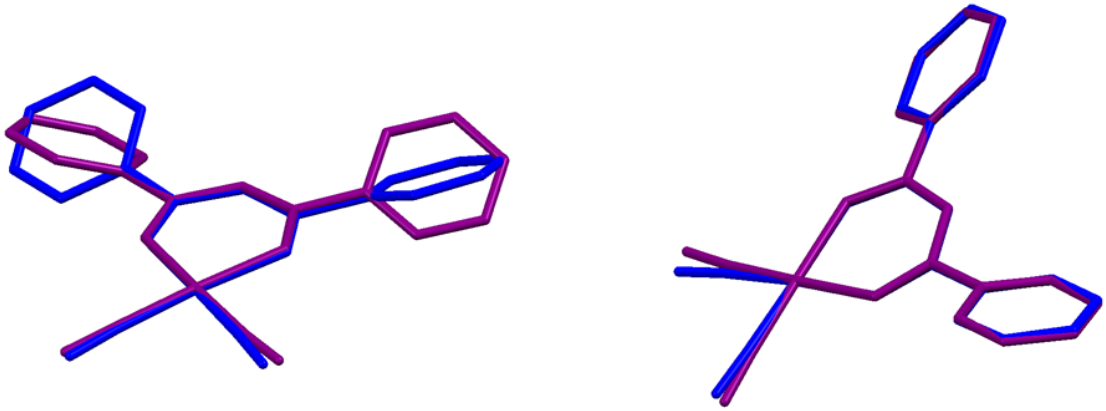

Figure 4.43: Overlay of the two molecules found in the asymmetric unit of [Rh(dbm)(CO)$_2$] molecule A= purple, molecule B= blue). The overlays are presented in two different orientations of the molecules clearly showing differences in the orientation of the phenyl rings and the position of the carbonyl moieties between the two molecules.

As with the previous structures, metallophilic interactions were also observed for the [Rh(dbm)(CO)$_2$] structure. Figure 4.44 gives a representation of these interactions between neighbouring rhodium(I) centres. The interactions are along the shortest cell axis (*a*-axis= 7.0256(2) Å) in the unit cell which is consistent with the other metallophilic interactions encountered in the previous structures. Alternating Rh···Rh distances of 3.487(1) Å and 3.563(1) Å were determined along the one-dimensional metal chain. Following [Rh(bzac)(CO)$_2$] (3.308(3) Å and 3.461(3) Å) the [Rh(dbm)(CO)$_2$] complex displayed the shortest Rh···Rh distances.

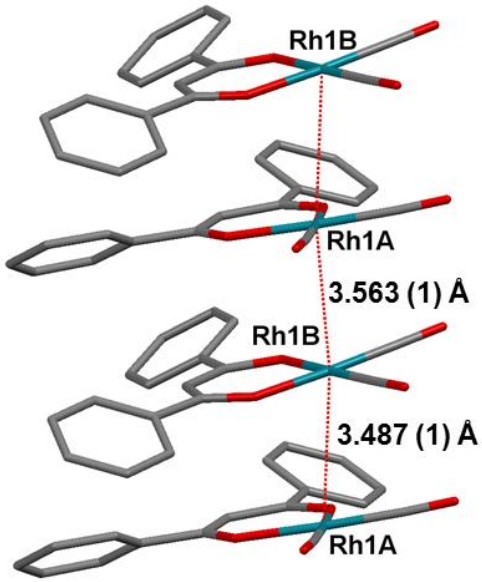

Figure 4.44: Illustration of the Rh···Rh interactions (indicated in red) between neighbouring molecules in [Rh(dbm)(CO)$_2$] along the *a*-axis of the unit cell.

The Rh(I) centres displayed angles of 170.52(1)° (Rh1a-Rh1b-Rh1a) and torsion angles of 143.3(3)° between coordinating β-diketonato moeites (C4a-Rh1a···Rh1b-C4b) along the one-dimensional metal chain. The staggered arrangement of the neighbouring molecules in the 1-D chain is illustrated in Figure 4.45.

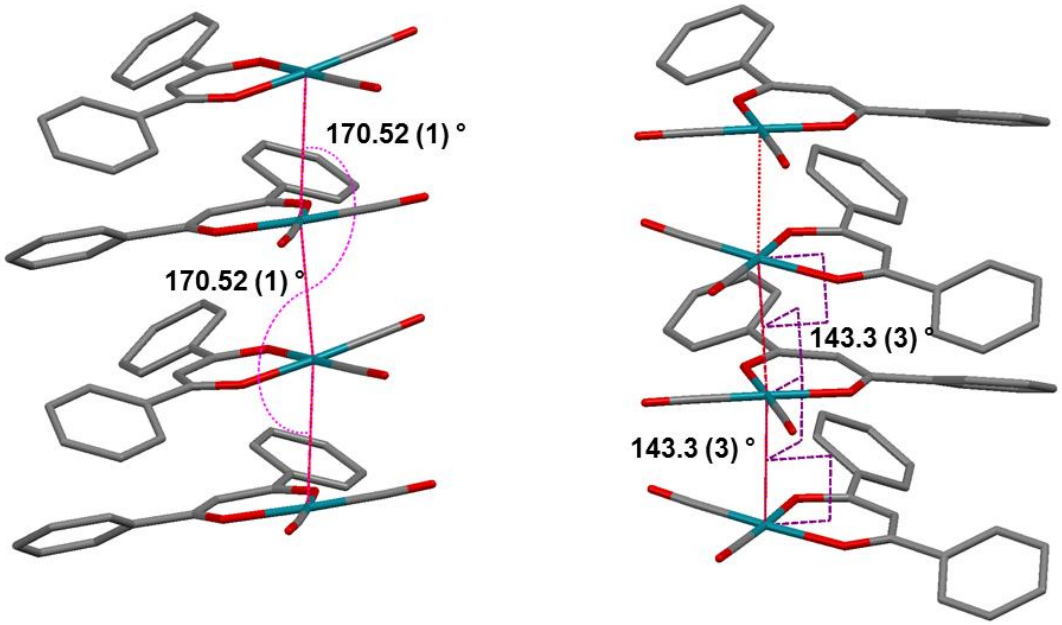

Figure 4.45: a) Rh···Rh interactions between neighbouring Rh(I) centres with angles of 170.52(1)°; b) Torsion angles of 143.3(3)° between coordinating β-diketonato moieties (C4a-Rh1a···Rh1b-C4b) revealed a staggered arrangement of molecules along the 1-D chain.

One hydrogen bond (Figure 4.46) was observed in the structure between the H10 and O6 atoms with detail related to the hydrogen bond given in Table 4.15.

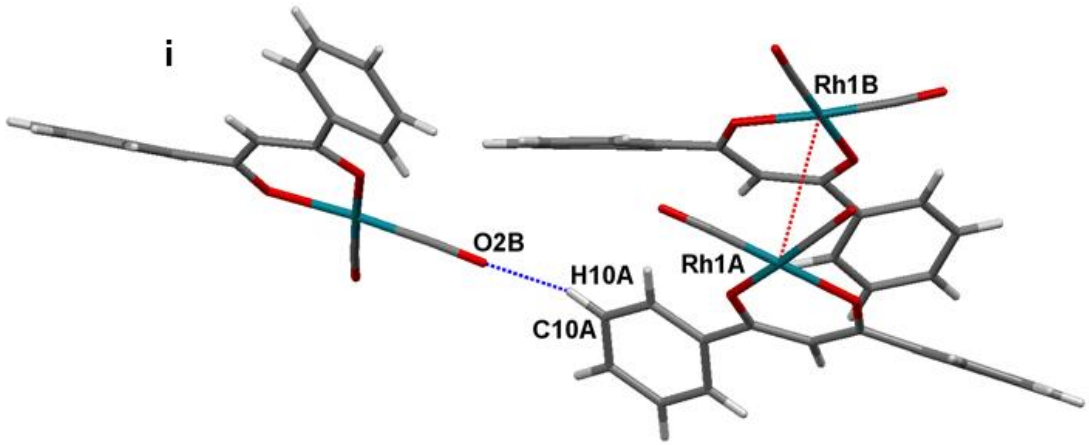

Figure 4.46: Hydrogen bond between an oxygen atom of the carbonyl moiety and hydrogen atom of one of the phenyl rings between neighbouring molecules in [Rh(dbm)(CO)$_2$].

Table 4.15: Hydrogen-bond geometry for [Rh(dbm)(CO)$_2$].

D-H···A	dD-H (Å)	dH···A (Å)	dD···A (Å)	Angle D-H···A (°)
C10-H10···O6^{i}	0.93	2.495	3.279(6)	142.2

Symmetry codes: i) 1-x, 1/2-y, -1/2+z.

O···O soft contacts exist between neighbouring molecules of [Rh(dbm)(CO)$_2$] as illustrated in Figure 4.47. The O1a···O1a (2.924(4) Å) and O1b···O1b (2.931(4) Å) contacts result in dimers forming between neighbouring molecules of [Rh(dbm)(CO)$_2$] in a head-to-head motif.

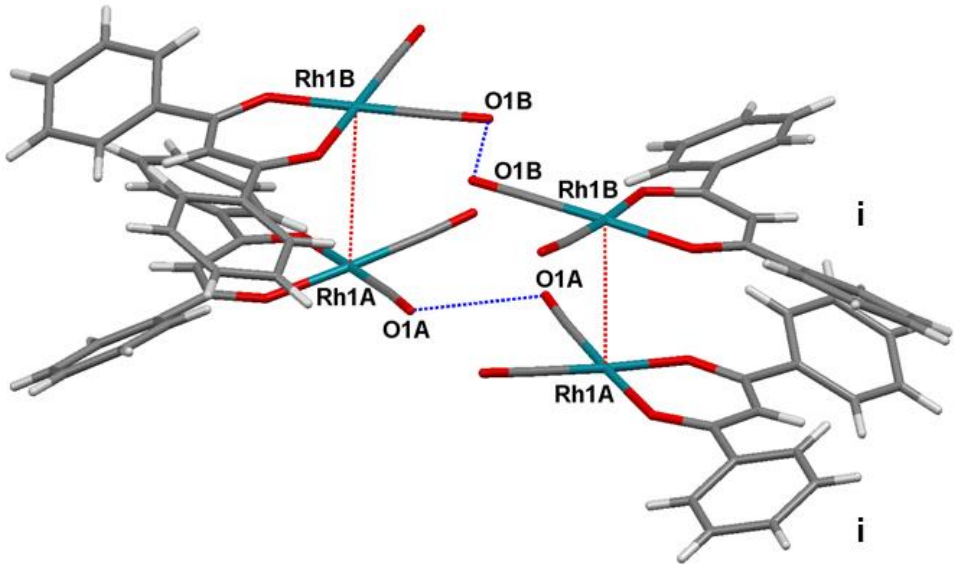

Figure 4.47: O···O soft contacts between neighbouring molecules result in dimers of molecules in [Rh(dbm)(CO)$_2$] (Symmetry operation: i) x, -y,1-z).

Illustrated in Figure 4.48, the packing diagram of [Rh(dbm)(CO)$_2$] clearly shows the dominating effect of metallophilic interactions in the packing within the unit cell. This is consistent with the packing diagrams observed for [Rh(bzac)(CO)$_2$] (Section 4.3), [Rh(F$_3$-bzac)(CO)$_2$] (Section 4.4) and [Rh(F$_3$-4Clbzac)(CO)$_2$] (Sections 4.5 and 4.6).

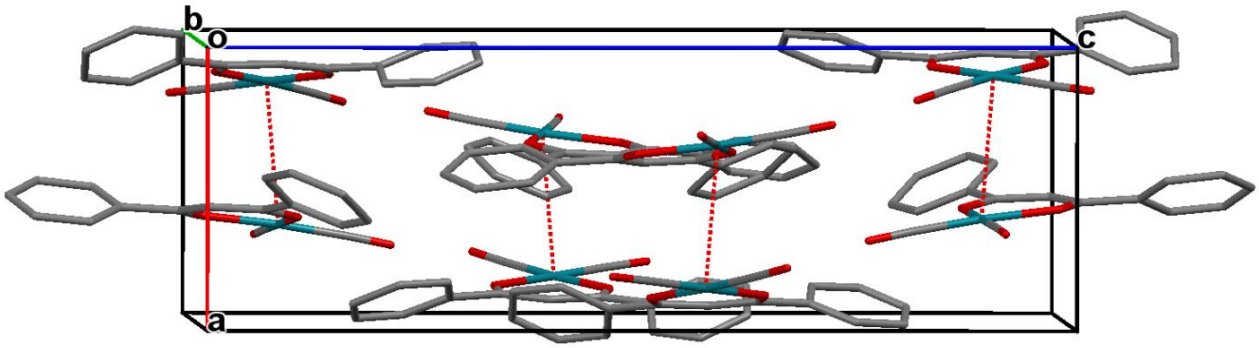

Figure 4.48: Packing of [Rh(dbm)(CO)$_2$] along an off-centered *b*-axis showing the dominating influence metallophilic interactions have on the stability of the crystal lattice.

4.8 Conclusion

Five solid-state structures of four Rh(I) complexes with different coordinated β-diketonato ligands were presented in this chapter. All of the structures displayed metallophilic interactions as well as other interactions such as halogen···halogen interactions and hydrogen bonding within the crystal lattices.

A complete discussion of all the structures evaluated during this study will be presented in Chapter 8 including the five structures presented in this chapter. This will allow for a better evaluation of the effect that subtle changes on the coordinating β-diketonato ligands may have on the metallophilic interactions and ultimately the construction of 1-D metal chains.

In the coming chapters, additional structures will be presented with the introduction of other electronic and steric changes to the coordinating ligands to allow for the manipulation of the metallophilic interactions and the physical properties associated with the crystals.

Chapter 5: Crystallographic Study of $[Rh(acac)(CO)_2]$, $[Rh(3Cl\text{-}acac)(CO)_2]$, $[Rh(CN\text{-}acac)(CO)_2]$ and $[Rh(pyruv)(CO)_2]$

5.1 Introduction

This chapter focusses on the structures obtained for rhodium(I) complexes of which changes were mostly introduced on the methine carbon of the coordinating β-diketonato ligand. The well-known $[Rh(acac)(CO)_2]$ structure is included in this chapter as its structure is to be used as a reference point in comparing the different structures obtained in the study (see Chapter 8). The four ligands that were successfully coordinated to rhodium and will be discussed in this chapter are illustrated in scheme 5.1.

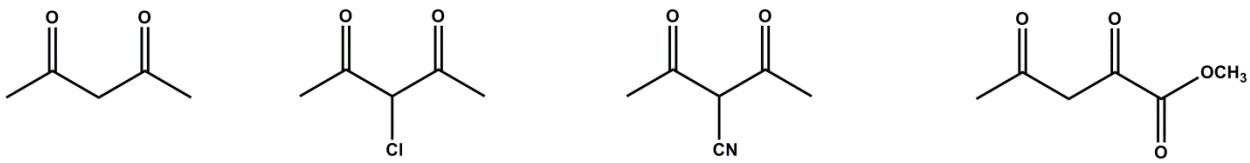

Acetylacetone **(acacH)** | 3-Chloro-2,4-pentanedione **(3Cl-acacH)** | 3-Cyano-2,4-pentanedione **(CN-acacH)** | Methyl acetopyruvate **(pyruvH)**

Scheme 5.1: Different β-diketone ligands coordinated to rhodium in the design of nano-wired materials utilizing metallophilic interactions.

The chapter will include a discussion on each rhodium(I) complex obtained by coordination of the above mentioned ligands as well as comparisons between the four structures.

5.2 Experimental

The reflection data of $[Rh(acac)(CO)_2]$, $[Rh(3Cl\text{-}acac)(CO)_2]$, $[Rh(CN\text{-}acac)(CO)_2]$ and $[Rh(pyruv)(CO)_2]$ were collected on a Bruker X8 Apex II 4K Kappa CCD diffractometer using graphite monochromated Mo Kα radiation (λ= 0.70926 Å) with ω- and φ-scans at 100(2) K. The Apex II software package[1] was utilized along with the optimum measurement method in collecting more than a hemisphere of reciprocal space as predicted by COSMO.[2] Frame integration and data reduction was performed using the SAINT-Plus and XPREP software

[1] **Apex2**, Version 2012.10-0, Bruker AXS Inc.,Madison, Wisconsin, USA, **2012**.
[2] **COSMO**, Version 1.48, Bruker AXS Inc., Madison, Wisconsin, USA, **2003**.

packages and SADABS[3] was made use of for multi-scan absorption correction.[4] The structures were solved using SIR92[5], SIR97[6], SIR2002[7], DIRDIF[8] or Superflip[9] with refinement performed using the WinGX software package[10] that incorporates SHELXL[11]. All atoms were refined anisotropically with the exception of hydrogen atoms. The hydrogen atoms were positioned geometrically and refined utilizing a riding model with fixed C-H distances of 0.98 Å (CH) [U_{iso}(H)= 1.2 Ueq] for methyl hydrogens and methine hydrogens with fixed C-H distances of 0.95 Å (CH) [U_{iso}(H)= 1.2 Ueq]. Molecular diagrams were generated with the Mercury software package[12] with a 50 % thermal ellipsoid probability for all non-hydrogen atoms. General crystal data and refinement parameters are represented in Table 5.1 with the complete list of atomic coordinates, equivalent anisotropic parameters and hydrogen coordinates of each data set given in Appendix A.

[3] **SADABS**, Version 2012/1, BrukerAXS Inc, Madison, Wisconsin, USA, **2012**.
[4] **SAINT-Plus**, Version 8.27B including XPREP, Bruker AXS Inc., Madison, Wisconsin, USA, **2012**.
[5] Altomare, A., Cascarano, G., Giacovazzo, C., Guagliardi, A., Burla, M. C., Polidori, G., Camalli, M., *J. Appl. Cryst.*, **1994**, *27*, 435-436.
[6] Altomare, A., Burla, M. C., Camalli, M., Cascarano, G. L., Giacovazzo, C., Guagliardi, A., Moliterni, A. G. G., Polidori, G., Spagna, R., *J. Appl. Cryst.*, **1999**, *32*, 115-119.
[7] Burla, M. C., Camalli, M., Carrozzini, B., Cascarano, G. L., Giacovazzo, C., Polidori, G., Spagna, R., *J. Appl. Cryst.*, **2003**, *36*, 1103.
[8] Beurskens, P. T., Admiraal, G., Beurskens, G., Bosman, W. P., Garcia-Granda, S., Gould, R. O., Smits, J. M. M., Smykalla, C., Crystallography Laboratory, University of Nijmegen, Toernooiveld, The Netherlands.
[9] Palatinus, L., Chapuis, G., *J. Appl. Cryst.*, **2007**, *40*, 786-790.
[10] **WinGX**. Farrugia, L. J., *J. Appl. Cryst.*, **2012**, *45*, 849–854.
[11] Sheldrick, G. M., *Acta Cryst.*, **2008**, *A64*, 112-122.
[12] **Mercury**, Macrae, C. F., Bruno, I. J., Chisholm, J. A., Edgington, P. R., McCabe, P., Pidcock, E., Rodriquez-Monge, L., Taylor, R., van de Streek, J., Wood, P. A., *J. Appl. Cryst.*, **2008**, *41*, 466-470.

Table 5.1: General crystal data for [Rh(acac)(CO)$_2$], [Rh(3Cl-acac)(CO)$_2$], [Rh(CN-acac)(CO)$_2$] and [Rh(pyruv)(CO)$_2$].

Crystallographic Data	[Rh(acac)(CO)$_2$]	[Rh(3Cl-acac)(CO)$_2$]	[Rh(CN-acac)(CO)$_2$]	[Rh(pyruv)(CO)$_2$]
Empirical Formula	$C_7H_7O_4Rh$	$C_7H_6ClO_4Rh$	$C_9H_6N_2O_4Rh$	$C_8H_7O_6Rh$
Molecular weight (g/mol)	258.04	292.48	482.88	302.05
Crystal system, space group	Triclinic, $P\bar{1}$	Orthorhombic, *Ccma*	Monoclinic, *C2/m*	Triclinic, $P\bar{1}$
a (Å)	6.523(2)	6.601(1)	15.697(9)	7.519(3)
b (Å)	7.768(3)	10.887(2)	6.474(3)	7.883(3)
c (Å)	9.182(3)	13.349(3)	14.446(8)	9.799(4)
***α* (°)**	106.09(2)	90.0	90.0	103.18(1)
***β* (°)**	91. 20(1)	90.0	90.35(3)	110.93(1)
***γ* (°)**	100.28(1)	90.0	90.0	99.94(1)
Volume (Å^3)	438.7(5)	914.3(6)	1468.0(1)	507.1(5)
Z	2	8	4	2
Density calculated (g/ cm^3)	1.954	2.125	2.185	1.978
Absorption coefficient (mm^{-1})	1.917	2.136	2.619	1.689
***F* (000)**	252	1136	920	296
Crystal size (mm^3)	0.215 x 0.227 x 0.909	0.15 x 0.16 x 0.44	0.002 x 0.289 x 0.616	0.14 x 0.15 x 0.72
Morphology, colour	Needle, red	Needle, red	Plate, purple	Needle, red
***Θ* range for data collection**	2.78 to 30.78	3.58 to 27.98	1.41 to 28.0	2.34 to 28.0
Completeness for collection (%)	99.0	99.8	99.8	99.5
Index ranges	-8≤ *h* ≥8 -10≤ *k* ≥10 -11≤ *l* ≥12	-8≤ *h* ≥8 -27≤ *k* ≥27 -17≤ *l* ≥17	-20≤ *h* ≥20 -8≤ *k* ≥8 -18≤ *l* ≥19	-9≤ *h* ≥9 -10≤ *k* ≥10 -12≤ *l* ≥12
Reflections collected	7061	21467	17217	8156
Independent reflections	4675	1199	1929	2429
Observed reflections	1887 (R_{int}= 0.0511)	1110 (R_{int}= 0.0538)	1253 (R_{int}= 0.1097)	2253 (R_{int}=0.0523)
Max. and min. transmission	0.407 and 0.746	0.602 and 0.746	0.588 and 0.746	0.376 and 0.798
Data/ restraints/ parameters	2100/ 0/ 109	1199/ 0/ 79	1929/ 0/ 107	2429/ 0/ 136
Goodness-of-fit on F^2	1.15	1.04	1.109	1.206
Final R indices	R1= 0.0447 wR2= 0.1439	R1= 0.0232 wR2= 0.0618	R1= 0.0700 wR2= 0.2336	R1= 0.257 wR2= 0.0725
R indices	R1= 0.0505 wR2= 0.1618	R1= 0.0254 wR2= 0.0634	R1= 0.0994 wR2= 0.2670	R1= 0.315 wR2= 0.1021
Largest diff. Peak and hole (e.Å^{-3})	0.87 and -2.30	0.82 and -0.88	1.94 and -1.73	1.01 and-1.61

5.3 Crystal structure of [Rh(acac)(CO)$_2$]

The structure reported for the [Rh(acac)(CO)$_2$] complex is a re-determination of the solid-state structure of the complex which was synthesized by Bonati and Wilkinson[13] in 1964 as the first rhodium(I) complex coordinated to a β-diketonato ligand. The structure of the complex was however only proposed by Ugo *et al.*[14] in 1967 whilst the first X-ray determination of the structure was performed and reported by Huq and Skapski[15] in 1974. The initial structure determination by Huq and Skapski[15] was performed at 20 °C and as such a re-determination was performed at 100 K with the aim of obtaining more accurate data.

As this study focuses on the comparison of various rhodium(I) complexes coordinated with β-diketonato ligands an accurate comparison to the relatively basic structure of [Rh(acac)(CO)$_2$] is essential. Data obtained for the structure determination of [Rh(acac)(CO)$_2$] that was treated in a similar matter to the other structures reported in this study would result in better correlations and comparisons between the structures. Table 5.2 offers a comparison of the unit cell dimensions found in this study for the structure of [Rh(acac)(CO)$_2$] with those reported by Huq and Skapski[15] in their structure determination performed in 1974.

Table 5.2: Comparison of the cell dimensions for the structure determined in this study as well as the published structure of [Rh(acac)(CO)$_2$] by Huq and Skapski[15].

Cell dimension	This Study	Published[15]
a	6.523(2)	6.5189(5)
b	7.768(3)	7.7614(8)
c	9.182(3)	9.205(1)
α	106.09(2)	106.04(1)
β	91. 20(1)	91.15(1)
γ	100.28(1)	100.21(1)
Space group	Triclinic, *P*$\bar{1}$	Triclinic, *P*$\bar{1}$
Z	2	2
Z'	1	1
Temperature (K)	100	293

As can be seen from Table 5.2, small differences in the unit cell dimensions exist for the two structure determinations. The slight deviations could be attributed to the different temperatures at which the collections were performed. Lower temperature collections typically result in smaller unit cell dimensions as a result of a small contraction of the unit

[13] Bonati, F., Wilkinson, G., *J. Chem. Soc.*, **1964**, 3156.
[14] Bailey, N. A., Coates, E., Robertson, G. B., Bonati, F., Ugo, R., *Chem. Commun.*, **1967**, 1041.
[15] Huq, F., Skapski, A. C., *J. Cryst. Mol. Struct.*, **1974**, *4*, 411-418.

cell. This is in part due to the vibrational parameters of the individual atoms in the molecule becoming restricted as the temperature is lowered.[16]

Very little other crystallographic information could be obtained from the published structure of [Rh(acac)$(CO)_2$] with no information available with regards to the R values or completeness of the data collection. These are valuable indicators of the reliability of a structure determination. In addition to these reasons the motivation for a unified correlation between the structures of this study to that of [Rh(acac)$(CO)_2$] resulted in an inclusion of the re-determination of the structure in our study.

The complex, (acetylacetonato-κ^2O,O)dicarbonylrhodium(I), crystallized in the triclinic space group $P\bar{1}$ with only one independent molecule in the asymmetric unit. The molecular structure as well as the numbering scheme is represented in Figure 5.1. General crystallographic information of the crystal structure is referred to in Table 5.1 with selected bond lengths and angles given in Table 5.3. Selected bond lengths and angles found for the published structure are included for comparison. For comprehensive information regarding bond distances and angles related to the structure refer to Appendix A.

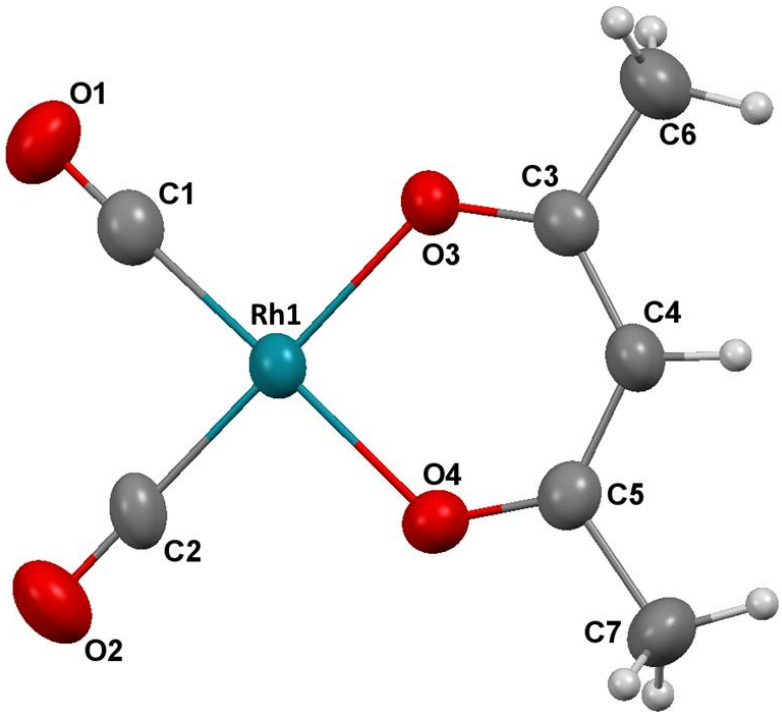

Figure 5.1: Molecular structure of [Rh(acac)$(CO)_2$] with atom numbering scheme (thermal ellipsoid probability= 50 %). Hydrogen atom labels have been omitted for clarity.

[16] Julian, M. M., *Foundations of Crystallography with Computer Applications*, CRC Press, Boca Raton, United States of America, **2015**, 21.

Table 5.3: Selected bond distances and angles of [Rh(acac)(CO)$_2$] for the structure found in this study as well as the published structure by Huq and Skapski[15].

Atoms	This Study	Published[15]
	Distance (Å)	
Rh1-C1	1.865(8)	1.831(7)
Rh1-C2	1.838(6)	1.831(7)
Rh1-O3	2.036(4)	2.040(4)
Rh1-O4	2.047(5)	2.044(4)
C1-O1	1.127(9)	1.155(8)
C2-O2	1.142(7)	1.144(7)
C3-O3	1.273(7)	1.285(6)
C5-O4	1.259(7)	1.498(7)
O3···O4[a]	2.900(6)	2.909

[a] Bite distance

Atoms	This Study	Published[15]
	Angle (°)	
C1-Rh1-C2	88.4(3)	88.9(3)
O3-Rh1-O4	90.5(2)	89.8(3)
C1-Rh1-O4	178.5(2)	-
C2-Rh1-O3	179.2(2)	-
C3-C4-C5	126.5(4)	127.1(5)
C1-Rh1-O3	90.9(3)	90.5(2)
C2-Rh1-O4	90.2(2)	90.8(2)
O3-C3···O4-C5[b]	179.84(3)	179.88

[b] Torsion angle between C3-O3 and C5-O4

All of the distances reported in Table 5.3 are well in range for the respective bond types such as the R1-C1 and Rh1-C2 distances of 1.865(8) Å and 1.838(6) Å (see Chapter 4 and 6). The slight differences between the two carbonyl bonds are interesting to note as the complex was expected to display a complete symmetrical geometry due to the symmetrical β-diketonato ligand coordinated to the rhodium(I) centre. For the published structure this was indeed the case as noted by the Rh1-C1 and Rh1-C2 distances of 1.831(7) Å.

The rhodium(I) complex displayed a square planar geometry as was seen with the other complexes discussed in Chapter 4. The angles between the rhodium(I) centre and the coordinating atoms display an almost perfectly square planar geometry with angles of nearly 90°. Only the 88.4(3)° angle of C1-Rh1-C2 showed slight deviation from the ideal 90° as can be seen in Figure 5.3.

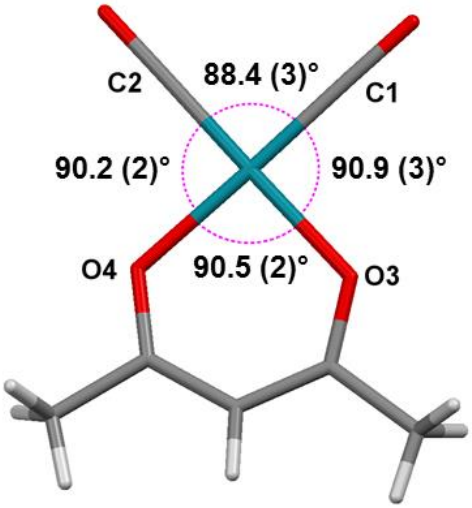

Figure 5.3: Represenation of the relatively undistorted square planar geometry observed in [Rh(acac)(CO)$_2$] as illustrated by the angles between the coordinating moiety of atoms.

The only intermolecular interactions found in the structure of [Rh(acac)(CO)$_2$] were metallopilic interactions found between Rh(I) centres of neighbouring molecules. These interactions result in the formation of a one-dimensional metal chain along one direction infinitely within the crystal lattice. These interactions were found to occur along the shortest cell axis of the unit cell of [Rh(acac)(CO)$_2$] (*a*-axis= 6.523(3) Å) and are illustrated in Figure 5.4. Rh···Rh interactions were found to alternate with distances of 3.254(3) Å and 3.274(3) Å repeated throughout the one-dimensional metal chain between neighbouring rhodium(I) centres.

As was discussed in Chapter 2, the strength of metallophilic interactions between metal centres is dependent upon the electronic influences brought upon by the coordinating ligands as well as the steric hindrance that some ligands might offer. [17,18,19] In the case of acetylacetonato the the methyl moieties are regarded as slighlty electron donating and as a result there is an increase of electron density at the rhodium(I) centre. With the increased electron density present on the metal centre the dz^2 orbitals are enlarged. As was mentioned in Chapter 2 metallophilic interactions between d^8 metal centres occurs primarily *via* overlap of the dz^2 orbitals and hence in the case of the enlarged dz^2 orbitals, overlap between neighbouring rhodium(I) centres in [Rh(acac)(CO)$_2$] is enhanced. This results in strengthened metallophilic interactions with shorter Rh-Rh distances as a result.

[17] Mégnamisi-Bélombé, M., *J. Solid Chem.*, **1979**, *27*, 389-396.
[18] Ferraris, G., Viterbo, D., *Acta Cryst.*, **1969**, *B25*, 2066-2070.
[19] Krogmann, K., Stephan, D., *Z. Anorg. Allg. Chem.*, **1968**, *362*, 290-300.

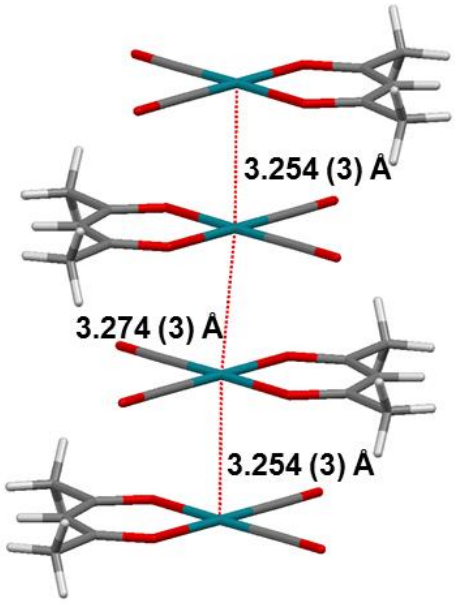

Figure 5.4: Rh···Rh interactions (indicated in red) between neighbouring molecules of [Rh(acac)(CO)$_2$] with Rh-···Rh distances of 3.254(3) Å and 3.274(3) Å.

As depicted in Figure 5.5 the Rh(I) centres connected *via* metallophilic interactions are in an almost linear arrangement with angles of 175.45(3)° between rhodium(I) centres (Rh1-Rh1-Rh1) in the one-dimensional metal chain. The ligands were found to be arranged in an eclipsed arrangement with angles of 180.0(2)° determined between the R-groups (C4-Rh1···Rh1-C4) of neighbouring molecules.

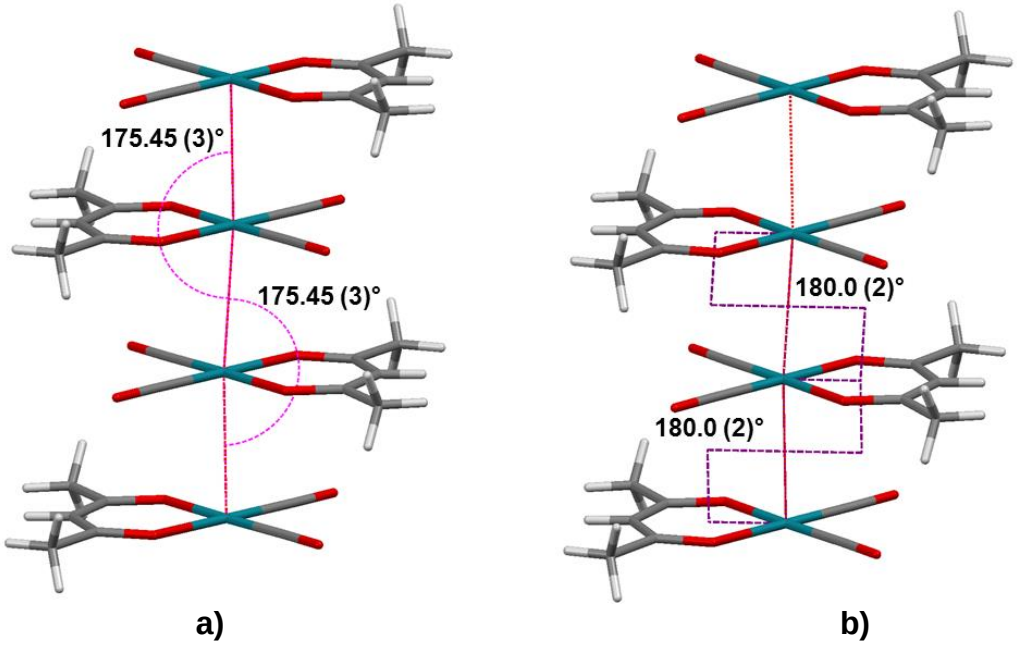

Figure 5.5: a) Angles of 175.45(3)° between Rh(I) centres (Rh1-Rh1-Rh1) are repeated throughout the crystal structure; b) Torsion angles of 180.0(2)° between coordinating β-diketonato ligands (C5-Rh1···Rh1-C5) of neighbouring molecules indicate an eclipsed arrangement of R-groups.

No other intermolecular interactions are found in the structure of [Rh(acac)$(CO)_2$] highlighting the importance of metallophilic interactions in the packing of molecules in the crystal lattice. The extended packing diagram for [Rh(acac)$(CO)_2$] in Figure 5.6 shows how the metallophilic interactions connect the molecules in the crystal structure in a head-to-tail motif along the *c*-axis between two metallophilic chains.

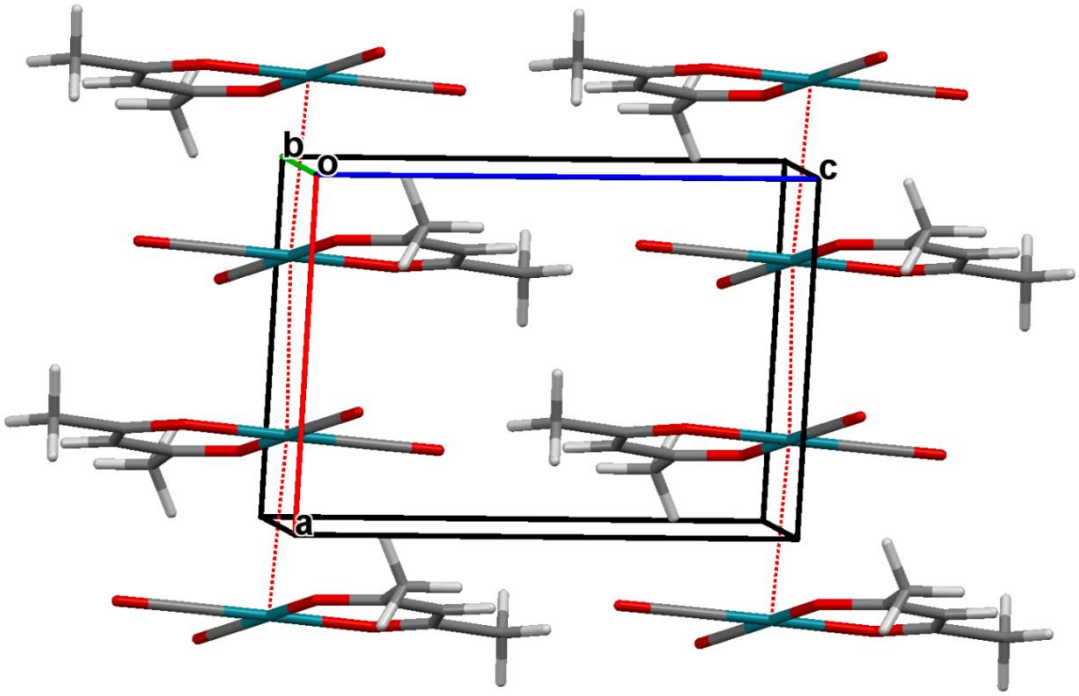

Figure 5.6: Extended packing diagram of [Rh(acac)$(CO)_2$] viewed along an off-centered *b*-axis highlighting the dominating effect metallophilic interactions have on the packing of molecules in the crystal lattice.

5.4 Crystal structure of [Rh(3Cl-acac)$(CO)_2$]

The complex, dicarbonyl(3-chloroacetylacetonato-κ^2O,O)rhodium(I), crystallized in the orthorhombic space group *Ccma* with only one independent molecule in the asymmetric unit and 8 molecules in the unit cell. Figure 5.7 represents the molecular structure as well as the numbering scheme of [Rh(3Cl-acac)$(CO)_2$] with selected bond lengths and angles given in Table 5.4.

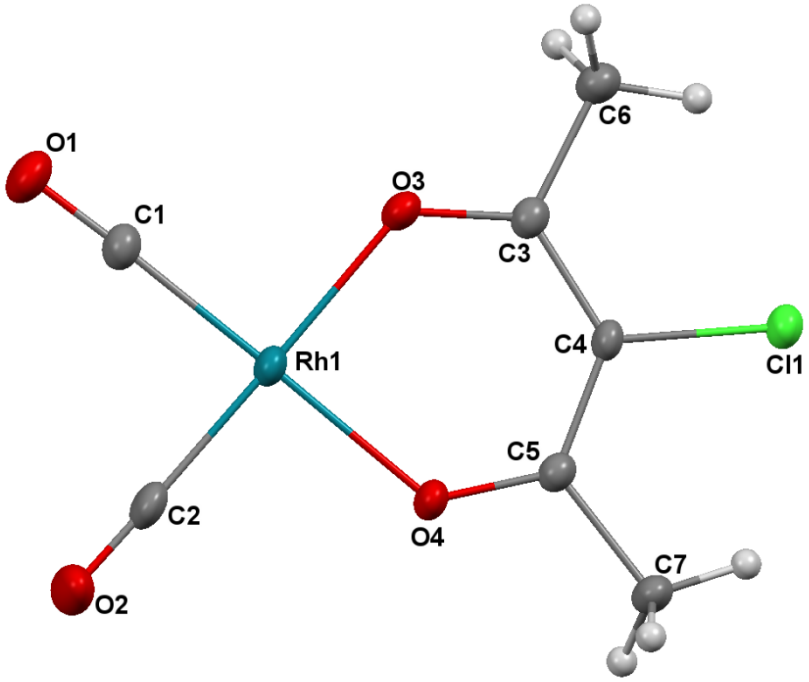

Figure 5.7: Molecular structure of [Rh(3Cl-acac)(CO)$_2$] with atom numbering scheme (thermal ellipsoid probability= 50 %). Hydrogen atom labels have been omitted for clarity.

Table 5.4: Selected bond distances and angles of [Rh(3Cl-acac)(CO)$_2$].

Atoms	Distance (Å)
Rh1-C1	1.854(4)
Rh1-C2	1.848(4)
Rh1-O3	2.026(3)
Rh1-O4	2.034(3)
C1-O1	1.130(5)
C2-O2	1.135(5)
C3-O3	1.272(4)
C5-O4	1.281(4)
C4-Cl1	1.757(4)
O3···O4[a]	2.850(3)

[a] Bite distance

Atoms	Angle (°)
C1-Rh1-C2	87.2(2)
O3-Rh1-O4	89.2(1)
C1-Rh1-O4	178.9(1)
C2-Rh1-O3	179.1(1)
C3-C4-C5	126.5(3)
C1-Rh1-O3	91.9(1)
C2-Rh1-O4	91.8(1)
O3-C3-C4	124.2(3)
O4-C5-C4	124.5(3)
O3-C3···O4-C5[b]	180.0(3)

[b] Torsion angle between C3-O3 and C5-O4

The bond distances reported for [Rh(3Cl-acac)(CO)$_2$] are in good agreement with the bond lengths of [Rh(acac)(CO)$_2$]. The carbonyl bond distances of 1.854(4) Å and 1.848(4) Å for Rh1-C1 and Rh1-C2 are in good agreement with the reported bond lengths of 1.865(8) Å

and 1.838(6) Å for [Rh(acac)(CO)$_2$]. The Rh1-O3 and Rh1-O4 bond distances of 2.026(3) Å and 2.034(3) Å are slightly shorter than those of [Rh(acac)(CO)$_2$] (2.036(4) Å and 2.047(5) Å).

As is evidenced in the angles reported in Table 5.4 almost no distortion of the square planar geometry was noted in [Rh(3Cl-acac)(CO)$_2$]. The only angle with a slight deviation from the ideal 90° is the C1-Rh1-C2 angle of 87.2(2)°.

The structures of [Rh(acac)(CO)$_2$] and [Rh(3Cl-acac)(CO)$_2$] were expected to be fairly similar as only a chlorine atom in [Rh(3Cl-acac)(CO)$_2$] differentiates the two molecules chemically. An overlay of the two molecules is represented in Figure 5.8 showing almost identical structures for [Rh(acac)(CO)$_2$] and [Rh(3Cl-acac)(CO)$_2$].

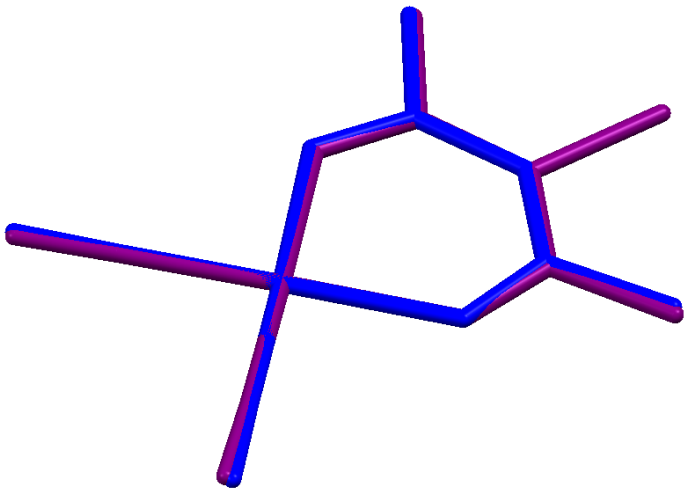

Figure 5.8: Overlay of [Rh(3-Clacac)(CO)$_2$] (purple) and [Rh(acac)(CO)$_2$] (blue) reveal an almost perfect overlay between the two molecules.

As was observed in the [Rh(acac)(CO)$_2$] complex, the dominating influence in the packing of molecules in the crystal lattice of [Rh(3Cl-acac)(CO)$_2$] are metallophilic interactions between neighbouring Rh(I) centres. These interactions occur along the *a*-axis (6.601(1) Å) of the unit cell with a fixed distance of 3.317(2) Å between rhodium(I) centres as illustrated in Figure 5.9. The packing along the shortest cell axis is consistent with the stacking of molecules observed in [Rh(acac)(CO)$_2$] (see Section 5.3). The Rh···Rh distance reported for this complex is slighlty longer than the Rh···Rh distances found between molecules in the structure of [Rh(acac)(CO)$_2$] (3.254(3) Å and 3.274(3) Å). The slightly longer Rh···Rh distances in [Rh(3Cl-acac)(CO)$_2$] could be the result of less dz^2 interaction between metal centres as the Cl atom is highly electron withdrawing thereby removing electron density from the rhodium(I) centre.

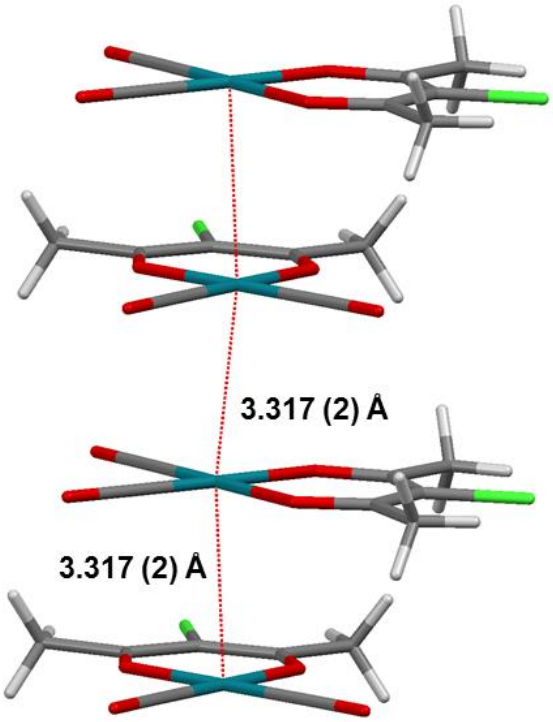

Figure 5.9: Rh···Rh interactions (indicated in red) between neighbouring molecules form a one-dimensional metal chain along the *a*-axis in [Rh(3Cl-acac)(CO)$_2$].

The molecules were found to stack in a distorted linear arrangement with angles of 168.66(2)° between Rh(I) centres (Rh-Rh-Rh) as can be seen in Figure 5.10. This is slightly less linear than was found for the molecules of [Rh(acac)(CO)$_2$] with reported angles of 175.45(3)°. The molecules are stacked in a staggered arrangement with torsion angles of 103.34(3)° between coordinating moieties (C4-Rh1···Rh1-C4). This is in contrast to the [Rh(acac)(CO)$_2$] complex which displayed an eclipsed arrangement of molecules (180.0(2)°) along the one-dimensional metal chain. The staggered arrangement could potentially be adopted by the molecules to accommodate the fairly large chlorine subsitutent and prevent steric hindrance in the establishment of metallophilic interactions in the one-dimensional metal chain.

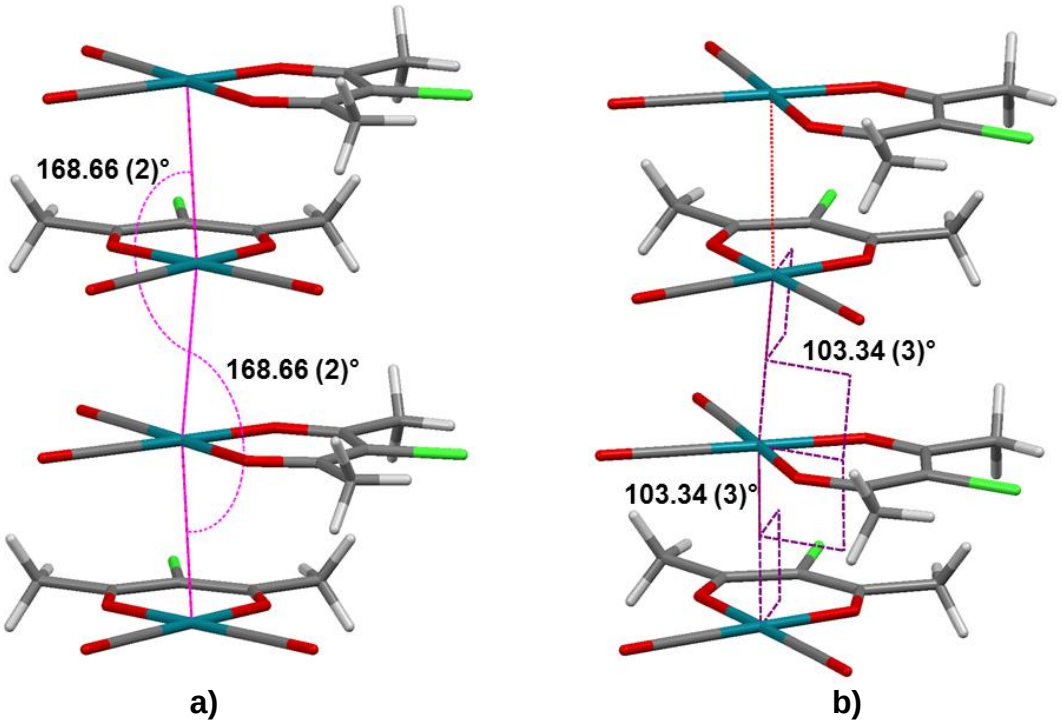

Figure 5.10: a) An angle of 168.66(2)° (Rh1-Rh1-Rh1) is found between neighbouring Rh centres along the 1-D chain; b) Torsion angles of 103.34(3)° between coordinating β-diketonato ligands (C4-Rh1···Rh1-C4) revealed a staggered arrangement of R-groups in [Rh(3Cl-acac)$(CO)_2$].

The crystal lattice of [Rh(3Cl-acac)$(CO)_2$] is further stabilized by soft contacts illustrated in Figure 5.11 with relevant information given in Table 5.5. The O1-O2 soft contacts are arranged in a head-to-head manner that leads to dimer formation between neighbouring molecules. The dimer formation is further supported by the O2-C7 interactions found in a side-ways orientation between molecules in a head-to-tail fashion.

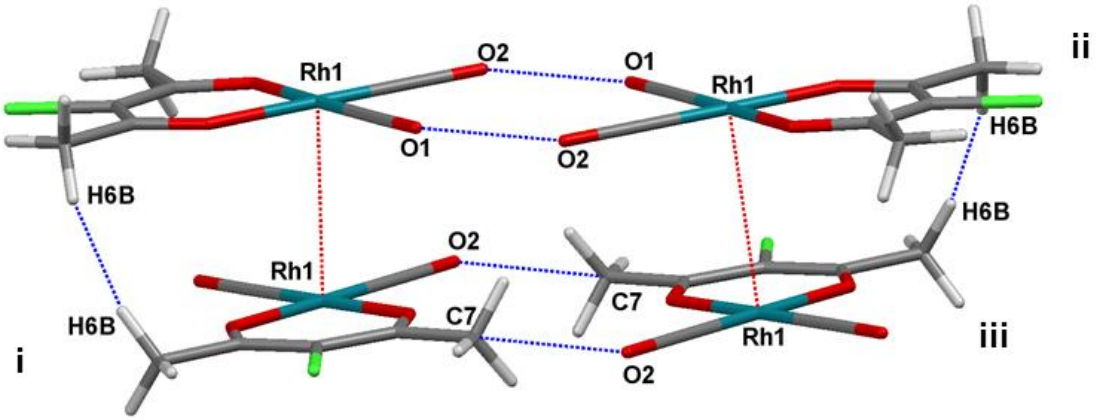

Figure 5.11: Soft contacts (indicated in blue) between oxygen atoms of neighbouring molecules in a head-to-head fashion induce dimer formation in [Rh(3Cl-acac)$(CO)_2$]. Contacts between oxygen and carbon atoms in head-to-tail orientation support the dimer formation between neighbouring molecules. Soft contacts involving a hydrogen atom adds further stability to the crystal lattice.

Table 5.5: Data of intermolecular soft contacts involving oxygen and hydrogen atoms in [Rh(3Cl-acac)(CO)$_2$].

Atoms	Distance (Å)
O1•••O2^{ii}	3.031(2)
O2^{i}•••C7^{iii}	3.205(3)
H6B•••H6B^{i}	2.023

Symmetry codes: i) 3/2- x, y, 3/2-z; ii) x, -y, -z; iii) ½+x, -y, ½-z.

Additionally, it was noted that the interactions are associated with different symmetry elements in the unit cell as illustrated in Figure 5.12. Inversion centres are encountered between the interactions (yellow dots) and a glide plane was found to run parallel to these interactions along the *a*-axis.

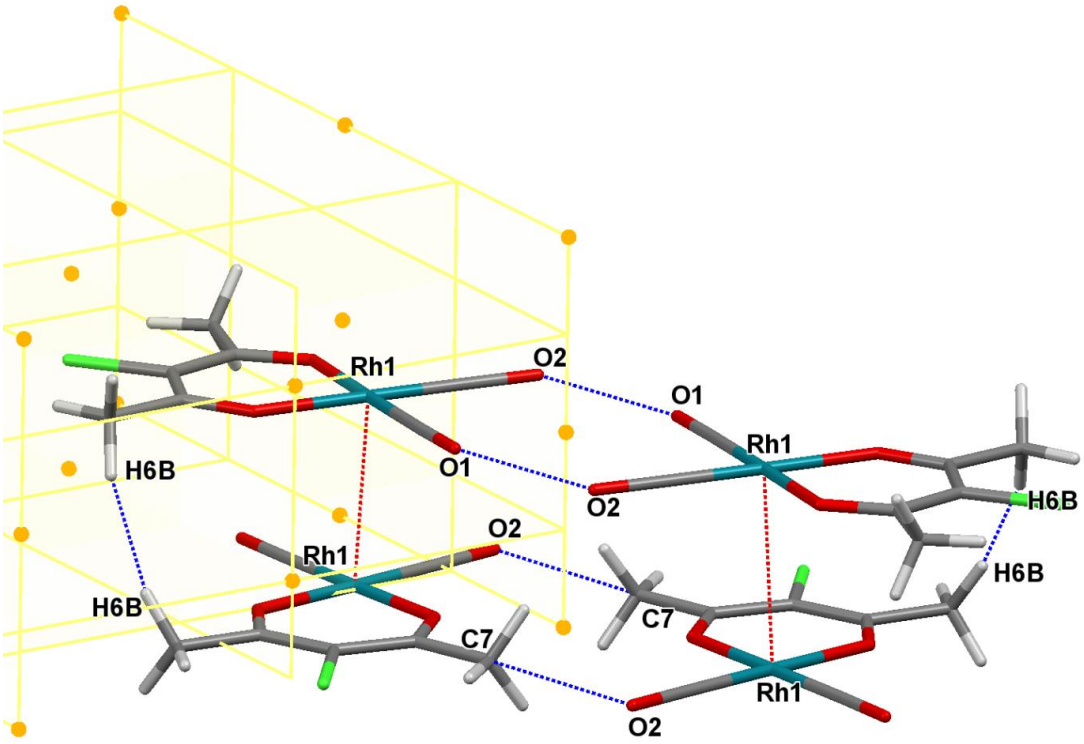

Figure 5.12: Soft contacts observed for [Rh(3Cl-acac)(CO)$_2$] are associated with various symmetry elements. Inversion centres (yellow dots) are found between the interactions of the molecules as well as a glide plane (yellow planes) running parallel to the interactions.

The packing diagram of [Rh(3Cl-acac)(CO)$_2$] is illustrated in Figure 5.13 with the dominating influence of metallophilic interactions clearly visible in the arrangement of molecules.

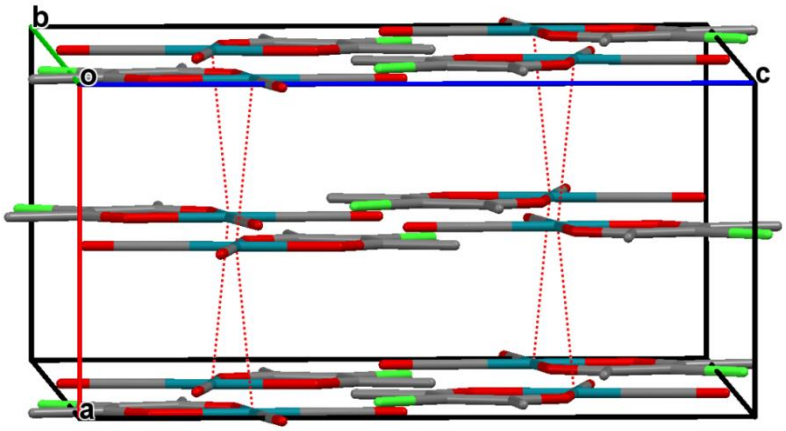

Figure 5.13: Packing of molecules of [Rh(3Cl-acac)(CO)$_2$] viewed along an off-centered *b*-axis illustrates the dominating effect that the metallophilic interactions have on the packing of molecules in the crystal lattice.

5.5 Crystal structure of [Rh(CN-acac)(CO)$_2$]

The complex, dicarbonyl(3-cyanoacetylacetonato-κ^2*O,O*)rhodium(I), crystallized in the monoclinic space group *C2/m* with only one independent molecule in the asymmetric unit and *Z*= 4. The molecular structure with numbering scheme is represented in Figure 5.14. General crystallographic information of the crystal structure is referred to in Table 5.1 with selected bond lengths and angles given in Table 5.6. For comprehensive information regarding bond distances and angles related to the structure refer to Appendix A.

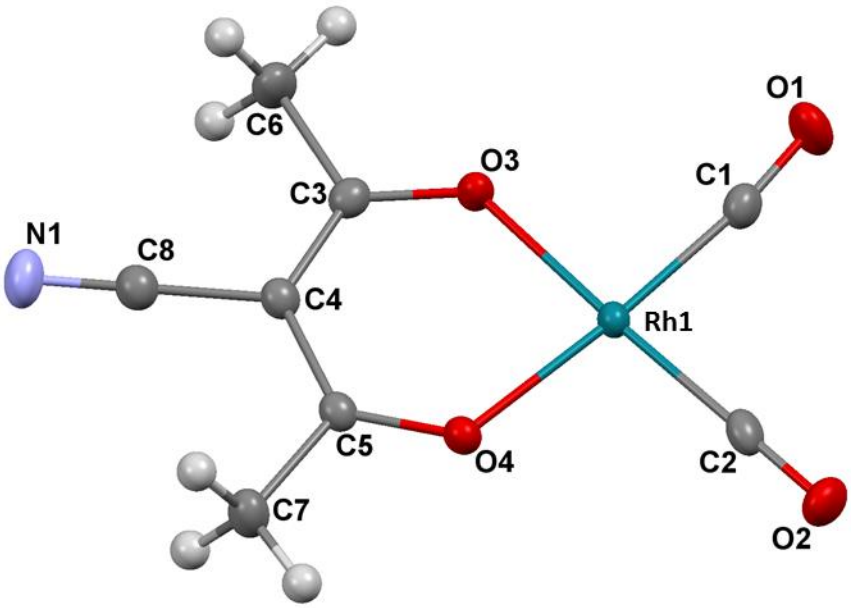

Figure 5.14: Molecular structure of [Rh(CN-acac)(CO)$_2$] with atom numbering scheme (thermal ellipsoid probability= 50 %). Hydrogen atom labels have been omitted for clarity.

Table 5.6: Selected bond distances and angles of [Rh(CN-acac)(CO)$_2$].

Atoms	Distance (Å)
Rh1-C1	1.852(3)
Rh1-C2	1.854(3)
Rh1-O3	2.035(2)
Rh1-O4	2.045(2)
C1-O1	1.124(4)
C2-O2	1.133(3)
C3-O3	1.267(3)
C5-O4	1.269(3)
C4-C8	1.441(4)
C8-N1	1.136(4)
O3···O4[a]	2.870(3)

[a] Bite distance

Atoms	Angle (°)
C1-Rh1-C2	90.7(1)
O3-Rh1-O4	89.40(9)
C1-Rh1-O4	176.25(9)
C2-Rh1-O3	177.7(1)
C3-C4-C5	126.2(2)
C1-Rh1-O3	86.9(1)
C2-Rh1-O4	92.9(1)
C4-C8-N1	179.7(3)
O3-C3···O4-C5[b]	2.7(4)

[b] Torsion angle between C3-O3 and C5-O4.

The carbonyl bond distances of Rh1-C1 (1.852(3) Å) and Rh1-C2 (1.854(3) Å) are longer than those reported for the structures of [Rh(acac)(CO)$_2$] (1.865(8) Å and 1.838(6) Å). This could possibly be due to the electronic influence of the substituted methine carbon by a highly electron withdrawing cyano group. This results in an electron poorer metal centre and hence less electron density available for π-back donation to the carbonyl moieties resulting in weaker bonds and longer rhodium-carbon distances.

Cyano groups are typically bonded *via* the carbon atom to the methine carbon position as illustrated in Figure 5.14. Further evidence to corroborate this are the C4-C8 (1.441(4) Å) and C8-N1 (1.136(4) Å) distances. The C4-C8 distance of 1.441(4) Å is typical for a carbon-carbon bond with notable literature references reporting distances of 1.424 Å[20] and 1.446 Å[21] for this type of bond involving a cyano group. The carbon-nitrogen bond of C8-N1 (1.136(4) Å) as found in the cyano group is of triple bond character and as such the length of this bond is considerbly shorter than single or double bonds with a typical literature value reported as 1.144 Å.[22] The triple bond character of C8-N1 can further be established by the C4-C8-N1

[20] Voutsas, G., Tzavellas, L. C., Tsiamis, C., *Struct. Chem.*, **1999**, *10*, 53-57.
[21] Burrows, D. A., Cassar, K., Mahon, M. F., Warren, J. E., *Dalton Trans.*, **2007**, 2499-2509.
[22] Pogozhev, D., Baudron, S. A., Hosseini, M. W., *Inorg. Chem.*, **2010**, *49*, 331-338.

bond angle of 179.7(3)°. Bond angles for a triple bond in the cyano group are typically near linear with typical angles of 179.06°[23] and 179.51°[24] reported in the CSD.

For the geometry around the Rh1 centre an almost perfect square planar geometry was observed with C1-Rh1-C2 (90.7(1)°) and O3-Rh1-O4 (89.40(9)°) angles close to the ideal 90° expected for this geometry.

As with the structures discussed in Sections 5.3 and 5.4, metallophilic interactions were encountered between neighbouring molecules in [Rh(CN-acac)$(CO)_2$]. Figure 5.15 illustrates how the Rh(I) centres of different molecules are connected in the one-dimensional metal chain. Rh···Rh distances of 3.197(2) Å and 3.224(3) Å were found to alternate between rhodium(I) centres infinitely along the 1-D chain. The Rh···Rh distances were slightly shorter than those in [Rh(acac)$(CO)_2$] (3.254(3) Å and 3.274(3) Å). As with all of the previous structures the interactions were again observed along the shortest cell-axis (*b*-axis (6.474(3) Å)) of the unit cell.

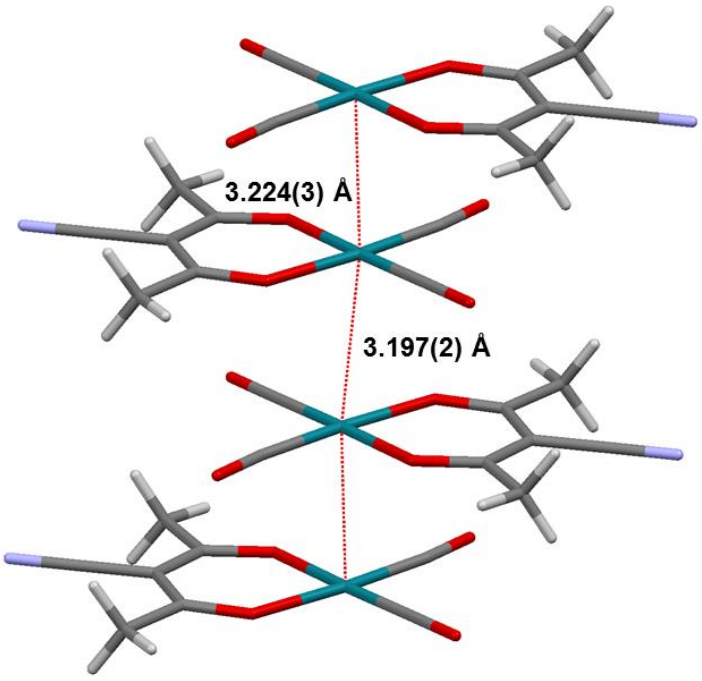

Figure 5.15: Rh···Rh interactions observed between neighbouring molecules in [Rh(CN-acac)$(CO)_2$] result in the formation of infinite one-dimensional metal chains along the *b*-axis.

Figure 5.16 illustrates the angles and torsions that exist along the one-dimensional metal chain facilitated *via* the metallophilic interactions. The angles of 166.5(3)° between the rhodium centres reveal significant deviation from a perfecly linear arrangement along the 1-D chain whilst the torsion angles of 180.0(3)° indicate an eclipsed arrangement of R-groups

[23] Yoshida, Y., Nishikiori, S, Kuroda, R., Yuge, H., *Chem. Eur. J.*, **2013**, *19*, 3451-3457.
[24] Tsiamis, C., Hazidimitriou, A. G., Tzavellas, L. C., *Inorg. Chem.*, **1998**, *37*, 2903-2909.

along the chain. A similar situation was noted for [Rh(acac)$(CO)_2$] with torsion angles of 180.0(2)° between R-groups.

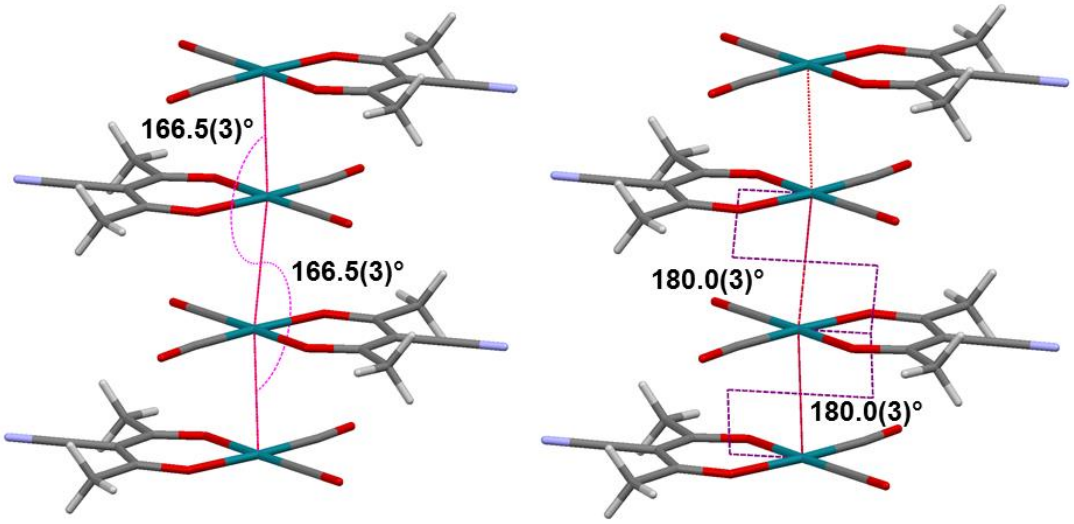

Figure 5.16: a) Angles of 166.5(3)° are found between neighbouring Rh centres (Rh-Rh-Rh) along the 1-D chain; b) Torsion angles of 180.0(3)° between coordinating β-diketonato ligands revealed an eclipsed arrangement of R-groups in [Rh(CN-acac)$(CO)_2$].

In addition to the metallophilic interactions observed in [Rh(CN-acac)$(CO)_2$], interactions between oxygen and carbon atoms occur between neighbouring molecules. These interactions are illustrated in Figure 5.17 with detail related to the interactions given in Table 5.7.

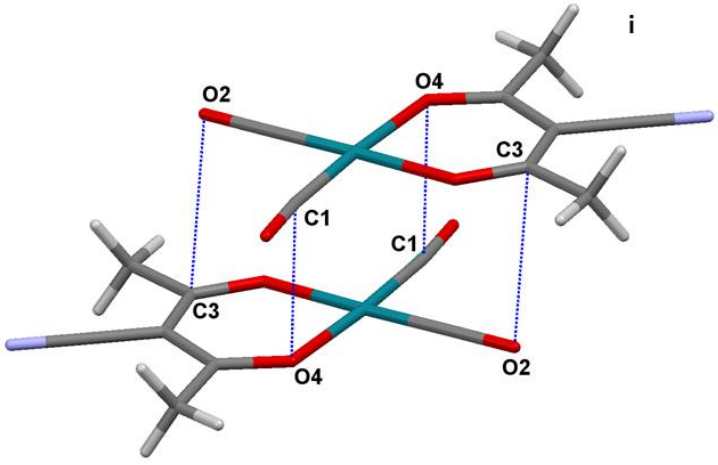

Figure 5.17: Soft contacts involving oxygen (indicated in blue) observed between neigbhouring molecules of [Rh(CN-acac)$(CO)_2$] (symmetry code: i) -x, -y, 1-z).

Table 5.7: Detail of the soft contacts involving oxygen in [Rh(CN-acac)$(CO)_2$].

Atoms	Distance (Å)
O4···C1^{i}	3.193(2)
C3···O2^{i}	3.215(3)

Symmetry codes: i) -x, -y, 1-z.

The packing diagram for [Rh(CN-acac)$(CO)_2$] illustrated in Figure 5.18 along an off-centrered *b*-axis clearly shows the metallophilic interactions as the main contributor within the arrangement of molecules in the crystal lattice stabilized by oxygen···carbon soft contacts.

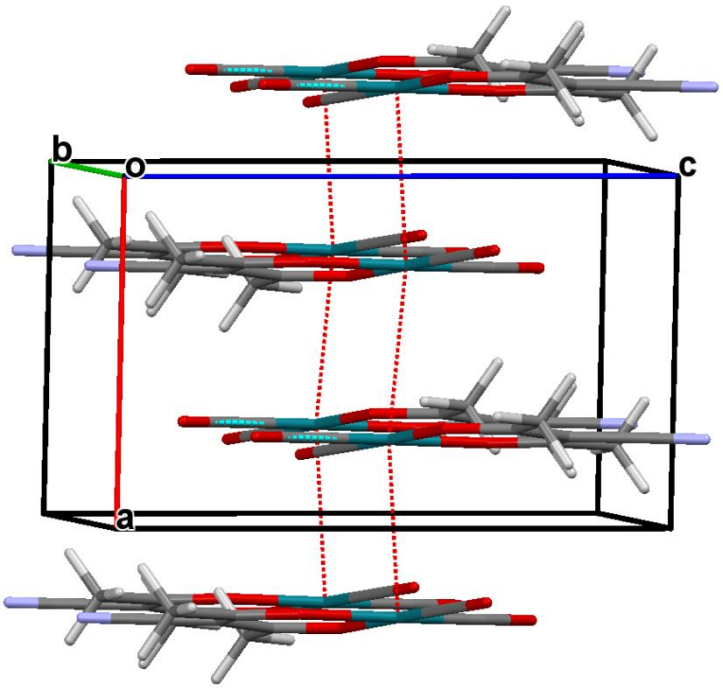

Figure 5.18: The extended packing diagram of [Rh(CN-acac)$(CO)_2$] viewed along an off-centred *b*-axis clearly shows the significant effect of the metallophilic interactions in the arrangement of molecules within the unit cell.

5.6 Crystal structure of [Rh(pyruv)$(CO)_2$]

The complex, dicarbonyl(methyl-4-oxo-2-oxypent-2-enoato-κ^2O,O')rhodium(I), crystallized in the triclinic spacegroup $P\bar{1}$ with only one independent molecule in the asymmetric unit. The molecular structure as well as the numbering scheme for the structure is represented in Figure 5.19. General crystallographic information of the crystal structure is referred to in Table 5.1 with selected bond lengths and angles given in Table 5.8. For comprehensive information regarding bond distances and angles related to the structure refer to Appendix A.

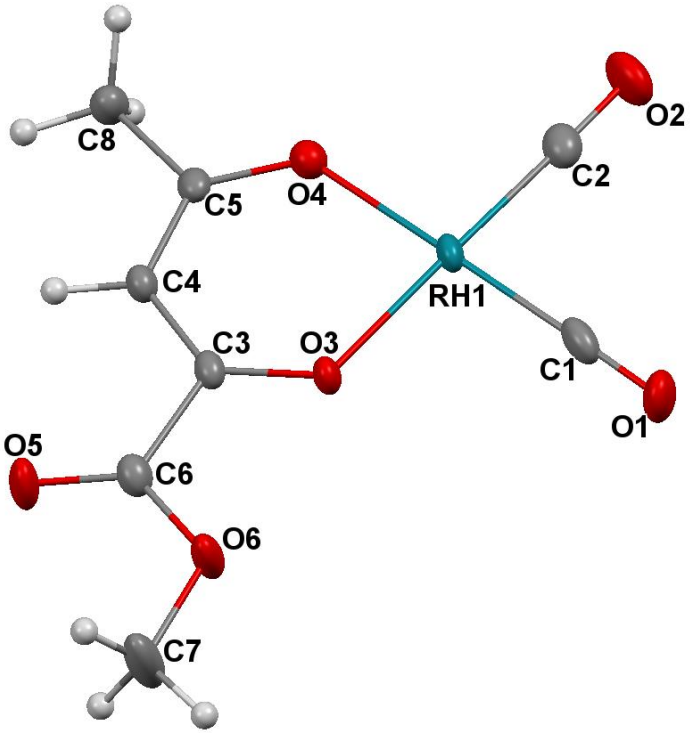

Figure 5.19: Molecular structure of [Rh(pyruv)(CO)$_2$] with atom numbering scheme (thermal ellipsoid probability= 50 %). Hydrogen atom labels have been omitted for clarity.

Table 5.8: Selected bond distances and angles of [Rh(pyruv)(CO)$_2$].

Atoms	Distance (Å)
Rh1-C1	1.852(4)
Rh1-C2	1.852(4)
Rh1-O3	2.043(3)
Rh1-O4	2.053(3)
C1-O1	1.141(5)
C2-O2	1.139(5)
C3-O3	1.283(4)
C5-O4	1.269(4)
C6-O5	1.200(4)
O6-C7	1.441(4)
O3···O4[a]	2.911(4)

[a] Bite distance

Atoms	Angle (°)
C1-Rh1-C2	89.7(2)
O3-Rh1-O4	90.6(1)
C1-Rh1-O4	176.9(1)
C2-Rh1-O3	177.7(1)
C3-C4-C5	124.7(3)
C1-Rh1-O3	90.2(1)
C2-Rh1-O4	89.3(2)
O3-C3···O4-C5[b]	179.44(3)

[b] Torsion angle between C3-O3 and C5-O4.

As can be seen from the data given in Table 5.8 the bond distances are well in agreement with the bond lengths reported in the previous structures. The reported bond lengths of Rh1-C1 and Rh1-C2 with distances of 1.852(4) Å are well in the range for this bond type. The

reported bond lengths are comparable to those reported for [Rh(3Cl-acac)$(CO)_2$] (1.854(4) Å and 1.848(4) Å).

The coordinating β-diketonato ligand is an unsymmetrical ligand with carbonyl and methoxy functional group substituents connected to the methyl carbon of the β-diketonato ligand. The electronic influence of these substituents are seemingly restricted in the subsequent rhodium(I) complex as only slight differences exist in the bond distances between the oxygen atoms of the coordinating ligand to the rhodium centre. The Rh1-O3 and Rh1-O4 bonds with distances of 2.043(3) Å and 2.053(3) Å are seemingly unaffected by the electron withdrawing moieties of the substituents on the β-diketonato backbone. The C3-O3 and C5-O4 distances of 1.283(4) Å and 1.269(4) Å show slightly more pronounced differences in bond strength as the C3-O3 bond is slightly weakened by the electron withdrawing effect of the substituent group on C3.

The molecule displayed a typical square planar geometry as was observed for all the other Rh(I) complexes discussed in this chapter. As can be seen from the angles reported in Table 5.8 the geometry shows almost no distortion from the ideal 90° angles expected within the coordination moiety. The C2-Rh1-O4 angle showed the greatest deviation from this ideal geometry with a reported angle of 89.3(2)°. It was noted that the pyruvate substituent on the coordinating β-diketonato ligand was slightly distorted out of the horizontal plane constructed through C1, C2, O3 and O4 as illustrated in Figure 5.20. The pyruvate group was found to be twisted above the plane at an angle of 5.74°.

Figure 5.20: Distortion of the pyruvate substituent of the coordinating β-diketonato ligand out of the equatorial plane constructed through the coordinating moiety at an angle of 5.74°.

As with the structures of [Rh(acac)$(CO)_2$] and [Rh(3Cl-acac)$(CO)_2$], metallaphilic interactions are encountered between Rh(I) centres of neighbouring molecules. However, in contrast to the previously discussed structures (Sections 5.3, 5.4 and 5.5) these interactions are limited to two molecules that results in dimer formation as illustrated in Figure 5.21. Rh···Rh distances of 3.134(3) Å were found between neighbouring metal centres. Interestingly, these interactions were not encountered along a specific cell axis of the unit cell as was seen with the previous structures.

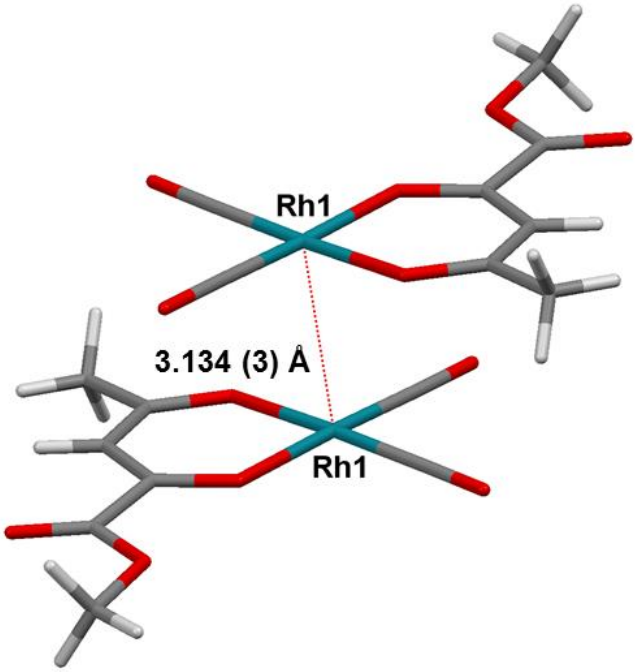

Figure 5.21: Rh···Rh interactions (indicated in red) between neighbouring molecules are restricted to dimer formation in [Rh(pyruv)$(CO)_2$].

Soft contacts were observed between oxygen atoms of the carbonyl moieties of two different molecules in a head-to-head fashion as is depicted in Figure 5.22. A O5···O5^{i} distance of 2.960(3) Å was determined between the molecules also leading to the formation of dimers.

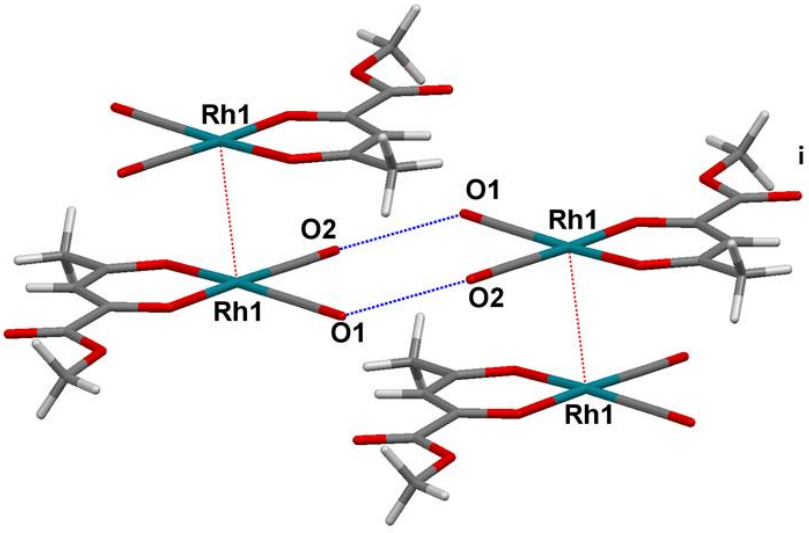

Figure 5.22: Soft contacts present in [Rh(pyruv)$(CO)_2$] between oxygen atoms of the carbonyl moieties of the molecules lead to dimer formation. (Symmetry code: i) 2-x, 1-y, 2-z.)

Furthermore, in conjunction with these soft contacts, a bifurcated hydrogen bond exists between O5 and hydrogen atoms of a neighbouring molecule in a tail-to-tail motif as seen in Figure 5.23. Details of the hydrogen bond are given in Table 5.9.

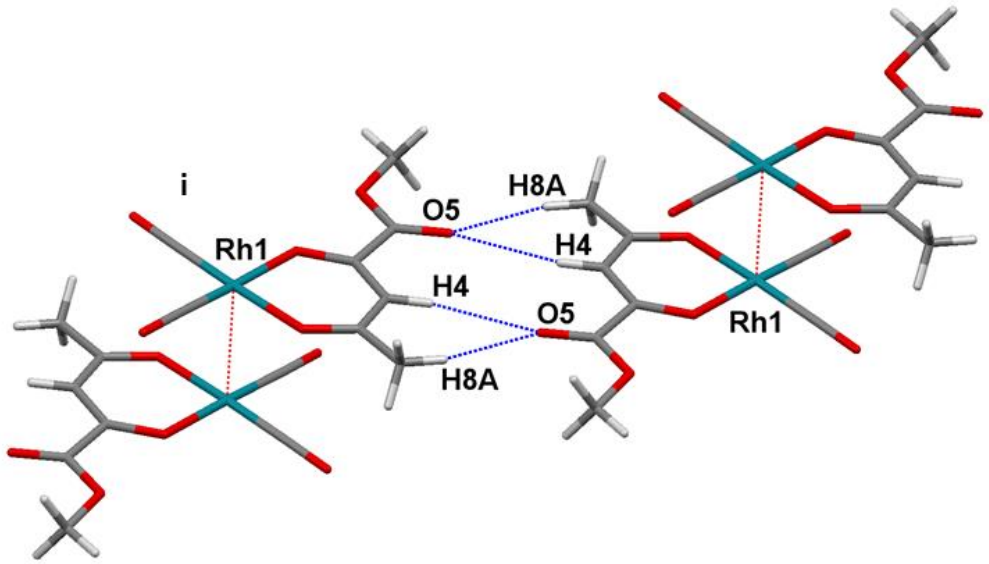

Figure 5.23: A bifurcated hydrogen bond exists between O5 and hydrogen atoms of a neighbouring molecule in [Rh(pyruv)(CO)$_2$] leading to dimer formation in a tail-to-tail motif. Symmetry code: i) 1+x, -1+y, z.

Table 5.9: Hydrogen bond geometry for [Rh(pyruv)(CO)$_2$].

D-H···A	dD-H (Å)	dH···A (Å)	dD···A (Å)	Angle D-H···A (°)
C4-H4···O5^{i}	0.95	2.563	3.464 (5)	158.4
C8-H8A···O5^{i}	0.98	2.593	3.541 (5)	162.9

Symmetry codes: i)1+x, -1+y, z.

The packing of molecules in [Rh(pyruv)(CO)$_2$] is heavily influenced by the Rh···Rh dimers that are formed *via* metallophilic interactions as seen in Figure 5.24. It was expected that the structure of [Rh(pyruv)(CO)$_2$] would display a similar stacking of molecules along a one-dimensional chain as was observed for the structures of [Rh(acac)(CO)$_2$], [Rh(3Cl-acac)(CO)$_2$] and [Rh(CN-acac)(CO)$_2$]. One explanation to why this did not occur could be the competing strengths of the other interactions found in this structure. The strong hydrogen bond as well as the soft contacts involving oxygen atoms between neighbouring molecules could be preventing metallophilic interactions from occurring as has been suggested in literature.[25]

[25] Pathaneni, S. S., Desiraju, G. R., *J. Chem. Soc., Dalton Trans.*, **1993**, 319-322.

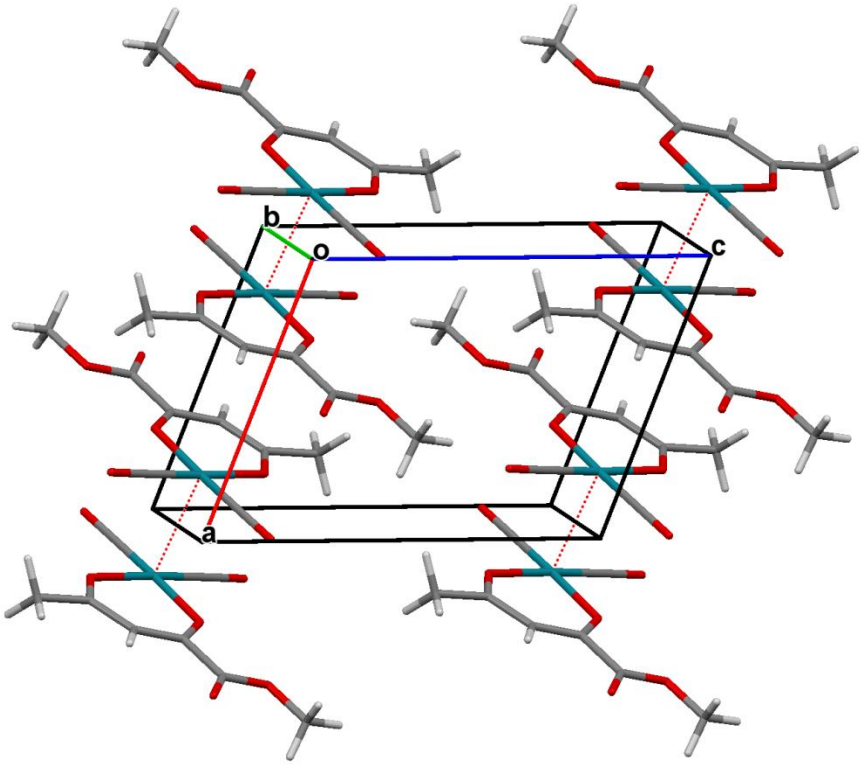

Figure 5.24: Packing diagram of [Rh(pyruv)(CO)$_2$] viewed along an off-centered *b*-axis.

5.7 Conclusion

Four rhodium(I) complexes and their solid-state structures were evaluated and discussed in this chapter. In three of these structures unique metallophilic interactions were found that lead to the growth of one-dimensional metal chains along a specific direction within the crystal lattice.

In each of these rhodium(I) complexes a different coordinating β-diketonato ligand was used. This was purposefully done to provide a means by which to evaluate the effects of different substituents in the coordinating ligands on the rhodium(I) centre and the potential metallophilic interactions that are expected in these complexes.

In the next chapter three rhodium(I) complexes will be discussed with altered substituents on the methyl carbon positions of the coordinating β-diketonato ligands.

Chapter 6: Crystallographic Study of [Rh(tfac)(CO)$_2$], [Rh(piv)(CO)$_2$] and [Rh(dipiv)(CO)$_2$]

6.1 Introduction

This chapter forms part of the over-arching crystallographic study involving the coordination of different β-diketone ligands to rhodium(I) metal centres. The aim in the design of these coordination complexes is to allow the establishment of metallophilic interactions between Rh(I) centres. Square planar coordination of metals with d^8 or d^{10} electronic configurations such as in Rh(I) complexes have been known to exhibit these interactions (see Section 2.4.1, Chapter 2). The current study is aimed at exploring the potential use of these interactions in the construction of nano-wired structures.

The choice of coordinating ligand to a metal centre has been shown to influence the metallophilic interactions.[1] In our study, the effect of changes to the electronic as well as the steric nature of different coordinating β-diketonato ligands in coordination to the rhodium(I) centre, and in turn the metallophilic interaction, was evaluated.

This chapter focuses on three Rh(I) complexes whose structural data were obtained by single crystal X-ray diffraction. The three ligands (scheme 6.1) used in coordination to rhodium(I) yielded the complexes [Rh(tfac)(CO)$_2$], [Rh(piv)(CO)$_2$] and [Rh(dipiv)(CO)$_2$].

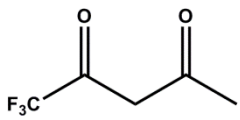

1,1,1-Trifluoro-2,4-pentanedione
(tfacH)

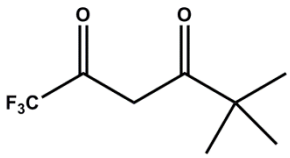

1,1,1-Trifluoro-5,5-dimethyl-2,4-hexanedione
(pivH)

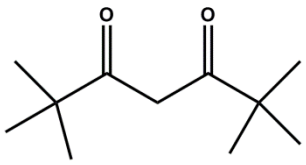

2,2,6,6-Tetramethyl-3,5-heptanedione
(dipivH)

Scheme 6.1: Different β-diketone ligands yielding rhodium(I) complexes with metallophilic interactions in the solid-state.

Two of these complexes contain fluorinated substituents that are regarded as highly electron withdrawing. It was anticipated that these ligands would have a significant effect on the electronic environment experienced by the metal in each complex. The 2,2,4,4-tetramethyl-

[1] Connick, W. B., Marsh, R. E., Schaefer, W. P., Gray, H. B., *Inorg. Chem.*, **1997**, *36*, 913-922.

3,5-heptanedione (dipivH) ligand has two *t*-butyl substituents on the β-diketone backbone which offers electron donating as well as significant steric bulk to the molecule.

Each of the above mentioned complexes will be discussed, highlighting the different bond and geometric properties associated with each solid-state structure. Particular focus will be given to the metallophilic interactions within the solid state by highlighting Rh···Rh distances, angles along the one-dimensional metal chain as well as torsion angles of the coordinating moieties. Additionally, intermolecular interactions contributing to the stability of the crystal lattice will be evaluated along with the packing encountered within each unit cell.

6.2 Experimental

The reflection data for [Rh(tfac)$(CO)_2$], [Rh(piv)$(CO)_2$] and [Rh(dipiv)$(CO)_2$] were collected on a Bruker X8 Apex II 4K Kappa CCD diffractometer using graphite monochromated Mo Kα radiation (λ= 0.70926 Å) with ω- and φ-scans at 100(2) K. The Apex II software package[2] was utilized along with the optimum measurement method in collecting more than a hemisphere of reciprocal space as predicted by COSMO.[3] Frame integration and data reduction was performed using the SAINT-Plus and XPREP software packages and SADABS[4] was made use of for multi-scan absorption correction.[5] The structures were solved using SIR92[6], SIR97[7], SIR2002[8], DIRDIF[9] or Superflip[10] with refinement performed using the WinGX software package[11] that incorporates SHELXL[12]. All atoms were refined anisotropically with the exception of hydrogen atoms. The hydrogen atoms were positioned geometrically and refined utilizing a riding model with fixed C-H distances of 0.98 Å (CH) [U_{iso}(H)= 1.2 Ueq] for methyl hydrogens and methine hydrogens with fixed C-H distances of 0.95 Å (CH) [U_{iso}(H)= 1.2 Ueq]. Molecular diagrams were generated with the Mercury software package[13] with a 50 % thermal ellipsoid probability for all non-hydrogen atoms. General crystallographic data and refinement parameters are represented in Table 6.1 with

[2] **Apex2**, Version 2012.10-0, Bruker AXS Inc.,Madison, Wisconsin, USA, **2012**.
[3] **COSMO**, Version 1.48, Bruker AXS Inc., Madison, Wisconsin, USA, **2003**.
[4] **SADABS**, Version 2012/1, BrukerAXS Inc, Madison, Wisconsin, USA, **2012**.
[5] **SAINT-Plus**, Version 8.27B including XPREP, Bruker AXS Inc., Madison, Wisconsin, USA, **2012**.
[6] Altomare, A., Cascarano, G., Giacovazzo, C., Guagliardi, A., Burla, M. C., Polidori, G., Camalli, M., *J. Appl. Cryst.*, **1994**, *27*, 435-436.
[7] Altomare, A., Burla, M. C., Camalli, M., Cascarano, G. L., Giacovazzo, C., Guagliardi, A., Moliterni, A. G. G., Polidori, G., Spagna, R., *J. Appl. Cryst.*, **1999**, *32*, 115-119.
[8] Burla, M. C., Camalli, M., Carrozzini, B., Cascarano, G. L., Giacovazzo, C., Polidori, G., Spagna, R., *J. Appl. Cryst.*, **2003**, *36*, 1103.
[9] Beurskens, P. T., Admiraal, G., Beurskens, G., Bosman, W. P., Garcia-Granda, S., Gould, R. O., Smits, J. M. M., Smykalla, C., Crystallography Laboratory, University of Nijmegen, Toernooiveld, The Netherlands.
[10] Palatinus, L., Chapuis, G., *J. Appl. Cryst.*, **2007**, *40*, 786-790.
[11] **WinGX**. Farrugia, L. J., *J. Appl. Cryst.*, **2012**, *45*, 849–854.
[12] Sheldrick, G. M., *Acta Cryst.*, **2008**, *A64*, 112-122.
[13] **Mercury**, Macrae, C. F., Bruno, I. J., Chisholm, J. A., Edgington, P. R., McCabe, P., Pidcock, E., Rodriquez-Monge, L., Taylor, R., van de Streek, J., Wood, P. A., *J. Appl. Cryst.*, **2008**, *41*, 466-470.

the complete list of atomic coordinates, equivalent anisotropic parameters and hydrogen coordinates of each data set given in Appendix A.

Table 6.1: General crystal data for [Rh(tfac)(CO)$_2$], [Rh(piv)(CO)$_2$] and [Rh(dipiv)(CO)$_2$].

Crystallographic Data	[Rh(tfac)(CO)$_2$]	[Rh(piv)(CO)$_2$]	[Rh(dipiv)(CO)$_2$]
Empirical Formula	$C_7H_7F_3O_4Rh$	$C_{10}H_{10}F_3O_4Rh$	$C_{13}H_{19}O_4Rh$
Molecular weight (g/mol)	312.01	354.09	342.19
Temperature (K)	100(2)	100(2)	100(2)
Crystal system, space group	Triclinic, $P\bar{1}$	Orthorhombic, *Pbcn*	Monoclinic, $P2_1/m$
***a* (Å)**	6.760(6)	6.467(2)	12.54(1)
***b* (Å)**	7.922(7)	18.477(5)	6.613(7)
***c* (Å)**	9.613(8)	20.682(6)	18.04(2)
***α* (°)**	79.80(3)	90.0	90.0
***β* (°)**	89.91(3)	90.0	98.44(2)
***γ* (°)**	77.18(3)	90.0	90.0
Volume (Å^3)	493.7(7)	2471.4(1)	1479.8(1)
Z	2	8	4
Density calculated (g/ cm^3)	2.099	1.903	1.536
Absorption coefficient (mm^{-1})	1.765	1.423	1.157
***F* (000)**	300	1392	696
Crystal size (mm^3)	0.108 x 0.178 x 0.722	0.287 x 0.682 x 0.882	0.078 x 0.111 x 0.877
Morphology, colour	Needle, orange	Cuboid, purple	Needle, purple
***Θ* range for data collection**	2.68 to 25.97	1.97 to 28.00	1.41 to 28.0
Completeness for collection (%)	85.1	99.9	99.1
Index ranges	-8≤ *h* ≥8 -10≤ *k* ≥10 -12≤ *l* ≥12	-8≤ *h* ≥8 -24≤ *k* ≥24 -27≤ *l* ≥27	-16≤ *h* ≥16 -8≤ *k* ≥8 -23≤ *l* ≥23
Reflections collected	4827	56825	18987
Independent reflections	2027	2991	3847
Observed reflections	1067 (R_{int}= 0.0633)	2703 (R_{int}= 0.0547)	1680 (R_{int}= 0.1854)
Max. and min. transmission	0.429 and 0.746	0.453 and 0.746	0.487 and 0.746
Data/ restraints/ parameters	1067/ 0/ 118	2991/ 0/ 163	3847/ 0/ 159
Goodness-of-fit on F^2	1.280	1.240	1.109
Final R indices	R1= 0.1448 wR2= 0.3705	R1= 0.0265 wR2= 0.0811	R1= 0.1352 wR2= 0.3308
R indices	R1= 0.1924 wR2= 0.4318	R1= 0.0315 wR2= 0.0981	R1= 0.2324 wR2= 0.4325
Largest diff. Peak and hole (e.Å^{-3})	1.81 and -1.98	0.52 and -1.06	3.72 (0.06 Å from Rh1B) and -1.71 (1.92 Å from O4A)

6.3 Crystal structure of [Rh(tfac)(CO)$_2$]

As was mentioned in Chapter 3 many challenges were faced in the obtainment of crystals for the different rhodium(I) complexes. In the case of the [Rh(tfac)(CO)$_2$] complex only a few crystals of relatively poor quality could be obtained from various recrystallization attempts (see Section 3.3.4). As a result, the poor quality of the crystals is reflected in the low completeness of 85 % for the subsequent data collection as well as the high R and Goodness-of-Fit values (see Table 6.1). With respect to this study the data collection could still yield sufficient data to determine the structure of [Rh(tfac)(CO)$_2$] which will be discussed in this section.

The complex, dicarbonyl(1,1,1-trifluoro-2,4-pentanedionato-κ^2O,O')rhodium(I), crystallized in the triclinic space group $P\bar{1}$ with only one independent molecule in the asymmetric unit. The molecular structure as well as the numbering scheme is represented in Figure 6.1. General crystallographic information of the crystal structure is referred to in Table 6.1 with selected bond lengths and angles related to the structure given in Table 6.2. For comprehensive information regarding bond distances and angles associated with the structure, refer to Appendix A.

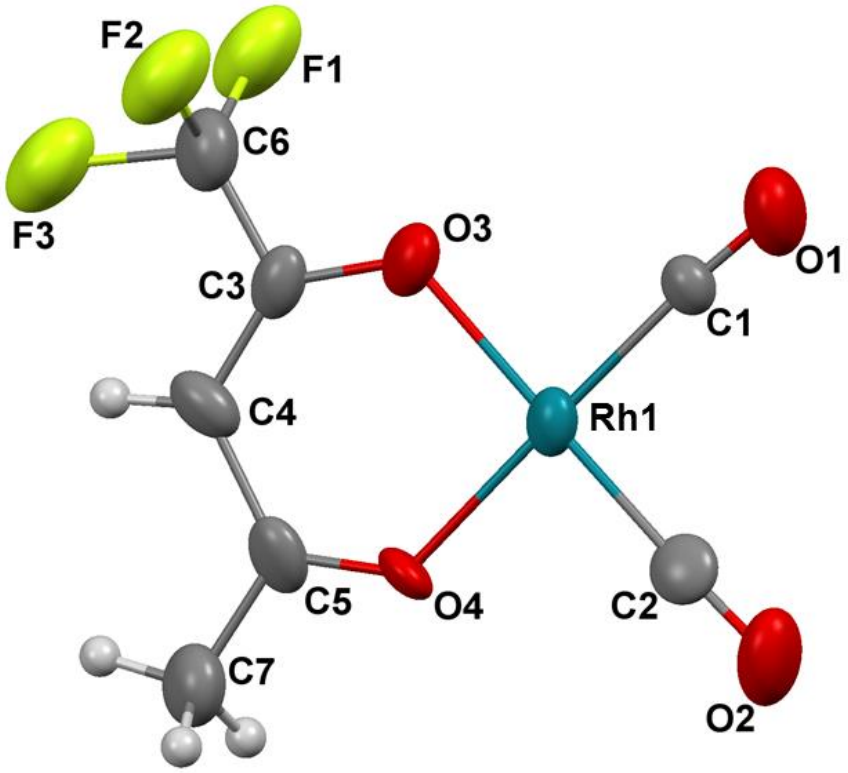

Figure 6.1: Molecular structure of [Rh(tfac)(CO)$_2$] with atom numbering scheme (thermal ellipsoid probability = 50 %). Hydrogen atom labels have been omitted for the sake of clarity.

Table 6.2: Selected bond distances and angles of [Rh(tfac)(CO)$_2$].

Atoms	Distance (Å)
Rh1-C1	1.85(2)
Rh1-C2	1.86(2)
Rh1-O3	2.03(2)
Rh1-O4	2.04(2)
C1-O1	1.12(2)
C2-O2	1.13(3)
C3-O3	1.29(3)
C5-O4	1.26(2)
C4-C3	1.38(3)
C4-C5	1.54(3)
C6-F1	1.41(2)
C6-F2	1.33(2)
C6-F3	1.54(3)
O3···O4[a]	2.91(3)

[a] Bite distance

Atoms	Angle (°)
C1-Rh1-C2	89.3(1)
O3-Rh1-O4	91.1(6)
C1-Rh1-O4	178.9(5)
C2-Rh1-O3	179.2(1)
C3-C4-C5	119.3(2)
C1-Rh1-O3	90.0(8)
C2-Rh1-O4	89.6(9)
O3-C3-C4	132.5(2)
O4-C5-C4	125.5(2)
O3-C3···O4-C5[b]	3(3)

[b] Torsion angle between C3-O3 and C5-O4

The bond distances reported in Table 5.2 reveal a square planar geometry for [Rh(tfac)(CO)$_2$] involving the coordination moiety of Rh1, C1, C2, O3 and O4. The Rh1-C1 and Rh1-C2 bonds are almost identical with bond distances of 1.85(2) Å and 1.86(2) Å respectively. The same could be said of the Rh1-O3 and Rh1-O4 bonds with distances of 2.03(2) Å and 2.04(2) Å. The symmetrical nature around the square planar Rh(I) centre is reflected in the bond angles of C1-Rh1-C2 (89.3(1)° and O3-Rh1-O4 (91.1(6)°). These angles along with those of C1-Rh1-O3 (90.0(8)°) and C2-Rh1-O4 (89.6(9)°) further reveal the square planar geometry for the Rh(I) complex.

A significant difference exists between the O3-C3-C4 (132.5(2)°) and O4-C5-C4 (125.5(2)°) bond angles. The larger bond angle of O3-C3-C4 is associated with the trifluoro substituent on the C3 carbon of the β-diketonato ligand. The effect of the trifluoro substituent on the geometry of the molecule is further evident in the bond distances of C4-C3 (1.38(3) Å) in contrast to the longer C4-C5 bond with a reported bond length of 1.54(3) Å.

The molecule was found to be virtually planar along the horizontal coordination plane with all atoms intersected by the equatorial plane constructed through the coordination moiety of C1,

C2, O3 and O4. The equatorial plane is illustrated in Figure 6.2 with the planarity of the molecule clearly visible. The fluorine atoms are positioned out of the horizontal plane with the exception of F3.

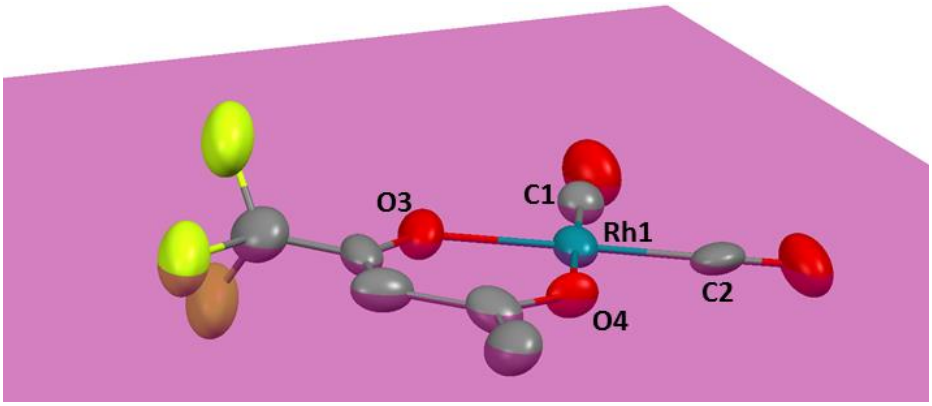

Figure 6.2: The equatorial plane constructed through the coordination moiety of atoms C1, C2, O3 and O4 was found to intersect all the atoms with the exception of the fluorine atoms in [Rh(tfac)(CO)$_2$].

The structure of [Rh(tfac)(CO)$_2$] was expected to be fairly similar to [Rh(acac)(CO)$_2$] (see Section 5.3, Chapter 5). This assumption was made based on literature sources indicating a tendency of the trifluoro moiety to be disorded over two positions interchanging with the methyl moiety in complexes containing the same ligand.[14,15] This suggests that the space occupancy of the trifluoro and methyl moieties are fairly similar and raised the question as to whether similarities exist between the structure determined for the [Rh(acac)(CO)$_2$] complex (Section 5.3, Chapter 5) and the [Rh(tfac)(CO)$_2$] complex. An overlay of the two molecules is depicted in Figure 6.3 showing slight differences in the orientation of the carbonyl bonds as well as the methyl carbons in [Rh(acac)(CO)$_2$].

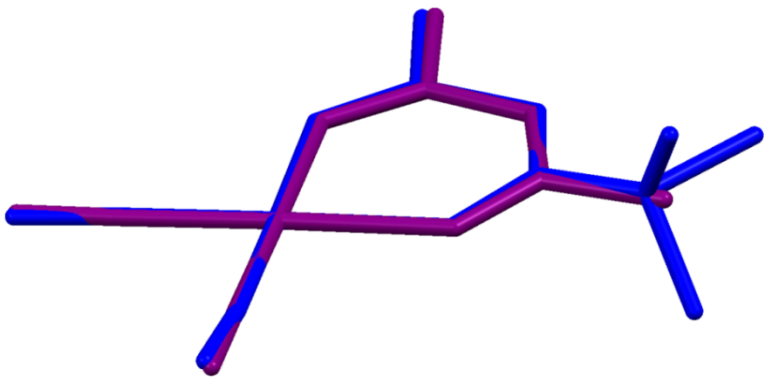

Figure 6.3: Overlay of [Rh(acac)(CO)$_2$] (purple) and [Rh(tfac)(CO)$_2$] (blue) indicating differences in the position of the carbonyl bonds and the methyl carbon moiety between the molecules.

[14] Bennet, D. W., Siddiquee, T. A., Haworth, D. T., Lindeman, S. V., *J. Chem. Crystallogr.*, **2007**, *37*, 207-212.
[15] Lai, Y. H., Chen, Y. L., Chi, Y., Liu, C. S., Carty, A. J., Peng, S. M., Lee, G. H., *J. Mater. Chem.*, **2003**, *13*, 1999-2006.

Metallophilic interactions were observed between Rh(I) centres of neighbouring molecules along the *a*-axis (6.760(9) Å) of the unit cell in [Rh(tfac)$(CO)_2$]. The tendency for metallophilic interactions to be encountered along the shortest cell axis was also observed for the structures discussed in Chapters 4 and 5. The metallophilic interactions encountered in [Rh(tfac)$(CO)_2$] are illustrated in Figure 6.4 with Rh···Rh distances of 3.384(3) Å and 3.385(3) Å. These alternating Rh···Rh distances are repeated throughout the crystal lattice along a one-dimensional chain constructed *via* the Rh(I) centres. These chains can be considered as "coordination polymeric" chains. Alternatively, these infinite polymeric structures can also be considered as mono coordinative nano-wires.

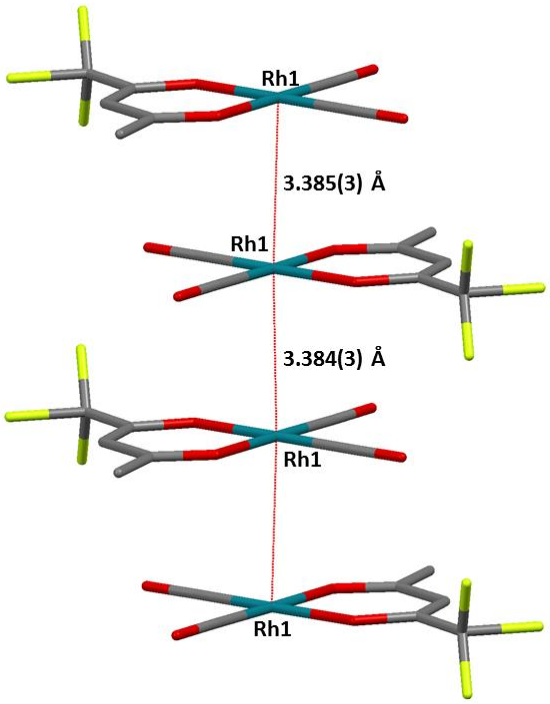

Figure 6.4: Metallophilic interactions (indicated in red) between neighbouring molecules of [Rh(tfac)$(CO)_2$] with Rh···Rh distances of 3.384(3) Å and 3.385(3) Å.

As depicted in Figure 6.5, the Rh(I) centres connected *via* metallophilic interactions are in a linear arrangement with angles of 173.93(3)° found between Rh1-Rh1-Rh1 of different molecules in the one-dimensional metal chain. The ligands were found to be arranged in a perfectly eclipsed arrangement with torsion angles of 180.0(2)° between C4-Rh1 and C4-Rh1 of different molecules. A similar arrangement was noted for the [Rh(bzac)$(CO)_2$] complex discussed in Chapter 4 (Section 4.3).

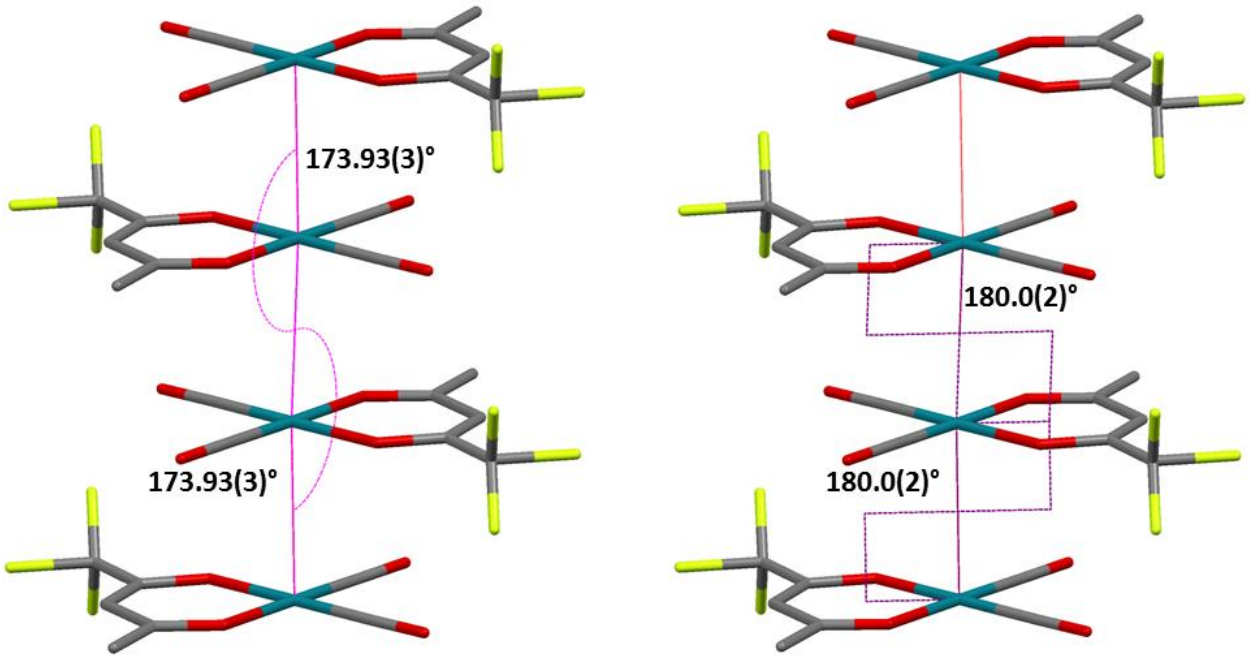

Figure 6.5: a) The angle between neighbouring Rh centres in [Rh(tfac)(CO)$_2$] (173.93(3)°); b) Torsion angles of 180.0(2)° between coordinating β-diketonato ligands revealed an eclipsed arrangement of R-groups between molecules as required by the symmetry.

Interestingly, the metallophilic interactions in [Rh(tfac)(CO)$_2$] are seemingly stabilized by another class of intermolecular interactions. Halogen bonding involving the fluorine atoms of [Rh(tfac)(CO)$_2$] are encountered in the crystal lattice.

The halogen bonds encountered in [Rh(tfac)(CO)$_2$] involve the fluorine atoms of the trifluoro substituent on the β-diketonato ligand and the oxygen atoms of the carbonyl moieties. These interactions are illustrated in Figure 6.6 with information related to the halogen bonds summarized in Table 6.3. The halogen bonds were found to extend along the one-dimensional metal chain in a head-to-tail motif providing additional stability to the crystal lattice.

Halogen bonds are typically encountered along the bond at angles of approximately 180° between donor and acceptor sites. This holds true except in cases where secondary interactions are found to disrupt this arrangement.[16] In [Rh(tfac)(CO)$_2$], it appears as if the metallophilic interactions along the one-dimensional chain prevent the halogen bonds of adopting the preferred conformation of bond angles of 180° with an angle of 117.08(3)° for C6-F2···O2.

[16] Metrangola, P., Murray, J. S., Pilati, T., Politzer, P., Resnatti, G., Terraneo, G., *Cryst. Growth Des.*, **2011**, *11*, 4238-4246.

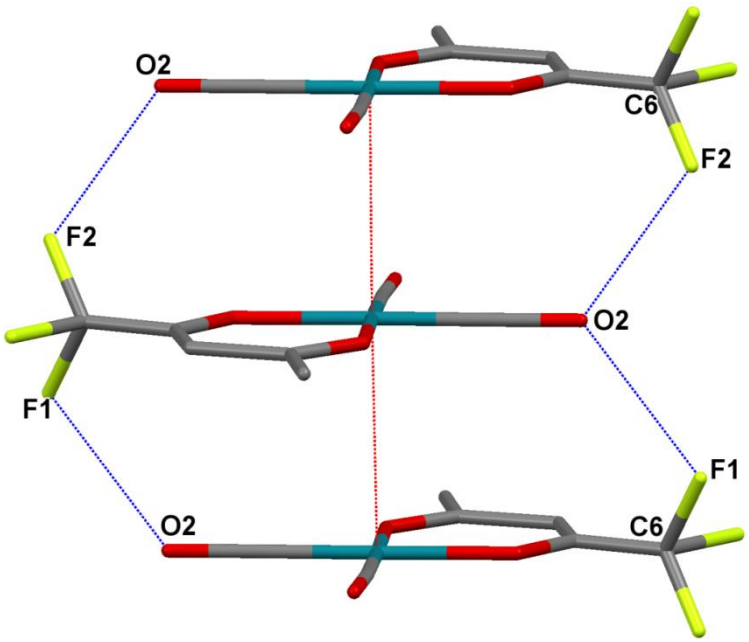

Figure 6.6: Halogen bonds existing between fluorine atoms of the β-diketonato ligand and oxygen atoms of the carbonyl oxygen in [Rh(tfac)(CO)$_2$].

Halogen bonds were also observed between neighbouring molecules along the *c*-axis of the unit cell. Figure 6.7 depicts these interactions of F3 with the oxygen atom of the carbonyl group of [Rh(tfac)(CO)$_2$] in a head-to-tail manner. Detail of the halogen bond is given in Table 6.3.

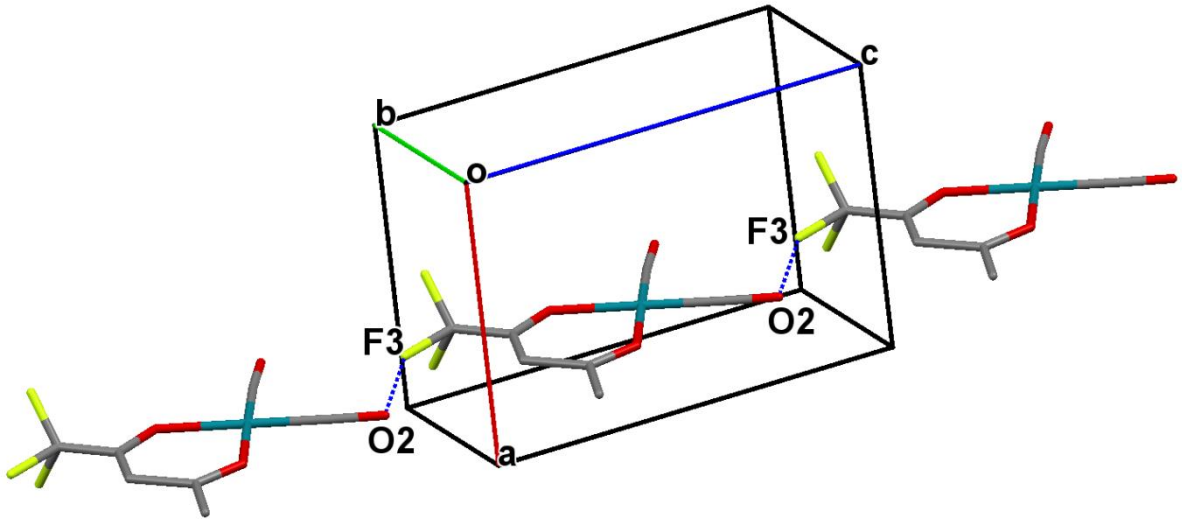

Figure 6.7: Halogen bonds between F3 and the oxygen atom of the carbonyl moiety in [Rh(tfac)(CO)$_2$] extend between neighbouring molecules in a head-to-tail motif along the *c*-axis.

Table 6.3: Halogen-bond geometry for [Rh(tfac)(CO)$_2$] as depicted in Figure 6.6 and 6.7.

D-X···A	dD-X (Å)	dX···A (Å)	dD···A (Å)	Angle D-X···A (°)
C6-F2···O2^{i}	1.33(2)	2.78(2)	3.56 (2)	117.08(3)
C6-F1···O2^{ii}	1.41(2)	2.85(2)	3.69 (3)	112.38(3)
C6-F3···O2^{iii}	1.54(3)	2.91(3)	4.28 (3)	147.53(3)

Symmetry codes: i) 1-x,1-y,1-z; ii) 2-x,1-y,1-z; iii) x,y,1+z.

The halogen bonds involving F1 and F3 atoms were observed to connect four molecules of [Rh(tfac)(CO)$_2$] with one another in a pseudo 8-membered ring system. This arrangement is depicted in Figure 6.8.

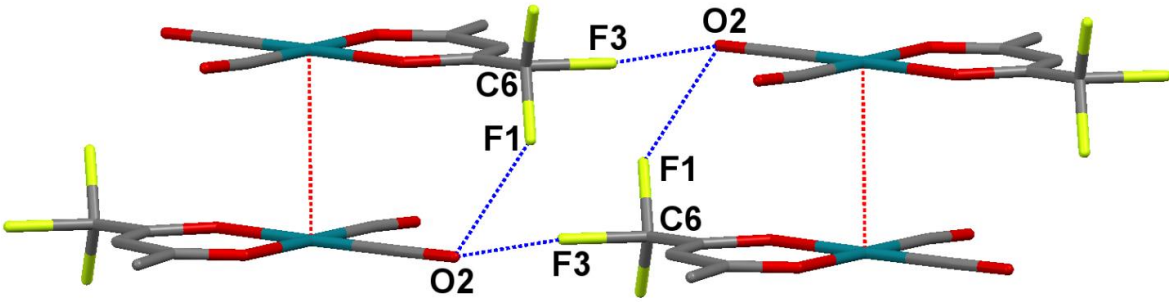

Figure 6.8: Halogen bonds connect four molecules in [Rh(tfac)(CO)$_2$] in a pseudo 8-membered ring system; defined by an inversion centre.

By introducing functional groups that possess the potential to form such interactions the directionality within the arrangement of molecules may be manipulated as is the case in [Rh(tfac)CO$_2$]. As discussed in Chapter 2 this type of manipulation of functional groups to facilitate certain interactions within solid-state structures forms the basis of crystal engineering. For [Rh(tfac)(CO)$_2$], the intermolecular interactions between the molecules lead to the formation of planes of molecules as can be seen in Figure 6.9.

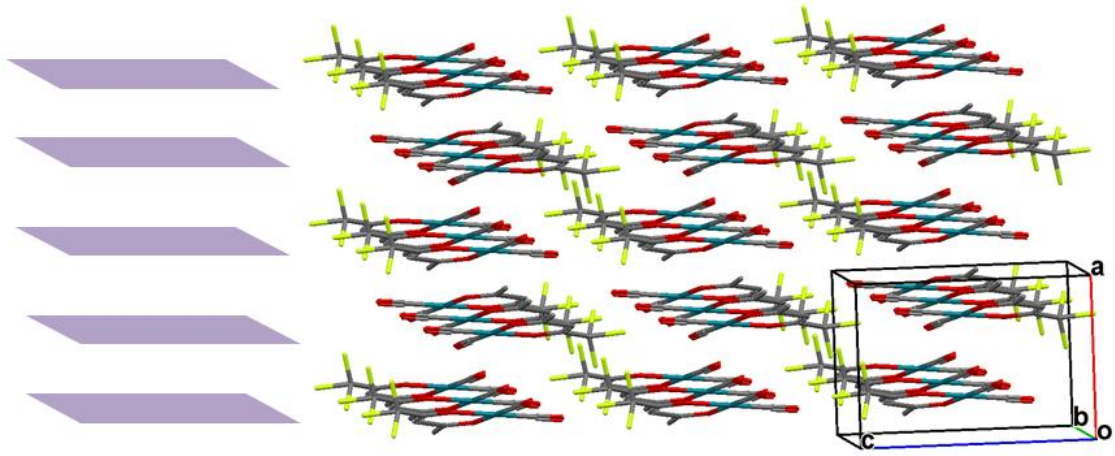

Figure 6.9: Molecules arranged along planes *via* the intermolecular interactions found in [Rh(tfac)(CO)$_2$].

The extended packing diagram for [Rh(tfac)(CO)$_2$] is illustrated in Figure 6.10 and clearly shows the dominating effect that the interactions have on the arrangement of molecules

within the crystal lattice. The metallophilic interactions, in addition with the halogen bonds encountered in this structure, allows for the dimensionality of the structure to be extended along two directions. Metallophilic interactions result in structuring of molecules along the *a*-axis whilst the halogen bonds were encountered along the *c*-axis of the lattice.

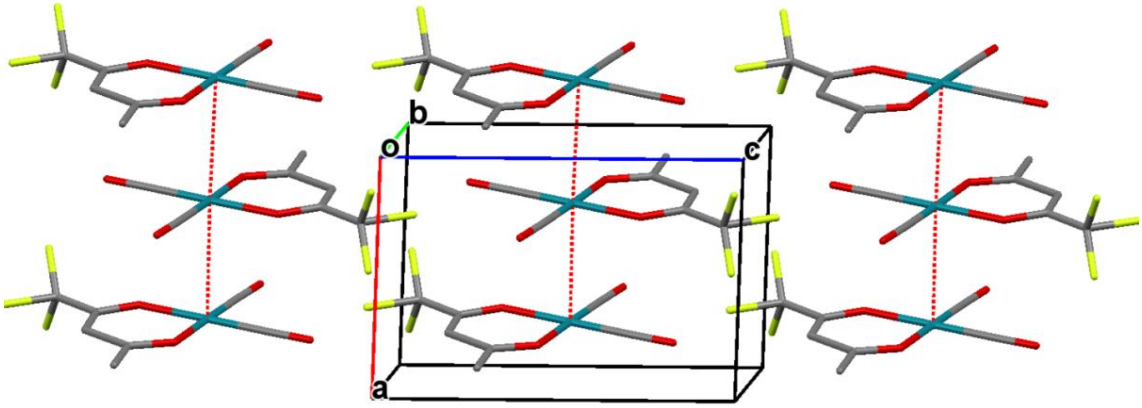

Figure 6.10: Extended packing diagram of [Rh(tfac)(CO)$_2$] viewed along an off-centered *b*-axis reveals the dominating effect that intermolecular interactions have on the arrangement of molecules within the crystal lattice.

6.4 Crystal structure of [Rh(piv)(CO)$_2$]

The complex, dicarbonyl(1,1,1-trifluoro-5,5-dimethyl-2,4-hexanedionato-κ^2O,O')rhodium(I), crystallized in the orthorhombic space group *Pbcn* with one molecule in the asymmetric unit. The molecular structure as well as the atom numbering scheme is represented in Figure 6.11. General crystallographic information of the crystal structure is referred to in Table 6.1 with selected bond lengths and angles given in Table 6.4. For comprehensive information regarding bond distances and angles, refer to Appendix A.

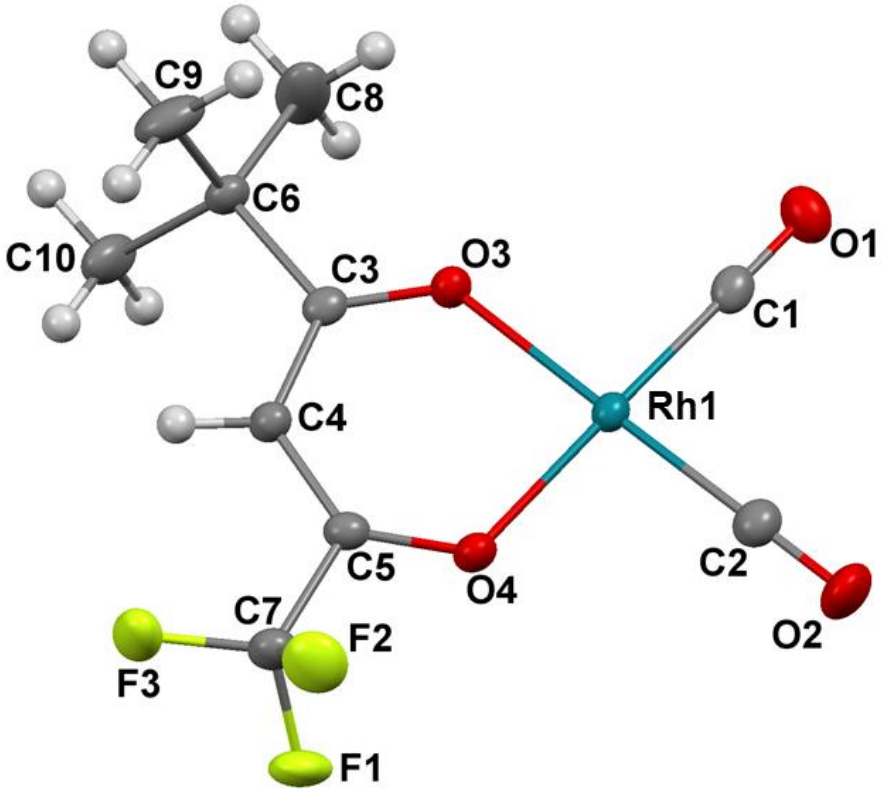

Figure 6.11: Molecular structure of [Rh(piv)(CO)$_2$] with atom numbering scheme (thermal ellipsoid probability = 50 %). Hydrogen atom labels have been omitted for the sake of clarity.

Table 6.4: Selected bond distances and angles of [Rh(piv)(CO)$_2$].

Atoms	Distance (Å)
Rh1-C1	1.839(2)
Rh1-C2	1.852(3)
Rh1-O3	2.047(2)
Rh1-O4	2.038(2)
C1-O1	1.131(3)
C2-O2	1.128(3)
C3-O3	1.258(3)
C5-O4	1.270(3)
C4-C3	1.411(3)
C4-C5	1.370(3)
C3-C6	1.531(3)
C5-C7	1.524(3)
C6-C8	1.520(3)
C6-C9	1.536(3)
C6-C10	1.531(3)
C7-F1	1.343(3)
C7-F2	1.338(3)
C7-F3	1.325(3)
O3···O4[a]	2.885(2)

[a] Bite distance

Atoms	Angle (°)
C1-Rh1-C2	89.0(1)
O3-Rh1-O4	89.87(7)
C1-Rh1-O4	177.32(7)
C2-Rh1-O3	179.14(9)
C3-C4-C5	124.3(2)
C1-Rh1-O3	90.14(8)
C2-Rh1-O4	90.9(1)
O3-C3-C4	124.2(2)
O4-C5-C4	130.8(2)
C3-O3···C5-O4[b]	1.7(2)

[b] Torsion angle between C3-O3 and C5-O4

The bond distances reported in Table 6.4 reveal a molecule that is unsymmetrical in terms of bond distances and angles. This is evident in the Rh1-C1 and Rh1-C2 bonds that differ significantly with bond distances of 1.839(2) Å and 1.852(3) Å respectively. The unsymmetrical nature of the molecule is further seen with the Rh1-O3 and Rh1-O4 bond lengths of 2.047(2) Å and 2.038(2) Å. Also the C3-O3 and C5-O4 bonds differ substantially with bond distances of 1.258(3) Å and 1.270(3) Å respectively. The differences observed in the molecule are attributed to the two different substituents that are present on the C3 and C5 carbons of the coordinating β-diketonato ligand. The trifluoro moiety present on C5 is electron withdrawing as opposed to the *t*-butyl group situated on C3 that is regarded as electron donating as well as being quite sterically demanding.[17,18]

The expected square planar geometry for [Rh(piv)$(CO)_2$] is distorted with bond angles of C1-Rh1-C2 (89.0(1)°) and C2-Rh1-O4 (90.9(1)°) deviating from the 90° angles expected for the ideal geometry. A similar square planar geometry was observed in [Rh(tfac)$(CO)_2$] (see Section 6.3)

Rh···Rh interactions were again noted between neighbouring molecules along the shortest cell axis of the unit cell (*a*-axis = 6.467(2) Å). These interactions, illustrated in Figure 6.12, with Rh···Rh distances found to alternate between 3.184(2) Å and 3.289(3) Å along the one-dimensional metal chain. The distances are considerably shorter than those reported for [Rh(tfac)$(CO)_2$] (3.384(3) Å and 3.385(3) Å), i.e. up to 0.2 Å.

[17] Stang, P. J., Rappoport, Z., Hanack, M., Subramanian, L. R., *Vinyl Cations*, Academic Press, New York, United States of America, **1979**, 257.
[18] Meurant, G., *Research in Chemical Kinetics*, Elsevier Science B. V., Amsterdam, The Netherlands, **1994**, 187.

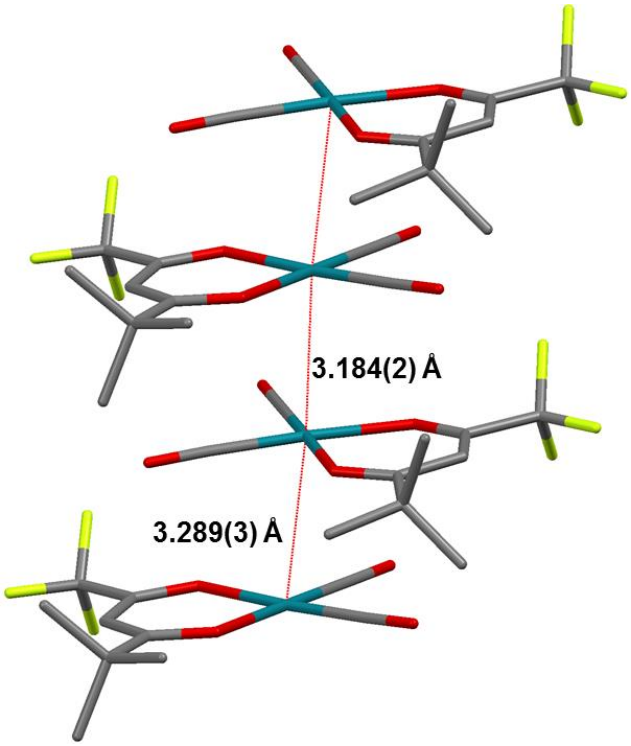

Figure 6.12: Rh···Rh interactions (indicated in red) between neighbouring molecules of [Rh(piv)(CO)$_2$] with Rh···Rh distances of 3.184(2) Å and 3.289(3) Å.

Figure 6.13 illustrates the angles and torsion angles between the stacked molecules along the chain of metallophilic interactions. The angles between the Rh(I) centres are 175.6(3)° along three consecutive metal centres. The angle indicates a small distortion from a near linear arrangement of molecules along the one-dimensional metal chain. Even smaller angles of 173.93(3)° were found between metal centres in [Rh(tfac)(CO)$_2$] (see Section 6.3). Torsion angles of 141.4(2)° between C4-Rh1 and C4-Rh1 (β-diketone ligands) of different molecules results in a slightly staggered arrangement of molecules as illustrated in Figure 6.13 (b). This is in contrast to the eclipsed formation that was noted in [Rh(tfac)(CO)$_2$] (180.0(2)°).

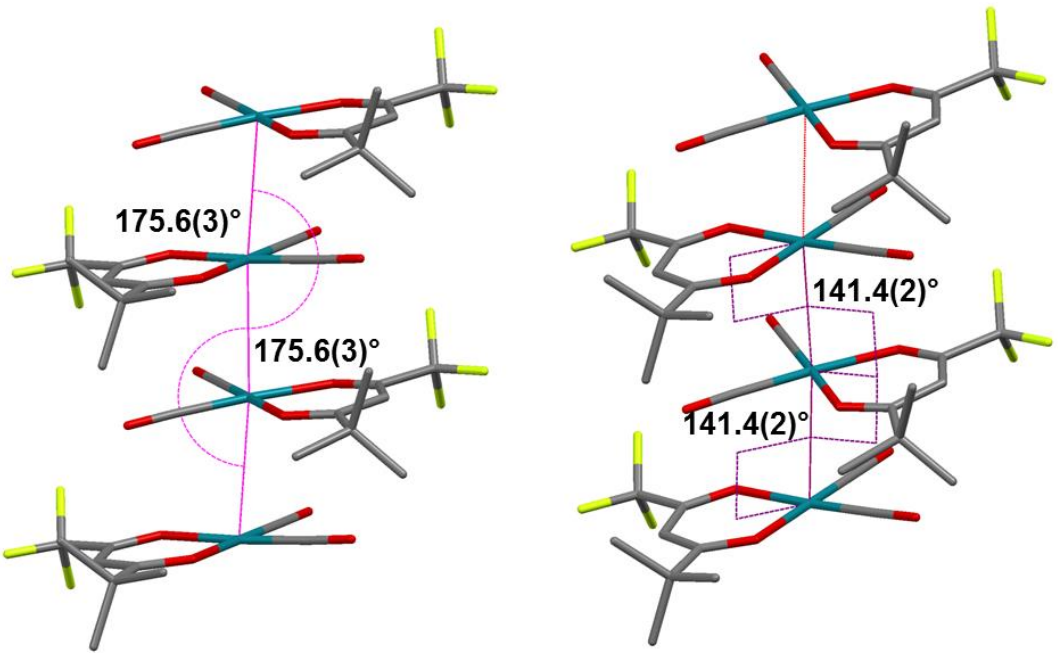

Figure 6.13: a) The angle between neighbouring Rh centres in [Rh(piv)(CO)$_2$] was found as 175.6(3)°; b) Torsion angles of 141.4(2)° between coordinating β-diketonato ligands revealed a staggered arrangement of R-groups between molecules.

Other soft contacts were observed in [Rh(piv)(CO)$_2$] between O1···C3^{ii} (3.159(2) Å, symmetry operation: ii) 1-x, y, ½-z) and a halogen bond between C7-F3···O1^{i}. These contacts are presented in Figure 6.14 with details of the halogen bond given in Table 6.5. The halogen bond is extended along the *c*-axis between molecules resulting in a polymeric chain within the crystal lattice as illustrated in Figure 6.15.

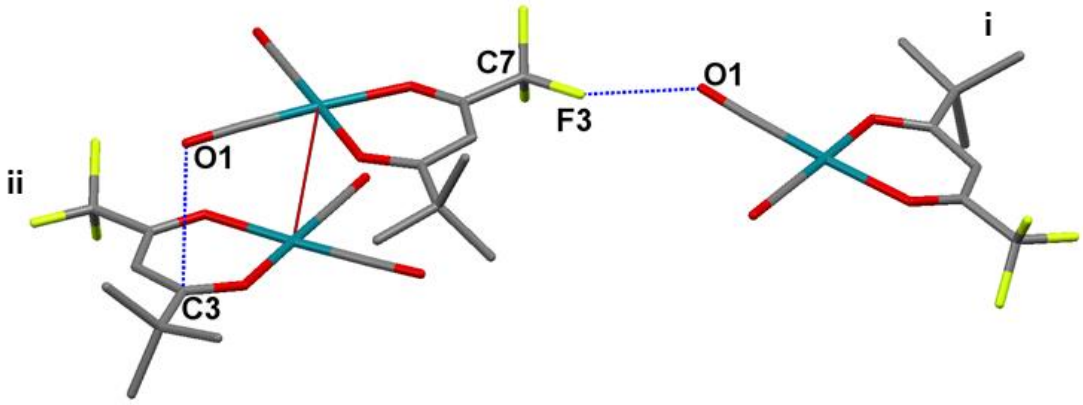

Figure 6.14: A soft contact between O1···C3 and a halogen bond C7-F3···O1^{i} involving the trifluoro substituent of the β-diketonato ligand in [Rh(piv)(CO)$_2$].

Table 6.5: Halogen-bond geometry for [Rh(piv)(CO)$_2$] as depicted in Figure 6.14 and 6.15.

D-X···A	dD-X (Å)	dX···A (Å)	dD···A (Å)	Angle D-X···A (°)
C7-F3···O1^{i}	1.33(3)	2.85(2)	3.74 (3)	122.5(4)

Symmetry codes: i) 1/2-x,1/2-y,1/2+z.

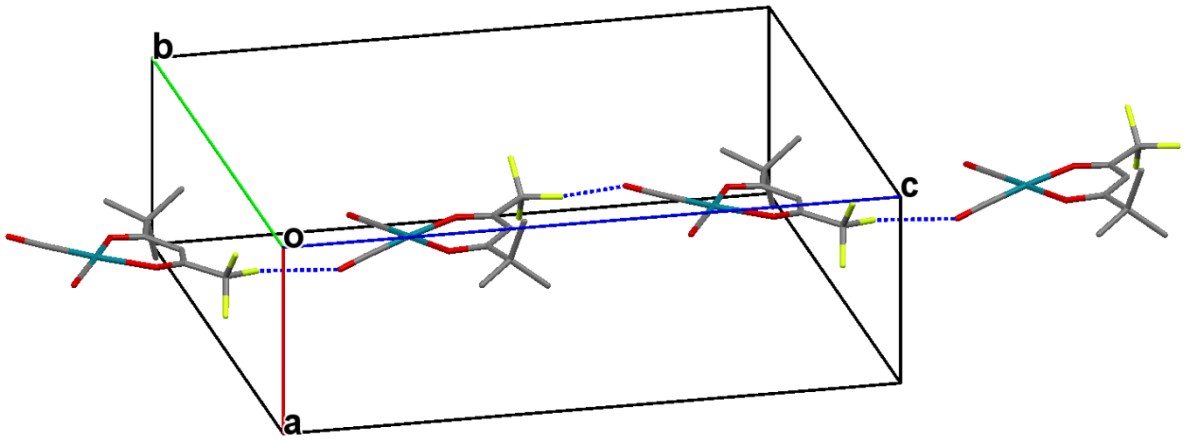

Figure 6.15: The halogen bond of C7-F3···O1 (indicated in blue) results in a polymeric chain when extended along the *c*-axis in [Rh(piv)(CO)$_2$].

As was seen with [Rh(tfac)(CO)$_2$], the combination of metallophilic interactions and halogen bonding leads to the construction of planes of molecules within the packing of [Rh(piv)(CO)$_2$]. These planes are illustrated in Figure 6.16 with the *a*-axis defined by the metallophilic interactions and the *c*-axis by the halogen bonds. The *b*-axis has only weak van der Waals packing which results in the construction of sort of “nano-plates”.

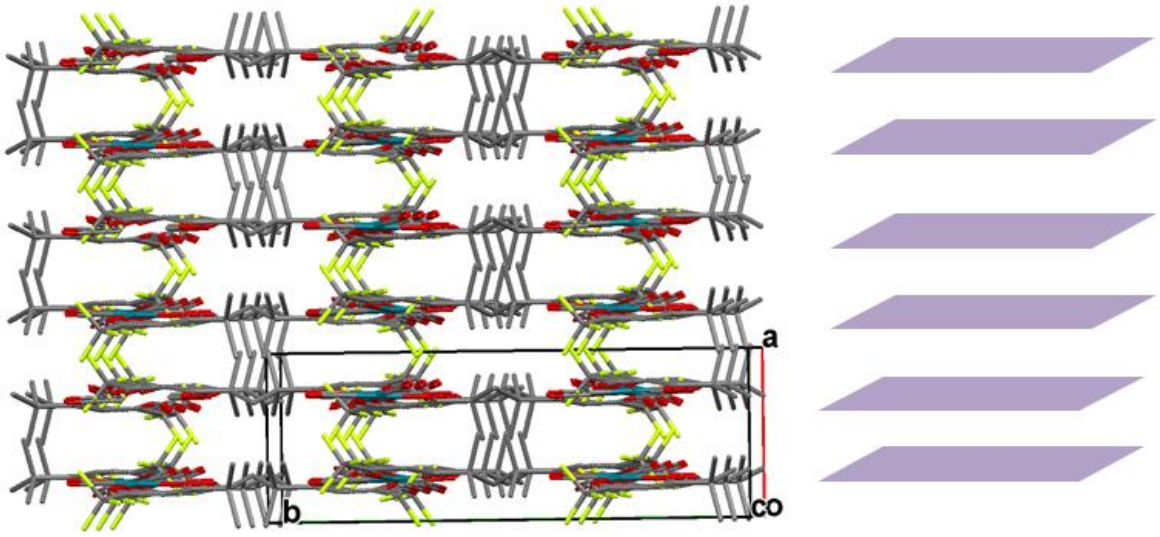

Figure 6.16: Metallophilic interactions along the *a*-axis and halogen bonding along the *c*-axis lead to the construction of “nano-plates” in [Rh(piv)(CO)$_2$].

The packing diagram for [Rh(piv)CO)$_2$] along a slightly off-centered *b*-axis is given in Figure 6.17. The influence of metallophilic interactions (indicated in red) in the arrangement of molecules within the crystal lattice, is clearly visible.

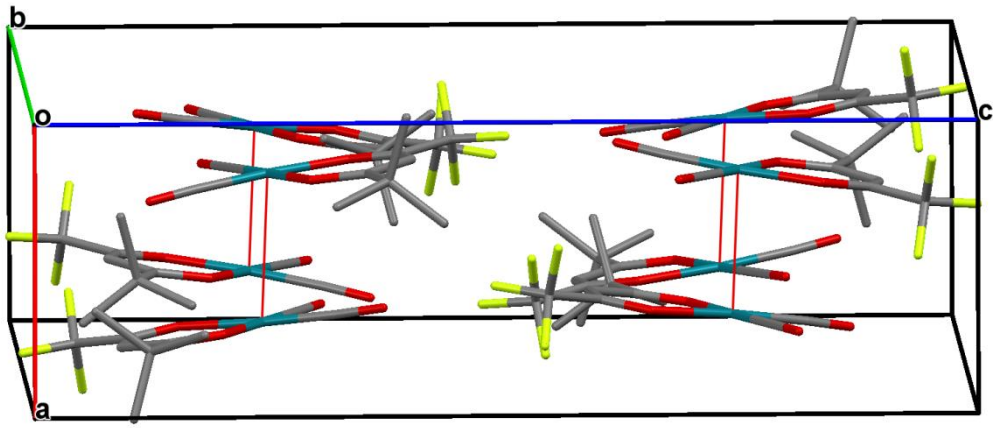

Figure 6.17: Packing diagram of [Rh(piv)(CO)$_2$] viewed along an off-centred *b*-axis illustrating the dominating effect of metallophilic interactions (indicated in red) in the arrangement of molecules in the crystal.

6.5 Crystal structure of [Rh(dipiv)(CO)$_2$]

As was the case with [Rh(tfac)(CO)$_2$], only a few crystals could be obtained from the synthesis of the [Rh(dipiv)(CO)$_2$] complex (see Section 3.3.7, Chapter 3). These crystals were of relatively poor quality which is reflected in the data collection (see Table 6.1). A very high R-value of 18 % is reported for the structure determination but a reasonably Goodness-of-fit value (1.109) and good completeness for the data collection (99.1 %) led to the structure to be included in this work.

The complex, dicarbonyl(2,2,6,6-tetramethyl-3,5-heptanedionato-κ^2*O,O*)rhodium(I), crystallized in the monoclinic space group $P2_1/m$ with 1 crystallographic pseudo dimeric complex in the asymmetric unit. The pseudo complex is actually made up of 2 molecular entities which is crystallographically viewed as a single entity due to the effect of the metallophilic interactions. The molecular structures as well as the numbering scheme are represented in Figure 6.18. General crystallographic information of the crystal structure is referred to in Table 6.1 with selected bond lengths and angles given in Table 6.6. For comprehensive information regarding bond distances and angles refer to Appendix A.

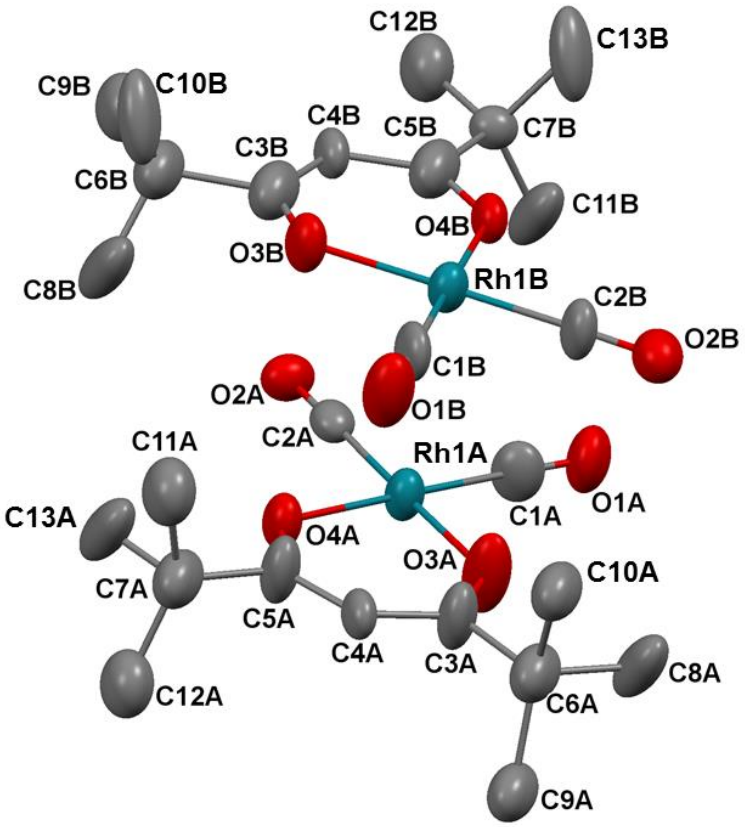

Figure 6.18: Molecular structures of [Rh(dipiv)$(CO)_2$] with atom numbering scheme (thermal ellipsoid probability = 50 %). Hydrogen atoms have been omitted for the sake of clarity.

Table 6.6: Selected bond distances and angles of [Rh(dipiv)$(CO)_2$].

Atoms	Distance (Å)	
	Molecule A	Molecule B
Rh1-C1	1.87(2)	1.85(2)
Rh1-C2	1.87(3)	1.87(2)
Rh1-O3	2.02(2)	2.02(2)
Rh1-O4	2.05(2)	2.03(2)
C1-O1	1.14(2)	1.14(2)
C2-O2	1.12(2)	1.14(2)
C3-O3	1.28(2)	1.29(3)
C5-O4	1.24(2)	1.29(3)
C4-C3	1.39(3)	1.43(3)
C4-C5	1.36(3)	1.42(3)
C3-C6	1.57(3)	1.58(3)
C5-C7	1.55(3)	1.53(3)
C6-C8	1.57(3)	1.50(2)
C6-C9	1.69(2)	1.54(3)
C6-C10	1.69(2)	1.50(2)
C7-C11	1.38(3)	1.53(2)
C7-C12	1.64(2)	1.64(2)
C7-C13	1.64(2)	1.53(2)
O3···O4[a]	2.84 (2)	2.86(2)

[a] Bite distance

Atoms	Angle(°)	
	Molecule A	Molecule B
C1-Rh1-C2	88.0(9)	88.3(9)
O3-Rh1-O4	88.6(6)	89.9(5)
C1-Rh1-O4	178.8(7)	178.9(7)
C2-Rh1-O3	178.2(7)	179.4(7)
C3-C4-C5	127(2)	124(2)
C1-Rh1-O3	90.2(8)	91.1(8)
C2-Rh1-O4	93.2(7)	90.7(7)
O3-C3-C4	123(2)	127(2)
O4-C5-C4	126(2)	125(2)
C3-O3···C5-O4[b]	180.1(2)	180.2(2)

[b] Torsion angle between C3-O3 and C5-O4

The bond distances of Rh1-C1a (1.87(2) Å) and Rh1a-C2a (1.87(3) Å) reveal a fairly symmetrically arranged molecule. Similarly the Rh1b-C1b (1.85(2) Å) and Rh1b-C2b (1.87(2) Å) bonds of molecule **B** revealed the similarity of the bonds. The symmetrical nature of the two molecules could be attributed to the symmetrical nature of the coordinating β-diketonato ligand in [Rh(dipiv)$(CO)_2$] containing two *t*-butyl substituents on the C3 and C5 carbon positions.

Small differences were noted between the two molecules of [Rh(dipiv)$(CO)_2$] with notable bond angles of O3a-Rh1a-O4a (88.6(9)°) and O3b-Rh1b-O4b (89.9(5)°) both illustrating a distorted square planar geometry. The angles of the coordinating moiety around each Rh(I) centre is illustrated in Figure 6.19. Clear differences are present between the two molecules with C2a-Rh1a-O4a (93.2(7)°) and C2b-Rh1b-O4b (90.7(7)°) notably different in the distorted square planar geometries.

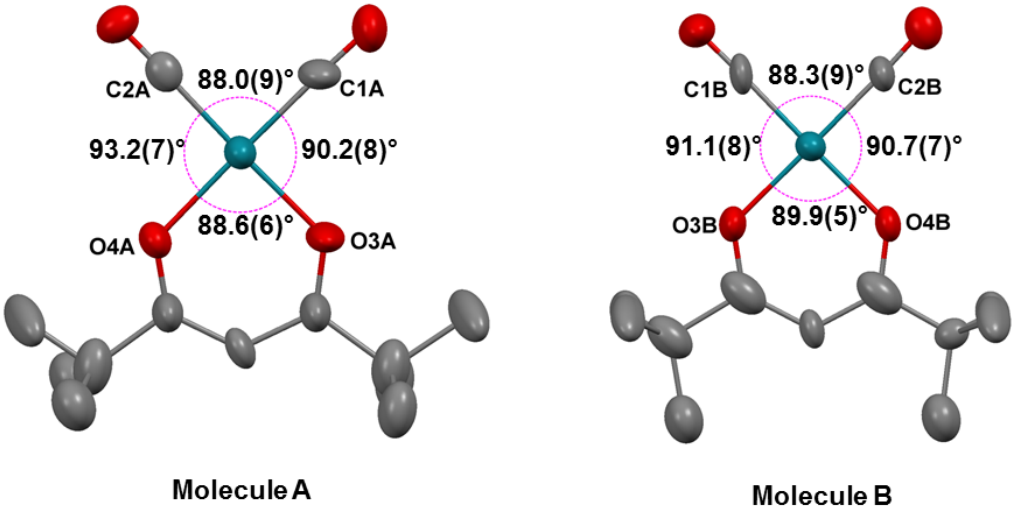

Molecule A Molecule B

Figure 6.19: Bond angles between the coordinating moiety of atoms C1, C2, O3 and O4 in [Rh(dipiv)$(CO)_2$] display a distorted square planar geometry for the two molecules.

Metallophilic interactions were encountered between the two molecules of [Rh(dipiv)$(CO)_2$] that extend into a one-dimensional metal chain along the *b*-axis (6.613(7) Å). These

interactions are illustrated in Figure 6.20 with consistent Rh···Rh distances of 3.307(3) Å. The Rh···Rh distances are slightly longer than those reported for [Rh(piv)$(CO)_2$] (3.184(2) Å and 3.289(3) Å) (see Section 6.4). Even longer Rh···Rh distances were however noted in [Rh(tfac)$(CO)_2$] (3.384(3) Å and 3.385(3) Å) (see Section 6.3).

Figure 6.21 illustrates the angles and torsions in which the molecules are arranged along the one-dimensional metal chain. The angles between Rh(I) centres were found to be 178.5(2)° (Rh1a-Rh1b-Rh1a) as measured along the linearly arranged molecules. Torsion angles of 140.9(3)° between the R-groups measured between C4a-Rh1a and C4b-Rh1b of different molecules results in a staggered arrangement along the 1-D chain. These values closely resembled those reported for [Rh(piv)$(CO)_2$] with angles of 175.6(3)° and torsion angles of 141.4(2)°.

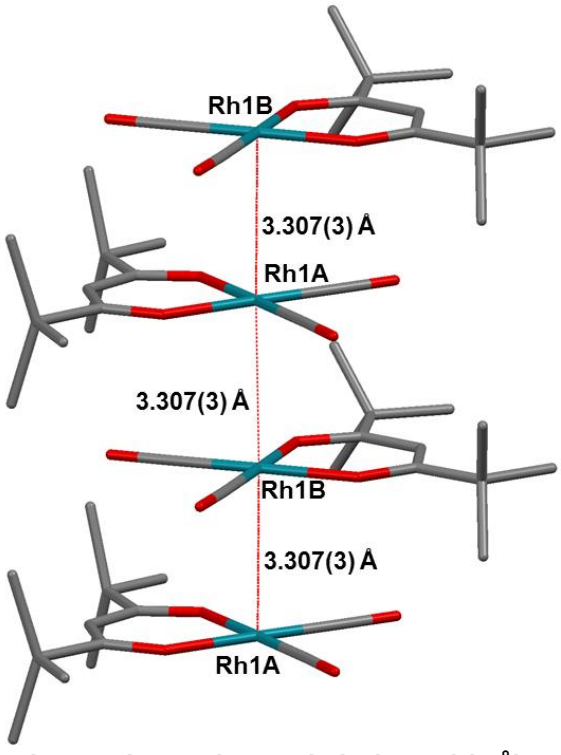

Figure 6.20: Metallophilic interactions Rh1a···Rh1b (3.307(3) Å) are extended into a one-dimensional chain along the crystallographic *b*-axis in [Rh(dipiv)$(CO)_2$].

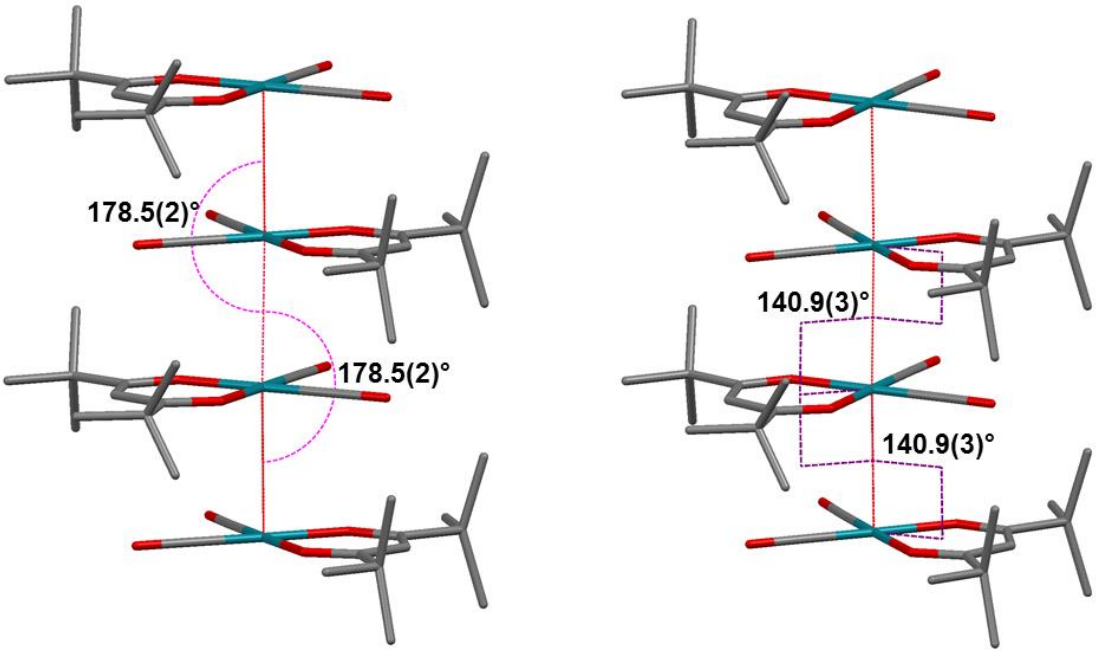

Figure 6.21: a) The angle between neighbouring Rh centres in [Rh(dipiv)(CO)$_2$] (178.5(2)°); b) Torsion angles of 140.9(3)° between coordinating β-diketonato ligands revealed a staggered arrangement of R-groups between molecules.

Other intra- and intermolecular soft contacts were observed in [Rh(dipiv)(CO)$_2$] and are illustrated in Figure 6.22. A bifurcated interaction was noted involving H11b within an intramolecular hydrogen bond with O1b as well as a soft contact with H11b of another molecule. Details of the interactions are given in Table 6.7.

Table 6.7: Hydrogen-bond geometry of C12a-H11b···O1b and detail of soft contacts found in [Rh(dipiv)(CO)$_2$].

D-X···A	dD-H (Å)	dH···A (Å)	dD···A (Å)	Angle D-X···A (°)
C12a-H12b···O1b	0.96	2.31	3.26(3)	173.3
H12b···H11b^{i}	-	-	2.39(2)	-
H9a···H9a^{i}	-	-	2.28(3)	-
C9a···C9a^{i}	-	-	3.38(3)	-

Symmetry codes: i) x,1+y, z.

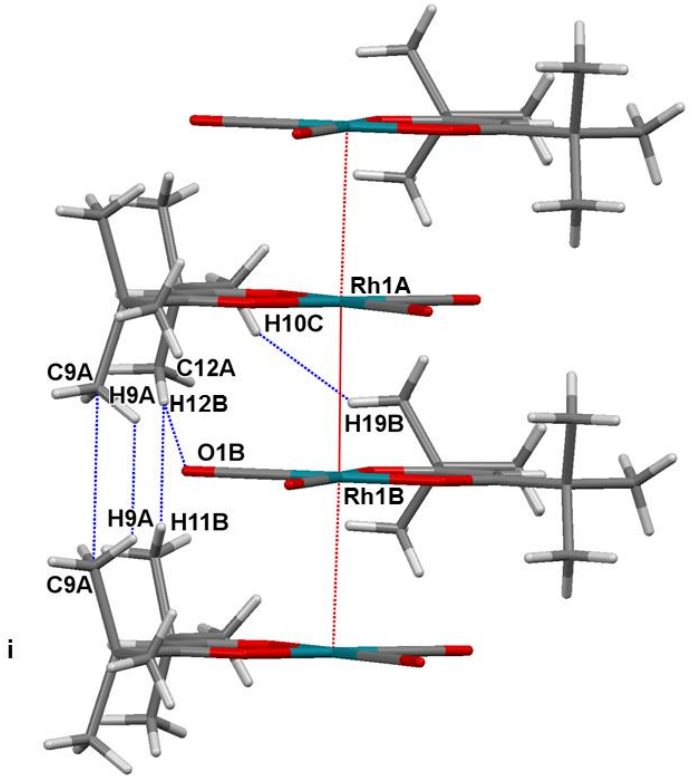

Figure 6.22: Intra- and intermolecular interactions in [Rh(dipiv)$(CO)_2$].

The packing diagram for [Rh(dipiv)$(CO)_2$] is given in Figure 6.23 viewed along an off centered *a*-axis which clearly shows the dominating effect of the Rh···Rh interactions on the arrangement of molecules within the crystal lattice.

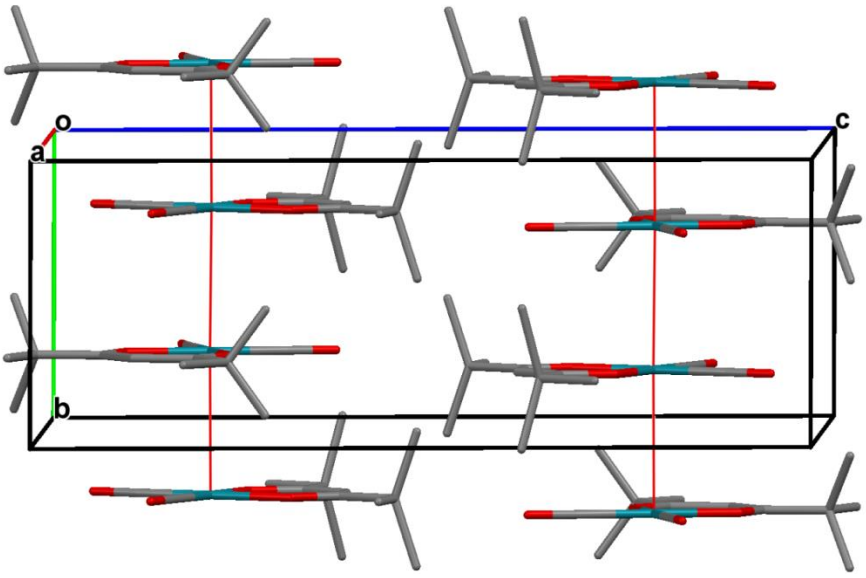

Figure 6.23: Packing diagram of [Rh(dipiv)$(CO)_2$] viewed along an off-centred *a*-axis showing the dominating effect of metallophilic interactions (indicated in red) in the arrangement of molecules in the crystal lattice.

6.6 Conclusion

The solid-state structures of three novel rhodium(I) complexes were evaluated and discussed in this chapter. Different Rh···Rh distances were reported for the three structures ([Rh(tfac)$(CO)_2$] = 3.384(3), 3.385(3) Å; [Rh(piv)$(CO)_2$] = 3.184(2), 3.289(3) Å and [Rh(dipiv)$(CO)_2$] = 3.307(3) Å) respectively. Additionally, the angles of the Rh(I) centres that are arranged in the chain as well as the torsion angles between R-groups of molecules were found to be different for each molecule. The Rh-Rh-Rh angles for [Rh(piv)$(CO)_2$] (175.6(3)°) and [Rh(dipiv)$(CO)_2$] (178.5(2)°) showed the greatest linearity in comparison to [Rh(tfac)$(CO)_2$] (173.93(3)°). The arrangement of molecules along the chain were also shown to be staggered in [Rh(piv)$(CO)_2$] and [Rh(dipiv)$(CO)_2$] whilst being eclipsed in [Rh(tfac)$(CO)_2$].

A preliminary kinetic investigation undertaken for this study will be discussed in the next Chapter. Substitution reactions of square planar complexes were shown in Chapter 2 to link the reactivity of a complex with the electronic environment experienced by the metal centre. It is anticipated that such studies will provide an additional parameter by which to evaluate the range of rhodium(I) complexes synthesized for this study. Ultimately, all of these individual parameters will be compared in relation to the Rh···Rh interactions and physical properties found in the solid-state for these rhodium(I) complexes in Chapter 8.

Chapter 7: Preliminary Reactivity and Equilibrium Evaluation of Carbonyl Substitution by a Bulky Tertiary Phosphine in [Rh(acac)-$(CO)_2$]

7.1 Introduction

This PhD study is concerned with the design and assembly of nano-wired materials *via* the use of metallophilic interactions between metal centres along one-dimensional metal chains. These one-dimensional metal chains have shown promise as materials with conductive properties.[1] However, in the development of any new material for potential application, an understanding of the relevant fundamental chemistry of the material is required. In the rhodium(I) complexes synthesized for this study this would imply an in-depth understanding of the changes induced on the metal centre by using different substituents in the coordinating β-diketonato ligands. By understanding the effects of using different coordinating ligands on the rhodium(I) centre within these complexes the engineering of new materials with desirable properties may become more viable.

The observation that rhodium(I) complexes and most other square-planar d^8 metal systems undergo associative substitution mechanisms (see Section 2.8, Chapter 2) provides a unique measure by which to evaluate metal complexes in terms of their reactivity. Furthermore, the reactivity of metal complexes in substitution reactions can be directly linked to the electronic environment experienced by the metal centre. Complexes containing electron poorer metal centres, more prone to nucleophilic attack, undergo substitution reactions faster and vice versa.[2]

Thus, by investigating substitution reactions of different [Rh(β-diketonato)$(CO)_2$] complexes not only can the reactivity of the complexes be evaluated but valuable information can be gained with regards to the electronic environment at the rhodium(I) centre. It is thus anticipated that any correlation found between the electronic environment at the rhodium(I) centre and the reactivity of

[1] Bera, J. K., Dunbar, K. R., *Angew. Chem., Int. Ed.*, **2002**, *41*, 4453-4457.
[2] Van Eldik, R., Bowman-James, K., *Advances in Inorganic Chemistry*, Academic Press, London, United Kingdom, **2007**, 296.

the rhodium(I) complexes can also be linked to the different coordinating β-diketonato ligands and their corresponding properties. This trend will hopefully be extended to some of the other parameters evaluated in the rhodium(I) complexes such as the ^{103}Rh chemical shifts, characteristics such as the colour exhibited by the compounds and the Rh···Rh distances along the one-dimensional metal chains in the solid-state (see Chapter 8).

7.2 General Reaction Mechanism

It is known that dicarbonyl Rh(I) complexes of the general form [Rh(*L,L'*-Bid)$(CO)_2$] undergo substitution reactions by tertiary phosphine entering nucleophiles with the corresponding loss of one carbonyl ligand.[3,4,5] The general carbonyl substitution reaction of (acetylacetonato-κ^2-*O,O)*dicarbonylrhodium(I), [Rh(acac)$(CO)_2$] with a bulky entering ligand tri(o-tolyl)phosphine is therefore considered in this study as illustrated in Scheme 7.1.

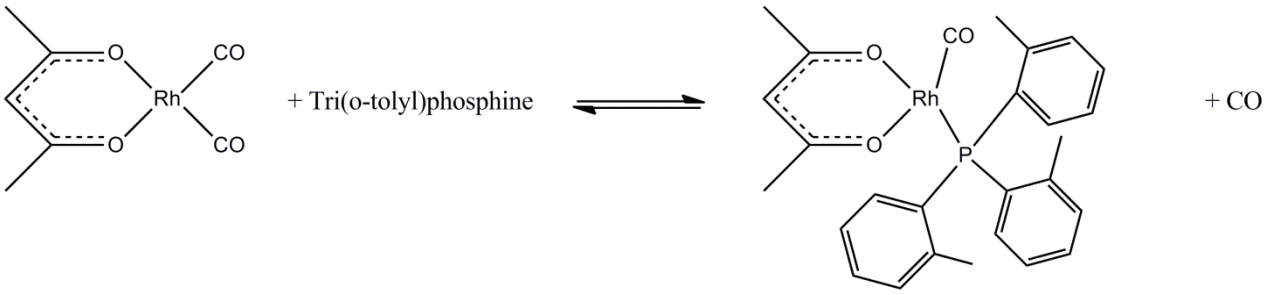

Scheme 7.1: General carbonyl substitution reaction of [Rh(acac)$(CO)_2$] by tri(o-tolyl)phosphine.

It is known, and was discussed in Chapter 2 (see Section 2.8) that square planar substitution reactions by entering nucleophiles generally follow a direct or solvent assisted (solvolysis) associative reaction pathway.[6] These two pathways are illustrated in Figure 7.1 with the [Rh(acac)$(CO)_2$] complex as reactant presented as [Rh(L)$(CO)_2$] (**1**) and the substituted product [Rh(acac)(CO)$(P(otol)_3$] as [Rh(L)(CO)$(P(otol)_3$)] (**2**), *via* a potential parallel solvent complex [Rh(L)(S)(CO)] (**3**). Of importance in the substitution process in this study is the fact that the substituted CO ligand (in this case a gas) also has to be incorporated in all rate laws and thermodynamic calculations (see Section 7.6).

[3] Bonati, F., Wilkinson, G., *J. Chem. Soc*., **1964**, 3156-3160.
[4] Serron, S. Huang, J., Nolan, S. P., *Organometallics*, **1998**, *17*, 534-539.
[5] Hartley, F. R., *Supported Metal Complexes*, D. Reidel Publishing Company, Dordrecht, The Netherlands, **1985**, 223.
[6] Elding, L. I., Gröning, A. B., *Inorg. Chim. Acta*, **1980**, *38*, 59-66.

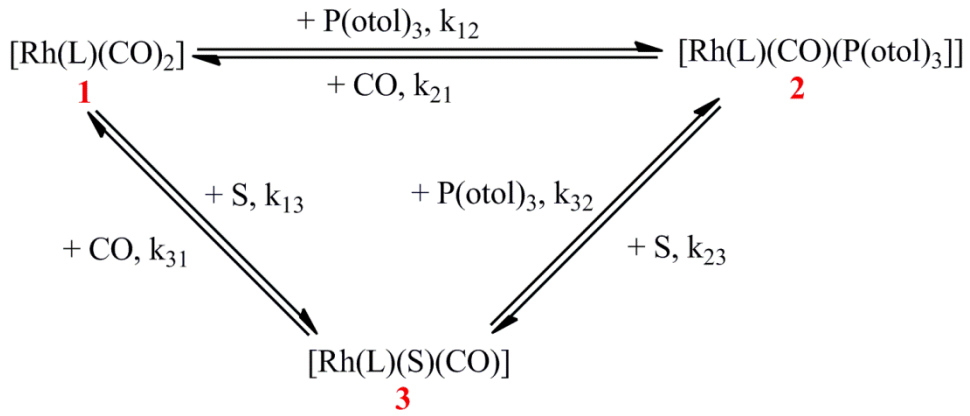

Figure 7.1: Schematic representation of a square planar substitution reaction with parallel direct substitution and solvent assisted pathways. The species are numbered in the following manner: [Rh(acac)(CO)$_2$] = 1; [Rh(acac)(CO)(P(otol)$_3$)] = 2; [Rh(acac)(S)(CO)] = 3; S= denotes the solvent. The subscripts of the rate constants represent the numbers of the species involved during the specific reaction, e.g. k_{12} describes the rate constant for the substitution reaction of complex 1 to 2. Solvent concentrations have been incorporated in the rate constants k_{13} and k_{23}.

From the reaction mechanism illustrated in Figure 7.1 the following expression can be derived (see Appendix for full derivation) describing the relationship between the value of k_{obs} and the concentrations of the various species in solution under conditions where an equilibrium (denoted by K_{eq}) exists[7,8,9]:

$$k_{obs} = k_{12}([P(\text{otol})_3] + \frac{[CO]}{K_{eq}}) + \frac{\frac{k_{13}k_{32}}{K_{eq}k_{31}}[CO] + k_{13}\frac{k_{32}}{k_{31}}[P(\text{otol})_3]}{[CO] + \frac{k_{32}}{k_{31}}[P(\text{otol})_3]} \qquad \text{(Eq. 7.1)}$$

In equation 7.1, K_{eq} is used to denote the equilibrium constant for the formation of the final product, [Rh(acac)(CO)(P(otol)$_3$)]. The equilibrium constant can be defined as the rate of the forward reactions divided by the rate of the reverse reactions with the direct and solvent assisted pathways in equilibrium. This gives equation 7.2[10]:

$$K_{eq} = \frac{k_{12}}{k_{21}} = \frac{k_{13}k_{32}}{k_{23}k_{31}} \qquad \text{(Eq. 7.2)}$$

In the case of large equilibrium constants, equation 7.1 can be simplified to the well-known two term rate law that is normally encountered for square planar substitution reactions.[11,12,13,14] This rate law can be given as:

$$k_{obs} = k_{12}[P(\text{otol})_3] + k_{13} \qquad \text{(Eq. 7.3)}$$

[7] Otto, S., *PhD Thesis*, University of the Free State, Bloemfontein, South Africa, **1999**.
[8] Kirsten, L., *MSc Dissertation*, University of Johannesburg, Johannesburg, South Africa, **2005**.
[9] Romeo, R., Arena, G., Scolara, L. M., Plutino, M. R., *Inorg. Chim. Acta*, **1995**, *240*, 81-92.
[10] Seguin, J. Y., Zador, M., *Inorg. Chim. Acta.*, **1976**, *20*, 203-206.
[11] De Waal, D. J. A., Robb, W., *Inorg. Chim. Acta*, **1978**, *26*, 91-96.
[12] Gray, H. B., Olcott, R. J., *Inorg. Chem.*, **1962**, *1*, 481-485.
[13] Pearson, R. G., Gray, H. B., Basolo, F., *J. Am. Chem. Soc.*, **1960**, *82*, 787-792.
[14] Otto, S., Roodt, A., *J. Organomet. Chem.*, **2006**, *691*, 4626-4632.

If the observed rate constants under these conditions are plotted against [P(otol)$_3$] a linear relationship will exist with the slope indicated as the k_{12} term and the intercept as the k_{13} constant (solvent assisted pathway).

However, under equilibrium conditions (small K_{eq} values) the concentration of the leaving group, CO in this case, can contribute significantly to the overall rate and the full equation (Eq. 7.1) describing the observable rate is obeyed.

The equilibrium constant of the reaction, K_{eq}, can be obtained kinetically, but may also be calculated from spectroscopic measurements (e.g. UV/Vis or NMR).

7.3 Experimental Procedures

7.3.1 Reagents

All reagents and chemicals were of analytical grade and purchased from Sigma-Aldrich South Africa. Reagents were used without further purification. The preparation and characterization of [Rh(acac)(CO)$_2$] as well as the final substituted phosphine complex, [Rh(acac)(CO)(P(otol)$_3$)] were described in Chapter 3 (see Sections 3.3.3 and 3.3.17).

The stability of the two reactants, [Rh(acac)(CO)$_2$] and tri(o-tolyl)phosphine was investigated in dimethyl formamide (DMF) over a period of 48 hours. The stability of the solutions was confirmed over this period. Fresh solutions were however prepared during each investigation since aged solutions are expected to potentially show artifacts due to slow decomposition and other potential side reactions.

7.3.2 Equipment

Kinetic measurements were initially performed on a Varian Cary 50 Conc. UV/Visible spectrophotometer. Temperature control of the reaction solutions was maintained to within ± 0.1 °C by means of a circulating water bath system. Faster reactions were monitored on a Hi-Tech SF-61DX2 Stopped-flow instrument, equipped with a circulating water bath, for which the dead time of the mixing unit was estimated to be less than 2.0 ms. The Stopped-flow instrument is a multiple wavelength apparatus used in the Diode-Array mode in which initial reactions were collected in order to validate the wavelength at which considerable absorbance change occurs. After the specific wavelength was selected, the Stopped-flow system was changed to the more sensitive Photo-Multiplier setup in order to collect the most accurate data. The Hi-Tech Stopped-flow instrument is Microsoft Windows operated with KinetAsyst Stopped-Flow Kinetic Studio

software[15] for the acquisition and analysis of kinetic data. Rate constants determined by Stopped-flow techniques are given as the average of at least four individual runs. ^{31}P NMR spectroscopic data were obtained on a Bruker Avance II 600 MHz spectrometer at 242.99 MHz (4096 scans, pulse of 30° and delay time of 0.1 seconds). ^{31}P NMR spectra were referenced externally to 85 % H_3PO_4 (δ= 0 ppm). The Scientist Micromath program, version 2.01[16] was used to fit all of the data to selected functions. The solid lines in the figures represent computer least-squares fits of data, while experimental values are represented as individual points, denoted by selected symbols. All the experimental data is given in the Appendix.

7.3.3 Treatment of Data

The Beer-Lambert law incorporated with the first-order exponential yields the following equation for the evaluation of absorbance change *vs.* time in simple-first order reactions.

$$A_t = A_\infty - (A_\infty - A_0)e^{k_{obs}t} \qquad \text{(Eq. 7.4)}$$

The pseudo first-order rate constant, k_{obs}, may be obtained by a least squares fit of the absorbance *vs.* time data.

7.4 General Considerations

The substitution reaction of a carbonyl group by a bulky phosphine, tri(o-tolyl)phosphine, in [Rh(acac)$(CO)_2$] was first investigated by P. Ebenebe[17] within the Chemistry Department of the University of the Free State in 1998. It was hoped to extend the study of Ebenebe[17] to the range of rhodium(I) complexes synthesized in this study to provide an additional parameter by which to evaluate the different electronic environments experienced by the rhodium(I) centre. This would hopefully result in a correlation with some of the solid-state characteristics exhibited by these complexes such as the metallophilic interactions between rhodium(I) centres (see Chapter 8).

As was mentioned in Section 7.1, substitution reactions of d^8 square planar metal complexes offer an opportunity to investigate the reactivity of a metal centre within metal complexes containing different coordinating ligands. These types of substitution reactions have been found to proceed at very fast reaction rates.

In order to study these fast reactions a bulky phosphine ligand such as tri(o-tolyl)phosphine was selected as entering ligand as it has been shown that increased steric bulk can considerably slow

[15] TgK Scientific Kinetic Studion, Version 1.0.8.32278, Copyright © **2008**, TgK Scientific.
[16] Micromath Scientist for Windows, Version 2.01, Copyright © **1986 – 1995**, MicroMath, Inc.
[17] Ebenebe, P., *MSc Dissertation*, University of the Free State, Bloemfontein, South Africa, **1998**.

the rate of reaction (see Section 2.8).[18] The bulkiness of the ligand is reflected in the large reported Tolman angle of the phosphine. It is known that the Tolman cone angle can be used as an effective parameter by which to estimate the amount of space that a phosphorous ligand occupies.[19,20] Tri(o-tolyl)phosphine has one of the largest reported cone angles (194°) with phosphines such as triphenylphosphine (145°) and tricyclohexylphosphine (170°) being less sterically demanding.[21,22,23]

In order to proceed with the preliminary kinetic investigations for this PhD study it was decided to initially repeat the substitution reaction of the carbonyl group by tri(o-tolyl)phosphine in $[Rh(acac)(CO)_2]$ as studied by Ebenebe[17].

The kinetic investigations of Ebenebe[17] were noted to have been conducted in acetone with fast reaction rates leading to studies utilizing Stopped-flow equipment. As certain Stopped-flow apparatuses are sensitive to solvents that can perish the plastic seals within the system acetone cannot be used in the setup available in this study. A replacement solvent had to be selected for this PhD investigation. A list of solvents with similar donicity and dielectric constant properties to acetone is presented in Table 7.1.

Table 7.1: Solvents and their properties relatable to acetone.

Solvent	Donicity (Dn)[24]	Dielectric constant[25]
Acetone	17.0	21.00
Benzene	0.1	2.30
Dimethyl sulfoxide	29.8	47.00
Dimethyl formamide	26.6	37.00
Methanol	19.0	32.70

Dimethyl formamide (DMF) was selected as the replacement solvent for this study as both acetone and dimethyl formamide are considered to be polar aprotic solvents, and DMF exhibited high solubility of the reactants and products in this study. The two solvents also display similar properties in terms of donicity and dielectric constants which was anticipated to result in similar rates and mechanism of substitution. Methanol was considered unsuitable due to it being regarded as a polar protic solvent whilst benzene is a non-polar solvent with substantially different solvent properties as seen in Table 7.1.

[18] Baddley, W. H., Basolo, F., *J. Am. Chem. Soc.*, **1966**, *88*, 2944-2950.
[19] Behr, A., Neubert, P., *Applied Homogeneous Catalysis*, Wiley-VCH, Weinhem, Germany, **2012**, 83.
[20] Tolman, C. A., *Chem. Rev.*, **1977**, *77*, 313-348.
[21] Pfennig, B. W., *Principles of Inorganic Chemistry*, Wiley & Sons, New Jersey, United States of America, **2015**, 641.
[22] Colacot, T., *New Trends in Cross-Coupling: Theory and Applications*, The Royal Society of Chemistry, Cambridge, United Kingdom, **2015**, 25.
[23] Noels, A. F., Graziani, M., Hubert, A. J., *Metal Promoted Selectivity in Organic Synthesis*, Springer Science + Business, Dordrecht, The Netherlands, **1991**, 217.
[24] Marcus, Y., *J. Solution Chem.*, **1984**, *13*, 599-624.
[25] Carey, F. A., Sundberg, R. J., *Advanced Organic Chemistry*, Kluwer Academic, New York, **2000**, 237.

7.5 Substitution Reaction Analysis by Slower UV/Vis and Stopped-flow Techniques

The reaction of tri(o-tolyl)phosphine with [Rh(acac)$(CO)_2$] in DMF was investigated at 25 °C using standard UV/Vis techniques. A typical change in absorbance spectra recorded can be seen in Figure 7.2 on the slower minute-to-hour UV/Vis spectrophotometric equipment. It is clear from Figure 7.2 (b), that the reaction proceeded at a fast rate with the reaction occurring almost instantaneously as the reaction solutions are mixed. The reaction proceeds to completion in under a minute time interval resulting in important data being lost when attempting the use of UV/Vis scanning equipment. This loss of data is unavoidable using slower minute-to-hour UV/Vis spectrophotometric equipment as the manual mixing time of ca. 60 seconds forms part of the initial experimental set up. It is however clear from this experiment (also confirmed by NMR, see Section 7.6.1) that only one, fast reaction occurs, even when monitored for 2 hours.

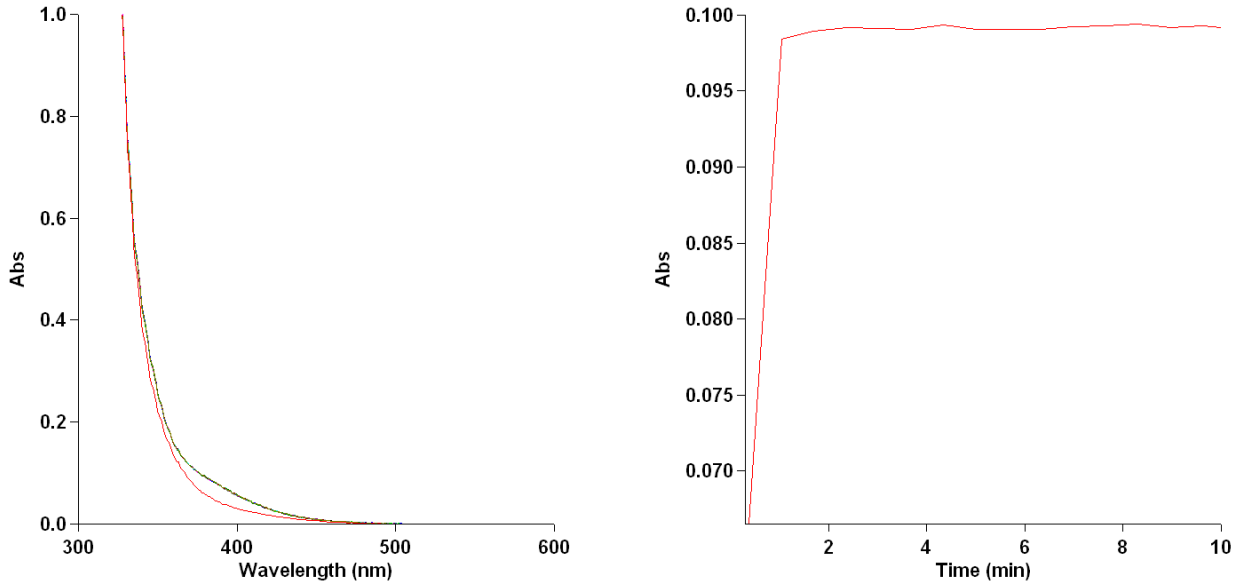

a) **b)**

Figure 7.2: a) Absorbance spectra of [Rh(acac)$(CO)_2$] (1.15 x 10^{-4} M) in the presence of [P(otol)$_3$] (1.5 x 10^{-3} M) over 120 minutes. b) The absorbance *vs.* time trace at 380 nm over ten minutes, Temp: 25 °C, DMF.

The fast reactions resulted in the use of millisecond-to-second Stopped-flow equipment to evaluate the substitution reaction. A typical change in absorbance spectra on the UV/Vis Stopped-flow using the Diode Array is represented in Figure 7.3 with a fitted (Eq. 7.4) change of absorbance against time plot in the right hand corner.

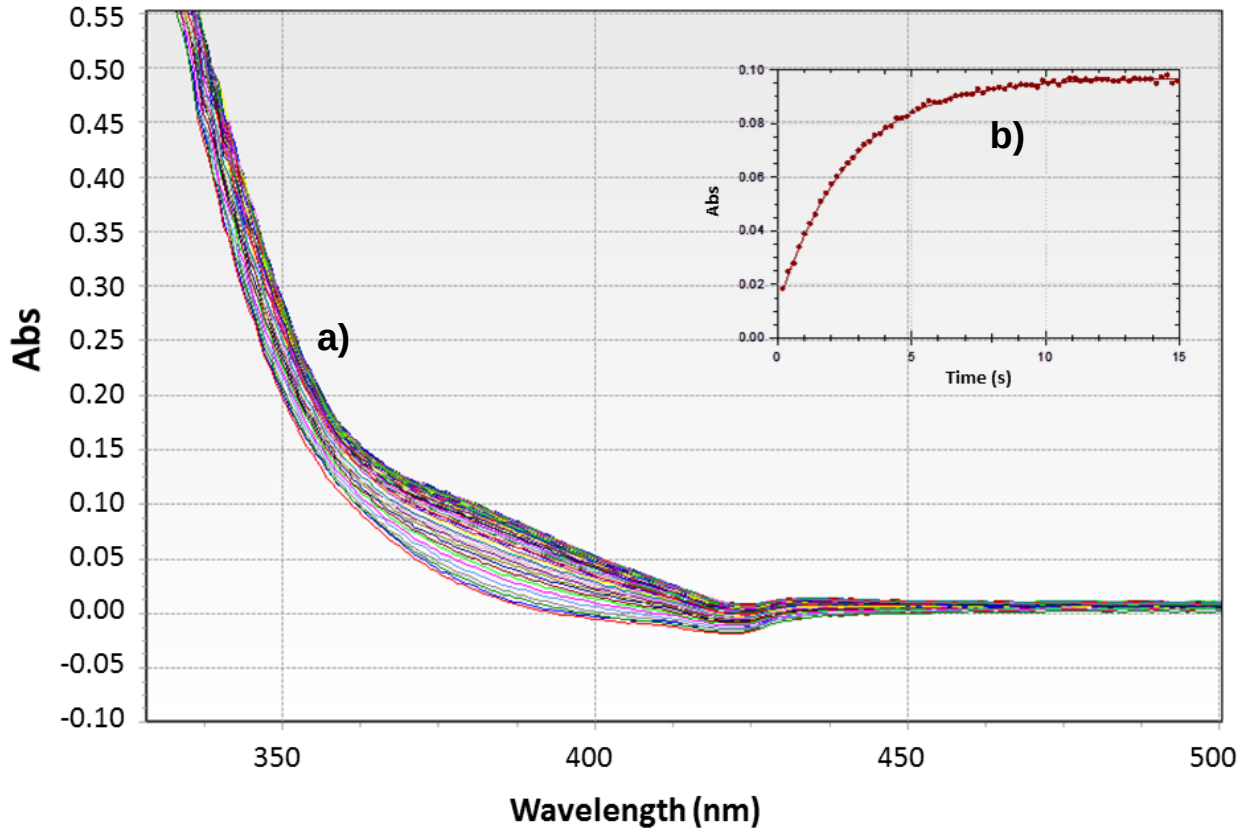

Figure 7.3: a) Absorbance spectra of $[Rh(acac)(CO)_2]$ (1.15×10^{-4} M) in the presence of $[P(otol)_3]$ (1.5×10^{-3} M). Insert (b) represents the absorbance *vs.* time trace at 380 nm which clearly shows the reaction reaching completion within ca. 10 seconds, Temp: 25 °C, DMF.

The k_{obs} values obtained from the reaction of $[Rh(acac)(CO)_2]$ with a series of concentrations for $[P(otol)_3]$ are presented in Figure 7.4 with a curvature of the data points clearly visible. The data related to the calculated k_{obs} values is summarized in Table 7.2 along with the data obtained by Ebenebe[17] for the same reaction of $[Rh(acac)(CO)_2]$ and $(P(otol)_3)$ performed in acetone.

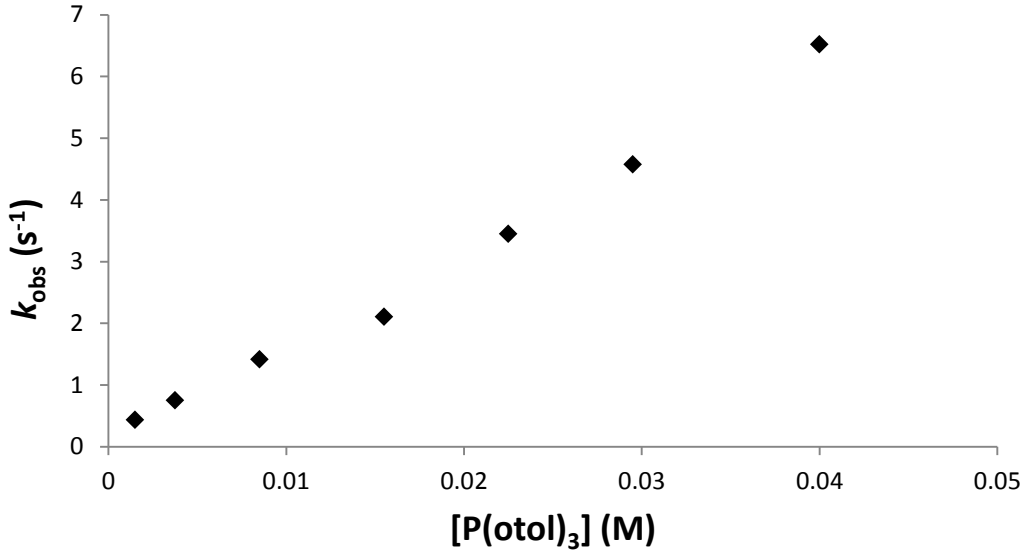

Figure 7.4: The rate constant dependence on $[P(otol)_3]$ for the carbonyl substitution in $[Rh(acac)(CO)_2]$ (1.15×10^{-4} M) at 25 °C found in DMF for this study.

Table 7.2: Observed rate constants at different concentrations of $[P(otol)_3]$ for the carbonyl substitution in $[Rh(acac)(CO)_2]$ at 25 °C found in this study as well as by the study conducted by Ebenebe[17].

This Study (DMF)		Study by Ebenebe[17] (Acetone)	
$[Rh(acac)(CO)_2]$ = 1.15 x 10^{-4} M		$[Rh(acac)(CO)_2]$ = 3.0 x 10^{-4} M	
$[P(otol)_3]$ (M)	k_{obs} (s^{-1})	$[P(otol)_3]$ (M)	k_{obs} (s^{-1})
1.50 x 10^{-3}	0.431(3)	**3.0 x 10^{-3}**	0.89(1)
3.75 x 10^{-3}	0.748(2)	**7.5 x 10^{-3}**	2.04(1)
8.50 x 10^{-3}	1.414(4)	**1.7 x 10^{-2}**	4.34(5)
1.55 x 10^{-2}	2.105(1)	**3.1 x 10^{-2}**	8.3(1)
2.25 x 10^{-2}	3.445(2)	**4.5 x 10^{-2}**	16(1)
2.95 x 10^{-2}	4.570(1)	**5.9 x 10^{-2}**	23(1)
4.00 x 10^{-2}	6.518(2)	**8.0 x 10^{-2}**	38(1)
		1.0 x 10^{-1}	48(3)

Upon critical analysis of the reaction mechanism proposed by Ebenebe[17] it was noted that the non-linear relationship found for the data was interpreted as the reaction proceeding according to *two different mechanistic pathways*. At lower concentrations of tri(o-tolyl)phosphine (0.003 M to 0.017 M) a slope (indicated in **blue** in Figure 7.5) with a zero intercept was interpreted as the reaction proceeding along a solvent assisted pathway (proceeding from species **1** to **3** and the final product **2**, see Figure 7.1). At higher phosphine concentrations the reaction was concluded to proceed *via* the direct substitution pathway (proceeding from species **1** to **2** in Figure 7.1) with a negative intercept according to a different slope (indicated in **red**) in Figure 7.5.

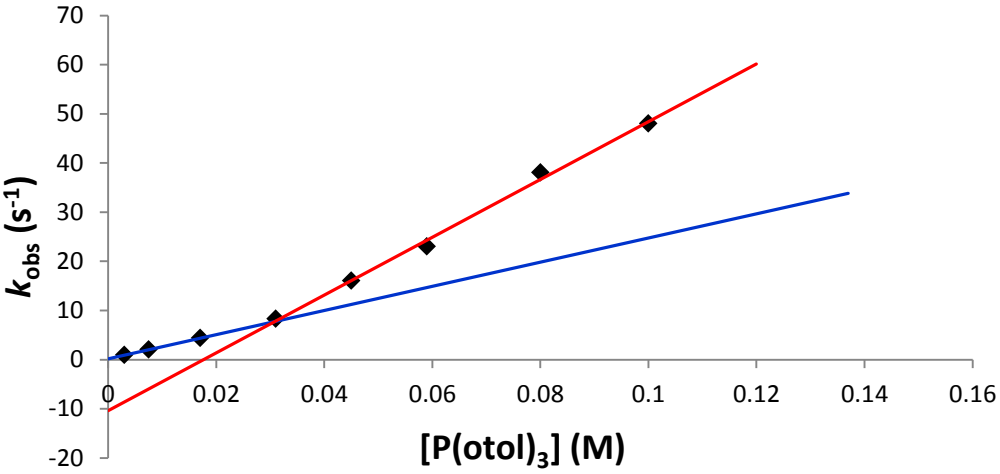

Figure 7.5: The rate constant dependence on $[P(otol)_3]$ for the carbonyl substitution in $[Rh(acac)(CO)_2]$ (3.0 x 10^{-4} M) at 25 °C reported by Ebenebe[17] in acetone. The assignment of two slopes was used to indicate the substitution reaction to occur along two different pathways as the concentration of phosphine varies.

The interpretation of two different reaction pathways concluded by Ebenebe[17] seems unlikely with a more acceptable explanation of the curvature of the data points due to the presence of an equilibrium in the reaction mechanism. In fact, experiments conducted during this PhD study clearly indicated an equilibrium present (see Section 7.6). The curvature of the data in the

observed rate constants *vs.* concentration of tri(o-tolyl)phosphine as found in this study is depicted in Figure 7.6 and suggests that the complete description of the rate constant in equation 7.1 holds for the reaction. A linear dependence on [$P(otol)_3$] would have implied the more generally encountered two-term rate law of equation 7.3.

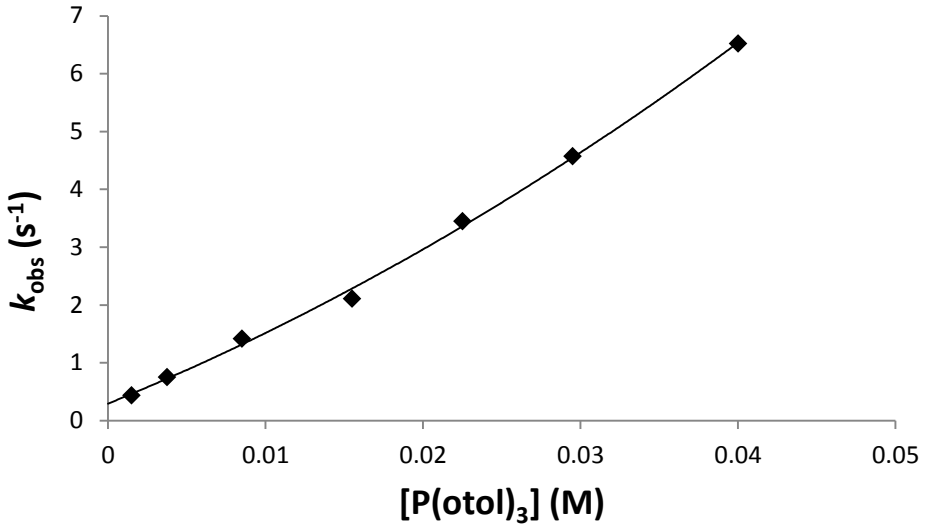

Figure 7.6: The rate constant dependence on [$P(otol)_3$] for the carbonyl substitution in [$Rh(acac)(CO)_2$] (1.15 x 10^{-4} M) found in this study fitted to a curved line, Temp= 25 °C, DMF.

A curvature fitting of the data reported by Ebenebe[17] is illustrated in Figure 7.7. In this comparison the fittings of the suggested two slopes as well as a curvature indicating the presence of an equilibrium reaction is shown. Similar examples of curved trends in k_{obs} *vs.* [ligand] plots have been seen for square planar substitutions indicating the presence of equilibrium conditions.[7,8,9]

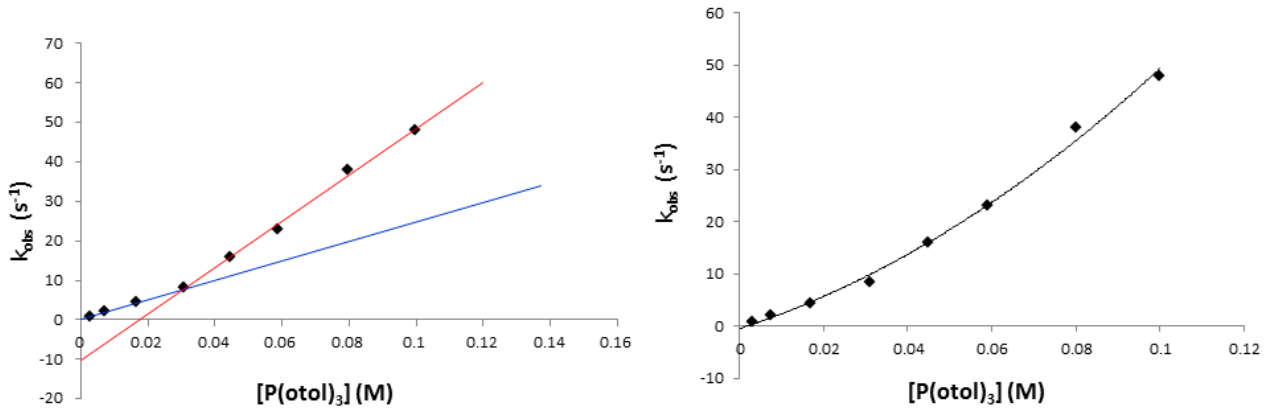

Figure 7.7: The rate constant dependence on [$P(otol)_3$] for the carbonyl substitution in [$Rh(acac)(CO)_2$] (3.0 x 10^{-4} M) found by Ebenebe[17] at 25 °C in acetone, fitted to two slopes as well as a curved line.

The curvature of the data obtained during the investigation of the substitution reaction of [$Rh(acac)(CO)_2$] and [$P(otol)_3$] led to the conclusion that an equilibrium reaction is indeed involved. Further tests were undertaken at this point to determine the equilibrium constant by appropriate experiments.

7.6 Determination of the Equilibrium Constant for the CO Substitution Reaction

To evaluate whether an equilibrium is present in the substitution reaction of [Rh(acac)$(CO)_2$] with [$P(otol)_3$], and to determine the value of the said constant, investigations by ^{31}P NMR and UV/Vis were performed that will be presented in the following sections.

7.6.1 Determination of K_{eq} by ^{31}P NMR

In order to determine whether an equilibrium exists in the substitution reaction of [Rh(acac)$(CO)_2$] and [$P(otol)_3$] ^{31}P NMR was used to evaluate the reaction. Spectra were collected for the reaction mixture of [$P(otol)_3$] (0.005 M) and three different [Rh(acac)$(CO)_2$] concentrations at 25 °C. The ^{31}P NMR spectra related to the three reaction mixtures are shown in Figure 7.8.

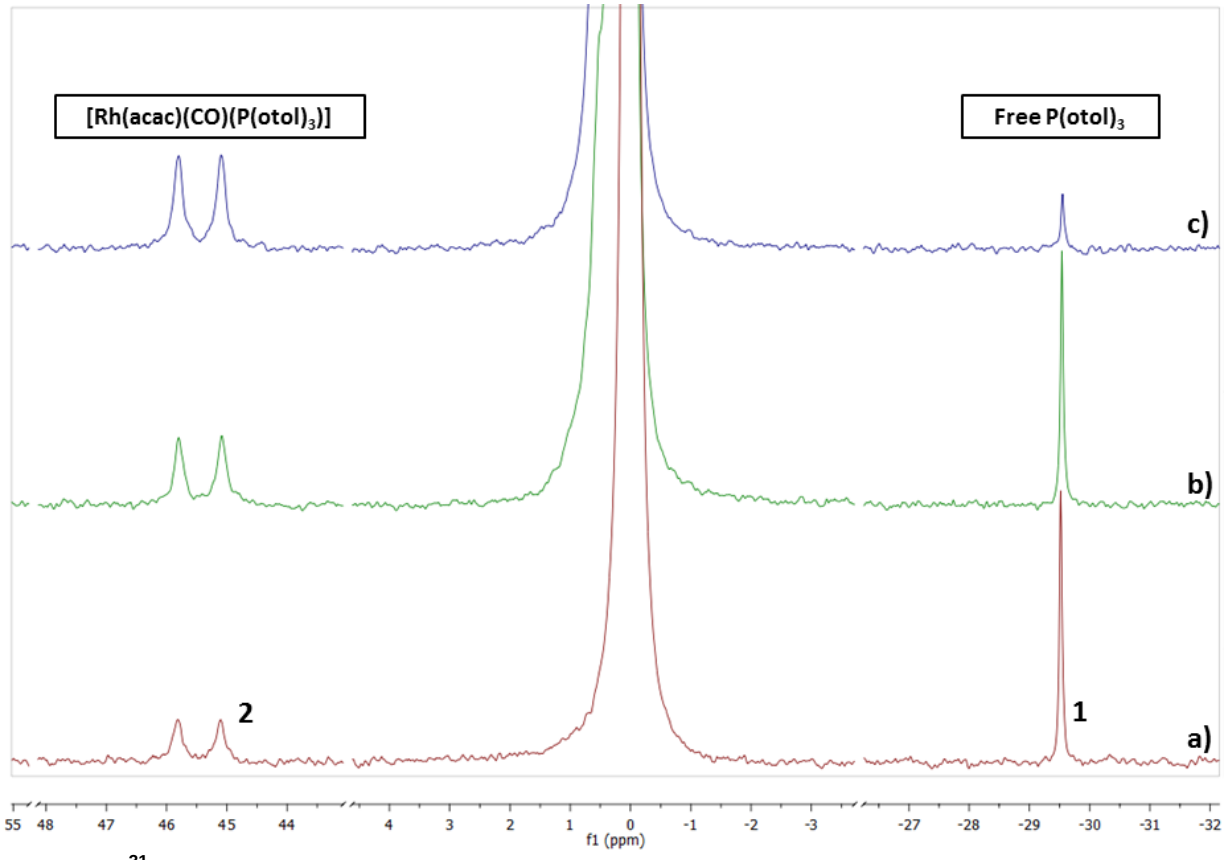

Figure 7.8: ^{31}P NMR spectra [(a)-(c)] of the reaction mixtures of [$P(otol)_3$] (0.005 M) and different concentrations of [Rh(acac)$(CO)_2$] in DMF at 25 °C. [Rh(acac)$(CO)_2$] in a) 0.005 M; b) 0.010 M and c) 0.020 M.

The ^{31}P NMR spectra showed that in each of the three experiments the reaction did not reach completion as free tri(o-tolyl)phosphine (labelled as peak **1** in Figure 7.8) was noted at -29.5 ppm in every spectrum. The peak at 45.4 ppm (labelled as peak **2**) was assigned as the substituted [Rh(acac)(CO)$(P(otol)_3$] product (typical doublet; $J_{Rh\text{-}P}$= 173.6 Hz) as confirmed in Chapter 3 (see Section 3.3.17).

The presence of the free phosphine in each spectrum indicated that an equilibrium was clearly influencing the system and the overall substitution reaction. The equilibrium equation for the substitution reaction of [Rh(acac)(CO)$_2$] and (P(otol)$_3$) is given by Eq. 7.5, where the 'eq subscripts denote the concentrations once equilibrium has been established:

$$K_{eq} = \frac{[Rh(acac)(CO)(P(\text{otol})_3)]_{eq}[CO]_{eq}}{[Rh(acac)(CO)_2]_{eq}[P(\text{otol})_3]_{eq}} \qquad \text{(Eq. 7.5)}$$

If integral values of the peak at -29.5 ppm are taken to represent the tri(o-tolyl)phosphine concentration at equilibrium and the integral of the peaks at 45.4 ppm as the concentration of [Rh(acac)(CO)(P(otol)$_3$)] at equilibrium (Figure 7.8) the concentration of the remaining species can be calculated. The integral values of the two peaks of each spectrum are expressed as a population number (sum of the populations of all peaks in each spectrum must equal 100) and is summarized in Table 7.2.

Table 7.2: Integral values of peaks 1 and 2 in Fig. 7.8 for the ^{31}P NMR spectra recorded for different [Rh(acac)(CO)$_2$] and [P(otol)$_3$] (0.005 M) at 25 °C, DMF.

Spectrum	[Rh(acac)(CO)$_2$]	Integral Peak 1	Integral Peak 2
a	0.005	49.2	50.8
b	0.010	37.5	62.5
c	0.020	8.9	91.1

As all of the values in Eq. 7.5 are known, K_{eq} may then be calculated using Eq. 7.5, see Table 7.3.

Table 7.3: Calculated experimental K_{eq} values from the ^{31}P NMR spectra (Fig. 7.8) for the reaction of different concentrations of [Rh(acac)(CO)$_2$] and [P(otol)$_3$] (0.005 M) at 25 °C, DMF.

Spectrum[b)]	[Rh(acac)(CO)$_2$] (M)	Concentrations at equilibrium (M)[a)]				K_{eq}*
		[Rh(acac)(CO)(P(otol)$_3$)]	[CO]	[P(otol)$_3$]	[Rh(acac)(CO)$_2$]	
a	0.005	0.0025	0.0025	0.0024	0.0024	1.0
b	0.010	0.0031	0.0031	0.0018	0.0069	0.8
c	0.020	0.0045	0.0045	0.0005	0.0150	3.0

* esd values on the calculated K_{eq} constants were estimated to be 10 - 20 %, no units. a) Calculated from known starting concentrations and integrals from peaks at equilibrium; b) [P(otol)$_3$]= 0.005 M.

From the experimentally determined equilibrium constants presented in Table 7.3 it can be seen that the different spectra gave similar small K_{eq} values indicating that the reaction proceeds under equilibrium conditions (see Section 7.2). The concentration of the substituted CO released into the reaction mixture can thus have a significant effect upon the reaction by inhibiting complete product formation.

In order to test whether [CO] does in fact influence the substitution reaction a second ^{31}P NMR experiment was designed in which conditions of one of the reaction mixtures with [Rh(acac)$(CO)_2$] (0.01 M) and [P(otol)$_3$] (0.005 M) was repeated but varying the [CO] at equilibrium in each spectrum. The original spectrum without any manipulation of [CO] is indicated in **red** in Figure 7.9.

CO gas was then bubbled through the reaction mixture for a period of several minutes to saturate the solution with CO thereby significantly increasing the [CO]. The resulting ^{31}P spectrum illustrated in **green** [Figure 7.9(**b**)] clearly shows that the free tri(o-tolyl)phosphine peak at -29.5 ppm has increased [to ca. double of that in (**a**)] with a simultaneous decrease in the product peak at 45.4 ppm [about half of that in (**a**)]. This clearly indicates that the concentration of CO in the reaction mixture shifted the equilibrium in favour of the unsubstituted [Rh(acac)$(CO)_2$] and [P(otol)$_3$] reactants.

In a further test, nitrogen gas was bubbled through the same saturated CO solution of [Rh(acac)$(CO)_2$] (0.01 M) and [P(otol)$_3$] (0.005 M). This was done to remove the CO gas in solution, driving the reaction to favour the [Rh(acac)(CO)(P(otol)$_3$)] complex (shifting of the equilibrium towards product formation). As can be seen by the spectrum indicated in **blue** in Figure 7.9(**c**) this indeed confirms to be the case with almost no free tri(o-tolyl)phosphine observed in solution (labeled as peak **1** at -29.4 ppm) with a substantial increase in the substituted product peak (labeled as peak **2** at 45.4 ppm) for [Rh(acac)(CO)(P(otol)$_3$].

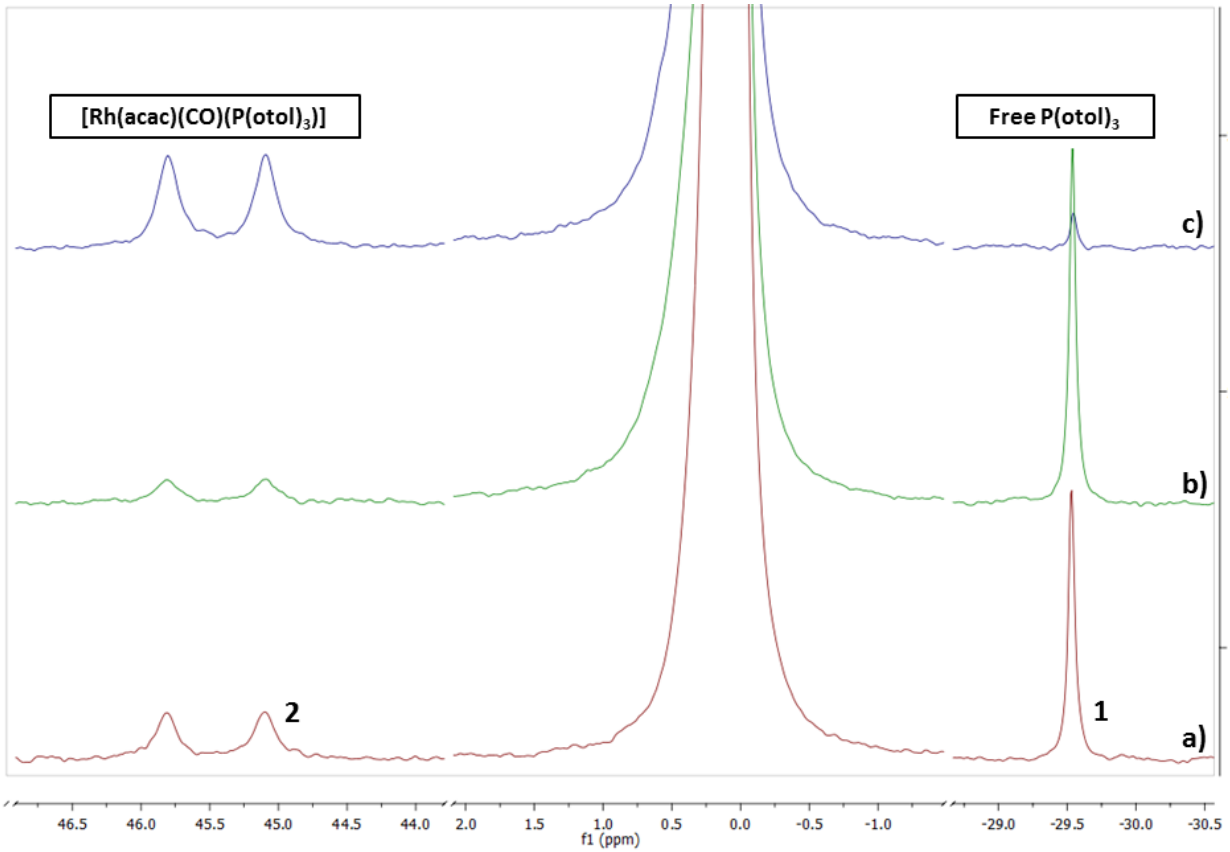

Figure 7.9: ^{31}P NMR spectra of the reaction mixtures of [Rh(acac)(CO)$_2$] (0.01 M) and [P(otol)$_3$] (0.005 M) in DMF at 25 °C under a) atmospheric conditions (red); b) a CO saturated solution (green) and c) nitrogen saturated solution (blue).

7.6.2 Determination of K_{eq} by UV/Vis

In order to confirm the experimental K_{eq} values obtained from the ^{31}P NMR spectra as discussed in Section 7.6.1 a UV/Vis experiment was designed to determine the equilibrium constant. Under these conditions the [Rh(acac)(CO)$_2$] (2.25 x 10^{-4} M) concentration was kept constant but varying the concentration of tri(o-tolyl)phosphine in DMF. The UV/Vis spectra obtained from the reaction of [Rh(acac)(CO)$_2$] and the varying concentration range of tri(o-tolyl)phosphine are represented in Figure 7.10.

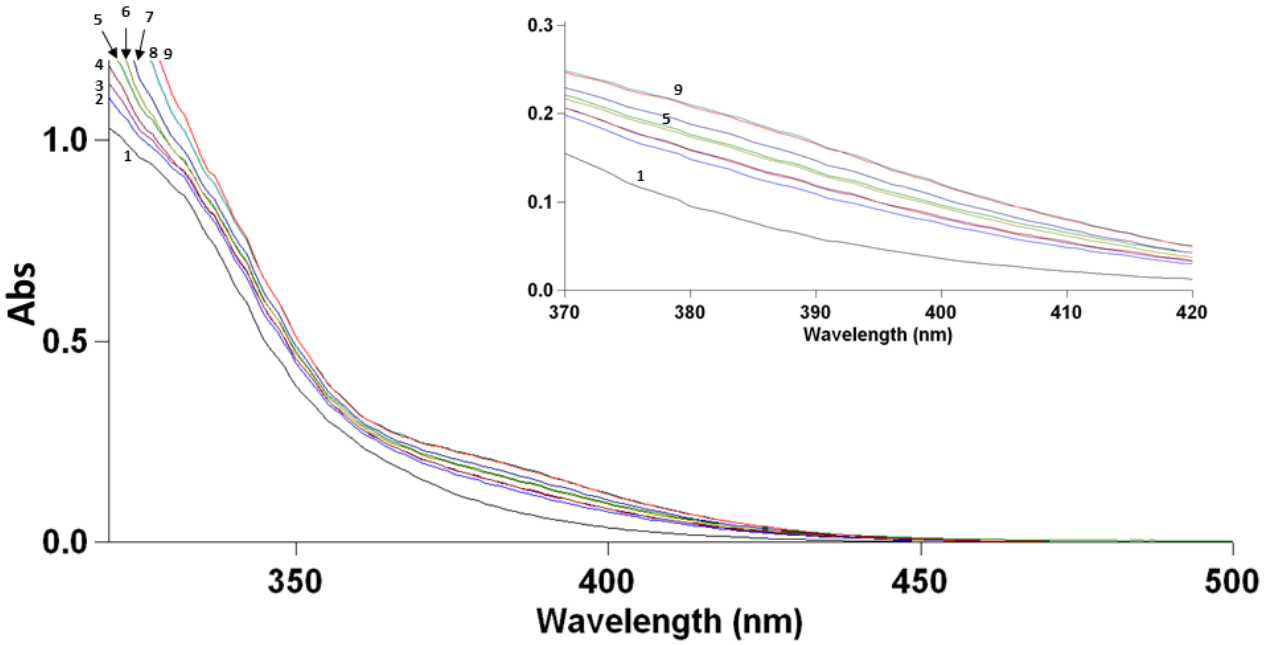

Figure 7.10: UV/Vis spectra of the reaction mixtures of [Rh(acac)(CO)$_2$] (2.5 x 10^{-4} M) and varying [P(otol)$_3$] concentrations in DMF at 25 °C, numbers denote the different [P(otol)$_3$] used as indicated in Table 7.4.

The UV/Vis spectra in Figure 7.10 yield the absorbance values at 380, 390 and 410 nm which are summarized in Table 7.4. The observed absorbance values at the three different wavelengths were then fitted to the equilibrium equation in a global fit as given below, and illustrated in Fig. 7.11, to calculate the K_{eq} value (full derivation in Appendix) with A^a_M and A^a_{ML} representing the absorbance values of the [Rh(acac)(CO)$_2$] and [Rh(acac)(CO)(P(otol)$_3$)] complexes, A^a_{obs} (a= different wavelengths) the observed absorbance and $[CO]_{eq}$ and $[P(otol)_3]_{eq}$ the [CO] and [P(otol)$_3$] at equilibrium:

$$A^a_{obs} = \frac{A^a_M[CO]_{eq} + A^a_{ML}K_{eq}[P(\text{otol})_3]_{eq}}{[CO]_{eq} + K_{eq}[P(\text{otol})_3]_{eq}} \qquad \text{(Eq. 7.5)}$$

Table 7.4: Recorded absorbance values at equilibrium and different wavelengths for the UV/Vis study of [Rh(acac)(CO)$_2$] (2.5 x 10^{-4} M) and varying [P(otol)$_3$] concentrations in DMF at 25 °C.

	[P(otol)$_3$] (M)	Abs (λ= 380 nm)	Abs (λ= 390 nm)	Abs (λ= 410 nm)
1	0	0.095	0.059	0.021
2	2.5 x 10^{-4}	0.148	0.109	0.048
3	3.5 x 10^{-4}	0.158	0.117	0.053
4	4.5 x 10^{-4}	0.159	0.118	0.055
5	6.0 x 10^{-4}	0.176	0.135	0.065
6	8.0 x 10^{-4}	0.173	0.133	0.061
7	1.0 x 10^{-3}	0.188	0.147	0.069
8	1.5 x 10^{-3}	0.208	0.165	0.079
9	2.0 x 10^{-3}	0.209	0.166	0.081

The fitted absorbance *vs.* [P(otol)$_3$] plots are given in Figure 7.11 and an experimental K_{eq} value of 1.0(4) was determined. This experimentally determined K_{eq} value by UV/Vis techniques is in good agreement with those values calculated in Section 7.6.1 by the ^{31}P NMR spectra results (Table 7.3) that were typically close to unity.

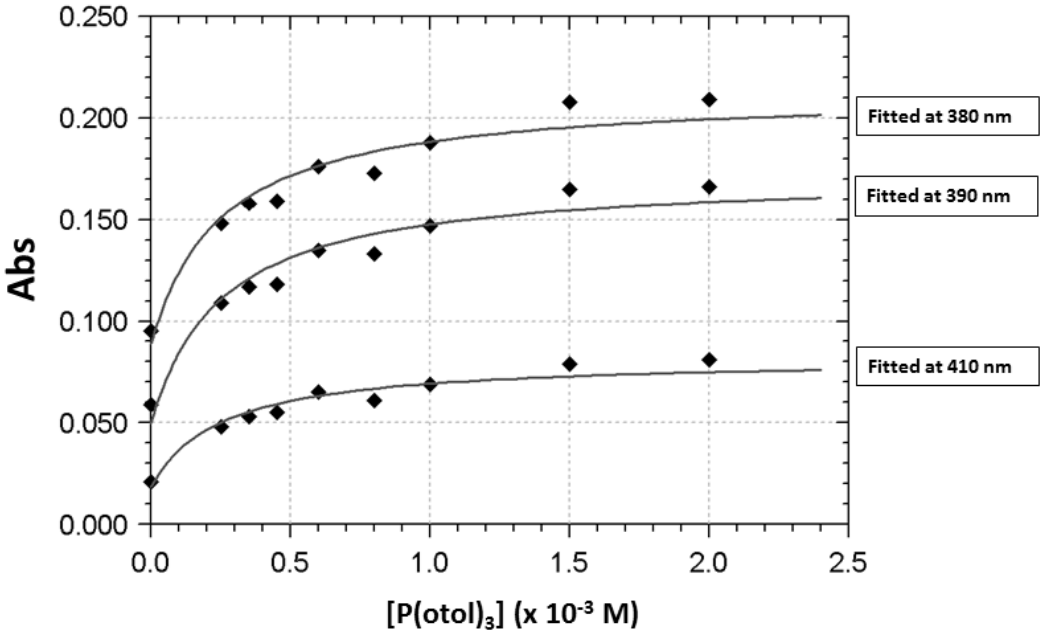

Figure 7.11: Global fit (see Appendix) with simulated (solid lines) plots of the A^{a}_{obs} *vs.* [P(otol)$_3$] according to Eq. 7.5 with experimental data (♦) fitted to the same equation at a= 380, 390 and 410 nm, respectively.

To confirm the ^{31}P NMR results with respect to the manipulation of the equilibrium by varied [CO] for the substitution reaction, an additional UV/Vis experiment was conducted. The UV/Vis spectrum of solutions of [Rh(acac)(CO)$_2$] (2.5 x 10^{-4} M) and [P(otol)$_3$] (2.5 x 10^{-4} M) before mixing was recorded and is represented in Figure 7.12 as spectrum **1**. The solutions were then mixed and the resulting UV/Vis spectrum labeled as **2** was obtained with a significant increase in absorbance observed. CO gas was then bubbled through the reaction mixture for several minutes and the UV/Vis spectrum (spectrum **3**) showed a return to the virtually original before mixing state of spectrum **1**. This indicated that the equilibrium had been shifted back to the original reactants of [Rh(acac)(CO)$_2$] and [P(otol)$_3$] by the addition of CO gas. Nitrogen gas was then bubbled through the same reaction mixture expelling the CO gas and resulted in the UV/Vis spectrum labeled as **4**. In this case, the absence of CO shifted the equilibrium towards the substituted product, [Rh(acac)(CO)(P(otol)$_3$)] with a similar spectrum as that of spectrum **2** (product formation favoured).

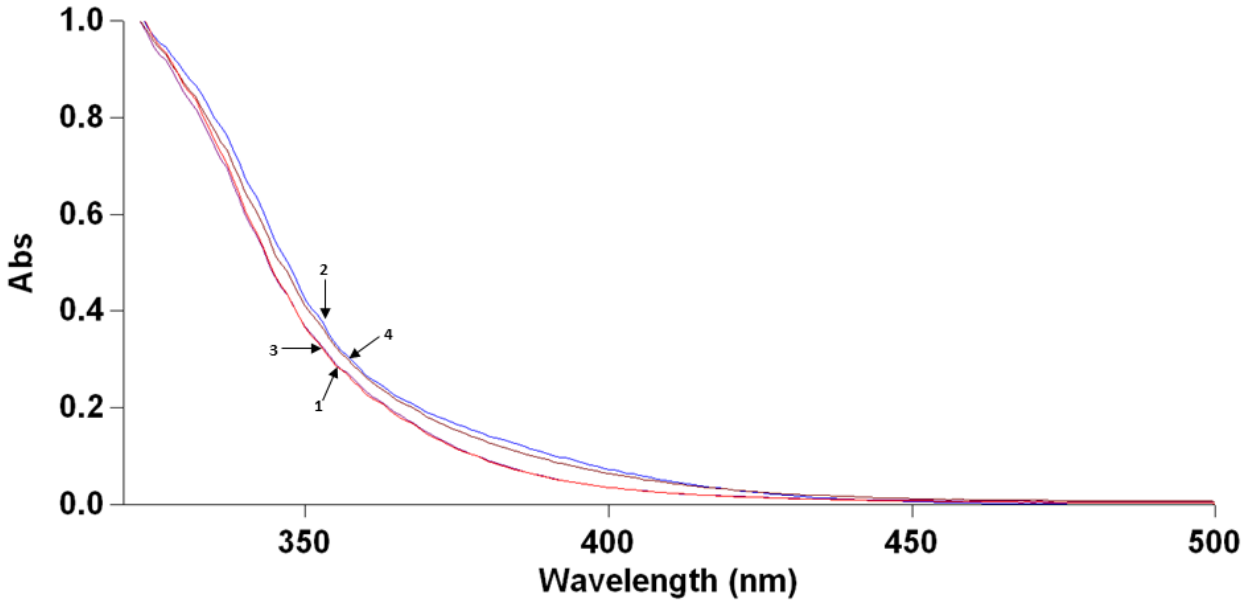

Figure 7.12: UV/Vis spectra of the reaction mixtures of [Rh(acac)(CO)$_2$] (2.5 x 10^{-4} M) and [P(otol)$_3$] (2.5 x 10^{-4} M) in DMF at 25 °C before mixing (1), mixed (2), in the presence of CO (3) and the presence of nitrogen (4) state.

7.6.3 Concluding Remarks on the Equilibrium Studies

It was shown in Sections 7.6.1 and 7.6.2 through ^{31}P NMR and UV/Vis experiments that an equilibrium is involved in the substitution reaction of [Rh(acac)(CO)$_2$] and [P(otol)$_3$] (small K_{eq} constant). This implies that the straightforward mechanistic assumption of an associative mechanism for the substitution reaction proceeding *via* a simple two-term rate law (Eq. 7.3) as interpreted by Ebenebe[17] is incorrect and that the complex rate law as presented in Eq. 7.1 actually holds. The data reported by Ebenebe[17] as well as the work presented here indicates a far more complex reaction mechanism involving equilibrium steps that was not included in detail as part of this PhD study. However, as discussed in detail in the following Section 7.7, the profile of the k_{obs} *vs.* [P(otol)$_3$] plots for the systems examined by Ebenebe[17] has fairly dominating direct pathways (k_{12} step in scheme 7.1), as defined by the slopes of the corresponding relationships, with the equilibria primarily contributing to the intercept values of the profiles. This enabled the fairly accurate estimation of the second-order rate constants k_{12} from the corresponding first-order constants as reported by Ebenebe[17]. These values are listed in Table 7.5.

7.7 Further Analysis of Second-order Rate Constants

Although the kinetic investigations into the substitution reaction of [Rh(acac)(CO)$_2$] and [P(otol)$_3$] indicated that a far more in-depth investigation is needed to evaluate the true mechanism by which the reaction proceeds valuable data may still be gained from the work conducted by Ebenebe[17].

For the comparison in this study of the reactivity of different [Rh(β-diketonato)$(CO)_2$] complexes, the reported k_{obs} values reported here as well as by Ebenebe[17] may still offer some value as a parameter by which to evaluate the electronic environment experienced by the rhodium(I) centre. The calculation of second-order rate constants can be useful in providing such a measure of reactivity.

Second-order rate constants (k_{12}) are used to describe the direct pathway of substitution related to the reaction of [Rh(acac)$(CO)_2$] and ($P(otol)_3$) that is mainly dependent on only the nature of the entering ligand (see Figure 7.1 and Eq. 7.3).

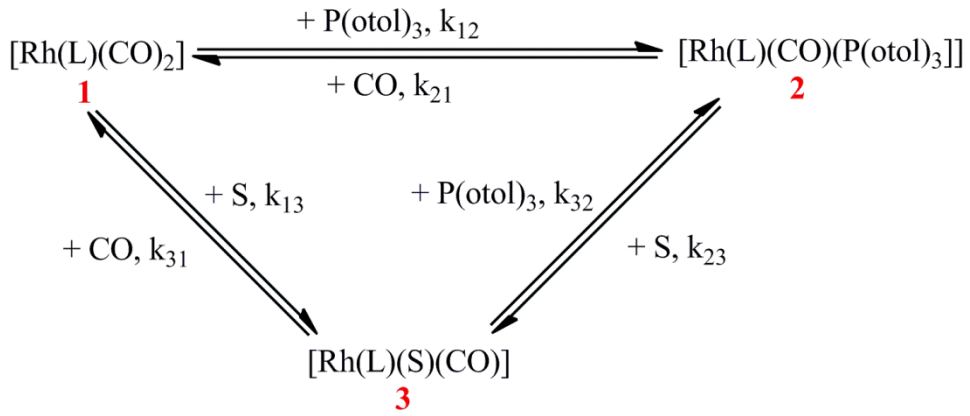

Figure 7.1: Schematic representation of a square planar substitution reaction with parallel direct substitution and solvent assisted pathways. The species are numbered in the following manner: [Rh(L)$(CO)_2$] = 1; [Rh(L)(CO)$(P(otol)_3)$] = 2; [Rh(L)(S)(CO)] = 3. The subscripts of the rate constants denote the numbers of the species involved during the specific reaction, e.g. k_{12} describes the rate constant for the substitution reaction of complex 1 to 2. Solvent concentrations have been incorporated in the rate constants k_{13} and k_{23}.

$$k_{obs} = k_{12}[P(\text{otol})_3] + k_{13} \qquad \text{(Eq. 7.3)}$$

As the solvent pathway is neglible in this case the k_{13} term is eliminated from equation 7.3 and the equation can be simplified. For a range of different rhodium(I) complexes with different coordinating β-diketonato ligands these second-order rate constants can thus be calculated using the following equation:

$$k_{12} = \frac{k_{obs}}{[P(\text{otol})_3]} \qquad \text{(Eq. 7.6)}$$

The calculated second-order rate constants from the work conducted by Ebenebe[17] can thus be used as a parameter by which to compare the reactivity of the rhodium(I) complexes containing different coordinating β-diketonato ligands. The second-order rate constants are summarized in Table 7.5 with the β-diketonato ligands coordinated in each rhodium(I) complex illustrated in Figure 7.13 along with their abbreviations.

Table 7.5: Approximated second-order rate constants for the carbonyl substitution in [Rh(β-diketonato)$(CO)_2$] complexes by tri(o-tolyl)phosphine at 25 °C reported by Ebenebe[17].

Complex	pK_a free ligand	[$P(otol)_3$] (M)	k_{obs} (s^{-1})	k_{12} ($M^{-1}.s^{-1}$) (Eq.7.6)
[Rh(dipiv)$(CO)_2$]	11.77	0.003	0.61(4)	2.0(1) x 10^2
[Rh(acac)$(CO)_2$]	8.95	0.003	0.89(1)	2.97(3) x 10^2
[Rh(dbm)$(CO)_2$]	9.35	0.003	2.49(4)	8.3(1) x 10^2
[Rh(tfac)$(CO)_2$]	6.30	0.003	49.2(9)	1.6(3) x 10^4
[Rh(F_3-bzac)$(CO)_2$]	6.30	0.003	123.6(1)	4.12(5) x 10^4
[Rh(hfac)$(CO)_2$]	4.43	0.0006	238.3(4)	3.97(7) x 10^5

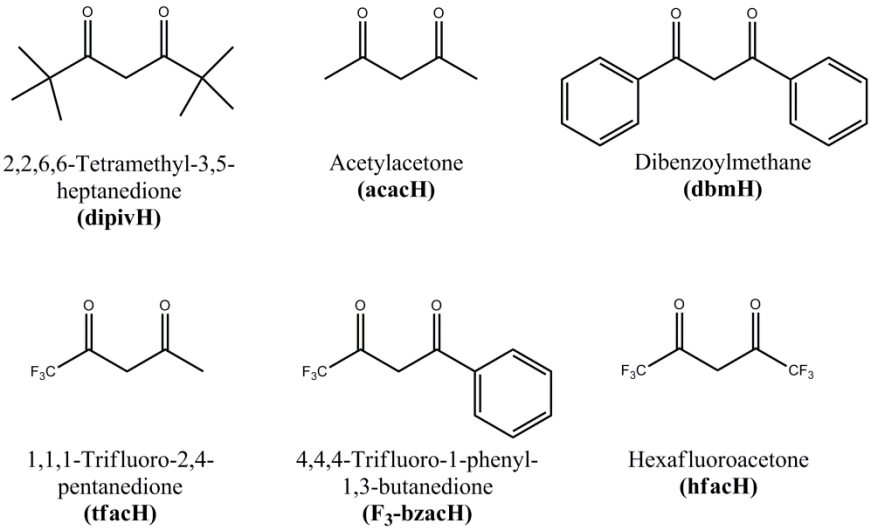

Figure 7.13: The different coordinating β-diketonato ligands and their abbreviations used in the rhodium(I) complexes of which second-order rate constants are reported in the substitution reaction of [Rh(β-diketonato)$(CO)_2$] and ($P(otol)_3$) in Table 7.5.

Interesting to note from the data presented in Table 7.5 is the increase in second-order rate constant (k_{12}) that is associated with a decrease of pK_a in the free uncoordinated β-diketone ligands. This relationship between the k_{12} constants and pK_a of the uncoordinated β-diketone ligands is illustrated in Figure 7.14.

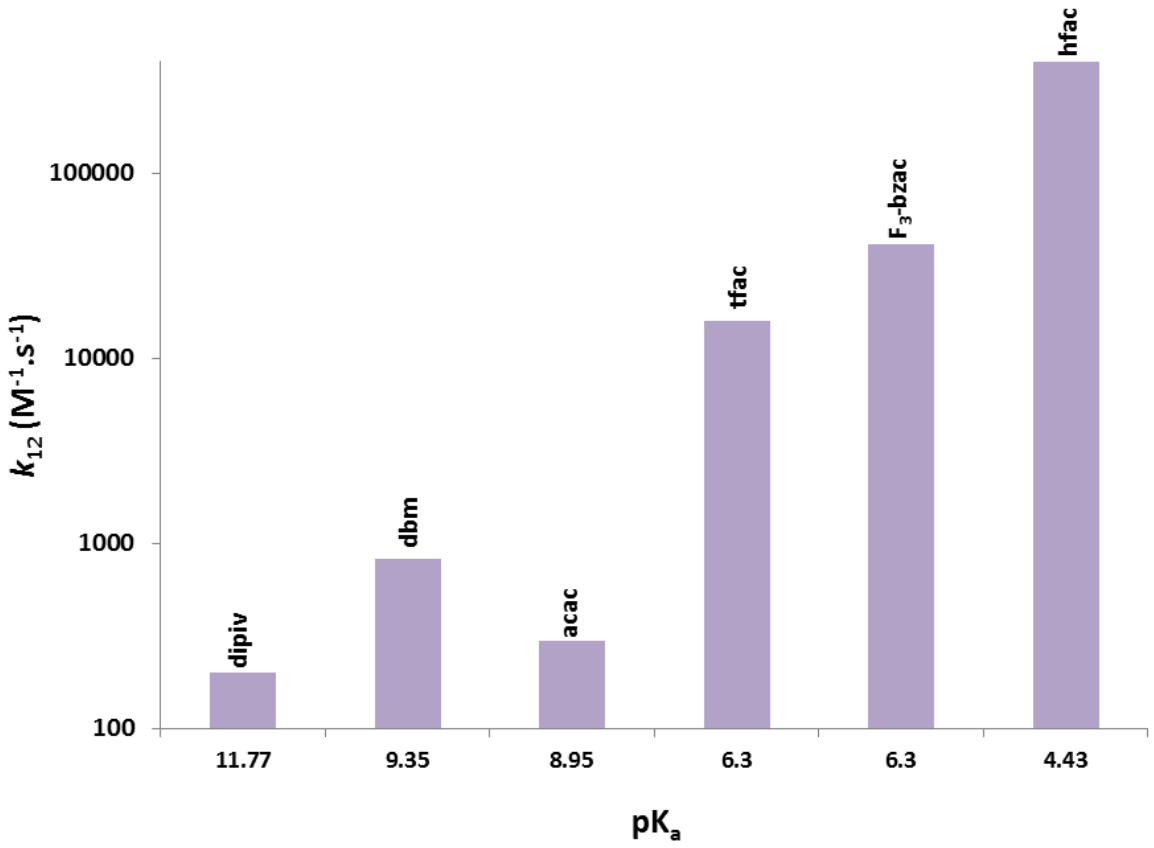

Figure 7.14: Second-order rate constants (k_{12}; seeTable 7.5) *vs.* pK_a of the uncoordinated β-diketone ligands in the substitution reaction of [Rh(β-diketonato)$(CO)_2$] and ($P(otol)_3$).

From Table 7.5 and Figure 7.14 it can be seen that the free ligand pK_a of 11.77 for the uncoordinated β-diketone ligand (dipivH) displayed the slowest rates of substitution with k_{12}= 2.0(1) x 10^2 $M^{-1}.s^{-1}$ for the coordinated complex, [Rh(dipiv)$(CO)_2$]. This is in contrast with the low pK_a of the free ligand, hfacH in [Rh(hfac)$(CO)_2$] (4.43) that resulted in the fastest substitution rate with a second-order rate constant of 3.97(7) x 10^5 $M^{-1}.s^{-1}$.

Table 7.5 also clearly shows how the seven order-of-magnitude increase in Bronsted basicity of the bidentate ligands manifests itself in a significant more than three order-of-magnitude in substitution reactivity decrease at the rhodium(I) centre (k_{12} values).

It was also noted that the rhodium(I) complexes containing electron withdrawing moieties in the coordinating β-diketonato ligands such as the trifluoro substituents in [Rh(tfac)$(CO)_2$], [Rh(F_3-bzac)$CO)_2$] and [Rh(hfac)$(CO)_2$] yielded the fastest rates. This trend suggests that by altering the substituents of the coordinating β-diketonato ligands in the rhodium(I) complexes and decreasing the electron density at the rhodium(I) centre, faster substitutions will occur. In contrast, as electron density is increased around the rhodium(I) centre by electron donating substituents in the coordinating β-diketonato ligands as found in the [Rh(acac)$(CO)_2$] k_{12}= 2.97(3) x 10^{-2} $M^{-1}.s^{-1}$) and [Rh(dipiv)$(CO)_2$] (k_{12}= 2.0(1) x 10^{-2} $M^{-1}.s^{-1}$) complexes, the substitution rates will decrease significantly in comparison to [Rh(hfac)$(CO)_2$] (k_{12}= 3.97(7) x 10^5 $M^{-1}.s^{-1}$).

7.8 Conclusion

In this chapter a preliminary kinetic investigation of a square planar substitution reaction in [Rh(acac)$(CO)_2$] by the bulky phosphine ligand P$(otol)_3$ was correlated with literature data and was expanded further upon. It was shown how a seemingly simple square planar substitution reaction can present numerous difficulties in order to correctly describe the reaction mechanism, with this investigation illustrating how significantly an equilibrium in the process can influence the reactivity profiles. The kinetic study conducted by Ebenebe[17] on the square planar substitution reactions of [Rh(β-diketonato)$(CO)_2$] complexes with (P$(otol)_3$) was interpreted as occurring *via* two different reaction pathways. In this study these conclusions were shown to be incorrect with the reaction rather occurring under equilibrium conditions, and significantly influenced by the concentration of the leaving CO ligand (small K_{eq} values).

In order to further correctly evaluate the reaction mechanism of the substitution reaction of [Rh(β-diketonato)$(CO)_2$] complexes with tri(o-tolyl)phosphine, extensive kinetic studies will have to be conducted which was not considered formally a part of this PhD study.

However, second-order rate constants were calculated from the k_{obs} values determined by Ebenebe[17] in the substitution reaction of different [Rh(β-diketonato)$(CO)_2$] complexes with (P$(otol)_3$). This provided a means by which to evaluate the electronic nature of the different rhodium(I) complexes which is one of the aims of this study.

These second-order rate constants showed that electron withdrawing substituents present on the coordinating β-diketonato ligand resulted in an increase in substitution rates, as expected to be favored during nucleophilic attack by an entering tertiary phosphine ligand. This coincided with a decrease in pK_a of the free uncoordinated β-diketone ligands with hfacH having the lowest pK_a and fastest substitution rates (see Table 7.5, Figure 7.14). Electron donating substituents on the coordinating β-diketonato ligands with higher pK_a values had slower substitution rates associated with the coordinated rhodium(I) complexes.

It is hoped that the correlation between pK_a and the reactivity of the rhodium(I) complexes will be further extended to some of the characteristics that were displayed in the solid-state structures of the rhodium(I) complexes (Chapters 4, 5 and 6). The correlations between all of the different parameters used to analyze the rhodium(I) complexes in this study will be presented in Chapter 8.

Chapter 8: Comparison of Different Solution and Solid-state Properties of [Rh(*O,O'*-Bid)$(CO)_2$] Complexes

8.1 Introduction

The aims as set out in Chapter 1 of this study is concerned with the design and assembly of nano-wired materials *via* the use of metallophilic interactions between metal centres along one-dimensional metal chains. The choice of rhodium as the central focus of the study was motivated by its vast applications in catalysis.[1,2,3] It was anticipated that the introduction of different steric and electronic changes to the metal centre could provide a better insight into the formation of these metallophilic interactions and the forces that govern the assembly of molecules into one-dimensional metal chains in the solid-state. These changes on the metal centre were brought about by using different coordinating β-diketonato ligands with electron withdrawing/ donating or sterically bulky substituents.

In addition to the solid-state study of the effects that the changes in coordinating ligands could have in the resulting rhodium(I) complexes, a preliminary study with regard to the reactivity of the metal centre was undertaken. This involved the investigation of the substitution reaction of one of the carbonyl moieties by a phosphine entering ligand. The kinetic study provided a link between the different coordinating ligands and the reactivity of the metal centre towards substitution reactions that would hopefully also manifest in the changes observed in the solid-state structures of the rhodium(I) complexes and the resulting one-dimensional metal chains.

In this chapter, it is anticipated to bring together all of the information gathered from the solution and solid-state evaluations conducted during the study to present some of the observations and correlations that were noted between the different rhodium(I) complexes. The subsections to follow will systematically present the correlations drawn between the different properties of the complexes as electronic and steric changes were introduced on the rhodium(I) centre. The

[1] Dickson, R., *Homogeneous Catalysis with Compounds of Rhodium and Iridium*, D. Reidel Puclishing Company, Dordrecht, The Netherlands, **1985**.
[2] Evans, P. A., *Modern Rhodium-Catalyzed Organic Reactions*, Wiley-VCH, Weinheim, Germany, **2005**, 2.
[3] Van Leeuwen, P. W. N. M., *Homogeneous Catalysis: Understanding the Art*, Kluwer Academic Publishers, Dordrecht, The Netherlands, **2004**, 139.

different coordinated β-diketonato ligands of the rhodium(I) complexes involved in the comparisons to be discussed in this chapter are represented in Figure 8.1 along with their short identification code that will be used throughout the subsections to follow.

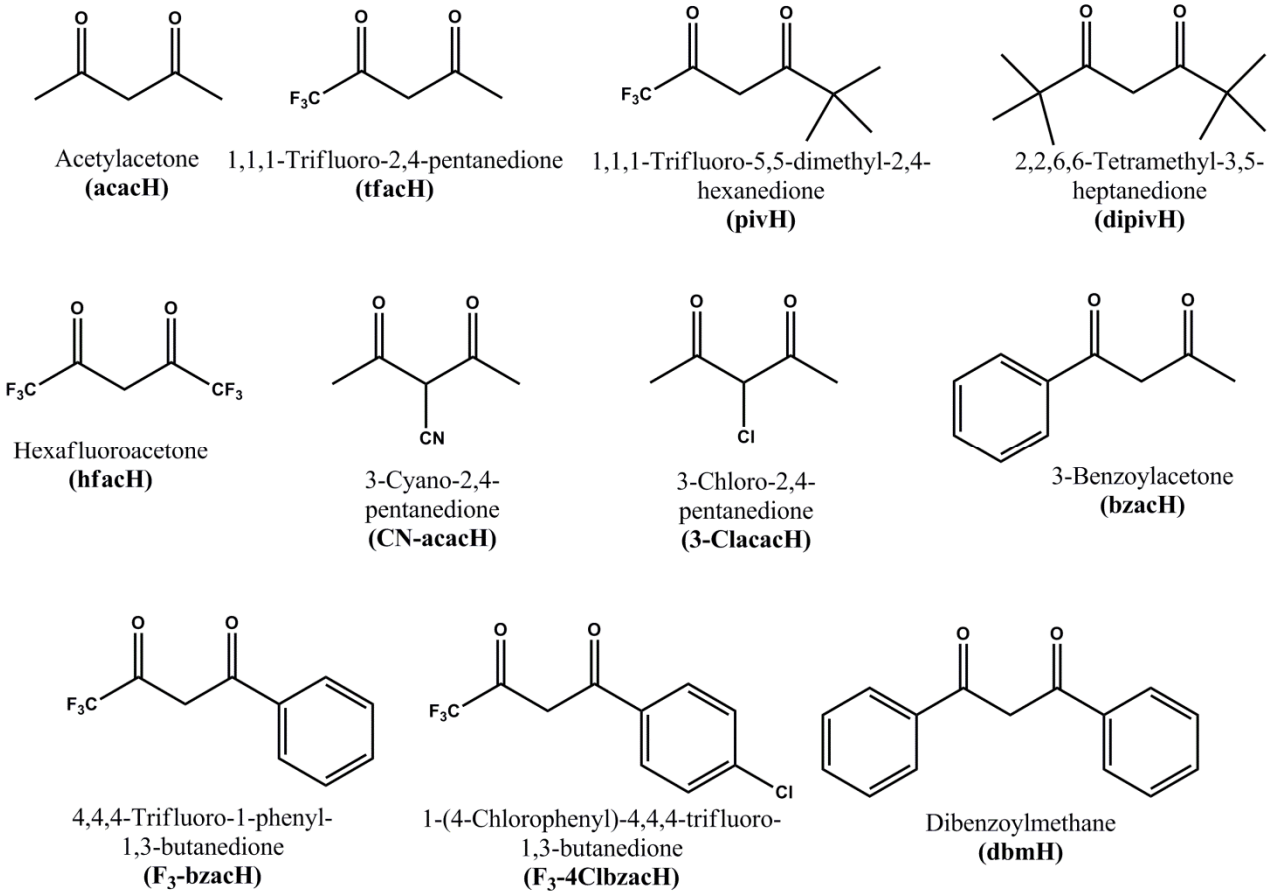

Figure 8.1: Representation of the different β-diketone ligands coordinated to rhodium(I) used for comparison in this chapter.

8.2 Correlations

8.2.1 Relationship Between the Bronsted pK_a Values of the Free Ligands and the ^{103}Rh Chemical Shift of the Coordinated Complexes

As was presented in Chapter 3 (Section 3.4) an approximate link was noted between the pK_a values of the free ligands and the ^{103}Rh chemical shifts reported for the different coordinated rhodium(I) complexes. The pK_a values of the free ligands along with the corresponding ^{103}Rh chemical shifts of the rhodium(I) complexes are given in Table 8.1. A graphical representation of the above data is listed in Figure 8.2 with a decrease in chemical shift clearly visible as the pK_a value increases for the different coordinating β-diketone ligands.

Table 8.1: pK_a values of the free ligands and the reported ^{103}Rh chemical shifts (Chapter 3) of the coordinated rhodium(I) complexes.

Complex	pK_a of the free ligand	^{103}Rh chemical shift (ppm)
$[Rh(hfac)(CO)_2]$	4.30[4]	357.5
$[Rh(tfac)(CO)_2]$	6.30[4]	319.2
$[Rh(F_3\text{-bzac})(CO)_2]$	6.30[4]	320.4
$[Rh(3Cl\text{-acac})(CO)_2]$	6.77[5]	297.7
$[Rh(piv)(CO)_2]$	6.99[6]	306.8
$[Rh(F_3\text{-4Clbzac})(CO)_2]$	7.55[7]	325.1
$[Rh(pyruv)(CO)_2]$	8.35[8]	311.1
$[Rh(bzac)(CO)_2]$	8.70[9]	284.0
$[Rh(acac)(CO)_2]$	8.95[4]	284.2
$[Rh(dbm)(CO)_2]$	9.35[4]	292.2
$[Rh(dipiv)(CO)_2]$	11.77[4]	270.2

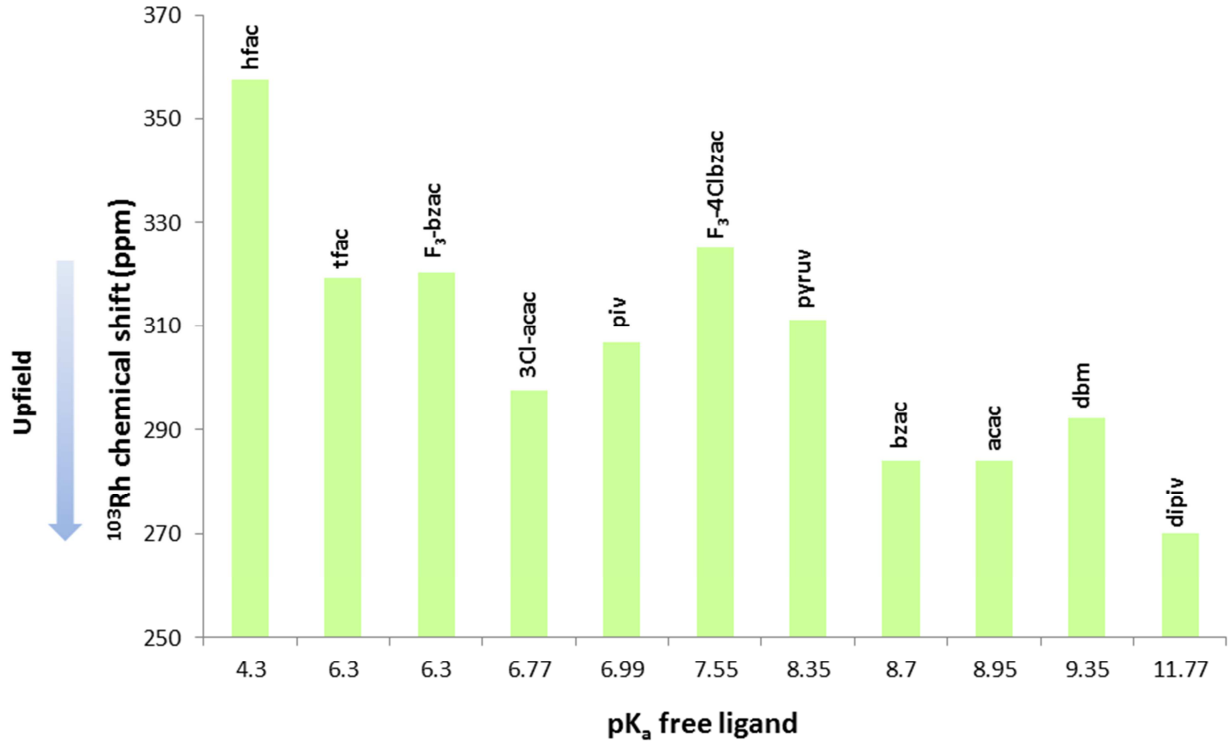

Figure 8.2: Schematic representation of the relationship between the pK_a values of the free β-diketone ligands and the reported ^{103}Rh chemical shifts of the coordinated complexes.

NMR chemical shifts can provide valuable information on the electronic environment experienced by the nuclei under investigation. For example, in ^{103}Rh NMR analysis, as electron density is increased around the rhodium(I) centre the shielding experienced by the rhodium nucleus will increase. As the shielding is increased, the chemical shift will move upfield (become lower).

[4] Ebenebe, P., *MSc Dissertation*, University of the Free State, Bloemfontein, South Africa, **1998**, 121.
[5] 3-Chloro-2,4-pentanedione (CAS: 1694-29-7), http://www.scbt.com/datasheet-251987-3-chloro-2-4-pentanedione.html, accessed: 26-05-15 (Calculated pK_a value).
[6] Canada-Vilalta, C., Huffman, J. C., Christou, G., *Polyhedron*, **2001**, 1785-1793.
[7] 1-(4-Chlorophenyl)-4,4,4-trifluorobutane-1,3-dione (CAS: 18931-60-7), http://en.chembase.cn/molecule-34967.html, accessed: 26-05-15 (Calculated pK_a value).
[8] Methyl-2,4-dioxopentanoate (CAS: 20577-61-1), http://en.chembase.cn/molecule-54218.html, accessed: 26-05-15 (Calculated pK_a value).
[9] Watarai, H., Takahashi, I., *Anal. Commun.*, **1998**, *38*, 289-292.

Investigating the ^{103}Rh chemical shifts of the different coordinated rhodium(I) complexes can thus provide information on the electron density present at the rhodium(I) centre. The different electron withdrawing or donating substituents on the coordinating β-diketonato ligands should effect the chemical shifts which can be related to the electronic environment around the rhodium(I) centre.

For example, in the case of [Rh(acac)$(CO)_2$] (δ= 284.2 ppm, Table 8.1) the methyl substituents are slightly electron donating[10] towards the metal centre as opposed to [Rh(tfac)$(CO)_2$] (δ= 319.2 ppm) with a trifluoro substituent exerting a highly electron withdrawing effect on the rhodium(I) centre. As electron density is removed from the rhodium(I) centre by the trifluoro substituent of the coordinating β-diketonato ligand, the rhodium(I) nucleus becomes less shielded. The less shielded rhodium(I) centre will result in a higher chemical shift as is observed for [Rh(tfac)$(CO)_2$] (δ= 319.2 ppm).

This effect was also observed between the [Rh(bzac)$(CO)_2$] (δ= 284.0 ppm) and [Rh(F_3-bzac)$(CO)_2$] (δ= 320.4 ppm) complexes. Both rhodium(I) complexes contain a phenyl substituent which is considered slightly electron withdrawing[11]. However, the [Rh(F_3-bzac)$(CO)_2$] complex contains an additional trifluoro electron withdrawing moiety as opposed to the slightly electron donating methyl substituent present in [Rh(bzac)$(CO)_2$]. The less electron density at the metal centre found in [Rh(F_3-bzac)$(CO)_2$] due to this electron withdrawing trifluoro group results in deshielding of the rhodium(I) nucleus and a larger chemical shift of 320.4 ppm.

A general correlation was noted in Figure 8.2 between the pK_a values of the uncoordinated β-diketone ligands and the ^{103}Rh chemical shifts of the coordinated rhodium(I) complexes. It was noted that ligands associated with high pK_a values had lower ^{103}Rh chemical shifts. [Rh(dipiv)$(CO)_2$] for example has a pK_a of 11.77 for the uncoordinated dipivH ligand and a ^{103}Rh chemical shift of 270.2 ppm. This is in contrast with lower pK_a values like that associated with hfacH (4.3) that had a higher ^{103}Rh chemical shift of 357.5 ppm in the coordinated [Rh(hfac)$(CO)_2$] complex.

Another observation that was made with regards to the electron withdrawing effects of the substituent groups on the electronic environment at the rhodium(I) centre relates to the chemical shift changes between [Rh(acac)$(CO)_2$] (δ= 284.2 ppm) and [Rh(3Cl-acac)$(CO)_2$] (δ= 297.7 ppm). In this case an electron withdrawing chlorine atom is located on the methine carbon position of the coordinating β-diketonato ligand as opposed to the hydrogen atom found in [Rh(acac)$(CO)_2$].

[10] Wermuth, C. G., *The Practice of Medicinal Chemistry*, Academic Press, San Diego, United States of America, **2008**, 435.
[11] Macomber, R. S., *Organic Chemistry*, University Science Books, Sausalita, United States of America, **1996**, 276.

The electron withdrawing group is separated three atoms away from the rhodium(I) centre in contrast to the two atoms separating the substituent from the rhodium(I) centre in [Rh(tfac)$(CO)_2$]. This would suggest that the electron withdrawing effect of the chlorine atom could be slightly less pronounced than for the previous examples. This agrees with the smaller increase in chemical shift that was observed for [Rh(3Cl-acac)$(CO)_2$] (δ= 297.7 ppm) as opposed to the large change for [Rh(tfac)$(CO)_2$] (δ= 319.2 ppm).

It would seem from Figure 8.2 as if the steric differences of the coordinating β-diketonato ligands had little effect on the ^{103}Rh chemical shift values. [Rh(acac)$CO)_2$] (δ= 284.2 ppm) and [Rh(bzac)$(CO)_2$] (δ= 284.0 ppm) have very similar chemical shifts even though the [Rh(bzac)$(CO)_2$] complex offers potentially significant steric bulk by the introduction of a phenyl substituent to the coordinating β-diketonato ligand. This reaffirms the initial statement that ^{103}Rh NMR can indeed be used as an effective tool to analyze the electronic environment experienced by the nucleus without the interference of a significant steric parameter.

8.2.2 Relationship Between the Bronsted pK_a Values of the Free Ligands and the Second-order Rate Constants in Substitution Reactions of the Coordinated Complexes

As was discussed in Chapter 7, a direct correlation between the pK_a values of the uncoordinated β-diketone ligands and the substitution rates of the coordinated [Rh(*O,O'*-Bid)$(CO)_2$] complexes with P$(otol)_3$ was observed. The calculated second-order rate constants of the CO substitution by P$(otol)_3$ are given in Table 8.2 with the relationship between the pK_a of the free ligands and the k_{12} values of the respective rhodium(I) complexes illustrated in Figure 8.3.

Table 8.2: Second-order rate constants for the carbonyl substitution of [Rh(β-diketonato)$(CO)_2$] complexes by tri(o-tolyl)phosphine at 25 ℃ reporte d by Ebenebe[12].

Complex	pK_a free ligand	[P$(otol)_3$] (M)	k_{obs} (s^{-1})	k_{12} ($M^{-1}.S^{-1}$) (Eq.7.6)
[Rh(dipiv)$(CO)_2$]	11.77	0.003	0.61(4)	2.0(1) x 10^2
[Rh(acac)$(CO)_2$]	8.95	0.003	0.89(1)	2.97(3) x 10^2
[Rh(dbm)$(CO)_2$]	9.35	0.003	2.49(4)	8.3(1) x 10^2
[Rh(tfac)$(CO)_2$]	6.30	0.003	49.2(9)	1.6(3) x 10^4
[Rh(F_3-bzac)$(CO)_2$]	6.30	0.003	123.6(1)	4.12(5) x 10^4
[Rh(hfac)$(CO)_2$]	4.43	0.0006	238.3(4)	3.97(7) x 10^5

[12] Ebenebe, P., *MSc Dissertation*, University of the Free State, Bloemfontein, South Africa, **1998**.

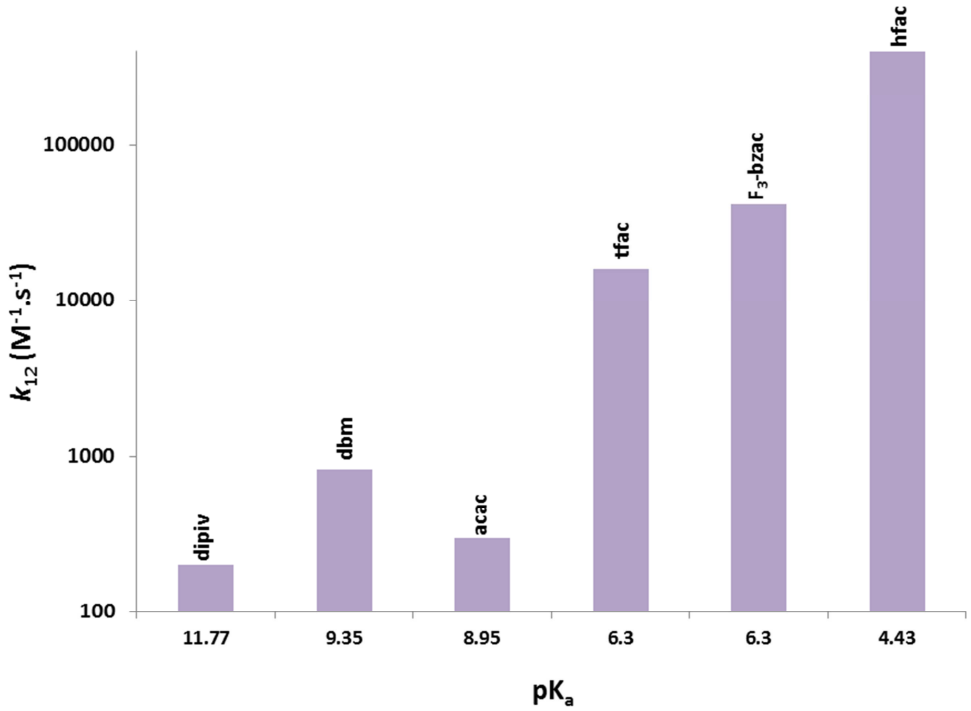

Figure 8.3: Schematic representation of the relationship between the pK_a values of the free β-diketone ligands and the reported second-order rate constants (k_{12}) of the substitution reaction of [Rh(*O,O'*-Bid)$(CO)_2$] with $P(otol)_3$.

It is clear from Figure 8.3 that lower pK_a values of the uncoordinated β-diketone ligands are associated with faster substitution rates for the corresponding coordinated rhodium(I) complexes. [Rh(hfac)$(CO)_2$] (k_{12}= 3.97(7) x 10^5 $M^{-1}.s^{-1}$) with the lowest pK_a of the free ligand, hfacH (4.3) had the largest k_{12} value indicating the rhodium(I) complex to have the fastest substitution rate. In contrast, [Rh(dipiv)$(CO)_2$] (k_{12}= 2.0(1) x 10^2 $M^{-1}.s^{-1}$) is associated with the highest pK_a value of the free ligand, dipivH (11.77), but displayed the slowest substitution rates.

A seven order-of-magnitude increase in Bronsted basicity of the bidentate ligands is associated with a three order-of-magnitude decrease in substitution reactivity at the rhodium(I) centre (k_{12} values) for the different rhodium(I) complexes.

Additionally, it was noted that rhodium(I) complexes with coordinating β-diketonato ligands containing electron-withdrawing substituents such as in [Rh(hfac)$(CO)_2$], [Rh(tfac)$(CO)_2$] and [Rh(F_3-bzac)$(CO)_2$] displayed the fastest substitution rates. For the rhodium(I) complexes with coordinating β-diketonato ligands containing electron-donating substituents, such as in [Rh(acac)$(CO)_2$] and [Rh(dipiv)$(CO)_2$], significantly slower substitution rates were observed.

8.2.3 Correlation of the UV/Vis Emission of the Rhodium(I) Complexes with Rh···Rh Interactions in the Solid-state

The different rhodium(I) complexes synthesized during this study displayed a unique range of colours ranging from yellow to purple, all accompanied by a green metallic lustre (see Chapter 3).

As was discussed in Chapter 2 many complexes containing metallophilic interactions display unique colour combinations that have been attributed to the interactions themselves with a direct link to the metal···metal distances found within the solid-state structures of these compounds (see Section 2.4.5).

The different colours observed for the rhodium(I) complexes synthesized in this study which also showed metallophilic interactions in the solid-state, are represented in Figure 8.4. One of the observations from this representation is that the coordinating β-diketonato ligands containing aliphatic substituents for example the [Rh(acac)$(CO)_2$], [Rh(3Cl-acac)$(CO)_2$] and [Rh(dipiv)$(CO)_2$] complexes all had relatively short Rh···Rh distances of 3.237(3) Å – 3.317(3) Å. Coincidentally, these complexes all exhibited a red or purple colour in the solid state. In contrast most of the rhodium(I) complexes with coordinating β-diketonates containing aromatic substituents displayed longer Rh···Rh distances (3.385(3) Å – 3.544(3) Å). These complexes were found to be orange or yellow hued.

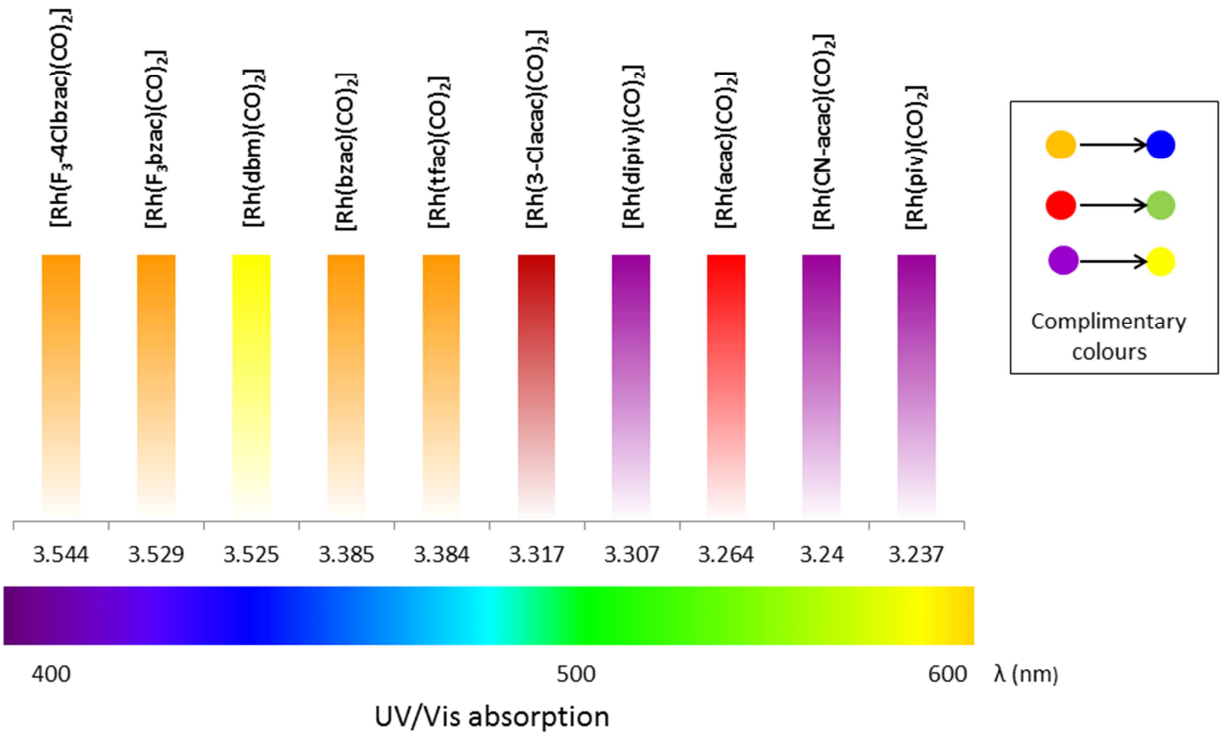

Figure 8.4: Representation of the colours exhibited by the different rhodium(I) complexes and the average Rh···Rh distances found in the solid-state (as determined by single crystal X-ray diffraction (Chapters 4, 5 and 6).

By comparing the colours of the individual complexes (emission) with their complimentary colours (absorbance) in the electromagnetic wave spectrum (Figure 8.4), the wavelength range at which each complex absorbs light in the solid state can be estimated. This comparison would suggest that orange or yellow coloured complexes absorb light in the 400 – 500 nm range whilst red and purple coloured complexes absorb light in the 500 – 600 nm range.

The wavelength range at which each complex absorbs light was found to correlate reasonably to the Rh···Rh distances in the solid-state structures of the different rhodium(I) complexes. Shorter Rh···Rh distances such as those reported for [Rh(acac)$(CO)_2$] (3.264(3) Å) and [Rh(piv)$(CO)_2$] (3.237(3) Å) are found at the longer wavelength range of 550 – 600 nm. Similarly, the longer Rh···Rh distances for [Rh(bzac)$(CO)_2$] (3.385(3) Å) and [Rh(F_3-bzac)$(CO)_2$] (3.529(3) Å) correlate to absorption at the shorter wavelength range of 400 – 470 nm. This coincides with literature reports that shorter Rh···Rh distances (~ 3.0 Å) are responsible for absorption maxima at a wavelength range of 500 – 600 nm whilst longer Rh···Rh distances (~ 3.8 nm) shifts these signals to 400 – 500 nm.[13]

Although most of the rhodium(I) complexes from this study displayed this trend reasonably, two exceptions were noted, namely the [Rh(dbm)$(CO)_2$] and [Rh(dipiv)$(CO)_2$] complexes. The reported average Rh···Rh distances in [Rh(dbm)$(CO)_2$] (3.525(3) Å) would suggest that the complex should exhibit an orange hue in the solid state if following the trend predicted from Figure 8.3. A similar situation exists for [Rh(dipiv)$(CO)_2$] that is coloured purple although the Rh···Rh distances of 3.307(3) Å would suggest a red coloured compound in the solid state.

8.2.4 Correlation of Electronic Influences on the Rhodium(I) Centre in Rhodium(I) Complexes with Rh···Rh Interactions in the Solid-state

Part of this study involved the investigation of the effect that changes to the substituents on the coordinating β-diketonato ligand could exert on the metallophilic interactions if any in the coordinated rhodium(I) complexes. If such changes could be observed it could also alter the assembly of the one-dimensional metal chain constructed of neighbouring molecules *via* metallophilic interactions between rhodium(I) centres.

This would imply in principle that the electronic effect of an electronic withdrawing substituent on the coordinating β-diketonato ligand could be extended to the metal centre and the metallophilic interactions throughout the one-dimensional metal chain in the solid state. The [Rh(acac)$(CO)_2$] and [Rh(tfac)$(CO)_2$] complexes offer such a comparison as the latter complex contains an electron withdrawing trifluoro moiety whilst still being similar in size and steric strain as the methyl moiety of [Rh(acac)$(CO)_2$]. Data related to these two rhodium(I) complexes are summarized in Table 8.3.

[13] Laurila, E., Tatikonda, R., Oresmaa, L., Hirva, P., Haukka, M., *Cryst. Eng. Comm.*, **2012**, *14*, 8401-8408.

Table 8.3: Summary of selected data related to [Rh(acac)(CO)$_2$] and [Rh(tfac)(CO)$_2$].

Complex	pK$_a$	Avg. d(Rh···Rh) (Å)	Rh chemical shift (ppm)	Angle Rh-Rh-Rh (°)	Torsion angle R-groups (°)
[Rh(acac)(CO)$_2$]	8.95	3.264(3)	284.2	175.45(3)	180.0(2)
[Rh(tfac)(CO)$_2$]	6.3	3.384(3)	319.2	173.93(3)	180.0(2)

From the ^{103}Rh chemical shift data presented in Table 8.3 it is clear that the electronic environment experienced by the rhodium(I) centre is different between the two complexes. The trifluoro moiety present in the [Rh(tfac)(CO)$_2$] complex reduces the electron density at the rhodium(I) centre that results in a higher chemical shift as mentioned in Section 8.2.1 (δ= 319.2 ppm).

A question that may be raised at this point is whether there is some additional steric contribution from the trifluoro moiety in the [Rh(tfac)(CO)$_2$] complex in comparison to the two methyl substituents present in [Rh(acac)(CO)$_2$]. In this regard a literature search revealed example cases of the trilfuoro moiety of the trifluoroacetylacetonato ligand in coordination to other metal centres being disordered over two positions between the methyl group and trifluoro substituent in the solid state structure determinations.[14,15] This would imply that the trifluoro group can easily "interconvert" to the methyl position as the space occupancy of these two substituents are relatively similar. The steric contribution of a trifluoro moiety in comparison to a methyl substituent is thus assumed to be relatively small in this comparison of [Rh(acac)(CO)$_2$] and [Rh(tfac)(CO)$_2$].

Further evidence to the similarity in steric properties between the two groups could potentially be seen in the observed linearity between the two different one-dimensional metal chains. For [Rh(acac)(CO)$_2$] an angle of 175.45(3)° along the rhodium centres (Rh-Rh-Rh) in the chain was noted and an angle of 173.93(3)° in the [Rh(tfac)(CO)$_2$] solid state structure. The difference between these two angles is relatively small. Moreover, the torsion angles between coordinated β-diketonato ligands of neighbouring molecules were found to be similar (180.0(2)°). As was mentioned in Section 2.4.4, the arrangement of molecules along the one-dimensional chains is highly influenced by the coordinating ligands. With both these structures displaying such similar spatial arrangements it would seem as if the only discernible difference between the ligands would indeed be the presence of the electron withdrawing trilfuoro substituent in [Rh(tfac)(CO)$_2$].

[14] Bennet, D. W., Siddiquee, T. A., Haworth, D. T., Lindeman, S. V., *J. Chem. Crystallogr.*, **2007**, *37*, 207-212.
[15] Lai, Y. H., Chen, Y. L., Chi, Y., Liu, C. S., Carty, A. J., Peng, S. M., Lee, G. H., *J. Mater. Chem.*, **2003**, *13*, 1999-2006.

Upon examination of the Rh···Rh distances encountered between the solid state structures of [Rh(acac)$(CO)_2$] (3.264(3) Å) and [Rh(tfac)$(CO)_2$] (3.384(3) Å) it was noted that the distances are considerably increased for the complex containing the trifluoro substituent. This would make sense when taking into account that the trifluoro group would remove electron density from the metal centre as the ^{103}Rh chemical shifts indicated. This results in less electron density available at the rhodium(I) centre for dz^2 orbital overlap between neighbouring molecules along the assembled one-dimensional metal chain. As was discussed in Chapter 2, the dz^2 orbital overlap is responsible for the establishment of metallophilic interactions between d^8 metal centres (see Section 2.4.3). As less orbital overlap can take place, the metallophilic interactions will weaken as in [Rh(acac)$(CO)_2$] ((3.264(3) Å) and [Rh(tfac)$(CO)_2$] (3.384(3) Å), observed in the increased Rh···Rh interactions respectively.

A second example of how the presence of electron withdrawing groups can alter the Rh···Rh distances and the resulting one-dimensional metal chain constructed from neighbouring molecules is in the comparison of the [Rh(F_3-4Clbzac)$(CO)_2$] and [Rh(F_3-bzac)$(CO)_2$] complexes. Once again data related to these two structures are summarized and presented in Table 8.4.

Table 8.4: Summary of selected data related to [Rh(F_3-bzac)$(CO)_2$] and [Rh(F_3-4Clbzac)$(CO)_2$].

Complex	pK_a	Avg. d(Rh···Rh) (Å)	Rh chemical shift (ppm)	Angle Rh-Rh-Rh (°)	Torsion angle R-groups (°)
[Rh(F_3-bzac)$(CO)_2$]	6.3	3.529(3)	320.4	167.50(2)	115.23(1)
[Rh(F_3-4Clbzac)$(CO)_2$]	7.55	3.544(3)	325.1	176.34(3)	97.61(3)

Both these rhodium(I) complexes contain trifluoro and phenyl ring substituents on the two methyl carbon positions of the coordinating β-diketonato ligands. In the case of [Rh(F_3-4Clbzac)$(CO)_2$], an additional electron withdrawing chlorine atom is located on the *para* position of the phenyl ring substituent. As phenyl rings are regarded only as slightly electron withdrawing due to the aromatic system being electron deficient the addition of the chlorine atom to the phenyl ring could result in more electron density being withdrawn from the metal centre towards the phenyl ring. The ^{103}Rh chemical shifts for [Rh(F_3-bzac)$(CO)_2$] (δ= 320.4 ppm) and [Rh(F_3-4Clbzac)$(CO)_2$] (δ= 325.1 ppm) agree with this as the electron poorer rhodium(I) centre in the [Rh(F_3-4Clbzac)$(CO)_2$] complex has a higher chemical shift value.

Upon examining the Rh···Rh distances in the solid-state structures of [Rh(F_3-bzac)$(CO)_2$] (3.529(3) Å) and [Rh(F_3-4Clbzac)$(CO)_2$] (3.544(3) Å) the addition of the electron withdrawing chlorine atom in [Rh(F_3-4Clbzac)$(CO)_2$] seems to lead to slightly longer Rh···Rh distances. Also

there is a remarkable difference in linearity between the one-dimensional chains encountered within each structure with the Rh-Rh-Rh angles of 167.50(2)° in [Rh(F_3-bzac)$(CO)_2$] less linear than the angles of 176.34(3)° found in [Rh(F_3-4Clbzac)$(CO)_2$].

In addition, the torsion angles between the coordinating β-diketonato ligands of neighbouring molecules in the two structures were found to be substantially different. Molecules in the one-dimensional chains of [RhF_3-4Clbzac)$(CO)_2$] (97.61(3)°) are in a staggered arrangement (see Section 2.4.4) whilst the molecules of [Rh(F_3-bzac)$(CO)_2$] are arranged at angles of 115.23(1)° along the chain. Chlorine atoms are substantially larger than hydrogen atoms and so this effect of different arrangements within the one-dimensional chains of the molecules could be attributed to a steric contribution of the chlorine atom in the molecule. It was also eluded to in Section 4.5 that the solid state structure of [Rh(F_3-4Clbzac)$(CO)_2$] contains halogen interactions between the chlorine atoms of different molecules. The torsion angles for the [Rh(F_3-4Clbzac)$(CO)_2$] complex (97.61(3)°) could thus also be influenced by a preferred orientation of the molecules to accommodate these interactions and to possibly add to the stability of the solid-state structure.

The previous two examples focussed on changes brought about in substituents to the two methyl carbon positions of the coordinating β-diketonato ligands and their effect on the metal centre with possible extension to the metallophilic interactions and one-dimensional metal chains. Electron withdrawing groups were also introduced on the methine carbon position to evaluate whether changes could be affected on the metal centre at the extended atom distance (three atoms separated from the rhodium(I) centre) in comparison to substituents on the methyl carbon positions (two atoms separated from the rhodium(I) centre). The two different substituent positions are illustrated in Figure 8.5 with the number of atoms separating the substituted groups from the metal centre indicated in red.

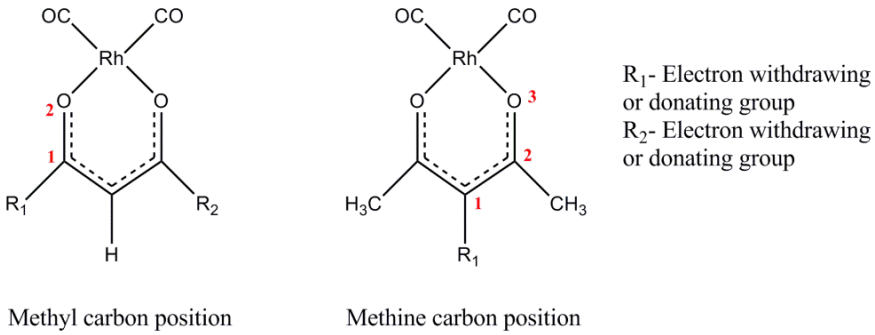

Figure 8.5: Schematic representation of the different carbon positions at which electron withdrawing substituents were introduced onto the coordinating β-diketonato ligands during this study.

Table 8.5 compares the two rhodium(I) complexes containing β-diketonato ligands with a substituent on the methine carbon position. The data clearly shows that the electron withdrawing effect of the chlorine substituent on the methine carbon position in [Rh(3Cl-acac)$(CO)_2$] does in

fact extend to the rhodium(I) centre as is evidenced in the ^{103}Rh chemical shift of 297.7 ppm which is considerably higher than that found for [Rh(acac)(CO)$_2$] (δ= 284.2 ppm). Also in [Rh(CN-acac)(CO)$_2$] (δ= 294.2 ppm) a higher chemical shift was observed.

Table 8.5: Summary of selected data related to [Rh(acac)(CO)$_2$], [Rh(3Cl-acac)(CO)$_2$] and [Rh(CN-acac)(CO)$_2$].

Complex	pK_a	Avg. d(Rh···Rh) (Å)	Rh chemical shift (ppm)	Angle Rh-Rh-Rh (°)	Torsion angle R-groups (°)
[Rh(acac)(CO)$_2$]	8.95	3.264(3)	284.2	175.45(3)	180.0(2)
[Rh(3Cl-acac)(CO)$_2$]	6.77	3.317(2)	297.7	168.88(2)	103.34(3)
[Rh(CN-acac)(CO)$_2$]	-	3.211(3)	294.2	166.5(3)	180.0(3)

However, the effect of the electron withdrawing groups on the methine carbon positions appear to be less pronounced than what was observed for [Rh(tfac)(CO)$_2$] (δ= 319.2) or [Rh(F$_3$-bzac)(CO)$_2$] (δ= 320.4 ppm). This could be due to the additional atom position separating the chlorine atom/ nitrile group from the metal centre as opposed to the two atom positions separating the electron withdrawing trifluoro moiety from the rhodium(I) centre in [Rh(tfac)(CO)$_2$].

The reduction in electron density experienced by the metal centre is possibly still reflected in the longer Rh···Rh distances found in [Rh(3Cl-acac)(CO)$_2$] (3.317(2) Å) as opposed to [Rh(acac)(CO)$_2$] (3.264(3) Å) albeit relatively small. The linearity of the one-dimensional metal chain along the Rh-Rh-Rh centres is disrupted upon coordination of the chlorine substituted β-diketonato ligand to the rhodium(I) centre. [Rh(acac)(CO)$_2$] (175.45(3)°) displayed a relatively linear arrangement as opposed to the smaller angles of 168.88(2)° in [Rh(3Cl-acac)(CO)$_2$]. Additionally, the torsion angles of 103.34(3)° between the coordinating β-diketonato ligands of neighbouring molecules in [Rh(3Cl-acac)(CO)$_2$] is significantly different from the eclipsed arrangement found in [Rh(acac)(CO)$_2$] (180.0(2)°). One explanation for this arrangement can possibly be attributed to the relative size constraint of the chlorine atom. To allow for effective packing of the molecules along the one-dimensional chain a smaller torsion angle could assist with less repulsion between chlorine atoms of different molecules within the packing of the crystal unit.

The Rh···Rh distances of [Rh(CN-acac)(CO)$_2$] (3.211(3) Å) are slightly shorter than those reported for [Rh(acac)(CO)$_2$]. This was unexpected as the decrease in electron density at the rhodium(I) centre should have resulted in longer Rh···Rh distances as was seen for [Rh(3Cl-acac)(CO)$_2$] (3.317(2) Å).

8.2.5 Correlation of Steric Influences on the Rhodium(I) Centre in Rhodium(I) Complexes with Rh···Rh Interactions in the Solid-state

As pointed out in the introduction, steric changes within the different coordinating β-diketonato ligands were also investigated for their possible influence on the rhodium(I) centre and potential simultaneous effect on the metallophilic interactions in the solid-state structures of these complexes. Two complexes that are compared for this reason are [Rh(acac)$(CO)_2$] and [Rh(dipiv)$(CO)_2$]. Data related to the solid-state structures of these two rhodium(I) complexes are summarized in Table 8.6.

Table 8.6: Summary of selected data related to [Rh(acac)$(CO)_2$] and [Rh(dipiv)$(CO)_2$].

Complex	pK_a	Avg. d(Rh···Rh) (Å)	Rh chemical shift (ppm)	Angle Rh-Rh-Rh (°)	Torsion angle R-groups (°)
[Rh(acac)$(CO)_2$]	8.95	3.264(3)	284.2	175.45(3)	180.0(2)
[Rh(dipiv)$(CO)_2$]	11.77	3.307(3)	270.2	178.5(2)	140.9(3)

These two rhodium(I) complexes were chosen for comparison due to the symmetrical nature of the coordinating β-diketonato ligands as well as the relatively low electron withdrawing or donating properties associated with the different substituents. In the case of [Rh(dipiv)$(CO)_2$] the two *t*-butyl groups are considered strongly electron donating.[16] From the ^{103}Rh chemical shifts some differences were observed at the metal centre due to the electron donating properties of the ligand. [Rh(dipiv)$(CO)_2$] has a lower chemical shift of 270.2 ppm signalling the increased electron density found at the metal centre due to the electron donating *t*-butyl group substituents.

The changes in chemical shift was comparable to changes noted between [Rh(acac)$(CO)_2$] (δ= 284.2 ppm) and [Rh(3Cl-acac)$(CO)_2$] (δ= 297.7 ppm). As was stated in Section 8.2.3 the electron withdrawing effects of the chlorine atom in [Rh(3Cl-acac)$(CO)_2$] are slightly decreased due to the larger atom separation from the metal centre. To this end, the small changes in the chemical shifts of the two rhodium(I) complexes discussed here are however only slight changes, with the steric contributions of the substituents being far more dominant.

The Rh···Rh distances increase slightly upon going from [Rh(acac)$(CO)_2$] (3.264(3) Å) to [Rh(dipiv)$(CO)_2$] (3.307(3) Å). This is contradictory to what would have been expected based on the smaller ^{103}Rh chemical shift value of 270.77 ppm in [Rh(dipiv)$(CO)_2$], which would have predicted shorter distances between rhodium(I) centres as the electron density is increased. An increased amount of electron density at the metal centre would have allowed for more effective dz^2 orbital overlap between neighbouring rhodium(I) centres and thus shorter Rh···Rh distances. The fact that the Rh···Rh distances are longer than expected suggests a strong steric contribution

[16] Peters, G. J., *Deoxynucleoside Analogs in Cancer Therapy*, Humana Press, New Jersey, **2006**, 364.

of the coordinating ligands preventing this more effective overlap from taking place. It was mentioned in Chapter 2 (Section 2.2.4) that the steric contribution of the coordinating ligands can contribute significantly to the metallophilic interactions that form. In this case it is concluded that the bulky *t*-butyl groups prevent closer interaction of the rhodium(I) centres thereby influencing the assembly of molecules along the one-dimensional metal chain.

Torsion angles of 140.9(3)° between the coordinated β-diketonato ligands of neighbouring molecules in a staggered arrangement along the one-dimensional chain provide further evidence to the steric strain imposed by the *t*-butyl groups. The molecules could be arranged in this manner along the chain to afford the least amount of steric strain from the bulky *t*-butyl substituents thereby assisting in the establishment of the metallophilic interactions between neighbouring molecules in spite of the significant steric strain imposed.

The examples of [Rh(acac)$(CO)_2$], [Rh(bzac)$(CO)_2$] and [Rh(dbm)$(CO)_2$] offer another comparison to evaluate the steric effect of ligands on the metallophilic interactions. Selected data for these three rhodium(I) complexes are presented in Table 8.7.

Table 8.7: Summary of selected data related to [Rh(acac)$(CO)_2$], [Rh(bzac)$(CO)_2$] and [Rh(dbm)$(CO)_2$].

Complex	pK_a	Avg. d(Rh···Rh) (Å)	Rh chemical shift (ppm)	Angle Rh-Rh-Rh (°)	Torsion angle R-groups (°)
[Rh(acac)$(CO)_2$]	8.95	3.264(3)	284.2	175.45(3)	180.0(2)
[Rh(bzac)$(CO)_2$]	8.70	3.385(3)	284.0	172.06(3)	180.0(2)
[Rh(dbm)$(CO)_2$]	9.35	3.525(1)	292.2	170.52(1)	143.3(3)

This data shows the slight electron withdrawing capability of the substituent phenyl rings evident in the ligand pK_a values and the ^{103}Rh chemical shift of [Rh(bzac)$(CO)_2$] (δ= 284.0 ppm) identical to the ^{103}Rh chemical shift of 284.2 ppm found for [Rh(acac)$(CO)_2$]. In the case of [Rh(dbm)$(CO)_2$] a slight decrease of electron density at the metal centre exists due to the electron withdrawing phenyl rings and a higher chemical shift of 292.2 ppm was found.

It was expected from the higher ^{103}Rh chemical shift value of [Rh(dbm)$(CO)_2$] (δ= 292.2 ppm) that the Rh···Rh distance would increase in comparison to those distances found for [Rh(acac)$(CO)_2$] (δ= 284.2 ppm). This was indeed the case with Rh···Rh distances of 3.525(1) Å in [Rh(dbm)$(CO)_2$] whereas Rh···Rh distances of 3.264(3) Å were found between rhodium(I) centres in [Rh(acac)$(CO)_2$].

If the electronic contribution of the phenyl rings was the only factor leading to the longer Rh···Rh distances of [Rh(dbm)$(CO)_2$] the relatively similar ^{103}Rh chemical shift found in [Rh(bzac)$(CO)_2$]

(δ= 284.0 ppm) in comparison to [Rh(acac)$(CO)_2$] (δ= 284.2 ppm) would lead to similar Rh···Rh distances as in [Rh(acac)$(CO)_2$]. Average Rh···Rh distances in [Rh(bzac)$(CO)_2$] were found to be 3.385(3) Å which are considerably longer than those of [Rh(acac)$(CO)_2$] (3.264(3) Å). This suggests that the weakening of the Rh···Rh interactions in [Rh(dbm)$(CO)_2$] as well as [Rh(bzac)$(CO)_2$] are not due to the weakly electron withdrawing phenyl substituents but are predominantly due to the steric contribution of the bulky nature of the phenyl rings.

Additionally, the linearity of the one-dimensional metal chain in [Rh(dbm)$(CO)_2$] appears to be affected by the steric strain imposed by the phenyl rings with Rh-Rh-Rh angles found to be 170.52(1)°. The torsion angles between coordinated β-diketonato ligands of 143.26(3)° suggest as is suspected in the case of [Rh(dipiv)$(CO)_2$] to be due to the arrangement of molecules to minimize the amount of steric strain experienced along the one-dimensional metal chain.

The torsion angles along the one-dimensional chains for [Rh(acac)$(CO)_2$] (180.0(2)°) and [Rh(bzac)$(CO)_2$] (180.0(2)°) reveal eclipsed arrangements of molecules opposed to the staggered arrangement in [Rh(dbm)$(CO)_2$] (143.26(3)°). This suggests that the addition of one phenyl substituent may be easily accommodated in the arrangement of molecules along the one-dimensional metal chains where as a second phenyl substituent provides a significant steric hindrance in the adoption of this geometry.

8.2.6 Steric Factors Influencing the Arrangement of Molecules along the One-Dimensional Metal Chains

As has been mentioned throughout this chapter the torsion angles along the one-dimensional chains appears not to be random but rather orchestrated by the arrangement of molecules to accommodate steric strain imposed by the coordinating β-diketonato ligands.

It was noted that in the case of molecules containing small coordinating β-diketonato ligands such as [Rh(acac)$(CO)_2$] or [Rh(tfac)$(CO)_2$] the arrangement of molecules in an eclipsed formation seems preferred with torsion angles of 180° between coordinating β-diketonato ligands of neighbouring molecules. The four rhodium(I) complexes to display this arrangement are summarized in Table 8.8.

Table 8.8: Summary of selected data related to [Rh(acac)(CO)$_2$], [Rh(tfac)(CO)$_2$], [Rh(CN-acac)(CO)$_2$] and [Rh(bzac)(CO)$_2$].

Complex	pK$_a$	Avg. d(Rh···Rh) (Å)	Rh chemical shift (ppm)	Angle Rh-Rh-Rh (°)	Torsion angle R-groups (°)
[Rh(acac)(CO)$_2$]	8.95	3.264(3)	284.2	175.45(3)	180.0(2)
[Rh(tfac)(CO)$_2$]	6.3	3.384(3)	319.2	173.93(3)	180.0(2)
[Rh(CN-acac)(CO)$_2$]	-	3.211(3)	294.2	166.5(3)	180.0(3)
[Rh(bzac)(CO)$_2$]	8.7	3.385(3)	284.0	172.06(3)	180.0(2)

In contrast, the molecules offering greater steric constraint to the arrangement of molecules along the one-dimensional chain adopt more staggered geometries as can be seen from the torsion angles listed in Table 8.9.

Table 8.9: Summary of selected data related to rhodium(I) complexes adopting staggered arrangements of molecules along the one-dimensional metal chain constructed from metallophilic interactions.

Complex	pK$_a$	Avg. d(Rh···Rh) (Å)	Rh chemical shift (ppm)	Angle Rh-Rh-Rh (°)	Torsion angle R-groups (°)
[Rh(piv)(CO)$_2$]	6.99	3.237(3)	306.8	175.6(3)	141.4(3)
[Rh(dipiv)(CO)$_2$]	11.77	3.307(3)	270.2	178.5(2)	140.9(3)
[Rh(3Cl-acac)(CO)$_2$]	6.77	3.317(2)	297.7	168.88(2)	103.34(3)
[Rh(F$_3$-bzac)(CO)$_2$]	6.3	3.529(3)	320.4	167.50(2)	115.23(1)
[Rh(F$_3$-4Clbzac)(CO)$_2$]	7.55	3.544(3)	342.2	176.34(3)	97.61(3)
[Rh(dbm)(CO)$_2$]	9.35	3.525(1)	292.2	170.52(1)	143.26(3)

Comparison of the data from Tables 8.8 and 8.9 suggests the steric strain brought about by the coordinating β-diketonato ligands might be affecting the arrangement of molecules along the one-dimensional metal chains found in the solid-state. In comparing for example [Rh(CN-acac)(CO)$_2$] (δ= 294.2 ppm) and [Rh(3Cl-acac)(CO)$_2$] (δ= 297.7 ppm) which offer similar electron withdrawing effects on the metal centre, the eclipsed arrangement of molecules in [Rh(CN-acac)(CO)$_2$] could in part be due to the smaller cyano group in relation to the larger chlorine substituent in [Rh(3Cl-acac)(CO)$_2$]. Additionally, the staggered arrangement of [Rh(3Cl-acac)(CO)$_2$] could be preferred to avoid repulsion of the chlorine atoms along the chain.

An added observation to how the coordinating ligands might influence the arrangement of the molecules along the one-dimensional metal chains is in the comparison of the two polymorphs of [Rh(F$_3$-4Clbzac)(CO)$_2$] that was isolated in this study. The concise data related to these two solid state structures are presented in Table 8.10.

Table 8.10: Summary of selected data related to the two polymorphs of [Rh(F_3-4Clbzac)$(CO)_2$] that were isolated during this study.

Complex	pK_a	Avg. d(Rh···Rh) (Å)	Rh chemical shift (ppm)	Angle Rh-Rh-Rh (°)	Torsion angle R-groups (°)
[Rh(F_3-4Clbzac)$(CO)_2$][i]	7.55	3.544(3)	325.1	176.34(3)	97.61(3)
[Rh(F_3-4Clbzac)$(CO)_2$][ii]	7.55	3.588(3)		168.36(6)	97.28(3)

i) Polymorph structure discussed in Section 4.4, ii) polymorph structure discussed in Section 4.5.

From the data given in Table 8.10 it is observed that the average Rh···Rh distances between the two polymorphs differ slightly (3.544(3) Å for polymorph **i** and 3.588(3) Å for polymorph **ii**). The angle at which the rhodium(I) centres are packed along the one-dimensional chains (Rh-Rh-Rh) were also found to differ significantly with 176.34(3)° for polymorph **i** and 168.36(6)° for polymorph **ii**.

However, one parameter that remained unchanged between the two polymorphs was the torsion angles at which the molecules are arranged along the one-dimensional chains. Both polymorphs had torsion angles of 97° between the coordinating β-diketonato ligands of neighbouring molecules. As was discussed in Sections 4.4 and 4.5, the intermolecular interactions involving these two polymorphs are significantly different thereby implying that the intermolecular interactions within each structure are not contributing significantly to the torsion angles along the one-dimensional chains. This would suggest that the most significant factor influencing the arrangement of the molecules along the one-dimensional metal chains was the coordinating ligands themselves.

8.3 Conclusion

In this chapter various comparisons of different properties of the rhodium(I) complexes of this study was presented. This included the physical properties such as colour exhibited by the rhodium(I) complexes that was correlated to the Rh···Rh distances found in the solid-state structures and the wavelength range of absorption. In totality, all of the parameters used in evaluation of the rhodium(I) complexes in this study can be illustrated schematically in Figure 8.6.

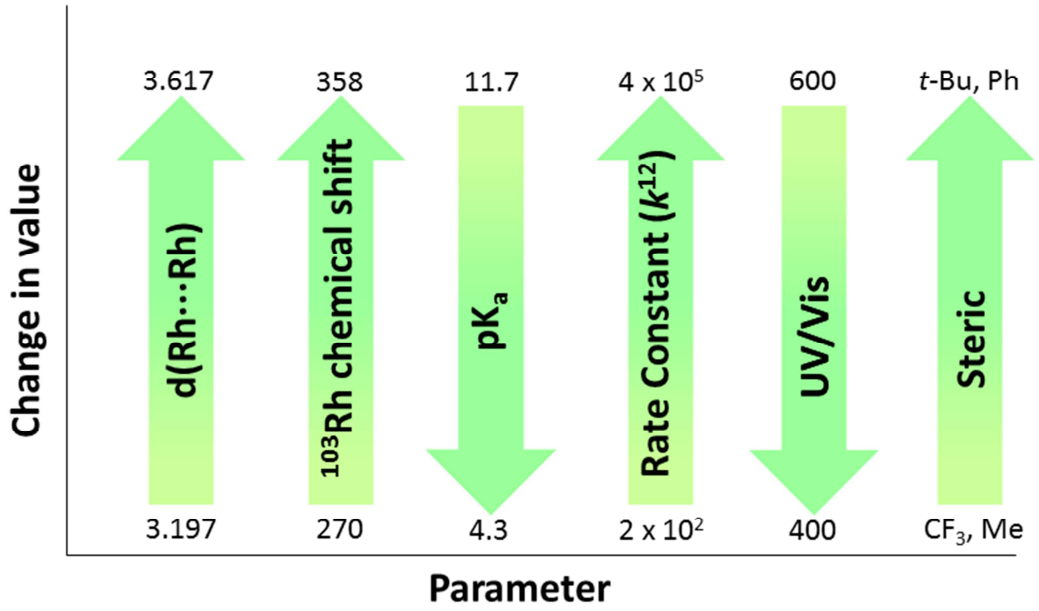

Figure 8.6: Schematic representation of all the parameters used in the evaluation of the rhodium(I) complexes of this study. In each case the general effect observed for the changes in the rhodium(I) complexes is illustrated with an increase or decrease in relation to the other parameters.

This illustration shows a general link in the increase of the Rh···Rh distances with an increase in the ^{103}Rh chemical shifts which in turn is associated with a decrease of pK_a value of the free ligands. A decrease in pK_a values of the free ligands resulted in faster substitution rates of the coordinated rhodium(I) complexes. Furthermore, an increase in Rh···Rh distances saw a decrease in the UV/Vis emission profile of the rhodium(I) complexes which was also shown to be influenced by the steric effects of the substituents on the coordinating β-diketonato ligands.

It is clear from Figure 8.6 that some six parameters were introduced in this study. All of these parameters, albeit some more important than others, show general and well-identifiable trends.

Following some of the trends that were discussed in this chapter a few guidelines may be applied in the future synthesis of compounds containing metallophilic interactions in particular for square planar rhodium(I) complexes:

i) In the design of systems that require a coloured complex with specific hue the system may be tailored for rhodium(I) systems by either using ligands containing aliphatic substituents to potentially yield a material with red or purple colouring. Alternatively, the use of aromatic substituents could lead to orange and yellow coloured compounds. The choice of ligand can thus potentially be used to tailor the physical properties of the resulting material as was seen in this study (Section 8.2.3).

ii) In cases where longer metal···metal distances are required within the one-dimensional chains the use of electron withdrawing groups as substituent on the coordinating ligand was shown to be effective. The position of the substituent also seems to affect the resulting metallophilic interactions as was seen with methyl *vs.* methine carbon

substituent positions (Section 8.2.4). The method of using small electron withdrawing groups could be effective if no disruption of the eclipsed arrangement of molecules along the constructed one-dimensional metal chains is required (Section 8.2.6).

iii) Alternatively, if longer metal···metal distanœs are required without specific preference to the arrangement of molecules along the one-dimensional metal chains, ligands containing aromatic substituents may be used (Section 8.2.5).

iv) If specific arrangements of molecules along the one-dimensional metal chains are required this may be influenced by using smaller coordinating β-diketonato ligands to facilitate eclipsed formations or larger coordinating β-diketonato ligands that could result in more staggered arrangements (Section 8.2.6).

A complete evaluation of the study will be presented in the next chapter with some of the successes and challenges of the study highlighted. Recommendations on future work to continue this study will also be given.

Chapter 9: Evaluation of Study

9.1 Introduction

One of the main motivations for this study (see Section 1.2, Chapter 1) was to gain further insight into the chemistry and properties of different [Rh(*O,O'*-Bid)$(CO)_2$] complexes that can be used in the design of nano-wired assemblies with potential applications. The study was undertaken to evaluate any correlations that might exist between the changes brought on the rhodium(I) centre by using different coordinating β-diketonato ligands and the subsequent one-dimensional chains constructed *via* metallophilic interactions in the solid-state. The findings of this investigation are discussed below.

9.2 Evaluation

9.2.1 Synthesis of Rhodium(I) Complexes and Characterization

One of the central aims in this study involved the synthesis of various rhodium(I) complexes with different coordinating β-diketonato ligands. This was done to evaluate the influence of using different substituents in the coordinating β-diketonato ligands on the rhodium(I) centre. The different substituents were chosen for their electron withdrawing/ donating as well as steric properties.

In this regard, several rhodium(I) complexes were successfully synthesized and characterized during this study (see Chapter 3). Characterization of the rhodium(I) complexes included use of UV/Vis, IR and NMR spectroscopy. From this characterization, a general trend was noted between the ^{103}Rh chemical shifts found for the rhodium(I) complexes and the pK_a values of the uncoordinated β-diketone ligands. It was observed that a decrease in pK_a of the free ligand resulted in higher ^{103}Rh chemical shifts (see Section 3.4). A relationship was also established between the ^{103}Rh chemical shifts and the CO stretching frequencies of the different rhodium(I) complexes with an increase in stretching frequency (asymmetric and symmetric) associated with an increase in ^{103}Rh chemical shift.

Furthermore, it was established that the ^{103}Rh chemical shifts reported for the coordinated complexes could be used to highlight the different electronic environments experienced at the

rhodium(I) centre upon coordination. For example, rhodium(I) complexes containing electron withdrawing substituents in the coordinating β-diketonato ligands had higher ^{103}Rh chemical shifts as the electron density at the rhodium(I) centre was decreased. In contrast, electron donating substituents in the coordinating β-diketonato ligands resulted in lower ^{103}Rh chemical shifts for the rhodium(I) complex.

9.2.2 Single Crystal X-ray Diffraction Study of [Rh(*O,O'*-Bid)(CO)$_2$] Complexes

The solid-state structures of the rhodium(I) complexes that could successfully be determined by single crystal X-ray diffraction during the study was discussed in Chapters 4, 5 and 6. Detailed insight into the solid-state structures with a focus on the geometric properties such as bond distances and angles as well as the important intermolecular interactions that were found in the crystal packing was given.

In each case metallophilic interactions were found between neighbouring rhodium(I) centres of these complexes that were extended into one-dimensional chains in the solid-state. The [Rh(pyruv)(CO)$_2$] complex was the only exception to this with the molecules noted to assemble into dimeric structures. The metallophilic interactions were presented with detail given on the Rh···Rh distances, angles of the linear chains as well as the torsions between neighbouring molecules for each of the rhodium(I) complexes. The crystallographic study of these rhodium(I) complexes revealed significant differences to exist in the one-dimensional chains with Rh···Rh distances and the geometric arrangement of molecules seemingly affected by the use of the different coordinating β-diketonato ligands to the rhodium(I) centre.

9.2.3 Preliminary Substitution and Equilibrium Investigation of [Rh(acac)(CO)$_2$]

To further evaluate the electronic environment experience by the rhodium(I) centre in these complexes a substitution kinetic study was undertaken and was discussed in Chapter 7. A preliminary kinetic investigation of a square planar substitution reaction of [Rh(acac)(CO)$_2$] by a bulky phosphine ligand was presented. It was also shown how a seemingly simple substitution reaction was complicated by an important equilibrium that exists for the reaction. This equilibrium was investigated using ^{31}P NMR and UV/Vis techniques and was shown to be dependent on the [CO] within the reaction.

However, second-order rate constants could still be estimated from literature values (see Section 7.7) that provided a measure of reactivity for the different [Rh(*O,O'*-Bid)$(CO)_2$] complexes that could be correlated with the different electronic environments experienced by the rhodium(I) centre. A relationship was established once again between the pK_a of the uncoordinated β-diketonato ligands and the coordinated rhodium(I) complexes. Substitution rates were seen to increase significantly as the pK_a of the free ligand was decreased rendering a decrease in electron density at the Rh(I) centre more prone to nucleophilic attack. It was seen that the seven order-of-magnitude increase in Bronsted basicity of the bidentate ligands results in a significant more than three order-of-magnitude in substitution reactivity decrease at the rhodium(I) centre (k_{12} values) (see Section 7.7).

9.2.4 Correlation Study

The final chapter included in this study (Chapter 8) focused on comparing different properties associated with the rhodium(I) complexes and relating those properties to the changes that were introduced in each complex by using different coordinating β-diketonato ligands. It was shown that the physical properties such as colour exhibited by the rhodium(I) complexes could directly be correlated to changes in Rh···Rh distances found in the solid-state structures. It was also shown how changes to the electronic environment of the rhodium(I) centre led to changes in the metallophilic interactions along the one-dimensional chains in the rhodium(I) complexes. Furthermore, greater steric bulk in the rhodium(I) complexes could be used to increase the Rh···Rh distances as well as influence the arrangement of the molecules along the one-dimensional chains. A general schematic representation to illustrate the relationship of all the parameters used to evaluate the rhodium(I) complexes was also presented. Reasonable trends in six different parameters were rated.

9.3 Future Work

Immediate future projects that could serve to quantify and optimize the research undertaken in this study are summarized below:

i) Expand the research on these rhodium(I) complexes to include theoretical calculations to gain a better understanding of the orbital overlap that takes place between rhodium(I) centres. This will also aid in understanding the effects brought

about in the metallophilic interactions by using different substituents in the coordinating β-diketonato ligands.

ii) Perform conductivity and solid-state spectroscopic studies on the current range of rhodium(I) complexes. This could include studies determining the effect of temperature on the metallophilic interactions and whether this could result in any physical changes of the material.

iii) Conduct a complete kinetic investigation of the substitution reaction of [Rh(*O,O'*-Bid)$(CO)_2$] complexes to assess the importance of equilibrium reactions and subsequently derive a full rate law describing the complete reaction.

iv) Expand the current study to investigate other transition metals and their metallophilic interactions by using the same series of coordinating ligands. This could provide valuable information on the role of the metal within the one-dimensional chains and physical properties of the bulk material.

v) Investigate future applications of these rhodium(I) complexes to be used in electronic or optic technologies.

The opportunities surrounding this research are great and diverse, and establishing a knowledge base of how fundamental chemistry impacts the ultimate construction of these nano-wired assemblies at the macroscopic scale will become vital in developing technologies that make use of such systems.

Appendix

Appendix A: Crystallographic Data

A 1. Supplementary Data for [Rh(bzac)(CO)$_2$]

Table A 1.1: Atomic coordinates and equivalent isotropic displacement parameters (Å^2) for [Rh(bzac)(CO)$_2$]. U(eq) is defined as one third of the trace of the orthogonalized U^{ij} tensor.

Atom	*x*	*y*	*z*	U_{eq}
C(1)	-1975(2)	3057(2)	5305(1)	17(1)
C(2)	1228(2)	2372(2)	5822(1)	18(1)
C(3)	-247(2)	2091(2)	3698(1)	13(1)
C(4)	1565(2)	1654(2)	3726(1)	16(1)
C(5)	2848(2)	1630(2)	4242(1)	16(1)
C(6)	-1396(2)	2156(2)	3096(1)	13(1)
C(7)	-945(2)	1102(2)	2608(1)	16(1)
C(8)	-2006(2)	1219(2)	2049(1)	17(1)
C(9)	-3539(2)	2371(2)	1970(1)	17(1)
C(10)	-4015(2)	3411(2)	2455(1)	17(1)
C(11)	-2949(2)	3305(2)	3014(1)	15(1)
C(12)	4773(2)	1331(3)	4178(1)	18(1)
O(1)	-3239(2)	3453(2)	5494(1)	24(1)
O(2)	1933(2)	2329(2)	6306(1)	24(1)
O(3)	-1033(2)	2504(2)	4148(1)	15(1)
O(4)	2556(2)	1879(2)	4781(1)	18(1)
Rh(1)	140(1)	2443(1)	5030(1)	13(1)

Table A 1.2: Hydrogen coordinates and isotropic displacement parameters (Å^2) for [Rh(bzac)(CO)$_2$].

Atom	*x*	*y*	*z*	U_{eq}
H(4)	1964	1342	3357	19
H(7)	95	299	2658	20

H(8)	-1681	506	1719	21
H(9)	-4261	2449	1587	20
H(10)	-5068	4194	2403	20
H(11)	-3278	4019	3344	18
H(12A)	4874	1153	3753	27
H(12B)	5235	153	4404	27
H(12C)	5466	2493	4335	27

Table A 1.3: Anisotropic displacement parameters ($Å^2$) for $[Rh(bzac)(CO)_2]$. The anisotropic displacement factor exponent takes the form: $-2\pi^2[h^2a^{*2}U^{11} + \ldots + 2hka^*b^*U^{23}]$.

Atom	U^{11}	U^{22}	U^{33}	U^{12}	U^{13}	U^{23}
C(1)	24(1)	16(1)	10(1)	0(1)	0(1)	-3(1)
C(2)	20(1)	14(1)	19(1)	0(1)	4(1)	-4(1)
C(3)	17(1)	10(1)	12(1)	1(1)	2(1)	-3(1)
C(4)	18(1)	17(1)	13(1)	1(1)	4(1)	-1(1)
C(5)	17(1)	14(1)	16(1)	2(1)	3(1)	-2(1)
C(6)	16(1)	13(1)	11(1)	1(1)	2(1)	-2(1)
C(7)	18(1)	16(1)	15(1)	0(1)	3(1)	2(1)
C(8)	23(1)	17(1)	13(1)	-2(1)	3(1)	1(1)
C(9)	20(1)	17(1)	13(1)	2(1)	-1(1)	-1(1)
C(10)	17(1)	16(1)	17(1)	1(1)	1(1)	2(1)
C(11)	18(1)	14(1)	14(1)	-1(1)	4(1)	0(1)
C(12)	16(1)	24(1)	15(1)	1(1)	2(1)	-3(1)
O(1)	24(1)	31(1)	18(1)	-2(1)	6(1)	1(1)
O(2)	31(1)	26(1)	14(1)	0(1)	-3(1)	-6(1)
O(3)	17(1)	18(1)	11(1)	0(1)	2(1)	-1(1)
O(4)	16(1)	24(1)	15(1)	1(1)	2(1)	-3(1)
Rh(1)	15(1)	15(1)	9(1)	0(1)	2(1)	-3(1)

Table A 1.4: Complete listing of bond lengths (Å) for $[Rh(bzac)(CO)_2]$.

Bond	Distance	Bond	Distance
C(1)-O(1)	1.139(2)	C(7)-H(7)	0.9500
C(1)-Rh(1)	1.8538(18)	C(8)-C(9)	1.388(2)
C(2)-O(2)	1.138(2)	C(8)-H(8)	0.9500
C(2)-Rh(1)	1.8479(18)	C(9)-C(10)	1.391(2)

C(3)-O(3)	1.2837(19)	C(9)-H(9)	0.9500
C(3)-C(4)	1.399(2)	C(10)-C(11)	1.391(2)
C(3)-C(6)	1.496(2)	C(10)-H(10)	0.9500
C(4)-C(5)	1.397(2)	C(11)-H(11)	0.9500
C(4)-H(4)	0.9500	C(12)-H(12A)	0.9800
C(5)-O(4)	1.2779(19)	C(12)-H(12B)	0.9800
C(5)-C(12)	1.504(2)	C(12)-H(12C)	0.9800
C(6)-C(7)	1.396(2)	O(3)-Rh(1)	2.0497(12)
C(6)-C(11)	1.400(2)	O(4)-Rh(1)	2.0350(12)
C(7)-C(8)	1.388(2)		

Table A 1.5: Complete listing of bond angles (º) fo r [Rh(bzac)(CO)$_2$].

Angle	Value	Angle	Value
O(1)-C(1)-Rh(1)	177.49(15)	C(8)-C(9)-C(10)	119.75(15)
O(2)-C(2)-Rh(1)	178.54(16)	C(8)-C(9)-H(9)	120.1
O(3)-C(3)-C(4)	125.71(15)	C(10)-C(9)-H(9)	120.1
O(3)-C(3)-C(6)	115.68(14)	C(11)-C(10)-C(9)	120.02(15)
C(4)-C(3)-C(6)	118.58(14)	C(11)-C(10)-H(10)	120.0
C(5)-C(4)-C(3)	126.44(15)	C(9)-C(10)-H(10)	120.0
C(5)-C(4)-H(4)	116.8	C(10)-C(11)-C(6)	120.53(15)
C(3)-C(4)-H(4)	116.8	C(10)-C(11)-H(11)	119.7
O(4)-C(5)-C(4)	126.07(15)	C(6)-C(11)-H(11)	119.7
O(4)-C(5)-C(12)	114.95(14)	C(5)-C(12)-H(12A)	109.5
C(4)-C(5)-C(12)	118.97(14)	C(5)-C(12)-H(12B)	109.5
C(7)-C(6)-C(11)	118.84(15)	H(12A)-C(12)-H(12B)	109.5
C(7)-C(6)-C(3)	121.37(14)	C(5)-C(12)-H(12C)	109.5
C(11)-C(6)-C(3)	119.78(14)	H(12A)-C(12)-H(12C)	109.5
C(8)-C(7)-C(6)	120.49(15)	H(12B)-C(12)-H(12C)	109.5
C(8)-C(7)-H(7)	119.8	C(3)-O(3)-Rh(1)	125.21(11)
C(6)-C(7)-H(7)	119.8	C(5)-O(4)-Rh(1)	125.63(11)
C(7)-C(8)-C(9)	120.35(15)	C(2)-Rh(1)-C(1)	87.98(7)
C(7)-C(8)-H(8)	119.8	C(2)-Rh(1)-O(4)	88.53(6)
C(9)-C(8)-H(8)	119.8	C(1)-Rh(1)-O(4)	175.86(6)
C(2)-Rh(1)-O(3)	179.13(6)	O(4)-Rh(1)-O(3)	90.62(5)
C(1)-Rh(1)-O(3)	92.87(6)		

A 2. Supplementary Data for [Rh(F_3-bzac)($CO)_2$]

Table A 2.1: Atomic coordinates and equivalent isotropic displacement parameters (Å^2) for [Rh(F_3-bzac)($CO)_2$]. U(eq) is defined as one third of the trace of the orthogonalized U^{ij} tensor.

Atom	*x*	*y*	*z*	U_{eq}
C(1)	9516(5)	4200(4)	957(1)	27(1)
C(2)	10229(5)	3050(4)	270(1)	28(1)
C(3)	8955(5)	1308(4)	1677(1)	23(1)
C(4)	9039(5)	266(4)	1441(1)	24(1)
C(5)	9380(5)	180(4)	993(1)	26(1)
C(6)	8597(5)	1288(4)	2165(1)	21(1)
C(7)	9091(5)	356(4)	2429(1)	24(1)
C(8)	8828(5)	398(4)	2885(1)	25(1)
C(9)	8041(5)	1359(4)	3080(1)	23(1)
C(10)	7526(5)	2288(4)	2819(1)	24(1)
C(11)	7829(5)	2247(4)	2368(1)	24(1)
C(12)	9358(6)	-994(4)	775(1)	33(1)
O(1)	9428(4)	5162(3)	1013(1)	36(1)
O(2)	10608(4)	3322(3)	-80(1)	39(1)
O(3)	9127(3)	2289(2)	1503(1)	23(1)
O(4)	9706(4)	973(3)	710(1)	29(1)
F(1)	10995(4)	-1221(3)	582(1)	69(1)
F(2)	8043(4)	-1047(3)	464(1)	61(1)
F(3)	9006(7)	-1836(3)	1054(1)	86(1)
Rh(1)	9649(1)	2664(1)	852(1)	24(1)

Table A 2.2: Hydrogen coordinates and isotropic displacement parameters (Å^2) for [Rh(F_3-bzac)($CO)_2$].

Atom	*x*	*y*	*z*	U_{eq}
H(4)	8851	-405	1600	29
H(7)	9599	-295	2298	29
H(8)	9179	-219	3060	30
H(9)	7857	1383	3386	28
H(10)	6983	2930	2949	29
H(11)	7511	2876	2194	29

Table A 2.3: Anisotropic displacement parameters ($Å^2$) for [Rh(F_3-bzac)($CO)_2$]. The anisotropic displacement factor exponent takes the form: $-2\pi^2[h^2a^{*2}U^{11} + \ldots + 2hka^*b^*U^{23}]$.

Atom	U^{11}	U^{22}	U^{33}	U^{12}	U^{13}	U^{23}
C(1)	26(2)	33(3)	21(2)	5(2)	1(2)	2(2)
C(2)	26(2)	29(3)	30(3)	-4(2)	-5(2)	2(2)
C(3)	16(2)	24(3)	30(2)	0(2)	-4(2)	0(2)
C(4)	23(2)	23(3)	27(2)	-2(2)	-5(2)	0(2)
C(5)	21(2)	24(3)	33(2)	-3(2)	-5(2)	0(2)
C(6)	13(2)	24(2)	25(2)	2(2)	-2(1)	-5(2)
C(7)	18(2)	26(3)	27(2)	-4(2)	0(2)	-3(2)
C(8)	22(2)	27(3)	25(2)	5(2)	1(2)	-1(2)
C(9)	19(2)	30(3)	21(2)	1(2)	2(1)	-3(2)
C(10)	19(2)	29(3)	25(2)	-3(2)	1(2)	2(2)
C(11)	14(2)	26(3)	33(2)	2(2)	-5(2)	-1(2)
C(12)	32(2)	37(3)	29(3)	-7(2)	-1(2)	-2(2)
O(1)	45(2)	34(2)	30(2)	3(2)	3(1)	5(2)
O(2)	42(2)	49(2)	25(2)	5(2)	3(1)	1(2)
O(3)	24(1)	23(2)	23(2)	1(1)	-2(1)	1(1)
O(4)	30(1)	30(2)	25(2)	-2(1)	0(1)	-3(1)
F(1)	37(2)	55(2)	117(3)	-47(2)	11(2)	-1(2)
F(2)	55(2)	56(2)	72(2)	-33(2)	-29(2)	8(2)
F(3)	187(4)	29(2)	43(2)	-9(2)	20(2)	-21(2)
Rh(1)	23(1)	28(1)	21(1)	1(1)	-1(1)	1(1)

Table A 2.4: Complete listing of bond lengths (Å) for [Rh(F_3-bzac)($CO)_2$].

Bond	Distance	Bond	Distance
C(1)-O(1)	1.143(6)	C(6)-C(7)	1.395(5)
C(1)-Rh(1)	1.832(5)	C(7)-C(8)	1.385(5)
C(2)-O(2)	1.133(5)	C(8)-C(9)	1.386(6)
C(2)-Rh(1)	1.854(4)	C(9)-C(10)	1.390(6)
C(3)-O(3)	1.270(5)	C(10)-C(11)	1.377(6)
C(3)-C(4)	1.414(6)	C(12)-F(1)	1.315(5)
C(3)-C(6)	1.491(5)	C(12)-F(2)	1.317(5)
C(4)-C(5)	1.375(5)	C(12)-F(3)	1.320(6)

C(5)-O(4)	1.281(5)	O(3)-Rh(1)	2.043(3)
C(5)-C(12)	1.526(6)	O(4)-Rh(1)	2.030(4)
C(6)-C(11)	1.388(6)		

Table A 2.5: Complete listing of bond angles (º) for [Rh(F_3-bzac)($CO)_2$].

Angle	Value	Angle	Value
O(1)-C(1)-Rh(1)	178.6(4)	F(1)-C(12)-F(2)	106.7(4)
O(2)-C(2)-Rh(1)	177.5(4)	F(1)-C(12)-F(3)	107.1(4)
O(3)-C(3)-C(4)	125.0(4)	F(2)-C(12)-F(3)	106.7(4)
O(3)-C(3)-C(6)	115.8(4)	F(1)-C(12)-C(5)	111.3(4)
C(4)-C(3)-C(6)	119.2(4)	F(1)-C(12)-F(2)	106.7(4)
C(5)-C(4)-C(3)	124.3(4)	F(2)-C(12)-C(5)	110.8(4)
O(4)-C(5)-C(4)	129.1(4)	F(3)-C(12)-C(5)	113.9(4)
O(4)-C(5)-C(12)	111.9(4)	C(3)-O(3)-Rh(1)	127.3(3)
C(4)-C(5)-C(12)	119.0(4)	C(5)-O(4)-Rh(1)	124.5(3)
C(11)-C(6)-C(7)	118.8(4)	C(1)-Rh(1)-C(2)	86.19(18)
C(11)-C(6)-C(3)	119.0(4)	C(1)-Rh(1)-O(4)	177.16(14)
C(7)-C(6)-C(3)	122.1(4)	C(2)-Rh(1)-O(4)	92.05(16)
C(8)-C(7)-C(6)	120.2(4)	C(1)-Rh(1)-O(3)	92.12(15)
C(7)-C(8)-C(9)	120.1(4)	C(2)-Rh(1)-O(3)	177.03(14)
C(8)-C(9)-C(10)	120.2(4)	O(4)-Rh(1)-O(3)	89.73(11)
C(11)-C(10)-C(9)	119.3(4)		
C(10)-C(11)-C(6)	121.4(4)		

A 3. Supplementary Data for [Rh(F_3-4Clbzac)($CO)_2$] i

Table A 3.1: Atomic coordinates and equivalent isotropic displacement parameters ($Å^2$) for [Rh(F_3-4Clbzac)($CO)_2$]. U(eq) is defined as one third of the trace of the orthogonalized U^{ij} tensor.

Atom	*x*	*y*	*z*	U_{eq}
C(1A)	4399(12)	6879(5)	7991(2)	19(2)
C(1B)	9154(12)	9094(4)	7952(2)	19(2)
C(1C)	10823(15)	8871(5)	10399(2)	24(2)
C(1D)	10721(15)	3858(5)	9437(2)	21(2)

C(2A)	3697(11)	7918(5)	8385(2)	23(2)
C(2B)	8711(12)	8118(6)	8380(2)	27(2)
C(2C)	10692(14)	9868(5)	10822(2)	32(2)
C(2D)	10545(14)	4865(5)	9015(2)	28(2)
C(3A)	5094(11)	8592(5)	7403(2)	18(2)
C(3B)	10179(10)	7307(5)	7415(2)	16(2)
C(3C)	10899(12)	10621(4)	9826(2)	19(2)
C(3D)	10874(13)	5623(4)	10008(2)	19(2)
C(4A)	5010(11)	9365(5)	7505(2)	17(2)
C(4B)	10222(11)	6554(5)	7542(2)	18(2)
C(4C)	10852(14)	11389(4)	9938(2)	20(2)
C(4D)	10902(17)	6389(4)	9892(2)	27(2)
C(5A)	4557(11)	9577(4)	7784(2)	16(2)
C(5B)	9779(10)	6381(5)	7827(2)	16(2)
C(5C)	10798(13)	11564(4)	10224(2)	19(2)
C(5D)	10820(20)	6567(5)	9605(2)	36(2)
C(6A)	5501(11)	8445(5)	7091(2)	16(2)
C(6B)	10599(12)	7420(4)	7104(2)	16(2)
C(6C)	10979(12)	10482(4)	9508(2)	17(2)
C(6D)	10965(12)	5493(4)	10326(2)	16(2)
C(7A)	5683(12)	9040(4)	6889(2)	18(2)
C(7B)	10662(13)	8188(4)	6993(2)	18(2)
C(7C)	11025(12)	11082(5)	9304(2)	23(2)
C(7D)	11013(12)	4719(4)	10425(2)	19(2)
C(8A)	6088(11)	8879(5)	6602(2)	21(2)
C(8B)	11055(11)	8324(5)	6705(2)	21(2)
C(8C)	11138(11)	10928(5)	9012(2)	24(2)
C(8D)	11063(12)	4552(5)	10721(2)	24(2)
C(9A)	6320(10)	8109(5)	6515(2)	20(2)
C(9B)	11360(11)	7696(5)	6523(2)	20(2)
C(9C)	11121(10)	10165(5)	8916(2)	20(2)
C(9D)	11060(11)	5176(5)	10913(2)	24(2)
C(10A)	6159(11)	7509(5)	6710(2)	23(2)
C(10B)	11315(11)	6934(5)	6624(2)	23(2)
C(10C)	11065(12)	9547(5)	9115(2)	21(2)
C(10D)	10996(12)	5939(5)	10819(2)	21(2)
C(11A)	5763(12)	7673(4)	6996(2)	17(2)

C(11B)	10932(12)	6794(4)	6914(2)	17(2)
C(11C)	10989(12)	9709(4)	9409(2)	20(2)
C(11D)	10949(13)	6106(5)	10528(2)	22(2)
C(12A)	4495(13)	10441(5)	7862(2)	20(2)
C(12B)	9803(11)	5537(5)	7923(2)	21(2)
C(12C)	10805(14)	12441(4)	10311(2)	21(2)
C(12D)	10830(20)	7416(5)	9518(2)	36(2)
O(1A)	4533(10)	6227(4)	7989(2)	36(2)
O(1B)	9130(10)	9757(3)	7920(1)	25(1)
O(1C)	10849(11)	8205(3)	10382(1)	33(2)
O(1D)	10761(11)	3213(3)	9460(1)	29(1)
O(2A)	3379(10)	7899(4)	8628(1)	39(2)
O(2B)	8431(10)	8156(4)	8623(2)	38(2)
O(2C)	10594(12)	9805(4)	11067(1)	46(2)
O(2D)	10411(11)	4833(4)	8770(1)	41(2)
O(3A)	4783(7)	7991(3)	7559(1)	18(1)
O(3B)	9779(7)	7926(3)	7557(1)	17(1)
O(3C)	10894(9)	10012(3)	9983(1)	21(1)
O(3D)	10838(8)	5016(3)	9853(1)	20(1)
O(4A)	4144(9)	9150(3)	8003(1)	21(1)
O(4B)	9306(10)	6840(3)	8033(1)	22(1)
O(4C)	10788(10)	11129(3)	10450(1)	23(1)
O(4D)	10725(10)	6126(3)	9386(1)	25(1)
F(1A)	5194(9)	10895(3)	7653(1)	39(2)
F(1B)	10624(11)	5059(3)	7733(1)	52(2)
F(1C)	12324(9)	12622(3)	10469(2)	47(2)
F(1D)	9360(20)	7612(4)	9351(2)	111(3)
F(2A)	5474(8)	10594(3)	8101(1)	31(1)
F(2B)	8044(8)	5282(3)	7977(2)	57(2)
F(2C)	9265(10)	12609(3)	10471(1)	47(2)
F(2D)	12340(9)	7584(4)	9345(2)	70(3)
F(3A)	2694(7)	10674(3)	7911(1)	35(1)
F(3B)	10786(11)	5447(3)	8166(1)	44(1)
F(3C)	10751(14)	12913(3)	10086(1)	59(2)
F(3D)	11106(19)	7901(4)	9726(2)	111(3)
Cl(1B)	11902(3)	7862(2)	6159(1)	30(1)
Cl(1C)	11231(3)	9966(1)	8549(1)	28(1)

ClA	6845(3)	7916(1)	6154(1)	27(1)
Cl(1D)	11145(3)	4975(2)	11283(1)	31(1)
Rh(1A)	4232(1)	7961(1)	7993(1)	17(1)
Rh(1B)	9233(1)	8025(1)	7990(1)	18(1)
Rh(1C)	10789(1)	9944(1)	10424(1)	20(1)
Rh(1D)	10696(1)	4943(1)	9414(1)	20(1)

Table A 3.2: Hydrogen coordinates and isotropic displacement parameters ($Å^2$) for [Rh(F_3-4Clbzac)$(CO)_2$].

Atom	*x*	*y*	*z*	U_{eq}
H(4A)	5285	9771	7370	21
H(4B)	10588	6131	7421	21
H(4C)	10859	11810	9804	24
H(4D)	10987	6811	10026	33
H(7A)	5525	9567	6948	22
H(7B)	10431	8617	7119	21
H(7C)	10978	11609	9368	28
H(7D)	11010	4303	10289	23
H(8A)	6208	9291	6466	26
H(8B)	11114	8843	6633	25
H(8C)	11228	11345	8877	28
H(8D)	11098	4028	10789	29
H(10A)	6318	6983	6648	27
H(10B)	11545	6511	6496	27
H(10C)	11077	9022	9048	25
H(10D)	10984	6353	10957	25
H(11A)	5665	7257	7131	21
H(11B)	10894	6273	6985	20
H(11C)	10945	9291	9544	24
H(11D)	10906	6633	10464	27

Table A 3.3: Anisotropic displacement parameters ($Å^2$) for [Rh(F_3-4Clbzac)$(CO)_2$]. The anisotropic displacement factor exponent takes the form: $-2\pi^2[h^2a^{*2}U^{11} + \ldots + 2hka^*b^*U^{23}]$.

Atom	U^{11}	U^{22}	U^{33}	U^{12}	U^{13}	U^{23}
C(1A)	19(4)	24(4)	13(4)	0(3)	2(4)	-1(4)

C(1B)	12(3)	25(4)	19(4)	-8(3)	-1(4)	-1(3)
C(1C)	26(4)	27(5)	19(5)	3(4)	-3(5)	1(4)
C(1D)	29(4)	23(4)	11(4)	-3(3)	-3(4)	4(4)
C(2A)	19(4)	19(4)	32(6)	6(4)	2(4)	-5(3)
C(2B)	22(4)	31(5)	28(6)	-13(4)	1(4)	-3(4)
C(2C)	30(4)	29(5)	36(6)	0(4)	3(4)	7(5)
C(2D)	34(5)	20(4)	30(5)	-3(4)	0(4)	3(4)
C(3A)	12(3)	24(5)	18(5)	-1(4)	0(3)	2(3)
C(3B)	11(3)	16(4)	20(5)	-5(3)	-6(3)	0(3)
C(3C)	17(4)	19(4)	20(4)	3(3)	-3(4)	-5(4)
C(3D)	18(4)	19(4)	20(4)	4(3)	-1(4)	-1(4)
C(4A)	22(4)	19(4)	11(4)	3(3)	-1(3)	0(3)
C(4B)	26(4)	14(4)	14(4)	2(3)	-2(3)	1(3)
C(4C)	32(4)	14(4)	14(4)	0(3)	2(4)	2(4)
C(4D)	52(6)	11(4)	18(5)	-5(3)	3(5)	-1(4)
C(5A)	13(4)	7(3)	28(5)	-2(3)	-4(3)	-1(3)
C(5B)	12(3)	14(4)	22(5)	-1(3)	2(3)	-2(3)
C(5C)	14(3)	14(4)	30(5)	1(3)	2(4)	1(4)
C(5D)	71(5)	12(3)	25(4)	5(3)	-1(4)	-2(4)
C(6A)	10(3)	25(4)	13(4)	-1(3)	-2(3)	-1(3)
C(6B)	13(3)	13(3)	21(4)	-3(3)	-2(3)	4(3)
C(6C)	17(4)	14(4)	20(4)	-1(3)	-1(3)	-1(3)
C(6D)	14(3)	16(4)	17(4)	-3(3)	-4(3)	1(3)
C(7A)	17(3)	17(4)	21(4)	-2(3)	2(4)	0(4)
C(7B)	21(4)	16(4)	17(4)	0(3)	-3(4)	-1(3)
C(7C)	26(4)	21(4)	23(5)	1(3)	-1(4)	2(4)
C(7D)	22(4)	20(4)	15(4)	0(3)	0(4)	-2(3)
C(8A)	17(4)	25(4)	22(5)	7(3)	4(3)	8(3)
C(8B)	15(4)	23(4)	24(5)	5(3)	-3(3)	0(3)
C(8C)	22(4)	25(4)	24(5)	7(4)	-5(3)	2(3)
C(8D)	20(4)	24(4)	28(5)	10(4)	3(4)	-1(3)
C(9A)	15(4)	31(5)	14(4)	-5(4)	1(3)	-4(3)
C(9B)	12(4)	31(5)	17(5)	2(4)	1(3)	-1(3)
C(9C)	12(3)	30(5)	16(4)	-2(3)	1(3)	-4(3)
C(9D)	13(4)	39(5)	18(4)	2(4)	1(3)	1(4)
C(10A)	21(4)	18(4)	29(5)	-3(4)	-3(3)	-1(3)
C(10B)	20(4)	28(5)	20(5)	-7(4)	3(3)	9(3)

C(10C)	30(5)	17(4)	17(4)	-4(3)	0(4)	1(4)
C(10D)	21(4)	26(4)	15(4)	-3(3)	-1(4)	-2(4)
C(11A)	13(3)	18(4)	21(4)	1(3)	-1(4)	-1(3)
C(11B)	16(4)	10(3)	24(5)	0(3)	2(4)	6(3)
C(11C)	22(4)	15(4)	23(5)	0(3)	2(4)	-2(3)
C(11D)	29(4)	18(4)	20(4)	4(3)	1(4)	2(4)
C(12A)	22(4)	17(4)	22(5)	2(3)	3(4)	-3(3)
C(12B)	24(4)	16(4)	23(5)	1(3)	5(3)	-4(3)
C(12C)	22(4)	19(4)	21(4)	1(3)	5(4)	4(4)
C(12D)	71(5)	12(3)	25(4)	5(3)	-1(4)	-2(4)
O(1A)	38(4)	20(3)	50(4)	1(3)	2(4)	-6(3)
O(1B)	36(3)	14(3)	26(3)	-1(2)	-4(3)	-3(3)
O(1C)	41(4)	19(3)	40(4)	4(3)	2(4)	3(3)
O(1D)	37(3)	19(3)	30(4)	-1(2)	3(4)	5(3)
O(2A)	51(4)	47(5)	18(4)	6(3)	6(3)	-2(4)
O(2B)	49(4)	41(4)	25(4)	-7(3)	12(3)	-2(3)
O(2C)	59(4)	55(5)	23(4)	3(3)	-2(4)	13(4)
O(2D)	66(5)	40(4)	16(3)	1(3)	-4(3)	5(4)
O(3A)	24(3)	14(3)	15(3)	2(2)	0(2)	-5(2)
O(3B)	20(3)	12(3)	20(3)	0(2)	2(2)	0(2)
O(3C)	33(3)	13(2)	18(3)	1(3)	0(2)	3(3)
O(3D)	26(2)	13(2)	20(3)	-1(3)	-1(2)	3(3)
O(4A)	30(3)	15(3)	18(3)	2(2)	10(3)	-2(3)
O(4B)	24(3)	12(2)	29(3)	-2(2)	2(3)	-3(3)
O(4C)	33(3)	15(3)	20(3)	2(2)	-3(3)	2(3)
O(4D)	36(3)	20(3)	19(3)	0(2)	0(3)	7(3)
F(1A)	71(4)	16(3)	28(3)	0(2)	20(3)	-5(2)
F(1B)	100(5)	19(3)	36(3)	2(3)	22(3)	14(4)
F(1C)	37(3)	31(3)	74(5)	-16(3)	-22(3)	1(3)
F(1D)	222(8)	27(3)	84(4)	23(3)	3(6)	5(5)
F(2A)	40(3)	23(3)	29(3)	-8(2)	-15(3)	-4(2)
F(2B)	29(3)	29(3)	113(6)	23(4)	1(4)	-7(2)
F(2C)	39(3)	29(3)	73(4)	-13(3)	20(4)	10(3)
F(2D)	37(3)	42(4)	131(7)	55(4)	-8(4)	-12(3)
F(3A)	24(3)	24(3)	58(4)	-6(3)	0(3)	7(2)
F(3B)	63(4)	31(3)	38(3)	15(2)	-11(4)	0(3)
F(3C)	139(6)	15(3)	23(3)	-2(2)	0(4)	1(4)

F(3D)	222(8)	27(3)	84(4)	23(3)	3(6)	5(5)
Cl(1B)	22(1)	50(2)	19(1)	2(1)	1(1)	-1(1)
Cl(1C)	31(1)	35(1)	17(1)	-4(1)	1(1)	-3(1)
ClA	24(1)	38(1)	18(1)	-3(1)	4(1)	2(1)
Cl(1D)	29(1)	48(1)	17(1)	3(1)	0(1)	1(1)
Rh(1A)	20(1)	16(1)	16(1)	3(1)	0(1)	-2(1)
Rh(1B)	20(1)	15(1)	18(1)	-3(1)	1(1)	-1(1)
Rh(1C)	24(1)	17(1)	18(1)	3(1)	-1(1)	1(1)
Rh(1D)	27(1)	15(1)	17(1)	0(1)	2(1)	1(1)

Table A 3.4: Complete listing of bond lengths (Å) for [Rh(F_3-4Clbzac)$(CO)_2$].

Bond	Distance	Bond	Distance
C(1A)-O(1A)	1.113(9)	C(6C)-C(7C)	1.393(11)
C(1A)-Rh(1A)	1.860(7)	C(6C)-C(11C)	1.401(10)
C(1B)-O(1B)	1.139 (9)	C(6D)-C(11D)	1.402(11)
C(1B)-Rh(1B)	1.842(7)	C(6D)-C(7D)	1.402(10)
C(1C)-O(1C)	1.142(9)	C(7A)-C(8A)	1.378(11)
C(1C)-Rh(1C)	1.838(7)	C(7B)-C(8B)	1.376(12)
C(1D)-O(1D)	1.120(9)	C(7C)-C(8C)	1.371(12)
C(1D)-Rh(1D)	1.854(7)	C(7D)-C(8D)	1.395(12)
C(2A)-O(2A)	1.140(10)	C(8A)-C(9A)	1.386(12)
C(2A)-Rh(1A)	1.850(9)	C(8B)-C(9B)	1.381(12)
C(2B)-O(2B)	1.140(10)	C(8C)-C(9C)	1.378(12)
C(2B)-Rh(1B)	1.841(9)	C(8D)-C(9D)	1.388(12)
C(2C)-O(2C)	1.140(10)	C(9A)-C(10A)	1.369(12)
C(2C)-Rh(1C)	1.841(8)	C(9A)-ClA	1.736(7)
C(2D)-O(2D)	1.134(9)	C(9B)-C(10B)	1.386(12)
C(2D)-Rh(1D)	1.846(8)	C(9B)-Cl(1B)	1.744(8)
C(3A)-O(3A)	1.276(9)	C(9C)-C(10C)	1.399(11)
C(3A)-C(4A)	1.405(11)	C(9C)-Cl(1C)	1.733(7)
C(3A)-C(6A)	1.487(11)	C(9D)-C(10D)	1.378(12)
C(3B)-O(3B)	1.276(9)	C(9D)-Cl(1D)	1.740(7)
C(3B)-C(4B)	1.416(11)	C(10A)-C(11A)	1.376(11)
C(3B)-C(6B)	1.475(12)	C(10B)-C(11B)	1.384(12)
C(3C)-O(3C)	1.271(8)	C(10C)-C(11C)	1.385(12)
C(3C)-C(4C)	1.413(10)	C(10D)-C(11D)	1.374(11)

C(3C)-C(6C)	1.488(11)	C(12A)-F(2A)	1.319(10)
C(3D)-O(3D)	1.262(8)	C(12A)-F(3A)	1.332(9)
C(3D)-C(4D)	1.416(10)	C(12A)-F(1A)	1.331(9)
C(3D)-C(6D)	1.485(11)	C(12B)-F(2B)	1.320(9)
C(4A)-C(5A)	1.377(12)	C(12B)-F(3B)	1.327(9)
C(4B)-C(5B)	1.381(12)	C(12B)-F(1B)	1.325(10)
C(4C)-C(5C)	1.351(11)	C(12C)-F(3C)	1.318(8)
C(4D)-C(5D)	1.360(12)	C(12C)-F(1C)	1.320(11)
C(5A)-O(4A)	1.278(8)	C(12C)-F(2C)	1.330(10)
C(5A)-C(12A)	1.522(10)	C(12D)-F(3D)	1.286(12)
C(5B)-O(4B)	1.277(8)	C(12D)-F(1D)	1.322(16)
C(5B)-C(12B)	1.512(11)	C(12D)-F(2D)	1.348(14)
C(5C)-O(4C)	1.280(9)	O(3A)-Rh(1A)	2.037(5)
C(5C)-C(12C)	1.553(10)	O(3B)-Rh(1B)	2.037(5)
C(5D)-O(4D)	1.266(9)	O(3C)-Rh(1C)	2.038(4)
C(5D)-C(12D)	1.509(11)	O(3D)-Rh(1D)	2.030(4)
C(6A)-C(7A)	1.388(11)	O(4A)-Rh(1A)	2.032(4)
C(6A)-C(11A)	1.403(10)	O(4B)-Rh(1B)	2.037(5)
C(6B)-C(11B)	1.404(10)	O(4C)-Rh(1C)	2.034(5)
C(6B)-C(7B)	1.411(10)	O(4D)-Rh(1D)	2.031(5)

Table A 3.5: Complete listing of bond angles (º) for [Rh(F_3-4Clbzac)$(CO)_2$].

Angle	Value	Angle	Value
O(1A)-C(1A)-Rh(1A)	178.7(8)	C(10C)-C(11C)-C(6C)	120.5(7)
O(1B)-C(1B)-Rh(1B)	177.9(7)	C(10D)-C(11D)-C(6D)	119.5(8)
O(1C)-C(1C)-Rh(1C)	179.5(9)	F(2A)-C(12A)-F(3A)	106.5(7)
O(1D)-C(1D)-Rh(1D)	177.8(8)	O(3A)-C(3A)-C(6A)	116.2(7)
O(2A)-C(2A)-Rh(1A)	179.2(8)	C(4A)-C(3A)-C(6A)	119.4(8)
O(2B)-C(2B)-Rh(1B)	177.8(9)	O(3B)-C(3B)-C(4B)	123.2(8)
O(2C)-C(2C)-Rh(1C)	178.1(10)	O(3B)-C(3B)-C(6B)	115.7(7)
O(2D)-C(2D)-Rh(1D)	178.0(8)	C(4B)-C(3B)-C(6B)	121.2(7)
O(3A)-C(3A)-C(4A)	124.4(8)	O(3C)-C(3C)-C(4C)	123.6(7)
O(3A)-C(3A)-C(6A)	116.2(7)	O(3C)-C(3C)-C(6C)	115.6(7)
C(4A)-C(3A)-C(6A)	119.4(8)	C(4C)-C(3C)-C(6C)	120.8(7)
O(3B)-C(3B)-C(4B)	123.2(8)	O(3D)-C(3D)-C(4D)	123.2(7)
O(3B)-C(3B)-C(6B)	115.7(7)	O(3D)-C(3D)-C(6D)	116.0(7)

C(4B)-C(3B)-C(6B)	121.2(7)	F(2A)-C(12A)-F(1A)	107.6(7)
O(3C)-C(3C)-C(4C)	123.6(7)	F(3A)-C(12A)-F(1A)	106.5(7)
O(3C)-C(3C)-C(6C)	115.6(7)	F(2A)-C(12A)-C(5A)	112.0(7)
C(4C)-C(3C)-C(6C)	120.8(7)	F(3A)-C(12A)-C(5A)	110.9(7)
O(3D)-C(3D)-C(4D)	123.2(7)	F(1A)-C(12A)-C(5A)	112.7(7)
O(3D)-C(3D)-C(6D)	116.0(7)	F(2B)-C(12B)-F(3B)	106.0(7)
C(4D)-C(3D)-C(6D)	120.7(7)	F(2B)-C(12B)-F(1B)	108.6(8)
C(5A)-C(4A)-C(3A)	124.8(8)	F(3B)-C(12B)-F(1B)	105.4(7)
C(5B)-C(4B)-C(3B)	125.7(8)	F(2B)-C(12B)-C(5B)	111.1(7)
C(5C)-C(4C)-C(3C)	124.4(7)	F(3B)-C(12B)-C(5B)	111.5(7)
C(5D)-C(4D)-C(3D)	125.1(8)	F(1B)-C(12B)-C(5B)	113.6(7)
O(4A)-C(5A)-C(4A)	129.8(7)	F(3C)-C(12C)-F(1C)	108.4(8)
O(4A)-C(5A)-C(12A)	111.2(7)	F(3C)-C(12C)-F(2C)	106.3(8)
C(4A)-C(5A)-C(12A)	119.0(8)	F(1C)-C(12C)-F(2C)	106.4(7)
O(4B)-C(5B)-C(4B)	129.3(8)	F(3C)-C(12C)-C(5C)	113.1(7)
O(4B)-C(5B)-C(12B)	111.9(7)	F(1C)-C(12C)-C(5C)	111.8(7)
C(4B)-C(5B)-C(12B)	118.8(7)	F(2C)-C(12C)-C(5C)	110.5(7)
O(4C)-C(5C)-C(4C)	131.6(7)	F(3D)-C(12D)-F(1D)	112.9(10)
O(4C)-C(5C)-C(12C)	110.7(7)	F(3D)-C(12D)-F(2D)	100.9(9)
C(4C)-C(5C)-C(12C)	117.7(7)	F(1D)-C(12D)-F(2D)	101.5(9)
O(4D)-C(5D)-C(4D)	130.4(8)	F(3D)-C(12D)-C(5D)	114.9(8)
O(4D)-C(5D)-C(12D)	111.1(8)	F(1D)-C(12D)-C(5D)	113.4(10)
C(4D)-C(5D)-C(12D)	118.5(8)	F(2D)-C(12D)-C(5D)	111.6(10)
C(7A)-C(6A)-C(11A)	117.9(7)	C(3A)-O(3A)-Rh(1A)	127.3(5)
C(7A)-C(6A)-C(3A)	123.0(7)	C(3B)-O(3B)-Rh(1B)	127.8(5)
C(11A)-C(6A)-C(3A)	119.1(7)	C(3C)-O(3C)-Rh(1C)	128.1(5)
C(11B)-C(6B)-C(7B)	118.7(7)	C(3D)-O(3D)-Rh(1D)	128.1(5)
C(11B)-C(6B)-C(3B)	122.6(7)	C(5A)-O(4A)-Rh(1A)	123.0(5)
C(7B)-C(6B)-C(3B)	118.7(7)	C(5B)-O(4B)-Rh(1B)	123.2(5)
C(7C)-C(6C)-C(11C)	118.5(7)	C(5C)-O(4C)-Rh(1C)	122.2(5)
C(7C)-C(6C)-C(3C)	123.3(7)	C(5D)-O(4D)-Rh(1D)	123.1(5)
C(11C)-C(6C)-C(3C)	118.2(7)	C(2A)-Rh(1A)-C(1A)	88.7(4)
C(11D)-C(6D)-C(7D)	119.5(7)	C(2A)-Rh(1A)-O(4A)	90.6(3)
C(11D)-C(6D)-C(3D)	122.9(7)	C(1A)-Rh(1A)-O(4A)	177.8(3)
C(7D)-C(6D)-C(3D)	117.6(7)	C(2A)-Rh(1A)-O(3A)	178.8(3)
C(8A)-C(7A)-C(6A)	121.1(7)	C(1A)-Rh(1A)-O(3A)	90.6(3)
C(8B)-C(7B)-C(6B)	120.9(7)	O(4A)-Rh(1A)-O(3A)	90.2(2)

C(8C)-C(7C)-C(6C)	121.4(8)	C(1B)-Rh(1B)-C(2B)	90.1(4)
C(8D)-C(7D)-C(6D)	120.8(7)	C(1B)-Rh(1B)-O(3B)	89.7(3)
C(7A)-C(8A)-C(9A)	119.4(8)	C(2B)-Rh(1B)-O(3B)	179.3(3)
C(7B)-C(8B)-C(9B)	119.2(8)	C(1B)-Rh(1B)-O(4B)	179.7(3)
C(7C)-C(8C)-C(9C)	119.7(8)	C(2B)-Rh(1B)-O(4B)	89.8(3)
C(9D)-C(8D)-C(7D)	117.9(8)	O(3B)-Rh(1B)-O(4B)	90.4(2)
C(10A)-C(9A)-C(8A)	120.9(8)	C(1C)-Rh(1C)-C(2C)	89.5(4)
C(10A)-C(9A)-ClA	120.3(7)	C(1C)-Rh(1C)-O(4C)	179.3(3)
C(8A)-C(9A)-ClA	118.8(7)	C(2C)-Rh(1C)-O(4C)	90.7(3)
C(8B)-C(9B)-C(10B)	121.5(8)	C(1C)-Rh(1C)-O(3C)	89.7(3)
C(8B)-C(9B)-Cl(1B)	119.6(7)	C(2C)-Rh(1C)-O(3C)	179.3(3)
C(10B)-C(9B)-Cl(1B)	118.9(7)	O(4C)-Rh(1C)-O(3C)	90.1(2)
C(8C)-C(9C)-C(10C)	120.5(7)	C(2D)-Rh(1D)-C(1D)	89.2(4)
C(8C)-C(9C)-Cl(1C)	120.0(7)	C(2D)-Rh(1D)-O(4D)	90.6(3)
C(10C)-C(9C)-Cl(1C)	119.5(6)	C(1D)-Rh(1D)-O(4D)	178.9(3)
C(10D)-C(9D)-C(8D)	121.9(8)	C(2D)-Rh(1D)-O(3D)	179.2(3)
C(10D)-C(9D)-Cl(1D)	119.8(7)	C(1D)-Rh(1D)-O(3D)	90.1(3)
C(8D)-C(9D)-Cl(1D)	118.3(7)	O(4D)-Rh(1D)-O(3D)	90.1(2)
C(9A)-C(10A)-C(11A)	119.5(8)		
C(11B)-C(10B)-C(9B)	119.6(8)		
C(11C)-C(10C)-C(9C)	119.4(7)		
C(11D)-C(10D)-C(9D)	120.4(8)		
C(10A)-C(11A)-C(6A)	121.2(7)		
C(10B)-C(11B)-C(6B)	120.2(7)		

A 4. Supplementary Data for [Rh(F_3-4Clbzac)($CO)_2$] ii

Table A 4.1: Atomic coordinates and equivalent isotropic displacement parameters (Å^2) for [Rh(F_3-4Clbzac)($CO)_2$]. U(eq) is defined as one third of the trace of the orthogonalized U^{ij} tensor.

Atom	*x*	*y*	*z*	U_{eq}
C(1A)	7030(20)	1820(17)	1022(8)	75(5)
C(1B)	12132(19)	2079(12)	3195(7)	48(3)
C(2A)	6620(30)	3462(14)	1682(11)	79(5)
C(2B)	11590(30)	3719(16)	1857(14)	88(6)
C(3A)	7568(14)	-490(11)	3244(7)	50(3)

C(3B)	12502(15)	-153(12)	1911(6)	49(3)
C(4A)	7411(14)	-26(12)	3905(6)	47(3)
C(4B)	12319(17)	331(14)	1043(7)	60(3)
C(5A)	7236(15)	1062(11)	3862(6)	45(2)
C(5B)	12016(18)	1483(14)	668(7)	56(3)
C(6A)	7850(20)	-1769(17)	3336(8)	67(3)
C(6B)	12784(14)	-1398(12)	2296(7)	50(3)
C(7A)	7998(16)	-2508(12)	4114(7)	52(3)
C(7B)	12828(18)	-1804(13)	3151(8)	56(3)
C(8A)	8260(20)	-3722(13)	4215(8)	60(3)
C(8B)	13100(19)	-2999(15)	3533(9)	70(4)
C(9A)	8328(18)	-4062(13)	3524(9)	56(3)
C(9B)	13261(18)	-3747(13)	3092(10)	63(4)
C(10A)	8230(20)	-3265(17)	2744(9)	72(4)
C(10B)	13210(20)	-3365(13)	2217(9)	64(3)
C(11A)	7951(16)	-2115(14)	2681(7)	58(3)
C(11B)	13011(16)	-2164(12)	1862(7)	53(3)
C(12A)	7197(16)	1357(15)	4624(8)	69(4)
C(12B)	11958(19)	1744(15)	-262(8)	67(3)
O(1A)	6930(20)	1810(16)	379(8)	110(4)
O(1B)	12260(20)	2021(12)	3857(7)	91(3)
O(2A)	6440(20)	4502(17)	1461(8)	110(4)
O(2B)	11200(20)	4781(12)	1646(7)	91(3)
O(3A)	7493(13)	167(8)	2500(5)	53(2)
O(3B)	12480(12)	474(9)	2387(5)	51(2)
O(4A)	7098(14)	1964(9)	3235(5)	56(2)
O(4B)	11902(15)	2321(11)	884(5)	68(3)
Rh(1A)	7074(1)	1900(1)	2079(1)	56(1)
Rh(1B)	12000(2)	2187(1)	2097(1)	53(1)
F(1A)	5680(20)	2248(16)	4645(6)	136(2)
F(1B)	13120(20)	2405(15)	-610(6)	136(2)
F(2A)	7170(20)	553(15)	5305(7)	136(2)
F(2B)	10310(20)	2556(16)	-585(7)	136(2)
F(3A)	8720(20)	1747(15)	4764(6)	136(2)
F(3B)	11440(20)	1081(16)	-613(7)	136(2)
Cl(1A)	8626(7)	-5509(5)	3630(4)	93(2)
Cl(1B)	13571(7)	-5214(4)	3553(4)	90(1)

Table A 4.2: Hydrogen coordinates and isotropic displacement parameters ($Å^2$) for [Rh(F_3-4Clbzac)$(CO)_2$].

Atom	*x*	*y*	*z*	U_{eq}
H(4A)	7435	-555	4433	57
H(4B)	12412	-169	721	72
H(7A)	7928	-2232	4570	62
H(7B)	12678	-1286	3462	67
H(8A)	8391	-4270	4741	72
H(8B)	13172	-3289	4109	84
H(10A)	8341	-3511	2274	87
H(10B)	13298	-3876	1904	77
H(11A)	7832	-1560	2158	69
H(11B)	13038	-1872	1288	64

Table A 4.3: Anisotropic displacement parameters ($Å^2$) for [Rh(F_3-4Clbzac)$(CO)_2$]. The anisotropic displacement factor exponent takes the form: $-2\pi^2[h^2a^{*2}U^{11} + \ldots + 2hka^*b^*U^{23}]$.

Atom	U^{11}	U^{22}	U^{33}	U^{12}	U^{13}	U^{23}
C(1A)	75(8)	98(13)	25(5)	7(6)	-1(5)	-3(8)
C(1B)	63(6)	56(7)	31(5)	-18(5)	4(5)	-18(5)
C(2A)	102(11)	44(8)	73(10)	6(7)	-14(8)	-15(7)
C(2B)	101(12)	55(10)	124(16)	-41(10)	20(11)	-34(9)
C(3A)	41(5)	60(7)	40(6)	-8(5)	-1(4)	-2(5)
C(3B)	46(5)	70(8)	31(5)	-17(5)	3(4)	-13(5)
C(4A)	47(5)	67(8)	28(5)	-12(5)	5(4)	-20(5)
C(4B)	68(7)	75(9)	38(6)	-28(6)	-5(5)	-6(6)
C(5A)	53(5)	57(7)	24(4)	-10(4)	-1(4)	-13(5)
C(5B)	54(6)	83(10)	35(6)	-14(6)	1(5)	-28(6)
C(6A)	63(5)	104(9)	36(4)	-7(5)	-7(4)	-40(5)
C(6B)	37(5)	63(8)	42(6)	-5(5)	-3(4)	-12(5)
C(7A)	54(6)	66(8)	36(5)	-15(5)	-3(4)	-15(5)
C(7B)	60(6)	63(8)	44(6)	-24(6)	-8(5)	-4(6)
C(8A)	81(8)	56(8)	57(7)	-26(6)	12(6)	-33(7)
C(8B)	62(7)	82(11)	51(7)	9(7)	-18(6)	-23(7)
C(9A)	56(6)	53(8)	68(8)	-22(6)	2(6)	-26(5)

C(9B)	45(6)	56(8)	83(10)	-10(7)	8(6)	-18(5)
C(10A)	57(7)	102(14)	56(8)	-17(8)	2(6)	-27(8)
C(10B)	88(9)	61(9)	60(8)	-28(7)	8(7)	-38(7)
C(11A)	48(6)	80(10)	39(6)	-15(6)	4(5)	-10(6)
C(11B)	59(6)	63(8)	41(6)	-25(5)	5(5)	-11(5)
C(12A)	42(5)	98(12)	54(7)	-4(7)	-16(5)	-17(6)
C(12B)	63(5)	104(9)	36(4)	-7(5)	-7(4)	-40(5)
O(1A)	110(7)	136(10)	59(5)	-1(6)	2(5)	-18(7)
O(1B)	129(7)	84(7)	64(5)	-11(4)	12(5)	-46(6)
O(2A)	110(7)	136(10)	59(5)	-1(6)	2(5)	-18(7)
O(2B)	129(7)	84(7)	64(5)	-11(4)	12(5)	-46(6)
O(3A)	68(5)	50(5)	33(4)	-12(3)	2(3)	-1(4)
O(3B)	57(4)	65(6)	34(4)	-19(4)	10(3)	-17(4)
O(4A)	75(5)	57(5)	30(4)	-7(3)	3(4)	-14(4)
O(4B)	74(6)	91(8)	34(4)	-10(5)	2(4)	-22(5)
Rh(1A)	52(1)	66(1)	33(1)	0(1)	3(1)	-7(1)
Rh(1B)	60(1)	63(1)	40(1)	-15(1)	3(1)	-23(1)
F(1A)	166(5)	180(7)	59(3)	-32(3)	3(3)	-42(5)
F(1B)	166(5)	180(7)	59(3)	-32(3)	3(3)	-42(5)
F(2A)	166(5)	180(7)	59(3)	-32(3)	3(3)	-42(5)
F(2B)	166(5)	180(7)	59(3)	-32(3)	3(3)	-42(5)
F(3A)	166(5)	180(7)	59(3)	-32(3)	3(3)	-42(5)
F(3B)	166(5)	180(7)	59(3)	-32(3)	3(3)	-42(5)
Cl(1A)	88(3)	72(3)	122(4)	-23(3)	12(3)	-34(2)
Cl(1B)	78(2)	64(3)	111(4)	-3(2)	2(2)	-15(2)

Table A 4.4: Complete listing of bond lengths (Å) for [Rh(F_3-4Clbzac)$(CO)_2$].

Bond	Distance	Bond	Distance
C(1A)-O(1A)	1.12(3)	C(7B)-C(8B)	1.41(2)
C(1A)-Rh(1A)	1.852(16)	C(8A)-C(9A)	1.385(19)
C(1B)-O(1B)	1.12(3)	C(8B)-C(9B)	1.36(2)
C(1B)-Rh(1B)	1.862(15)	C(9A)-C(10A)	1.40(2)
C(2A)-O(2A)	1.15(3)	C(9A)-Cl(1A)	1.732(15)
C(2A)-Rh(1A)	1.860(16)	C(9B)-C(10B)	1.44(2)
C(2B)-O(2B)	1.13(3)	C(9B)-Cl(1B)	1.731(15)
C(2B)-Rh(1B)	1.845(18)	C(10A)-C(11A)	1.38(2)

C(3A)-O(3A)	1.295(13)	C(10B)-C(11B)	1.42(2)
C(3A)-C(4A)	1.426(17)	C(12A)-F(2A)	1.301(18)
C(3A)-C(6A)	1.53(2)	C(12A)-F(3A)	1.341(19)
C(3B)-O(3B)	1.321(16)	C(12A)-F(1A)	1.36(2)
C(3B)-C(4B)	1.434(16)	C(12B)-F(3B)	1.29(2)
C(3B)-C(6B)	1.466(19)	C(12B)-F(1B)	1.315(19)
C(4A)-C(5A)	1.321(18)	C(12B)-F(2B)	1.35(2)
C(4B)-C(5B)	1.36(2)	O(3A)-Rh(1A)	2.023(9)
C(5A)-O(4A)	1.27(2)	O(3B)-Rh(1B)	1.999(10)
C(5A)-C(12A)	1.472(18)	O(4A)-Rh(1A)	2.038(10)
C(5B)-O(4B)	1.22(3)	O(4B)-Rh(1B)	2.032(10)
C(5B)-C(12B)	1.542(17)		
C(6A)-C(11A)	1.33(2)		
C(6A)-C(7A)	1.371(17)		
C(6B)-C(11B)	1.371(18)		
C(6B)-C(7B)	1.408(17)		
C(7A)-C(8A)	1.45(2)		

Table A 4.5: Complete listing of bond angles (°) for [Rh(F_3-4Clbzac)($CO)_2$].

Angle	Value	Angle	Value
O(1A)-C(1A)-Rh(1A)	176.9(16)	C(11A)-C(10A)-C(9A)	118.1(15)
O(1B)-C(1B)-Rh(1B)	178.3(12)	C(11B)-C(10B)-C(9B)	114.6(13)
O(2A)-C(2A)-Rh(1A)	174.5(16)	C(6A)-C(11A)-C(10A)	121.3(15)
O(2B)-C(2B)-Rh(1B)	175.0(19)	C(6B)-C(11B)-C(10B)	124.0(12)
O(3A)-C(3A)-C(4A)	121.1(12)	F(2A)-C(12A)-F(3A)	102.0(11)
O(3A)-C(3A)-C(6A)	114.4(11)	F(2A)-C(12A)-F(1A)	104.6(13)
C(4A)-C(3A)-C(6A)	124.5(11)	F(3A)-C(12A)-F(1A)	101.1(17)
O(3B)-C(3B)-C(4B)	122.2(13)	F(2A)-C(12A)-C(5A)	118.4(16)
O(3B)-C(3B)-C(6B)	117.2(10)	F(3A)-C(12A)-C(5A)	114.6(12)
C(4B)-C(3B)-C(6B)	120.5(12)	F(1A)-C(12A)-C(5A)	113.9(10)
C(5A)-C(4A)-C(3A)	127.0(11)	F(3B)-C(12B)-F(1B)	121.0(14)
C(5B)-C(4B)-C(3B)	122.0(13)	F(3B)-C(12B)-F(2B)	88.9(11)
O(4A)-C(5A)-C(4A)	130.1(11)	F(1B)-C(12B)-F(2B)	94.3(14)
O(4A)-C(5A)-C(12A)	111.3(12)	F(3B)-C(12B)-C(5B)	122.3(14)
C(4A)-C(5A)-C(12A)	118.5(11)	F(1B)-C(12B)-C(5B)	112.2(11)
O(4B)-C(5B)-C(4B)	135.7(13)	F(2B)-C(12B)-C(5B)	108.7(13)

O(4B)-C(5B)-C(12B)	113.7(13)	C(3A)-O(3A)-Rh(1A)	128.6(9)
C(4B)-C(5B)-C(12B)	110.4(14)	C(3B)-O(3B)-Rh(1B)	128.8(8)
C(11A)-C(6A)-C(7A)	123.3(17)	C(5A)-O(4A)-Rh(1A)	122.7(9)
C(11A)-C(6A)-C(3A)	119.9(13)	C(5B)-O(4B)-Rh(1B)	121.0(10)
C(7A)-C(6A)-C(3A)	116.7(13)	C(2A)-Rh(1A)-C(1A)	89.9(10)
C(11B)-C(6B)-C(7B)	119.6(13)	C(2A)-Rh(1A)-O(3A)	177.6(8)
C(11B)-C(6B)-C(3B)	122.9(11)	C(1A)-Rh(1A)-O(3A)	89.6(8)
C(7B)-C(6B)-C(3B)	117.5(13)	C(2A)-Rh(1A)-O(4A)	90.4(8)
C(6A)-C(7A)-C(8A)	117.7(13)	C(1A)-Rh(1A)-O(4A)	179.8(8)
C(6B)-C(7B)-C(8B)	118.3(14)	O(3A)-Rh(1A)-O(4A)	90.3(5)
C(9A)-C(8A)-C(7A)	118.1(13)	C(2B)-Rh(1B)-C(1B)	88.9(9)
C(9B)-C(8B)-C(7B)	121.4(13)	C(2B)-Rh(1B)-O(3B)	179.0(8)
C(8A)-C(9A)-C(10A)	121.4(15)	C(1B)-Rh(1B)-O(3B)	90.3(8)
C(8A)-C(9A)-Cl(1A)	118.9(11)	C(2B)-Rh(1B)-O(4B)	90.4(8)
C(10A)-C(9A)-Cl(1A)	119.7(13)	C(1B)-Rh(1B)-O(4B)	179.0(8)
C(8B)-C(9B)-C(10B)	122.0(14)	O(3B)-Rh(1B)-O(4B)	90.3(5)
C(8B)-C(9B)-Cl(1B)	121.8(12)	C(11A)-C(10A)-C(9A)	118.1(15)
C(10B)-C(9B)-Cl(1B)	116.2(13)	C(11B)-C(10B)-C(9B)	114.6(13)
O(1A)-C(1A)-Rh(1A)	176.9(16)	C(6A)-C(11A)-C(10A)	121.3(15)
O(1B)-C(1B)-Rh(1B)	178.3(12)	C(6B)-C(11B)-C(10B)	124.0(12)
O(2A)-C(2A)-Rh(1A)	174.5(16)	F(2A)-C(12A)-F(3A)	102.5(11)
O(2B)-C(2B)-Rh(1B)	175.0(19)	F(2A)-C(12A)-F(1A)	104.6(13)
O(3A)-C(3A)-C(4A)	121.1(12)	F(3A)-C(12A)-F(1A)	101.1(17)
O(3A)-C(3A)-C(6A)	114.4(11)	F(2A)-C(12A)-C(5A)	118.4(16)
C(4A)-C(3A)-C(6A)	124.5(11)	F(3A)-C(12A)-C(5A)	114.6(12)
O(3B)-C(3B)-C(4B)	122.2(13)	F(1A)-C(12A)-C(5A)	113.9(10)
O(3B)-C(3B)-C(6B)	117.2(10)	F(3B)-C(12B)-F(1B)	121.0(18)
C(4B)-C(3B)-C(6B)	120.5(12)	F(3B)-C(12B)-F(2B)	88.9(11)
C(5A)-C(4A)-C(3A)	124.9(16)	F(1B)-C(12B)-F(2B)	94.3(14)
C(5B)-C(4B)-C(3B)	122.0(13)	F(3B)-C(12B)-C(5B)	122.3(14)
O(4A)-C(5A)-C(4A)	130.1(11)	F(1B)-C(12B)-C(5B)	112.2(11)
O(4A)-C(5A)-C(12A)	111.3(12)	F(2B)-C(12B)-C(5B)	108.7(13)
C(4A)-C(5A)-C(12A)	118.5(11)	C(3A)-O(3A)-Rh(1A)	128.6(9)
O(4B)-C(5B)-C(4B)	135.7(13)	C(3B)-O(3B)-Rh(1B)	128.8(8)
O(4B)-C(5B)-C(12B)	113.7(13)	C(5A)-O(4A)-Rh(1A)	122.7(9)
C(4B)-C(5B)-C(12B)	110.4(14)	C(5B)-O(4B)-Rh(1B)	121.0(10)
C(11A)-C(6A)-C(7A)	123.3(17)	C(2A)-Rh(1A)-C(1A)	89.9(9)

C(11A)-C(6A)-C(3A)	119.9(13)	C(2A)-Rh(1A)-O(3A)	178.0(6)
C(7A)-C(6A)-C(3A)	116.7(13)	C(1A)-Rh(1A)-O(3A)	89.0(6)
C(11B)-C(6B)-C(7B)	119.6(13)	C(2A)-Rh(1A)-O(4A)	90.9(7)
C(11B)-C(6B)-C(3B)	122.9(11)	C(1A)-Rh(1A)-O(4A)	179.0(6)
C(7B)-C(6B)-C(3B)	117.5(13)	O(3A)-Rh(1A)-O(4A)	90.2(4)
C(6A)-C(7A)-C(8A)	117.7(13)	C(2B)-Rh(1B)-C(1B)	88.4(9)
C(6B)-C(7B)-C(8B)	118.3(14)	C(2B)-Rh(1B)-O(3B)	178.8(8)
C(9A)-C(8A)-C(7A)	118.1(13)	C(1B)-Rh(1B)-O(3B)	90.5(5)
C(9B)-C(8B)-C(7B)	121.4(13)	C(2B)-Rh(1B)-O(4B)	91.0(8)
C(8A)-C(9A)-C(10A)	121.4(15)	C(1B)-Rh(1B)-O(4B)	178.8(5)
C(8A)-C(9A)-Cl(1A)	118.9(11)	O(3B)-Rh(1B)-O(4B)	90.0(4)
C(10A)-C(9A)-Cl(1A)	119.7(13)		
C(8B)-C(9B)-C(10B)	122.0(14)		
C(8B)-C(9B)-Cl(1B)	121.8(12)		
C(10B)-C(9B)-Cl(1B)	116.2(13)		

A 5. Supplementary Data for [Rh(dbm)(CO)$_2$]

Table A 5.1: Atomic coordinates and equivalent isotropic displacement parameters (Å^2) for [Rh(dbm)(CO)$_2$]. U(eq) is defined as one third of the trace of the orthogonalized U^{ij} tensor.

Atom	*x*	*y*	*z*	U_{eq}
C(1A)	8298(6)	994(2)	5112(2)	32(1)
C(1B)	3272(6)	654(2)	5750(2)	30(1)
C(2A)	8138(5)	885(2)	6330(2)	29(1)
C(2B)	3112(5)	1367(2)	6719(2)	24(1)
C(3A)	9244(4)	3005(2)	5278(2)	16(1)
C(3B)	4079(4)	2385(2)	4755(1)	17(1)
C(4A)	9312(4)	3292(2)	5865(1)	16(1)
C(4B)	4244(4)	3011(2)	5075(1)	16(1)
C(5A)	9135(4)	2933(2)	6423(2)	17(1)
C(5B)	4155(4)	3093(2)	5714(2)	15(1)
C(6A)	9432(4)	3447(2)	4715(1)	16(1)
C(6B)	4207(4)	2384(2)	4067(1)	16(1)
C(7A)	10395(4)	4081(2)	4710(2)	18(1)
C(7B)	3713(4)	2962(2)	3714(1)	19(1)
C(8A)	10596(5)	4454(2)	4169(2)	21(1)

C(8B)	3911(5)	2945(2)	3077(1)	21(1)
C(9A)	9816(5)	4205(2)	3624(2)	22(1)
C(9B)	4618(5)	2360(2)	2785(2)	22(1)
C(10A)	8835(5)	3580(2)	3622(2)	21(1)
C(10B)	5102(5)	1782(2)	3134(2)	22(1)
C(11A)	8662(4)	3202(2)	4163(1)	19(1)
C(11B)	4876(4)	1789(2)	3769(2)	19(1)
C(12A)	9235(4)	3313(2)	7019(1)	16(1)
C(12B)	4394(4)	3804(2)	5993(1)	15(1)
C(13A)	8665(5)	4007(2)	7066(1)	19(1)
C(13B)	5343(4)	4338(2)	5686(2)	17(1)
C(14A)	8746(5)	4346(2)	7629(2)	24(1)
C(14B)	5565(5)	4979(2)	5965(2)	20(1)
C(15A)	9417(5)	4007(2)	8149(2)	25(1)
C(15B)	4824(5)	5098(2)	6553(2)	20(1)
C(16A)	9977(4)	3316(2)	8106(2)	24(1)
C(16B)	3866(5)	4574(2)	6857(2)	19(1)
C(17A)	9876(4)	2975(2)	7547(2)	21(1)
C(17B)	3662(4)	3928(2)	6581(1)	16(1)
O(1A)	8129(6)	669(2)	4683(1)	50(1)
O(1B)	3093(6)	74(2)	5674(1)	56(1)
O(2A)	7803(5)	463(2)	6681(2)	46(1)
O(2B)	2794(4)	1202(2)	7215(1)	40(1)
O(3A)	8989(4)	2359(1)	5157(1)	22(1)
O(3B)	3875(3)	1787(1)	4998(1)	21(1)
O(4A)	8886(3)	2274(1)	6479(1)	21(1)
O(4B)	3858(3)	2608(1)	6108(1)	18(1)
Rh(1A)	8598(1)	1591(1)	5775(1)	21(1)
Rh(1B)	3544(1)	1586(1)	5909(1)	17(1)

Table A 5.2: Hydrogen coordinates and isotropic displacement parameters (Å^2) for [Rh(dbm)(CO)$_2$].

Atom	*x*	*y*	*z*	U_{eq}
H(4A)	9492	3769	5890	20
H(4B)	4429	3409	4840	19
H(7A)	10906	4254	5075	22

H(7B)	3250	3359	3906	22
H(8A)	11256	4872	4170	25
H(8B)	3566	3329	2843	25
H(9A)	9950	4457	3260	26
H(9B)	4768	2355	2358	26
H(10A)	8295	3416	3258	26
H(10B)	5579	1388	2940	26
H(11A)	8024	2780	4158	23
H(11B)	5172	1396	3999	23
H(13A)	8230	4240	6718	23
H(13B)	5830	4263	5292	21
H(14A)	8349	4805	7657	29
H(14B)	6210	5331	5760	24
H(15A)	9492	4239	8525	30
H(15B)	4975	5529	6739	24
H(16A)	10419	3084	8454	29
H(16B)	3357	4654	7247	23
H(17A)	10242	2513	7522	26
H(17B)	3033	3574	6790	20

Table A 5.3: Anisotropic displacement parameters ($Å^2$) for $[Rh(dbm)(CO)_2]$. The anisotropic displacement factor exponent takes the form: $-2\pi^2[h^2a^{*2}U^{11} + \ldots + 2hka^*b^*U^{23}]$.

Atom	U^{11}	U^{22}	U^{33}	U^{12}	U^{13}	U^{23}
C(1A)	48(2)	17(2)	31(2)	6(2)	-1(2)	2(2)
C(1B)	51(2)	26(2)	14(2)	0(1)	6(2)	-3(2)
C(2A)	32(2)	22(2)	32(2)	2(2)	-2(2)	2(2)
C(2B)	38(2)	15(2)	20(2)	-1(1)	4(1)	-6(1)
C(3A)	13(1)	15(2)	20(2)	1(1)	1(1)	2(1)
C(3B)	14(1)	23(2)	12(1)	-2(1)	-1(1)	2(1)
C(4A)	16(1)	16(2)	17(2)	2(1)	1(1)	0(1)
C(4B)	16(1)	18(2)	14(2)	-1(1)	0(1)	-2(1)
C(5A)	12(1)	20(2)	18(2)	3(1)	1(1)	2(1)
C(5B)	10(1)	19(2)	16(1)	-1(1)	0(1)	2(1)
C(6A)	14(1)	16(2)	18(1)	1(1)	2(1)	3(1)
C(6B)	14(1)	22(2)	12(1)	-2(1)	0(1)	-1(1)
C(7A)	18(2)	17(2)	19(2)	-3(1)	0(1)	0(1)

C(7B)	17(1)	20(2)	18(2)	-2(1)	0(1)	-2(1)
C(8A)	23(2)	15(2)	24(2)	-1(1)	8(1)	2(1)
C(8B)	22(2)	24(2)	16(2)	1(1)	-2(1)	-5(1)
C(9A)	24(2)	23(2)	18(2)	4(1)	4(1)	8(1)
C(9B)	20(2)	32(2)	13(2)	-4(1)	3(1)	-6(1)
C(10A)	21(2)	27(2)	17(2)	-1(1)	-2(1)	6(1)
C(10B)	21(2)	26(2)	19(2)	-7(1)	2(1)	-1(1)
C(11A)	16(1)	20(2)	21(2)	-2(1)	0(1)	0(1)
C(11B)	20(2)	22(2)	16(2)	-3(1)	1(1)	1(1)
C(12A)	12(1)	20(2)	16(1)	2(1)	1(1)	0(1)
C(12B)	13(1)	16(2)	16(2)	-1(1)	-3(1)	2(1)
C(13A)	21(2)	19(2)	17(2)	3(1)	2(1)	1(1)
C(13B)	19(1)	21(2)	13(1)	1(1)	-2(1)	-1(1)
C(14A)	28(2)	23(2)	21(2)	0(1)	1(2)	0(2)
C(14B)	23(2)	18(2)	20(2)	4(1)	-4(1)	-2(1)
C(15A)	26(2)	31(2)	19(2)	-3(1)	-1(1)	-6(2)
C(15B)	24(2)	16(2)	21(2)	-3(1)	-8(1)	4(1)
C(16A)	21(2)	30(2)	21(2)	8(2)	-4(1)	1(1)
C(16B)	21(2)	21(2)	16(2)	-2(1)	-2(1)	5(1)
C(17A)	18(2)	23(2)	23(2)	5(1)	0(1)	2(1)
C(17B)	14(1)	20(2)	15(1)	1(1)	0(1)	0(1)
O(1A)	95(3)	22(2)	34(2)	-3(1)	-9(2)	-1(2)
O(1B)	115(3)	21(2)	33(2)	-5(1)	12(2)	-13(2)
O(2A)	59(2)	33(2)	47(2)	22(1)	4(2)	0(2)
O(3A)	32(1)	14(1)	21(1)	0(1)	2(1)	-1(1)
O(3B)	30(1)	19(1)	15(1)	0(1)	2(1)	0(1)
O(4A)	26(1)	17(1)	21(1)	3(1)	2(1)	2(1)
O(4B)	26(1)	16(1)	13(1)	0(1)	1(1)	0(1)
Rh(1A)	25(1)	13(1)	24(1)	3(1)	1(1)	1(1)
Rh(1B)	24(1)	15(1)	14(1)	0(1)	1(1)	0(1)

Table A 5.4: Complete listing of bond lengths (Å) for [Rh(dbm)(CO)$_2$].

Bond	Distance	Bond	Distance
C(1A)-O(1A)	1.130(7)	C(7B)-C(8B)	1.387(4)
C(1A)-Rh(1A)	1.854(6)	C(8A)-C(9A)	1.386(5)
C(1B)-O(1B)	1.129(7)	C(8B)-C(9B)	1.384(5)

C(1B)-Rh(1B)	1.846(6)	C(9A)-C(10A)	1.388(5)
C(2A)-O(2A)	1.141(7)	C(9B)-C(10B)	1.389(5)
C(2A)-Rh(1A)	1.845(6)	C(10A)-C(11A)	1.385(4)
C(2B)-O(2B)	1.1451(6)	C(10B)-C(11B)	1.386(5)
C(2B)-Rh(1B)	1.830(3)	C(12A)-C(17A)	1.391(4)
C(3A)-O(3A)	1.290(5)	C(12A)-C(13A)	1.400(4)
C(3A)-C(4A)	1.388(4)	C(12B)-C(17B)	1.394(4)
C(3A)-C(6A)	1.492(4)	C(12B)-C(13B)	1.395(4)
C(3B)-O(3B)	1.275(4)	C(13A)-C(14A)	1.384(4)
C(3B)-C(4B)	1.397(4)	C(13B)-C(14B)	1.385(5)
C(3B)-C(6B)	1.494(4)	C(14A)-C(15A)	1.387(5)
C(4A)-C(5A)	1.397(4)	C(14B)-C(15B)	1.393(5)
C(4B)-C(5B)	1.395(4)	C(15A)-C(16A)	1.392(5)
C(5A)-O(4A)	1.292(5)	C(15B)-C(16B)	1.382(5)
C(5A)-C(12A)	1.485(4)	C(16A)-C(17A)	1.380(5)
C(5B)-O(4B)	1.288(5)	C(16B)-C(17B)	1.390(4)
C(5B)-C(12B)	1.508(4)	O(3A)-Rh(1A)	2.015(3)
C(6A)-C(11A)	1.395(4)	O(3B)-Rh(1B)	2.024(3)
C(6A)-C(7A)	1.397(5)	O(4A)-Rh(1A)	2.025(3)
C(6B)-C(7B)	1.396(4)	O(4B)-Rh(1B)	2.028(2)
C(6B)-C(11B)	1.397(4)		
C(7A)-C(8A)	1.383(4)		

Table A 5.5: Complete listing of bond angles (º) for [Rh(dbm)(CO)$_2$].

Angle	Value	Angle	Value
O(1A)-C(1A)-Rh(1A)	175.3(3)	C(13A)-C(12A)-C(5A)	121.4(3)
O(1B)-C(1B)-Rh(1B)	177.6(3)	C(17B)-C(12B)-C(13B)	119.1(3)
O(2A)-C(2A)-Rh(1A)	177.6(4)	C(17B)-C(12B)-C(5B)	118.7(3)
O(2B)-C(2B)-Rh(1B)	176.5(3)	C(13B)-C(12B)-C(5B)	122.2(3)
O(3A)-C(3A)-C(4A)	125.4(3)	C(14A)-C(13A)-C(12A)	120.3(3)
O(3A)-C(3A)-C(6A)	113.5(3)	C(14B)-C(13B)-C(12B)	120.2(3)
C(4A)-C(3A)-C(6A)	121.2(3)	C(13A)-C(14A)-C(15A)	120.4(3)
O(3B)-C(3B)-C(4B)	125.9(3)	C(13B)-C(14B)-C(15B)	120.3(3)
O(3B)-C(3B)-C(6B)	114.7(3)	C(14A)-C(15A)-C(16A)	119.6(3)
C(4B)-C(3B)-C(6B)	119.4(3)	C(16B)-C(15B)-C(14B)	119.8(3)
C(3A)-C(4A)-C(5A)	126.2(3)	C(17A)-C(16A)-C(15A)	120.0(3)

C(5B)-C(4B)-C(3B)	125.8(3)	C(15B)-C(16B)-C(17B)	120.0(3)
O(4A)-C(5A)-C(4A)	125.6(3)	C(16A)-C(17A)-C(12A)	121.1(3)
O(4A)-C(5A)-C(12A)	114.3(3)	C(16B)-C(17B)-C(12B)	120.6(3)
C(4A)-C(5A)-C(12A)	120.1(3)	C(3A)-O(3A)-Rh(1A)	126.5(2)
O(4B)-C(5B)-C(4B)	125.8(3)	C(3B)-O(3B)-Rh(1B)	126.0(2)
O(4B)-C(5B)-C(12B)	114.5(3)	C(5A)-O(4A)-Rh(1A)	125.8(2)
C(4B)-C(5B)-C(12B)	119.7(3)	C(5B)-O(4B)-Rh(1B)	125.7(2)
C(11A)-C(6A)-C(7A)	118.5(3)	C(2A)-Rh(1A)-C(1A)	91.50(17)
C(11A)-C(6A)-C(3A)	118.3(3)	C(2A)-Rh(1A)-O(3A)	177.65(14)
C(7A)-C(6A)-C(3A)	123.2(3)	C(1A)-Rh(1A)-O(3A)	87.57(13)
C(7B)-C(6B)-C(11B)	119.2(3)	C(2A)-Rh(1A)-O(4A)	91.0(14)
C(7B)-C(6B)-C(3B)	122.0(3)	C(1A)-Rh(1A)-O(4A)	177.77(13)
C(11B)-C(6B)-C(3B)	118.8(3)	O(3A)-Rh(1A)-O(4A)	90.49(9)
C(8A)-C(7A)-C(6A)	120.7(3)	C(2B)-Rh(1B)-C(1B)	86.37(15)
C(8B)-C(7B)-C(6B)	120.0(3)	C(2B)-Rh(1B)-O(3B)	176.22(13)
C(7A)-C(8A)-C(9A)	120.1(3)	C(1B)-Rh(1B)-O(3B)	90.38(12)
C(9B)-C(8B)-C(7B)	120.7(3)	C(2B)-Rh(1B)-O(4B)	92.18(12)
C(8A)-C(9A)-C(10A)	119.9(3)	C(1B)-Rh(1B)-O(4B)	178.44(12)
C(8B)-C(9B)-C(10B)	119.5(3)	O(3B)-Rh(1B)-O(4B)	90.51(9)
C(11A)-C(10A)-C(9A)	119.9(3)		
C(11B)-C(10B)-C(9B)	120.3(3)		
C(10A)-C(11A)-C(6A)	120.9(3)		
C(10B)-C(11B)-C(6B)	120.3(3)		
C(17A)-C(12A)-C(13A)	118.6(3)		
C(17A)-C(12A)-C(5A)	119.9(3)		

A 6. Supplementary Data for [Rh(acac)(CO)$_2$]

Table A 6.1: Atomic coordinates and equivalent isotropic displacement parameters (Å^2) for [Rh(acac)(CO)$_2$]. U(eq) is defined as one third of the trace of the orthogonalized U^{ij} tensor.

Atom	*x*	*y*	*z*	U_{eq}
C(1)	3026(10)	7026(9)	-808(8)	41(1)
C(2)	2192(10)	3542(9)	-2050(7)	38(1)
C(3)	2721(5)	6065(5)	3286(5)	36(1)
C(4)	2270(5)	4257(5)	3309(5)	41(1)
C(5)	1928(5)	2727(5)	2056(5)	36(1)

C(6)	3056(6)	7558(6)	4768(5)	51(1)
C(7)	1458(6)	840(5)	2288(5)	51(1)
O(1)	3328(4)	8272(4)	-1232(4)	57(1)
O(2)	2013(4)	2632(5)	-3276(4)	59(1)
O(3)	2870(7)	6629(6)	2109(5)	36(1)
O(4)	1946(7)	2719(5)	683(5)	38(1)
Rh(1)	2504(1)	4992(1)	-72(1)	31(1)

Table A 6.2: Hydrogen coordinates and isotropic displacement parameters ($Å^2$) for $[Rh(acac)(CO)_2]$.

Atom	*x*	*y*	*z*	U_{eq}
H(4)	2191	4052	4259	49
H(6A)	2919	7025	5597	77
H(6B)	2033	8314	4804	77
H(6C)	4430	8286	4849	77
H(7A)	1471	952	3357	77
H(7B)	2500	165	1849	77
H(7C)	107	211	1807	77

Table A 6.3: Anisotropic displacement parameters ($Å^2$) for $[Rh(acac)(CO)_2]$. The anisotropic displacement factor exponent takes the form: $-2\pi^2[h^2a^{*2}U^{11} + \ldots + 2hka^*b^*U^{23}]$.

Atom	U^{11}	U^{22}	U^{33}	U^{12}	U^{13}	U^{23}
C(1)	35(2)	51(3)	39(3)	14(2)	7(2)	9(2)
C(2)	34(3)	53(3)	29(2)	15(2)	6(2)	8(2)
C(3)	30(2)	40(2)	36(2)	9(2)	1(1)	8(1)
C(4)	49(2)	42(2)	31(2)	11(2)	2(2)	8(1)
C(5)	32(2)	41(2)	40(2)	16(2)	6(1)	10(1)
C(6)	62(2)	48(2)	38(2)	6(2)	3(2)	9(2)
C(7)	70(2)	40(2)	49(3)	19(2)	5(2)	11(2)
O(1)	62(2)	55(2)	64(2)	33(2)	11(2)	12(2)
O(2)	61(2)	67(2)	39(2)	3(2)	3(2)	6(2)
O(3)	41(2)	37(2)	30(2)	10(2)	3(2)	8(1)
O(4)	41(2)	35(2)	40(2)	12(2)	6(2)	7(1)
Rh(1)	26(1)	39(1)	30(1)	11(1)	2(1)	7(1)

Table A 6.4: Complete listing of bond lengths (Å) for [Rh(acac)(CO)$_2$].

Bond	Distance	Bond	Distance
C(1)-O(1)	1.127(9)	C(3)-C(6)	1.506(6)
C(1)-Rh(1)	1.865(8)	C(4)-C(5)	1.387(5)
C(2)-O(2)	1.142(7)	C(5)-O(4)	1.259(6)
C(2)-Rh(1)	1.838(6)	C(5)-C(7)	1.517(6)
C(3)-O(3)	1.273(7)	O(3)-Rh(1)	2.036(4)
C(3)-C(4)	1.389(6)	O(4)-Rh(1)	2.047(5)

Table A 6.5: Complete listing of bond angles (°) for [Rh(acac)(CO)$_2$].

Angle	Value	Angle	Value
O(1)-C(1)-Rh(1)	178.8(6)	C(3)-O(3)-Rh(1)	125.0(3)
O(2)-C(2)-Rh(1)	179.3(6)	C(5)-O(4)-Rh(1)	125.3(3)
O(3)-C(3)-C(4)	126.4(4)	C(2)-Rh(1)-C(1)	88.4(3)
O(3)-C(3)-C(6)	114.5(4)	C(2)-Rh(1)-O(3)	179.19(13)
C(4)-C(3)-C(6)	119.1(4)	C(1)-Rh(1)-O(3)	90.9(3)
C(5)-C(4)-C(3)	126.5(4)	C(2)-Rh(1)-O(4)	90.2(2)
O(4)-C(5)-C(4)	126.3(4)	C(1)-Rh(1)-O(4)	178.54(16)
O(4)-C(5)-C(7)	114.1(4)	O(3)-Rh(1)-O(4)	90.52(18)
C(4)-C(5)-C(7)	119.5(4)		

A 7. Supplementary Data for [Rh(3Cl-acac)(CO)$_2$]

Table A 7.1: Atomic coordinates and equivalent isotropic displacement parameters (Å^2) for [Rh(3Cl-acac)(CO)$_2$]. U(eq) is defined as one third of the trace of the orthogonalized U^{ij} tensor.

Atom	*x*	*y*	*z*	U_{eq}
C(1)	5000	926(2)	994(3)	20(1)
C(2)	5000	-40(2)	2178(3)	23(1)
C(3)	5000	2124(2)	3389(3)	16(1)
C(4)	5000	1837(2)	4346(3)	16(1)
C(5)	5000	1174(2)	4557(3)	16(1)
C(6)	5000	2843(2)	3279(3)	22(1)
C(7)	5000	937(2)	5622(3)	22(1)

O(1)	5000	960(2)	150(2)	29(1)
O(2)	5000	-580(2)	2043(2)	39(1)
O(3)	5000	1809(1)	2571(2)	19(1)
O(4)	5000	729(1)	3891(2)	18(1)
Cl(1)	5000	2360(1)	5381(1)	20(1)
Rh(1)	5000	841(1)	2377(1)	15(1)

Table A 7.2: Hydrogen coordinates and isotropic displacement parameters ($Å^2$) for [Rh(3Cl-acac)$(CO)_2$].

Atom	*x*	*y*	*z*	U_{eq}
H(6A)	5000	3043	3944	32
H(6B)	3788	2978	2910	32
H(6C)	6212	2978	2910	32
H(7A)	5000	1306	6079	33
H(7B)	6212	675	5740	33
H(7C)	3788	675	5740	33

Table A 7.3: Anisotropic displacement parameters ($Å^2$) for [Rh(3Cl-acac)$(CO)_2$]. The anisotropic displacement factor exponent takes the form: $-2\pi^2[h^2a^{*2}U^{11} + \ldots + 2hka^*b^*U^{23}]$.

Atom	U^{11}	U^{22}	U^{33}	U^{12}	U^{13}	U^{23}
C(1)	23(2)	22(2)	15(2)	-2(1)	0	0
C(2)	32(2)	27(2)	11(2)	-1(1)	0	0
C(3)	16(2)	19(2)	14(2)	0(1)	0	0
C(4)	19(2)	17(2)	11(2)	-2(1)	0	0
C(5)	18(2)	18(2)	13(2)	1(1)	0	0
C(6)	27(2)	21(2)	17(2)	3(1)	0	0
C(7)	33(2)	18(2)	14(2)	2(1)	0	0
O(1)	37(2)	35(2)	15(1)	1(1)	0	0
O(2)	73(3)	22(2)	21(2)	-4(1)	0	0
O(3)	24(1)	20(1)	12(1)	2(1)	0	0
O(4)	25(1)	17(1)	11(1)	-1(1)	0	0
Cl(1)	27(1)	20(1)	14(1)	-2(1)	0	0
Rh(1)	18(1)	18(1)	10(1)	-1(1)	0	0

Table A 7.4: Complete listing of bond lengths (Å) for [Rh(3Cl-acac)(CO)$_2$].

Bond	Distance	Bond	Distance
C(1)-O(1)	1.130(5)	C(5)-C(7)	1.504(5)
C(1)-Rh(1)	1.854(4)	C(6)-H(6A)	0.9800
C(2)-O(2)	1.135(5)	C(6)-H(6B)	0.9800
C(2)-Rh(1)	1.848(4)	C(6)-H(6C)	0.9800
C(3)-O(3)	1.272(4)	C(7)-H(7A)	0.9800
C(3)-C(4)	1.408(5)	C(7)-H(7B)	0.9800
C(3)-C(6)	1.500(5)	C(7)-H(7C)	0.9800
C(4)-C(5)	1.405(5)	O(3)-Rh(1)	2.026(3)
C(4)-Cl(1)	1.757(4)	O(4)-Rh(1)	2.034(3)
C(5)-O(4)	1.281(4)		

Table A 7.5: Complete listing of bond angles (°) for [Rh(3Cl-acac)(CO)$_2$].

Angle	Value	Angle	Value
O(1)-C(1)-Rh(1)	178.2(4)	H(6B)-C(6)-H(6C)	109.5
O(2)-C(2)-Rh(1)	179.2(4)	C(5)-C(7)-H(7A)	109.5
O(3)-C(3)-C(4)	124.2(3)	C(5)-C(7)-H(7B)	109.5
O(3)-C(3)-C(6)	115.2(3)	H(7A)-C(7)-H(7B)	109.5
C(4)-C(3)-C(6)	120.6(3)	C(5)-C(7)-H(7C)	109.5
C(5)-C(4)-C(3)	126.5(3)	H(7A)-C(7)-H(7C)	109.5
C(5)-C(4)-Cl(1)	116.6(3)	H(7B)-C(7)-H(7C)	109.5
C(3)-C(4)-Cl(1)	116.9(3)	C(3)-O(3)-Rh(1)	128.2(2)
O(4)-C(5)-C(4)	124.5(3)	C(5)-O(4)-Rh(1)	127.4(2)
O(4)-C(5)-C(7)	114.8(3)	C(2)-Rh(1)-C(1)	87.15(17)
C(4)-C(5)-C(7)	120.7(3)	C(2)-Rh(1)-O(3)	179.09(14)
C(3)-C(6)-H(6A)	109.5	C(1)-Rh(1)-O(3)	91.89(14)
C(3)-C(6)-H(6B)	109.5	C(2)-Rh(1)-O(4)	91.77(14)
H(6A)-C(6)-H(6B)	109.5	C(1)-Rh(1)-O(4)	178.92(14)
C(3)-C(6)-H(6C)	109.5	O(3)-Rh(1)-O(4)	89.19(10)
H(6A)-C(6)-H(6C)	109.5		

A 8. Supplementary Data for [Rh(CN-acac)(CO)$_2$]

Table A 8.1: Atomic coordinates and equivalent isotropic displacement parameters (Å^2) for [Rh(CN-acac)(CO)$_2$]. U(eq) is defined as one third of the trace of the orthogonalized U^{ij} tensor.

Atom	*x*	*y*	*z*	U_{eq}
C(1)	2678(4)	2076(4)	6939(3)	19(1)
C(2)	2190(4)	-1603(4)	5899(3)	19(1)
C(3)	2918(4)	2182(4)	3131(3)	17(1)
C(4)	2630(4)	489(4)	1963(3)	16(1)
C(5)	2402(4)	-1324(4)	2004(3)	15(1)
C(6)	3210(5)	4010(4)	2926(3)	26(1)
C(7)	2222(5)	-2988(4)	649(3)	23(1)
C(8)	2593(4)	588(4)	585(3)	20(1)
N(1)	2555(4)	666(4)	-501(3)	29(1)
O(1)	2752(3)	3313(3)	7964(2)	29(1)
O(2)	1987(3)	-2730(3)	6353(2)	27(1)
O(3)	2932(3)	2328(3)	4406(2)	18(1)
O(4)	2351(3)	-1669(3)	3122(2)	16(1)
Rh(1)	2538(1)	234(1)	5149(1)	14(1)

Table A 8.2: Hydrogen coordinates and isotropic displacement parameters (Å^2) for [Rh(CN-acac)(CO)$_2$].

Atom	*x*	*y*	*z*	U_{eq}
H(6A)	3383	5019	3828	40
H(6B)	1995	4141	2422	40
H(6C)	4439	4034	2398	40
H(7A)	2075	-4107	847	34
H(7B)	3465	-2972	132	34
H(7C)	1009	-2951	100	34

Table A 8.3: Anisotropic displacement parameters ($Å^2$) for [Rh(CN-acac)$(CO)_2$]. The anisotropic displacement factor exponent takes the form: $-2\pi^2[h^2a^{*2}U^{11} + \ldots + 2hka^*b^*U^{23}]$.

Atom	U^{11}	U^{22}	U^{33}	U^{12}	U^{13}	U^{23}
C(1)	18(1)	23(2)	20(2)	12(1)	2(1)	1(1)
C(2)	14(1)	26(2)	15(1)	7(1)	3(1)	2(1)
C(3)	14(1)	18(1)	21(1)	10(1)	1(1)	1(1)
C(4)	13(1)	18(1)	17(1)	6(1)	2(1)	0(1)
C(5)	11(1)	17(1)	15(1)	5(1)	1(1)	0(1)
C(6)	38(2)	19(2)	24(2)	11(1)	5(1)	2(1)
C(7)	27(1)	22(2)	18(1)	7(1)	1(1)	-1(1)
C(8)	18(1)	21(2)	20(1)	7(1)	1(1)	0(1)
N(1)	31(1)	37(2)	22(1)	17(1)	2(1)	1(1)
O(1)	41(1)	22(1)	17(1)	2(1)	4(1)	-1(1)
O(2)	31(1)	26(1)	30(1)	19(1)	6(1)	4(1)
O(3)	24(1)	14(1)	15(1)	5(1)	1(1)	1(1)
O(4)	18(1)	15(1)	15(1)	5(1)	1(1)	2(1)
Rh(1)	14(1)	15(1)	12(1)	5(1)	1(1)	2(1)

Table A 8.4: Complete listing of bond lengths (Å) for [Rh(CN-acac)$(CO)_2$].

Bond	Distance	Bond	Distance
C(1)-O(1)	1.124(4)	C(4)-C(8)	1.441(4)
C(1)-Rh(1)	1.852(3)	C(5)-O(4)	1.269(3)
C(2)-O(2)	1.133(3)	C(5)-C(7)	1.496(4)
C(2)-Rh(1)	1.854(3)	C(8)-N(1)	1.136(4)
C(3)-O(3)	1.267(3)	O(3)-Rh(1)	2.035(2)
C(3)-C(4)	1.404(4)	O(4)-Rh(1)	2.045(2)
C(3)-C(6)	1.506(4)		
C(4)-C(5)	1.419(4)		

Table A 8.5: Complete listing of bond angles (°) fo r [Rh(CN-acac)$(CO)_2$].

Angle	Value	Angle	Value
O(1)-C(1)-Rh(1)	173.4(2)	C(5)-O(4)-Rh(1)	126.95(18)
O(2)-C(2)-Rh(1)	179.6(3)	C(1)-Rh(1)-C(2)	90.73(13)
O(3)-C(3)-C(4)	124.8(2)	C(1)-Rh(1)-O(3)	86.92(11)

O(3)-C(3)-C(6)	114.8(3)	C(2)-Rh(1)-O(3)	177.72(10)
C(4)-C(3)-C(6)	120.4(3)	C(1)-Rh(1)-O(4)	176.25(9)
C(3)-C(4)-C(5)	126.2(2)	C(2)-Rh(1)-O(4)	92.88(11)
C(3)-C(4)-C(8)	117.3(2)	O(3)-Rh(1)-O(4)	89.40(9)
C(5)-C(4)-C(8)	116.5(2)		
O(4)-C(5)-C(4)	124.9(2)		
O(4)-C(5)-C(7)	116.0(2)		
C(4)-C(5)-C(7)	119.1(2)		
N(1)-C(8)-C(4)	179.7(3)		
C(3)-O(3)-Rh(1)	127.62(18)		

A 9. Supplementary Data for [Rh(pyruv)(CO)$_2$]

Table A 9.1: Atomic coordinates and equivalent isotropic displacement parameters (Å^2) for [Rh(pyruv)(CO)$_2$]. U(eq) is defined as one third of the trace of the orthogonalized U^{ij} tensor.

Atom	*x*	*y*	*z*	U_{eq}
C(1)	7787(5)	1912(5)	8204(5)	23(1)
C(2)	9344(5)	2514(5)	11176(5)	24(1)
C(3)	6145(5)	6502(4)	8968(4)	16(1)
C(4)	6624(4)	7526(4)	10464(4)	17(1)
C(5)	7617(5)	7048(5)	11792(4)	17(1)
C(6)	4889(5)	7183(5)	7715(4)	19(1)
C(7)	3207(7)	6603(6)	5066(4)	39(1)
C(8)	7883(5)	8214(5)	13335(4)	24(1)
O(1)	7592(4)	798(4)	7143(3)	29(1)
O(2)	10138(4)	1789(4)	11984(4)	35(1)
O(3)	6563(4)	5033(3)	8484(3)	17(1)
O(4)	8271(4)	5668(4)	11793(3)	20(1)
O(5)	4370(4)	8533(3)	7975(3)	26(1)
O(6)	4435(4)	6078(4)	6314(3)	26(1)
Rh(1)	8071(1)	3739(1)	9899(1)	16(1)

Table A 9.2: Hydrogen coordinates and isotropic displacement parameters (Å^2) for [Rh(pyruv)(CO)$_2$].

Atom	*x*	*y*	*z*	U_{eq}
H(4)	6263	8628	10615	20
H(7A)	2944	5724	4082	59
H(7B)	3891	7810	5121	59
H(7C)	1949	6633	5145	59
H(8A)	7333	9237	13210	36
H(8B)	9299	8674	14020	36
H(8C)	7191	7492	13781	36

Table A 9.3: Anisotropic displacement parameters (Å^2) for [Rh(pyruv)(CO)$_2$]. The anisotropic displacement factor exponent takes the form: $-2\pi^2[h^2a^{*2}U^{11} + \ldots + 2hka^*b^*U^{23}]$.

Atom	U^{11}	U^{22}	U^{33}	U^{12}	U^{13}	U^{23}
C(1)	19(2)	22(2)	35(2)	18(2)	12(2)	11(2)
C(2)	20(2)	19(2)	32(2)	8(2)	11(2)	5(1)
C(3)	14(1)	13(2)	23(2)	7(1)	9(1)	5(1)
C(4)	16(1)	15(2)	20(2)	6(1)	8(1)	7(1)
C(5)	13(1)	13(2)	22(2)	4(1)	5(1)	2(1)
C(6)	19(2)	19(2)	23(2)	9(1)	12(1)	8(1)
C(7)	57(3)	45(3)	22(2)	12(2)	12(2)	39(2)
C(8)	27(2)	22(2)	19(2)	4(1)	5(1)	10(2)
O(1)	39(2)	20(1)	29(1)	4(1)	15(1)	15(1)
O(2)	34(2)	32(2)	47(2)	25(1)	12(1)	16(1)
O(3)	19(1)	14(1)	19(1)	6(1)	7(1)	9(1)
O(4)	20(1)	19(1)	22(1)	7(1)	7(1)	7(1)
O(5)	40(2)	21(1)	25(1)	10(1)	16(1)	20(1)
O(6)	36(1)	27(1)	18(1)	7(1)	9(1)	23(1)
Rh(1)	15(1)	12(1)	23(1)	7(1)	8(1)	7(1)

Table A 9.4: Complete listing of bond lengths (Å) for [Rh(pyruv)(CO)$_2$].

Bond	Distance	Bond	Distance
C(1)-O(1)	1.141(5)	C(5)-O(4)	1.269(4)
C(1)-Rh(1)	1.852(4)	C(5)-C(8)	1.503(5)

C(2)-O(2)	1.139(5)	C(6)-O(5)	1.200(4)
C(2)-Rh(1)	1.852(4)	C(6)-O(6)	1.333(4)
C(3)-O(3)	1.283(4)	C(7)-O(6)	1.441(4)
C(3)-C(4)	1.383(5)	O(3)-Rh(1)	2.043(3)
C(3)-C(6)	1.528(4)	O(4)-Rh(1)	2.053(3)
C(4)-C(5)	1.421(4)		

Table A 9.5: Complete listing of bond angles (º) fo r [Rh(pyruv)(CO)$_2$].

Angle	Value	Angle	Value
O(1)-C(1)-Rh(1)	178.9(3)	O(6)-C(6)-C(3)	111.4(3)
O(2)-C(2)-Rh(1)	178.7(4)	C(3)-O(3)-Rh(1)	123.7(2)
O(3)-C(3)-C(4)	129.0(3)	C(5)-O(4)-Rh(1)	126.3(2)
O(3)-C(3)-C(6)	115.4(3)	C(6)-O(6)-C(7)	114.8(3)
C(4)-C(3)-C(6)	115.5(3)	C(1)-Rh(1)-C(2)	89.69(18)
C(3)-C(4)-C(5)	124.7(3)	C(1)-Rh(1)-O(3)	90.24(14)
O(4)-C(5)-C(4)	125.5(3)	C(2)-Rh(1)-O(3)	177.72(11)
O(4)-C(5)-C(8)	115.8(3)	C(1)-Rh(1)-O(4)	176.85(12)
C(4)-C(5)-C(8)	118.7(3)	C(2)-Rh(1)-O(4)	89.32(15)
O(5)-C(6)-O(6)	124.9(3)	O(3)-Rh(1)-O(4)	90.63(11)
O(5)-C(6)-C(3)	123.7(3)		

A 10. Supplementary Data for [Rh(tfac)(CO)$_2$]

Table A 10.1: Atomic coordinates and equivalent isotropic displacement parameters (Å^2) for [Rh(tfac)(CO)$_2$]. U(eq) is defined as one third of the trace of the orthogonalized U^{ij} tensor.

Atom	*x*	*y*	*z*	U_{eq}
C(1)	6880(20)	7200(20)	5690(20)	58(4)
C(2)	7820(20)	3890(30)	6870(30)	74(5)
C(3)	7290(20)	5750(30)	1894(16)	73(6)
C(4)	7830(20)	4020(20)	1720(20)	75(5)
C(5)	8260(30)	2550(30)	3040(20)	81(5)
C(6)	6890(30)	7010(30)	700(20)	109(6)
C(7)	8800(30)	710(30)	2810(20)	109(6)

O(1)	6460(20)	8410(20)	6184(15)	104(5)
O(2)	8050(20)	3160(30)	7997(17)	107(6)
O(3)	7110(19)	6480(20)	2999(15)	74(4)
O(4)	8147(17)	2779(14)	4306(14)	58(3)
F(1)	8250(20)	8120(20)	365(13)	153(4)
F(2)	5010(30)	7950(20)	395(13)	153(4)
F(3)	7080(20)	6270(30)	-684(15)	153(4)
Rh(1)	7469(1)	5115(2)	5014(1)	61(1)

Table A 10.2: Hydrogen coordinates and isotropic displacement parameters ($Å^2$) for $[Rh(tfac)(CO)_2]$.

Atom	*x*	*y*	*z*	U_{eq}
H(4)	7944	3737	822	89
H(7A)	8843	703	1811	164
H(7B)	7810	96	3216	164
H(7C)	10114	149	3245	164

Table A 10.3: Anisotropic displacement parameters ($Å^2$) for $[Rh(tfac)(CO)_2]$. The anisotropic displacement factor exponent takes the form: $-2\pi^2[h^2a^{*2}U^{11} + \ldots + 2hka^*b^*U^{23}]$.

Atom	U^{11}	U^{22}	U^{33}	U^{12}	U^{13}	U^{23}
C(1)	54(7)	53(8)	76(10)	-26(7)	13(7)	-20(6)
C(2)	36(6)	90(14)	97(14)	-17(10)	-3(7)	-18(7)
C(3)	55(8)	123(17)	54(8)	-9(9)	3(6)	-50(10)
C(4)	58(7)	48(8)	124(14)	-23(9)	0(8)	-20(6)
C(5)	75(9)	104(14)	91(12)	-39(10)	16(9)	-62(10)
C(6)	95(10)	155(18)	97(11)	-38(10)	-9(8)	-57(11)
C(7)	95(10)	155(18)	97(11)	-38(10)	-9(8)	-57(11)
O(1)	127(10)	117(14)	84(9)	-35(9)	7(8)	-48(10)
O(2)	106(9)	153(17)	80(9)	-36(10)	20(8)	-55(11)
O(3)	68(6)	94(9)	66(7)	-7(7)	-13(6)	-34(7)
O(4)	62(5)	37(5)	84(8)	-30(5)	0(5)	-15(4)
F(1)	157(6)	189(11)	105(6)	21(6)	-18(4)	-56(6)
F(2)	157(6)	189(11)	105(6)	21(6)	-18(4)	-56(6)
F(3)	157(6)	189(11)	105(6)	21(6)	-18(4)	-56(6)
Rh(1)	50(1)	86(1)	55(1)	-18(1)	0(1)	-31(1)

Table A 10.4: Complete listing of bond lengths (Å) for [Rh(tfac)(CO)$_2$].

Bond	Distance	Bond	Distance
C(1)-O(1)	1.12(2)	C(5)-O(4)	1.26(2)
C(1)-Rh(1)	1.844(17)	C(5)-C(7)	1.47(3)
C(2)-O(2)	1.13(3)	C(6)-F(2)	1.33(2)
C(2)-Rh(1)	1.86(2)	C(6)-F(1)	1.41(2)
C(3)-O(3)	1.29(3)	C(6)-F(3)	1.54(3)
C(3)-C(6)	1.37(3)	O(3)-Rh(1)	2.030(15)
C(3)-C(4)	1.38(3)	O(4)-Rh(1)	2.041(16)
C(4)-C(5)	1.54(3)		

Table A 10.5: Complete listing of bond angles (°) f or [Rh(tfac)(CO)$_2$].

Angle	Value	Angle	Value
O(1)-C(1)-Rh(1)	174.8(16)	F(2)-C(6)-F(3)	94.7(15)
O(2)-C(2)-Rh(1)	179.3(16)	C(3)-C(6)-F(3)	114(2)
O(3)-C(3)-C(6)	110(2)	F(1)-C(6)-F(3)	96.3(16)
O(3)-C(3)-C(4)	132.5(17)	C(3)-O(3)-Rh(1)	123.9(14)
C(6)-C(3)-C(4)	117.5(19)	C(5)-O(4)-Rh(1)	127.6(13)
C(3)-C(4)-C(5)	119.3(18)	C(1)-Rh(1)-C(2)	89.3(10)
O(4)-C(5)-C(7)	116.9(19)	C(1)-Rh(1)-O(3)	90.0(8)
O(4)-C(5)-C(4)	125.5(18)	C(2)-Rh(1)-O(3)	179.2(1)
C(7)-C(5)-C(4)	117.6(17)	C(1)-Rh(1)-O(4)	178.9(5)
F(2)-C(6)-C(3)	119.9(18)	C(2)-Rh(1)-O(4)	89.6(9)
F(2)-C(6)-F(1)	109(2)	O(3)-Rh(1)-O(4)	91.1(6)
C(3)-C(6)-F(1)	118.1(15)		

A 11. Supplementary Data for [Rh(piv)(CO)$_2$]

Table A 11.1: Atomic coordinates and equivalent isotropic displacement parameters (Å^2) for [Rh(piv)(CO)$_2$]. U(eq) is defined as one third of the trace of the orthogonalized U^{ij} tensor.

Atom	*x*	*y*	*z*	U_{eq}
C(1)	2859(3)	1898(1)	1743(1)	19(1)
C(2)	2539(3)	3229(1)	2118(1)	24(1)

C(3)	2120(3)	1215(1)	3564(1)	16(1)
C(4)	1825(3)	1749(1)	4042(1)	18(1)
C(5)	1892(3)	2480(1)	3929(1)	18(1)
C(6)	2114(3)	417(1)	3762(1)	19(1)
C(7)	1557(4)	2991(1)	4497(1)	25(1)
C(8)	2828(5)	-57(2)	3204(2)	41(1)
C(9)	-111(3)	214(1)	3948(2)	36(1)
C(10)	3528(4)	302(1)	4346(1)	32(1)
O(1)	3164(3)	1619(1)	1266(1)	28(1)
O(2)	2595(3)	3772(1)	1869(1)	37(1)
O(3)	2376(2)	1349(1)	2973(1)	18(1)
O(4)	2163(2)	2830(1)	3408(1)	19(1)
Rh(1)	2459(1)	2339(1)	2530(1)	15(1)
F(1)	3146(3)	3455(1)	4554(1)	35(1)
F(2)	-144(2)	3392(1)	4407(1)	36(1)
F(3)	1348(3)	2655(1)	5059(1)	37(1)

Table A 11.2: Hydrogen coordinates and isotropic displacement parameters ($Å^2$) for $[Rh(piv)(CO)_2]$.

Atom	*x*	*y*	*z*	U_{eq}
H(4)	1569	1596	4463	22
H(8A)	2816	-555	3336	61
H(8B)	4206	79	3081	61
H(8C)	1913	6	2843	61
H(9A)	-560	513	4301	53
H(9B)	-158	-285	4076	53
H(9C)	-1005	288	3583	53
H(10A)	3074	603	4697	48
H(10B)	4922	427	4232	48
H(10C)	3475	-197	4476	48

Table A 11.3: Anisotropic displacement parameters ($Å^2$) for [Rh(piv)$(CO)_2$]. The anisotropic displacement factor exponent takes the form: $-2\pi^2[h^2a^{*2}U^{11} + \ldots + 2hka^*b^*U^{23}]$.

Atom	U^{11}	U^{22}	U^{33}	U^{12}	U^{13}	U^{23}
C(1)	12(1)	22(1)	23(1)	5(1)	-2(1)	1(1)
C(2)	21(1)	24(1)	27(1)	3(1)	0(1)	-2(1)
C(3)	10(1)	15(1)	23(1)	1(1)	-2(1)	1(1)
C(4)	19(1)	16(1)	20(1)	1(1)	1(1)	-1(1)
C(5)	15(1)	16(1)	22(1)	-2(1)	-1(1)	0(1)
C(6)	20(1)	13(1)	23(1)	1(1)	-1(1)	1(1)
C(7)	31(1)	18(1)	25(1)	-3(1)	-1(1)	-1(1)
C(8)	71(2)	20(1)	32(2)	-1(1)	9(1)	13(1)
C(9)	27(1)	20(1)	60(2)	4(1)	0(1)	-6(1)
C(10)	35(1)	21(1)	40(1)	9(1)	-13(1)	-2(1)
O(1)	25(1)	36(1)	23(1)	-2(1)	1(1)	3(1)
O(2)	51(1)	22(1)	37(1)	11(1)	-2(1)	-5(1)
O(3)	20(1)	16(1)	19(1)	1(1)	-1(1)	1(1)
O(4)	23(1)	14(1)	21(1)	1(1)	0(1)	-1(1)
Rh(1)	13(1)	15(1)	17(1)	3(1)	-1(1)	0(1)
F(1)	44(1)	21(1)	39(1)	-7(1)	-8(1)	-9(1)
F(2)	39(1)	31(1)	39(1)	-8(1)	4(1)	14(1)
F(3)	63(1)	24(1)	23(1)	-4(1)	5(1)	-1(1)

Table A 11.4: Complete listing of bond lengths (Å) for [Rh(piv)$(CO)_2$].

Bond	Distance	Bond	Distance
C(1)-O(1)	1.131(3)	C(6)-C(8)	1.520(3)
C(1)-Rh(1)	1.839(2)	C(6)-C(10)	1.531(3)
C(2)-O(2)	1.128(3)	C(6)-C(9)	1.536(3)
C(2)-Rh(1)	1.852(3)	C(7)-F(3)	1.325(3)
C(3)-O(3)	1.258(3)	C(7)-F(2)	1.338(3)
C(3)-C(4)	1.411(3)	C(7)-F(1)	1.343(3)
C(3)-C(6)	1.531(3)	O(3)-Rh(1)	2.0472(16)
C(4)-C(5)	1.370(3)	O(4)-Rh(1)	2.0378(17)
C(5)-O(4)	1.270(3)		
C(5)-C(7)	1.524(3)		

Table A 11.5: Complete listing of bond angles (°) f or [Rh(piv)(CO)$_2$].

Angle	Value	Angle	Value
O(1)-C(1)-Rh(1)	177.81(19)	F(3)-C(7)-F(2)	107.26(19)
O(2)-C(2)-Rh(1)	179.7(3)	F(3)-C(7)-F(1)	107.38(19)
O(3)-C(3)-C(4)	124.20(19)	F(2)-C(7)-F(1)	106.79(18)
O(3)-C(3)-C(6)	116.72(18)	F(3)-C(7)-C(5)	113.59(17)
C(4)-C(3)-C(6)	119.07(19)	F(2)-C(7)-C(5)	110.73(18)
C(5)-C(4)-C(3)	124.3(2)	F(1)-C(7)-C(5)	110.77(18)
O(4)-C(5)-C(4)	130.8(2)	C(3)-O(3)-Rh(1)	127.82(14)
O(4)-C(5)-C(7)	110.91(18)	C(5)-O(4)-Rh(1)	122.78(14)
C(4)-C(5)-C(7)	118.32(19)	C(1)-Rh(1)-C(2)	89.00(11)
C(8)-C(6)-C(10)	109.7(2)	C(1)-Rh(1)-O(4)	177.32(7)
C(8)-C(6)-C(3)	110.5(2)	C(2)-Rh(1)-O(4)	90.92(10)
C(10)-C(6)-C(3)	110.12(17)	C(1)-Rh(1)-O(3)	90.14(8)
C(8)-C(6)-C(9)	109.5(2)	C(2)-Rh(1)-O(3)	179.14(9)
C(10)-C(6)-C(9)	109.2(2)	O(4)-Rh(1)-O(3)	89.87(7)
C(3)-C(6)-C(9)	107.74(17)		

A 12. Supplementary Data for [Rh(dipiv)(CO)$_2$]

Table A 12.1: Atomic coordinates and equivalent isotropic displacement parameters (Å^2) for [Rh(dipiv)(CO)$_2$]. U(eq) is defined as one third of the trace of the orthogonalized U^{ij} tensor.

Atom	*x*	*y*	*z*	U_{eq}
C(1A)	8945(19)	7500	8890(11)	55(6)
C(1B)	8352(18)	2500	6951(11)	52(6)
C(2A)	6900(17)	7500	8378(11)	40(5)
C(2B)	9627(18)	2500	8223(11)	51(6)
C(3A)	9638(17)	7500	6781(12)	62(5)
C(3B)	5790(20)	2500	8059(17)	71(3)
C(4A)	8767(16)	7500	6204(11)	42(4)
C(4B)	5967(17)	2500	8860(11)	42(4)
C(5A)	7700(18)	7500	6267(12)	62(5)
C(5B)	7000(20)	2500	9296(16)	71(3)
C(6A)	10810(20)	7500	6541(15)	71(3)

C(6B)	4600(20)	2500	7621(16)	71(3)
C(7A)	6890(20)	7500	5534(16)	71(3)
C(7B)	7168(17)	2500	10148(10)	41(5)
C(8A)	11660(20)	7500	7280(13)	84(4)
C(8B)	4502(15)	4340(30)	7119(10)	84(4)
C(9A)	10960(16)	5060(20)	6326(12)	71(3)
C(9B)	3750(20)	2500	8156(14)	78(4)
C(11A)	5850(20)	7500	5700(13)	84(4)
C(11B)	7763(16)	4430(30)	10434(10)	84(4)
C(12A)	6703(18)	5170(20)	5245(12)	78(4)
C(12B)	6080(20)	2500	10476(14)	78(4)
O(1A)	9461(12)	7500	9468(9)	70(5)
O(1B)	8477(13)	2500	6336(8)	77(6)
O(2A)	6137(12)	7500	8634(8)	47(4)
O(2B)	10537(13)	2500	8377(8)	57(4)
O(3A)	9531(12)	7500	7476(8)	78(6)
O(3B)	6501(12)	2500	7621(7)	51(4)
O(4A)	7313(11)	7500	6861(7)	48(4)
O(4B)	7899(11)	2500	9026(6)	40(3)
Rh(1A)	8151(1)	7500	7928(1)	42(1)
Rh(1B)	8124(1)	2500	7940(1)	41(1)

A 13.

Table A 12.2: Hydrogen coordinates and isotropic displacement parameters (Å^2) for [Rh(dipiv)(CO)$_2$].

Atom	*x*	*y*	*z*	U_{eq}
H(4)	8935	7500	5719	51
H(15)	5368	2500	9109	51
H(8A)	12373	7537	7151	126
H(8B)	11569	6297	7562	126
H(8C)	11544	8667	7575	126
H(19A)	3805	4350	6817	126
H(19B)	5051	4306	6800	126
H(19C)	4586	5542	7422	126
H(9A)	10990	4251	6771	106
H(9B)	11616	4890	6117	106
H(9C)	10360	4636	5966	106

H(20A)	3863	3654	8481	117
H(20B)	3822	1285	8450	117
H(20C)	3046	2561	7869	117
H(10A)	5709	6243	5934	126
H(10B)	5350	7660	5246	126
H(10C)	5762	8597	6034	126
H(21A)	8432	4514	10237	126
H(21B)	7904	4403	10972	126
H(21C)	7326	5586	10273	126
H(11A)	6005	4721	5334	117
H(11B)	7248	4323	5514	117
H(11C)	6745	5107	4719	117
H(22A)	6118	3464	10877	117
H(22B)	5950	1177	10663	117
H(22C)	5500	2860	10089	117

Table A 12.3: Anisotropic displacement parameters ($Å^2$) for [Rh(dipiv)$(CO)_2$]. The anisotropic displacement factor exponent takes the form: $-2\pi^2[h^2a^{*2}U^{11} + \ldots + 2hka^*b^*U^{23}]$.

Atom	U^{11}	U^{22}	U^{33}	U^{12}	U^{13}	U^{23}
C(1A)	48(14)	88(19)	30(10)	0	13(10)	0
C(1B)	41(13)	76(17)	33(10)	0	-16(10)	0
C(2A)	41(13)	32(11)	46(12)	0	0(10)	0
C(2B)	35(13)	81(18)	34(10)	0	-5(9)	0
C(3A)	31(8)	111(16)	42(9)	0	0(7)	0
C(3B)	45(6)	64(7)	99(8)	0	0(5)	0
C(4A)	35(8)	49(9)	37(7)	0	-12(6)	0
C(4B)	35(8)	49(9)	37(7)	0	-12(6)	0
C(5A)	31(8)	111(16)	42(9)	0	0(7)	0
C(5B)	45(6)	64(7)	99(8)	0	0(5)	0
C(6A)	45(6)	64(7)	99(8)	0	0(5)	0
C(6B)	45(6)	64(7)	99(8)	0	0(5)	0
C(7A)	45(6)	64(7)	99(8)	0	0(5)	0
C(7B)	47(13)	38(12)	38(10)	0	8(9)	0
C(8A)	49(7)	143(11)	55(6)	0	-6(5)	0
C(8B)	49(7)	143(11)	55(6)	0	-6(5)	0
C(9A)	45(6)	64(7)	99(8)	0	0(5)	0

C(9B)	65(9)	95(12)	70(8)	0	-5(7)	0
C(11A)	49(7)	143(11)	55(6)	0	-6(5)	0
C(11B)	49(7)	143(11)	55(6)	0	-6(5)	0
C(12A)	65(9)	95(12)	70(8)	0	-5(7)	0
C(12B)	65(9)	95(12)	70(8)	0	-5(7)	0
O(1A)	38(9)	104(15)	65(11)	0	-2(8)	0
O(1B)	48(11)	142(18)	41(9)	0	10(8)	0
O(2A)	47(9)	47(9)	52(8)	0	18(7)	0
O(2B)	53(11)	57(10)	59(9)	0	-2(8)	0
O(3A)	44(10)	164(18)	26(7)	0	8(7)	0
O(3B)	41(9)	81(11)	29(7)	0	-2(6)	0
O(4A)	37(8)	70(10)	34(7)	0	-2(6)	0
O(4B)	34(8)	50(9)	34(7)	0	-5(6)	0
Rh(1A)	32(1)	64(1)	31(1)	0	3(1)	0
Rh(1B)	30(1)	58(1)	35(1)	0	5(1)	0

Table A 12.4: Complete listing of bond lengths (Å) for [Rh(dipiv)(CO)$_2$].

Bond	Distance	Bond	Distance
C(1A)-O(1A)	1.14(2)	C(6B)-C(8B)#2 [C10]	1.50(2)
C(1A)-Rh(1A)	1.87(2)	C(6B)-C(8B)	1.50(2)
C(1B)-O(1B)	1.14(2)	C(6B)-C(9B)	1.54(3)
C(1B)-Rh(1B)	1.85(2)	C(7A)-C(11A)	1.38(3)
C(2A)-O(2A)	1.12(2)	C(7A)-C(12A)#1 [C13]	1.635(18)
C(2A)-Rh(1A)	1.87(3)	C(7A)-C(12A)	1.635(18)
C(2B)-O(2B)	1.14(2)	C(7B)-C(11B)	1.53(2)
C(2B)-Rh(1B)	1.87(2)	C(7B)-C(11B)#2 [C13]	1.53(2)
C(3A)-O(3A)	1.28(2)	C(7B)-C(12B)	1.64(2)
C(3A)-C(4A)	1.39(3)	O(3A)-Rh(1A)	2.019(14)
C(3A)-C(6A)	1.57(3)	O(3B)-Rh(1B)	2.033(14)
C(3B)-O(3B)	1.29(3)	O(4A)-Rh(1A)	2.053(13)
C(3B)-C(4B)	1.43(3)	O(4B)-Rh(1B)	2.020(12)
C(3B)-C(6B)	1.58(4)		
C(4A)-C(5A)	1.36(3)		
C(4B)-C(5B)	1.42(3)		
C(5A)-O(4A)	1.24(2)		
C(5A)-C(7A)	1.55(3)		

C(5B)-O(4B)	1.29(3)		
C(5B)-C(7B)	1.53(3)		
C(6A)-C(8A)	1.57(3)		
C(6A)-C(9A)	1.688(16)		
C(6A)-C(9A)#1 [C10]	1.688(16)		

Symmetry transformations used to generate equivalent atoms:

#1 x,-y+3/2,z #2 x,-y+1/2,z

Table A 12.5: Complete listing of bond angles (º) f or [Rh(dipiv)(CO)$_2$].

Angle	Value	Angle	Value
O(1A)-C(1A)-Rh(1A)	177.8(19)	C(9B)-C(6B)-C(3B)	112(2)
O(1B)-C(1B)-Rh(1B)	179(2)	C(11A)-C(7A)-C(5A)	110(2)
O(2A)-C(2A)-Rh(1A)	178.5(18)	C(11A)-C(7A)-C(12A)#1	88.4(13)
O(2B)-C(2B)-Rh(1B)	178.5(18)	C(5A)-C(7A)-C(12A)#1	108.6(12)
O(3A)-C(3A)-C(4A)	123(2)	C(11A)-C(7A)-C(12A)	88.4(13)
O(3A)-C(3A)-C(6A)	120.0(19)	C(5A)-C(7A)-C(12A)	108.6(12)
C(4A)-C(3A)-C(6A)	116.8(19)	C(12A)#1-C(7A)-C(12A)	141(2)
O(3B)-C(3B)-C(4B)	127(2)	C(11B)-C(7B)-C(11B)#2	113(2)
O(3B)-C(3B)-C(6B)	113(2)	C(11B)-C(7B)-C(5B)	109.2(12)
C(4B)-C(3B)-C(6B)	120(2)	C(11B)#2-C(7B)-C(5B)	109.2(12)
C(5A)-C(4A)-C(3A)	127(2)	C(11B)-C(7B)-C(12B)	106.4(12)
C(5B)-C(4B)-C(3B)	124(2)	C(11B)#2-C(7B)-C(12B)	106.4(12)
O(4A)-C(5A)-C(4A)	126(2)	C(5B)-C(7B)-C(12B)	112.6(19)
O(4A)-C(5A)-C(7A)	117(2)	C(3A)-O(3A)-Rh(1A)	127.9(14)
C(4A)-C(5A)-C(7A)	117(2)	C(3B)-O(3B)-Rh(1B)	126.0(15)
O(4B)-C(5B)-C(4B)	125(2)	C(5A)-O(4A)-Rh(1A)	126.7(14)
O(4B)-C(5B)-C(7B)	113(2)	C(5B)-O(4B)-Rh(1B)	128.3(15)
C(4B)-C(5B)-C(7B)	123(2)	C(2A)-Rh(1A)-C(1A)	88.0(9)
C(8A)-C(6A)-C(3A)	108(2)	C(2A)-Rh(1A)-O(3A)	178.2(7)
C(8A)-C(6A)-C(9A)	96.4(12)	C(1A)-Rh(1A)-O(3A)	90.2(8)
C(3A)-C(6A)-C(9A)	101.6(11)	C(2A)-Rh(1A)-O(4A)	93.2(7)
C(8A)-C(6A)-C(9A)#1	96.4(12)	C(1A)-Rh(1A)-O(4A)	178.8(7)
C(3A)-C(6A)-C(9A)#1	101.6(11)	O(3A)-Rh(1A)-O(4A)	88.6(6)
C(9A)-C(6A)-C(9A)#1	148(2)	C(1B)-Rh(1B)-C(2B)	88.3(9)
C(8B)#2-C(6B)-C(8B)	107(2)	C(1B)-Rh(1B)-O(4B)	179.4(7)
C(8B)#2-C(6B)-C(9B)	111.7(14)	C(2B)-Rh(1B)-O(4B)	90.7(7)

C(8B)-C(6B)-C(9B)	111.7(14)	C(1B)-Rh(1B)-O(3B)	91.1(8)
C(8B)#2-C(6B)-C(3B)	106.8(15)	C(2B)-Rh(1B)-O(3B)	178.9(7)
C(8B)-C(6B)-C(3B)	106.8(15)	O(4B)-Rh(1B)-O(3B)	89.9(5)

Symmetry transformations used to generate equivalent atoms:

#1 x,-y+3/2,z #2 x,-y+1/2,z

Appendix B: Kinetic Investigations

B 1. Supplementary Data for Kinetic Measurements in Chapter 7.

The tables in this section give the observed first-order rate constants for the reactions described in Chapter 7. The ligand concentrations are given in mol.dm^{-3}; the first-order rate constant, k_{obs} is given in the unit s^{-1}; temperatures are given in ℃.

Table B 1: P(otol)$_3$ concentration dependence of the pseudo-first order rate constant for the substitution reaction between [Rh(acac)(CO)$_2$] and P(otol)$_3$ at 25 ℃.

[P(otol)$_3$]	k_{obs} (s^{-1})
1.50 x 10^{-3}	0.431(3)
3.75 x 10^{-3}	0.748(2)
8.50 x 10^{-2}	1.414(4)
1.55 x 10^{-2}	2.105(1)
2.25 x 10^{-2}	3.445(2)
2.95 x 10^{-2}	4.570(1)
4.00 x 10^{-2}	6.518(2)

Derivation of Equations used in Chapter 7:

Derivation of Eq. (7.1), (7.2) and (7.3):

Consider the mechanism as presented in Scheme B 1:

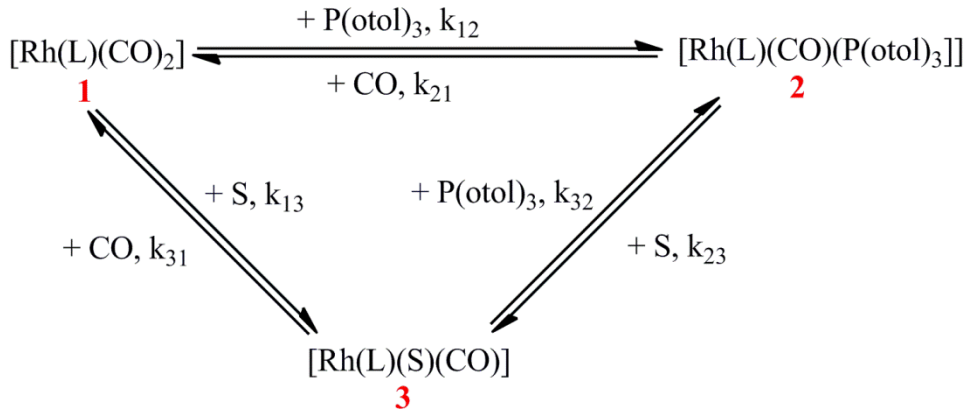

Scheme B 1: Schematic representation of a square planar substitution reaction with parallel direct substitution and solvent assisted pathways. The species are numbered in the following manner: [Rh(acac)(CO)$_2$] = 1; [Rh(acac)(CO)(P(otol)$_3$)] = 2; [Rh(acac)(S)(CO)] = 3; S= denotes the solvent. The subscripts of the rate constants represent the numbers of the species involved during the specific reaction, e.g. k_{12} describes the rate constant for the substitution reaction of complex 1 to 2. Solvent concentrations have been incorporated in the rate constants k_{13} and k_{23}.

$$\text{Set } k_{13} = k'_{13}[S] \quad and\ k_{23} = k'_{23}[S]$$

The rate expression for the formation of [Rh(L)(CO)(P(otol)$_3$] can be written as:

$$R=k_{12}[P(otol)_3][Rh(L)(CO)_2]+ k_{32}[P(otol)_3][Rh(L)(S)(CO)]- k_{21}[CO][Rh(L)(CO)(P(otol)_3)] - k_{23}[S][Rh(L)(CO)(P(otol)_3)] \quad \mathbf{A}$$

Under pseudo order conditions in both [CO] and [P(otol)$_3$] the stationary state can be approximated for [Rh(L)(S)(CO)] provided that $k_{32}[P(otol)_3]k_{31}[CO] >> k_{13}k_{23}$:

$$\frac{d[Rh(L)(S)(CO)]}{dt}=0=k_{13}[Rh(L)(CO)_2]+k_{23}[Rh(L)(CO)(P(otol)_3)]-k_{31}[CO][Rh(L)(S)(CO)]-k_{32}[P(otol)_3][Rh(L)(S)(CO)]$$

$$\therefore [Rh(L)(S)(CO)]=\frac{k_{13}[Rh(L)(CO)_2] + k_{23}[Rh(L)(CO)(P(otol)_3)]}{k_{31}[CO]+k_{32}[P(otol)_3]} \quad \mathbf{B}$$

Set **B** in **A**:

$$R=k_{12}[P(otol)_3][Rh(L)(CO)_2]+\frac{k_{32}k_{13}[P(otol)_3][Rh(L)(CO)_2]+k_{32}k_{23}[P(otol)_3][Rh(L)(CO)(P(otol)_3)]}{k_{31}[CO]+k_{32}[P(otol)_3]}-$$

$$k_{21}[CO][Rh(L)(CO)(P(otol)_3)] - k_{23}[S][Rh(L)(CO)(P(otol)_3)]$$

Manipulation of the equation can be done to give:

$$R = k_{12}[P(otol)_3][Rh(L)(CO)_2] - k_{21}[CO][Rh(L)(CO)(P(otol)_3)] +$$

$$\frac{k_{32}k_{13}[P(otol)_3][Rh(L)(CO)_2]+k_{32}k_{23}[P(otol)_3][Rh(L)(CO)(P(otol)_3)]-k_{23}k_{31}[CO][Rh(L)(CO)(P(otol)_3)]-k_{23}k_{32}[P(otol)_3][Rh(L)(CO)(P(otol)_3)]}{k_{31}[CO]+k_{32}[P(otol)_3]}$$

$$=k_{12}[P(otol)_3][Rh(L)(CO)_2]- k_{21}[CO][Rh(L)(CO)(P(otol)_3)]+\frac{k_{32}k_{13}[P(otol)_3][Rh(L)(CO)_2]-k_{23}k_{31}[CO][Rh(L)(CO)(P(otol)_3)]}{k_{31}[CO]+k_{32}[P(otol)_3]}$$

$$=k_{12}[P(otol)_3][Rh(L)(CO)_2]- k_{21}[CO][Rh(L)(CO)(P(otol)_3)]-\frac{k_{23}k_{31}[CO][Rh(L)(CO)(P(otol)_3)]-k_{32}k_{13}[P(otol)_3][Rh(L)(CO)_2]}{k_{31}[CO]+k_{32}[P(otol)_3]}$$

Integration then gives:

$$k_{obs}=k_{12}[P(otol)_3]-k_{21}[CO]+\frac{k_{23}k_{31}[CO]+k_{32}k_{13}[P(otol)_3]}{k_{31}[CO]+k_{32}[P(otol)_3]} \qquad \textbf{C}$$

Also at equilibrium the direct and solvent pathways are synchronized, resulting in:

$$K_{eq}=\frac{k_{12}}{k_{21}}=\frac{k_{13}k_{32}}{k_{23}k_{31}} \qquad \textbf{D} \text{ (Eq. 7.2)}$$

Substituting k_{21} and k_{23} from **D** into **C**:

$$k_{obs} = k_{12}[P(otol)_3] + \frac{k_{12}}{K_{eq}}[CO] + \frac{\frac{k_{13}}{K_{eq}}\frac{k_{32}}{k_{31}}k_{31}[CO]+k_{32}k_{13}[P(otol)_3]}{k_{31}[CO]+k_{32}[P(otol)_3]} \qquad \textbf{E}$$

The following simplified version of **E** can be given as follows:

$$k_{obs} = k_{12}([P(\text{otol})_3] + \frac{[CO]}{K_{eq}}) + \frac{\frac{k_{13}}{K_{eq}}\frac{k_{32}}{k_{31}}[CO]+k_{13}\frac{k_{32}}{k_{31}}[P(\text{otol})_3]}{[CO]+\frac{k_{32}}{k_{31}}[P(\text{otol})_3]} \qquad \text{(Eq. 7.1)}$$

If all steps are non-equilibrium reactions:

K_{eq}= large and $k_{31}\approx k_{23}\approx 0$

Then **E** simplifies to:

$$k_{obs}=k_{12}[P(otol)_3]+0[CO]+\frac{0[CO]+k_{32}k_{13}[P(otol)_3]}{0[CO]+k_{32}[P(otol)_3]} \quad \mathbf{E}$$

$$k_{obs} = k_{12}[P(otol)_3] + k_{13} \quad \text{(Eq. 7.3)}$$

Derivation of (Eq. 7.5):

Consider the reaction where $[Rh(L)(CO)_2]$ represents $[Rh(acac)(CO)_2]$ and $[Rh(L)(CO)(P(otol)_3]$ the $[Rh(acac)(CO)(P(otol)_3)]$ complexes:

$$[Rh(L)(CO)_2] + P(otol)_3 \rightleftharpoons [Rh(L)(CO)(P(otol)_3)] + CO$$

The equilibrium constant for the reaction can be expressed as follows:

$$K = \frac{[Rh(L)(CO)(P(otol)_3][CO]}{[Rh(L)(CO)_2][P(otol)_3]} \quad \mathbf{A}$$

Under equilibrium conditions, the observed absorbance (A^a_{obs}) for the reaction can be given as follows where A^a_M and A^a_{ML} represents the absorbance values of the $[Rh(acac)(CO)_2]$ and $[Rh(acac)(CO)(P(otol)_3]$ complexes:

$$A^a_{obs} = A_M + A_{ML}$$

Using the Beer-Lambert law, this equation can be expressed as:

$$= \varepsilon_M c^e_M + \varepsilon_{ML} c^e_{ML} \quad \mathbf{B}$$

The following term can be used to express the total concentration of rhodium in the reaction:

$$[M]_{tot} = [Rh(L)(CO)_2] + [Rh(L)(CO)(P(otol)_3] \quad \mathbf{C}$$

By substituting **A** into **C**:

$$[M]_{tot} = [Rh(L)(CO)_2] + \frac{K[Rh(L)(CO)_2][P(otol)_3]}{[CO]}$$

$$[Rh(L)(CO)_2]_{eq} = \frac{[M]_{tot}[CO]}{[CO]+K[P(otol)_3]} \quad \mathbf{D}$$

Likewise,

$$[M]_{tot} = [Rh(L)(CO)_2] + [Rh(L)(CO)(P(otol)_3] \quad \mathbf{C}$$

Can become **E** by substituting **A** into **C**:

$$[M]_{tot} = \frac{[Rh(L)(CO)(P(otol)_3][CO]}{K[P(otol)_3]} + [Rh(L)(CO)(P(otol)_3]$$

$$[Rh(L)(CO)(P(otol)_3]_{eq} = \frac{[M]_{tot}}{1+\frac{[CO]}{K[P(otol)_3]}} = \frac{[M]_{tot}K[P(otol)_3]}{[CO]+K[P(otol)_3]} \quad \textbf{E}$$

By substituting **D** and **E** into **B**:

$$A^a_{obs} = \frac{\varepsilon_M[M]_{tot}[CO]_{eq} + \varepsilon_{ML}[M]_{tot}K[P(otol)_3]_{eq}}{[CO]_{eq} + K[P(otol)_3]_{eq}}$$

This simplifies to:

$$A^a_{obs} = \frac{A^a_M[CO]_{eq}+A^a_{ML}K_{eq}[P(\text{otol})_3]_{eq}}{[CO]_{eq}+K_{eq}[P(\text{otol})_3]_{eq}} \quad \text{(Eq. 7.5)}$$

In most cases, the equilibrium concentrations of $[P(otol)_3]_{eq}$ and $[CO]_{eq}$ will be known when working under pseudo first-order conditions. Investigations undertaken in this study were not performed under pseudo first-order conditions with the specific goal of evaluating the equilibrium reaction in the presence of significant CO concentrations. For this reason, the data was modelled according to a global fit (with an estimated input of the equilibrium constant) using the quadratic equation to calculate the equilibrium concentrations of all the species. Several iterations were run to calculate the correct K_{eq} value. The model used for the global fittings was:

Ks = (RhCP*CO)/(RhC2*P)
A1obs = (A1m*(P-Pe) + A1ml*Ke*Pe) / ((P-Pe) + (Ke*Pe))
A2obs = (A2m*(P-Pe) + A2ml*Ke*Pe) / ((P-Pe) + (Ke*Pe))
A3obs = (A3m*(P-Pe) + A3ml*Ke*Pe) / ((P-Pe) + (Ke*Pe))
(Ke-1)*Pe*Pe + ((2*P) - Ke*P + (Ke*Rh))*Pe - (P*P) = 0
0 < Rh < 1
0 < P < 1
0 < Pe < 1